Predictive Control methods for Building Control and Demand Response

THÈSE N^{O} 7738 (2017)

PRÉSENTÉE LE 9 JUIN 2017

À LA FACULTÉ DES SCIENCES ET TECHNIQUES DE L'INGÉNIEUR

LABORATOIRE D'AUTOMATIQUE 3

PROGRAMME DOCTORAL EN GÉNIE ÉLECTRIQUE

ÉCOLE POLYTECHNIQUE FÉDÉRALE DE LAUSANNE

POUR L'OBTENTION DU GRADE DE DOCTEUR ÈS SCIENCES

PAR

Tomasz Tadeusz GORECKI

acceptée sur proposition du jury:

Prof. G. Ferrari Trecate, président du jury
Prof. C. N. Jones, directeur de thèse
Prof. A. Georghiou, rapporteur
Dr A. Parisio, rapporteuse
Prof. M. Paolone, rapporteur

ÉCOLE POLYTECHNIQUE
FÉDÉRALE DE LAUSANNE

Suisse
2017

Changer ses désirs plutôt que l'ordre du monde.
— René Descartes

Acknowledgements

As commonplace as it may sound, it is nevertheless true that this thesis would not quite be the same without the contributions of many people. I am grateful, even indebted to so many people that I will certainly forget to thank some of them. First, I warmly thank my supervisor, Colin Jones. His supervision made my PhD a great learning experience and a very enjoyable time. People often describe the PhD work as lonely, but it could not be more untrue in my case: it has been a pleasure to collaborate extensively with my colleagues on projects that could simply not have existed otherwise. Faran, my PhD twin, deserves a special mention. It has been a pleasure to work with him and I think we can be happy of what we achieved. I wish to particularly thank Altug, Faran and Luca for the collective effort that led to the LADR platform. It is a success that each of us has crucially contributed to. I am really spoiled because it is so easy to work with them. Our laboratory has a vivid atmosphere and a number of the scientific discussions we had have helped me greatly. I am thinking particularly of Georgios, Harsh, Altug, Sanket, Milan, Ioannis that have served me well as scientific sparring partners on numerous occasions.

Beyond work, I had a lot of fun working in LA and made great friends over the years. I am happy to have met Georgios, Altug, Tafarel, Andrea, Predrag, Milan, Faran, René, Luca, Francisco, Ye, Jean-Hubert, Martand, Kristoph, Harsh, Sanket, Ehsan, Ioannis, Truong, Ivan, Diogo, Michele, Raffaele, Philippe, Peter, Zlatko, Sean, Niketh, Basile, Mahdieh, Melanie, Timm... I can say I learned something from every person in the lab, on a scientific or personal level. I thank the professors of the laboratory, Colin, Roland, Dominique, Ali and Giancarlo for fostering a great working atmosphere in the laboratory. I thank the secretaries, Ruth, Eva, Francine, Margot for making my life easier and always answering my questions with great patience and professionalism. A special thanks goes to Christophe for infinite patience and help. Thanks to Sandra, Norbert and Francis for helping us greatly with the students on various occasions.

Big thanks to my friends, old and new. You have contributed to make this time here packed with good memories. Hopefully, we have others great times ahead of us.

My deepest thanks go to my family and especially my parents. Their influence is just indescribable and they have continuously pushed me to always do better, and I would not even be close to where I am without them.

Lausanne, May 26th, 2017 T. G.

Abstract

This thesis studies advanced control techniques for the control of building heating and cooling systems to provide demand response services to the power network. It is divided in three parts.

The first one introduces the MATLAB toolbox *OpenBuild* which aims at facilitating the design and validation of predictive controllers for building systems. In particular, the toolbox constructs models of building that are appropriate for use in predictive controllers, based on standard building description data files. It can also generate input data for these models that allows to test controllers in a variety of weather and usage scenarios. Finally, it offers co-simulation capability between MATLAB and EnergyPlus in order to test the controllers in a trusted simulation environment, making it a useful tool for control engineers and researchers who want to design and test building controllers in realistic simulation scenarios.

In the second part, the problem of robust tracking commitment is formulated: it consists of a multi-stage robust optimization problem for systems subject to uncertainty where the set where the uncertainty lies is part of the decision variables. This problem formulation is inspired by the need to characterize how an energy system can modify its electric power consumption over time in order to procure a service to the power network, for example Demand Response or Reserve Provision. A method is proposed to solve this problem where the key idea is to modulate the uncertainty set as the image of a fixed uncertainty set by a modifier function, which allows to embed the modifier function in the controller and by doing so convert the problem into a standard robust optimization problem. The applicability of this framework is demonstrated in simulation on a problem of reserve provision by a building. We finally detail how to derive infinite horizon guarantees for the robust tracking commitment problem.

The third part of thesis reports the experimental works that have been conducted on the Laboratoire d'Automatique Demand Response (LADR) platform, a living lab equipped with sensors and a controllable heating system. These experiments implement the algorithms developed in the second part of the thesis to characterize the LADR platform flexibility and demonstrate the closed-loop control of a building heating system providing secondary frequency control to the Swiss power network. In the experiments, we highlight the importance of being able to adjust the power consumption baseline around which the flexibility is offered in the intraday market and show how flexibility and comfort trade off.

Key words: MPC, predictive control, robust optimization, building control, ancillary services, demand response, frequency regulation, power consumption flexibility, smart grid, demand side management

Résumé

Cette thèse étudie des techniques de commandes avancées pour le contrôle des systèmes de chauffage et de refroidissement dans les batiments dans le but de fournir des services de Demande Réponse au réseau électrique. Elle est divisée en trois parties.

La première partie présente la toolbox MATLAB *OpenBuild* dont l'objectif est de faciliter le design et la validation de controlleurs prédictifs pour les batiments. En particulier, cette toolbox construit des modèles des batiments qui sont adaptés à la commande prédictive, basés sur des fichiers standards de description des données du batiment. Elle génere également les données d'entrée pour ces modèles pour différentes météo et types d'usage. Enfin, elle offre la possibilté de co-simuler entre MATLAB et EnergyPlus pour tester les algorithmes de commandes dans un environnement de simulation de qualité. Cela rend OpenBuild utile pour les ingénieurs en commande et les chercheurs qui veulent concevoir et tester des algorithmes de commande dans des conditions réalistes.

Dans la deuxième partie, le problème du 'robust tracking commitment' est formulé : il s'agit d'un problème d'optimization robuste multi-temps pour un système sujet à aléas oú l'ensemble dans lequel l'aléa réside fait partie des variables de décision. La formulation de ce problème est inspirée par le besoin de caractériser dans quelle mesure un système énergétique peut modifier sa consommation énergétique dans le temps pour fournir un service au réseau électrique, par exemple un service de demande réponse ou de puissance de réserve. Une méthode est proposée pour résoudre ce problème où l'idée maitresse est de moduler l'ensemble des aléas comme l'image d'un ensemble fixe par une fonction, ce qui permet d'inclure cette fonction dans le controlleur et, ce faisant, de transformer le problème en un problème d'optimisation robuste standard. L'applicabilité de cette approche est démontrée en simulation sur un exemple de batiment fournissant de la puissance de réserve au réseau. Enfin, nous montrons comment obtenir des garanties lorsqu'un horizon infini est considéré dans le problème "robust tracking commitment".

La troisième partie de la thèse rapporte les expériences qui ont été conduites sur le demonstratuer laboratoire d'automatique Demande Reponse (LADR), un laboratoire equipé de capteurs et d'un système de chauffage controllable. Ces expériences implémentent les algorithmes présentés dans la deuxième partie de la thèse pour calculer la flexibilité de la plateforme LADR et démontrent le contrôle en boucle fermée du chauffage d'un batiment fournissant de la régulation de fréquence secondaire au réseau électrique suisse. Dans les expériences, nous mettons en évidence l'importance de pouvoir ajuster la consommation électrique autour de laquelle la flexibilité est calculée sur le marché intra journalier et nous

montrons comment le niveau de flexibilité et de comfort peuvent être fixés simultanément.

Mots clefs : MPC, commande prédictive, optimisation robuste, contrôle des batiments, services systèmes, demande réponse, régulation de fréquence, flexibilité dans la consommation électrique, smart grid

Contents

List of Figures

List of Tables

1 Introduction

Massive changes are challenging today's electricity grid, both in its physical structure and its operation. Among the most cited factors driving these changes are:

- The deployment of large amounts of renewable energy resources, which causes more and more energy to be produced and injected into the power grid on distribution networks instead of the transmission network.
- The electrification of transport which also is expected to intensify the energy consumption on the lower levels of the electricity grid

The power grid is subject to stringent operating constraints, whereby generation and consumption need to balance at all times. This balancing is a complex task due to the relative unavailability and high cost of electricity storage resources. As a result, it is required to maintain part of the generation capacity as 'reserve' to act as a control resource to fill in for production/consumption mismatches at all times. Due to the increasing share of non-controllable (or less controllable) production units, mostly in the form of wind and solar power, the idea of using load side resources as reserves has been attracting a growing attention. Among other resources, buildings have been identified as potential providers of such services.

Buildings have long been studied for their potential for energy savings. For example, 37 % of the total final energy consumed in the European Union [109]) is consumed in buildings. As a consequence, buildings naturally represent a target of choice for the implementation of energy-efficiency measures. This is widely acknowledged and most countries have equipped themselves with policies that specifically focus on energy consumption in buildings. For example, in Switzerland, the Swiss Society of Engineers and Architects (SIA[1]) develops legal standards, regulations, and guidelines in architecture and construction, including energy-related aspects. The federal strategy for energy [31] plans for a periodic reinforcement of the SIA standards regarding energy-efficiency in buildings.

Improving control has been identified as having an important potential for energy efficiency in buildings. Industry players typically report energy or cost savings of up to 30% using modern advanced control systems [131].

[1] http://www.sia.ch/en/the-sia/

Accordingly, the control community has also explored the field of building control at large, proposing new advanced methods for 'traditional' building control and developing control methods for new equipment in buildings [99]. It was recognized early that buildings are good candidates for the deployment of predictive control methods, due to the relatively slow nature of the processes controlled and a somewhat less critical emphasis on safety, compared to other industrial applications. Most contributions featuring MPC for building control have focused on the supervisory control of various types of heating and cooling systems, as detailed in Chapter 2. Although the literature has repeatedly proven that implementation of MPC for buildings can be successful and outperform traditional building control methods, several hurdles remain for a large-scale deployment of MPC controllers in buildings. It is generally acknowledged that one of the most critical aspects is to obtain good quality prediction models for the controller. Models should combine good prediction capabilities and ease-of-use for control and optimization purposes, which typically translate into structural constraints on the model, such as linearity.

As buildings have been regarded more and more as potential providers of grid services, research has started to explore the technical and economic potential of buildings for this type of services. This manuscript follows this direction and attempts to answer the following questions:

1. How can the deployment of MPC controllers for building control application be streamlined?

2. How can one characterize the flexibility in power consumption a building or any electrical system can offer to the grid?

3. How can this flexibility be demonstrated in practice, and is it possible to 'optimally' offer flexibility to the power grid?

We report the research conducted over the course of the Ph.D. in three main parts. Each part tackles one of the questions above. Due to the relative independence of the parts, we purposefully keep this introductory chapter short, whereas each part provides a more extensive introduction of each topic.

Part I:The OpenBuild Toolbox

Modeling remains one of the main hurdles to the design of MPC controllers for building systems. While a number of high performance simulation tools are available, they are generally not considered fit for controller design, and even less for optimization based control. On the other hand, the thermodynamics in a building is well understood and can be modeled relatively simply, starting from the underlying physical phenomena involved. In collaboration with Faran A. Qureshi, another Ph.D. student at the Laboratoire d'Automatique, we have developed the toolbox *OpenBuild* for building thermal model extraction and building control. OpenBuild works in combination with the popular simulation environment EnergyPlus [25] to extract building description data and a quantitative description of the external factors driving the building thermal behaviour including weather, occupancy, and internal gains. Starting

from standard building description data, OpenBuild constructs entirely automatically a linear state space model that takes as inputs the energy inputs in each thermal zone of the building and as outputs the temperature in the buildings; along with the disturbance data that drives the system. This model is suitable for direct use in MPC and can conveniently be combined with custom models for the HVAC system or other auxiliary systems attached to the building (storage, local generation). We analyze the quality of the model obtained and its performance for control application and present a simple use case to illustrate the usefulness of the toolbox.

The contribution of the OpenBuild toolbox can be summarized as follows:

- It provides controller ready models of buildings that are particularly suited for predictive controllers
- It generates input data for those models for a variety of scenarios, allowing extensive testing of the controllers designed with the toolbox
- It allows cosimulation with EnergyPlus for model validation and controller testing

This part is based on the publication:

Tomasz T. Gorecki, Faran A. Qureshi, and Colin N. Jones. "OpenBuild : An Integrated Simulation Environment for Building Control". In: *2015 IEEE Multi-Conference on Systems and Control (MSC)*. 2015

Part II: Robust tracking commitment

Our objective is to investigate the provision of reserve services to the grid with loads. In this chapter, we introduce the *robust tracking commitment* problem. We establish that this problem offers a natural framework to quantify the flexibility of a load in terms of power consumption. We start from a general finite-horizon tracking problem for a system subject to disturbances and propose a method to solve the problem when the set in which the disturbance lies is part of the decision variables. The key to solve the problem is to model the uncertainty set as the image of a base set by a modifier function, which allows to recast the problem as a robust program and exploit the results of the robust programming literature. We show how quantifying the flexibility of a load can be cast as a robust tracking commitment problem and then introduce the concept of the 'virtual battery'. Finally, a discussion on infinite-horizon guarantees closes the chapter.

The main novelties introduced in this part are:

- To formalize the reserve provision problem as a robust tracking commitment problem, a tracking problem where the set of disturbances is part of the decision variables
- To show how to solve the robust tracking commitment problem and present cases where a tractable reformulation can be obtained

The content of this chapter is mostly taken from:

Tomasz T. Gorecki, Altuğ Bitlislioğlu, Giorgos Stathopoulos, and Colin N. Jones. "Guaranteeing input tracking for constrained systems: theory and application to demand response". In: *the 2015 American Control Conference (ACC)*. 2015

Altuğ Bitlislioğlu, Tomasz T. Gorecki, and Colin N. Jones. "Robust Tracking Commitment with Application to Demand Response". In: *IEEE Transactions on Automatic Control* (2016)

Part III: Experiments with Laboratoire d'automatique Demand Response (LADR)
In this part, we challenge the practical relevance of the concepts put forward in Part II in a series of experiments, where we explore the potential of secondary frequency control provision with buildings. After reporting about recent works that have looked at ancillary services provision with loads in experimental setups, we specifically look at the provision of secondary frequency control in the Swiss ancillary services market with a laboratory scale experimental testbed. The laboratoire d'automatique demand response testbed (LADR) is first introduced: it consists of a part of our laboratory equipped with sensors and a controllable electric heating system. We compute the maximum reserve the system is able to offer using the robust tracking commitment problem framework introduced in Chapter 5 and perform closed loop experiments of the system providing real-time power consumption tracking according to the regulations of the Swiss market. In addition, we show how comfort and reserve capacity can be optimally traded-off and emphasize the importance of the lead time at which the power consumption scheduled needs to be fixed by showing the difference between scheduling the baseline consumption on the day-ahead market against the intraday market.

The main novelties introduced in this part are:

- To demonstrate the applicability of the robust tracking commitment framework on an experimental testbed,
- To demonstrate closed-loop control of the heating system of a building providing secondary frequency control following the rules of the Swiss ancillary services market. Experiments were successful despite large uncertainties affecting the system, validating the robustness of the approach proposed,
- To discuss the importance of the intraday market and to show how power consumption flexibility and comfort trade off.

The content of this chapter is partly taken from:
Tomasz T. Gorecki, Luca Fabietti, Faran A. Qureshi, and Colin N. Jones. "Experimental Demonstration of Buildings Providing Frequency Regulation Services in the Swiss Market". In: *Energy and Buildings(accepted)* (2017)

Additional publications We provide here a short description of the following manuscripts that have been published or submitted during the Ph.D. and have not been included in the dissertation:

- Faran Ahmed Qureshi, Tomasz T. Gorecki, and Colin N. Jones. "Model Predictive Control for Market-Based Demand Response Participation". In: *19th World Congress of the International Federation of Automatic Control*. 2014

  In this study, we investigate the maximum possible profit for a commercial office building participating in New York's Day-Ahead Demand Response (DADR) program. We formulate an optimal control problem, assuming perfect knowledge of future weather, occupancy, and day-ahead electricity price predictions to examine the potential benefit of participation. Then, a practical control strategy based on the framework of Model Predictive Control is proposed, which enables a building to participate in the DADR program. The controller decides once every day, whether or not to participate in the Demand Response event, and then optimizes its electric consumption to increase savings. A simulation study is carried out using a building model extracted from an EnergyPlus model, real measured weather data, and real day-ahead spot market price data for New York. Savings in the range of 23% to 33% are reported.

- Luca Fabietti, Tomasz T. Gorecki, Faran A. Qureshi, Altuğ Bitlislioğlu, Ioannis Lymperopoulos, and Colin N. Jones. "Experimental Implementation of Frequency Regulation Services Using Commercial Buildings". In: *IEEE Transactions on Smart Grid* PP.99 (2016), pp. 1–1. ISSN: 1949-3053. DOI: 10.1109/TSG.2016.2597002

  This paper illustrates the potential of commercial buildings to act as frequency reserves providers through an experimental demonstration conducted in the LADR testbed. It presents the control methodology and compares two methods to solve the bidding problem, one based on robust programming and another based on a stochastic programming approach. It is observed how their level of conservatism differ, both in simulations and experiments. Experiments were conducted at night, when disturbances are minimal.

- Xuan Truong Nghiem, Altug Bitlislioğlu Altuğ, Tomasz T. Gorecki, Faran Ahmed Qureshi, and Colin Jones. "OpenBuildNet Framework for Distributed Co-Simulation of Smart Energy Systems". In: *Proceedings of the 14th International Conference on Control, Automation, Robotics and Vision*. 2016

  This paper introduces the open-source framework OpenBuildNet for distributed co-simulation of large-scale smart energy systems. Using a loose-coupling approach to co-simulate parallel processes, it can leverage and seamlessly integrate specialized simulation and computation tools in a common platform. Users can therefore benefit from the capabilities of state-of-the-art and widely used tools in each domain. OpenBuildNet is scalable and highly flexible as it uses a decentralized architecture, message-based communication, and peer-to-peer data exchange between subsystem nodes. It also provides a set of easy-to-use software tools tailored for researchers and engineers. This paper presents the architecture and tool suite of OpenBuildNet, and demonstrates its usefulness in a case study of controlling multiple buildings for demand response. Our contribution to this work, together with Faran A. Qureshi is

to give a brief overview of the OpenBuild toolbox, which can be used to generate models used in OpenBuildNet.

- Tomasz T. Gorecki and Colin N. Jones. "Constrained bundle methods with inexact minimization applied to the energy regulation provision". In: *IFAC World Congress (accepted)*. Toulouse, France, July 2017

  This paper presents initial results in the implementation of a constrained bundle method for solving large scale robust optimization problems. In this work, an alternative method is proposed to solve large scale robust optimization problems. It combines ideas from the bundle method literature for constrained nonsmooth optimization. Instead of assuming exact solutions to the minimization subproblems within the bundle method iterations, we propose to use an approximate solution to the minimization step and in particular to use the alternating direction method of multipliers (ADMM) to perform this step efficiently. Beside taking advantage of the celebrated robustness properties of ADMM, we observe that obtaining low accuracy solutions to the minimization quickly allows to solve larger problems faster.

OpenBuild Part I

This part of the thesis focuses on the development of the toolbox OpenBuild for modeling of buildings for control applications. We start by introducing the problem of building control in the Chapter 2 and we examine the shortcomings of the current practice of optimal control of buildings. In Chapter 3, we introduce the OpenBuild toolbox and demonstrate how it helps alleviating some of these shortcomings and give examples of its use. Finally, we review where the OpenBuild toolbox was used in Chapter 4 before providing a detailed description of the modeling procedure in Appendix.

The OpenBuild toolbox has been developed as a joint work between Tomasz Gorecki and Faran Qureshi, within the Green Energy Management of Structure (GEMS) project. As a consequence, this part of the thesis is co-authored and will appear for the most part identically in both theses.

2 Literature review

2.1 Building Control

2.1.1 The main objectives of building control

The objectives of building control and the most important aspects of room automation are discussed here. Building control aims to fulfill the following objectives, by order of importance:

- Maintain occupants' comfort in the building, for example keeping the temperature in occupied spaces at an appropriate level.
- Maintain the equipment in a safe operating mode, for example avoiding excessive cycling of compressors in heat pumps.
- Optimize the cost of operation of the building, for example by minimizing the energy consumption, using storage systems efficiently, and operating the equipment at its optimal coefficient of performance.

For the temperature management of the building, regulation and stability are not the primary control issues. The main issue is rather related to the economically efficient use of the heating, cooling, air-conditioning and ventilation system (HVAC) in order to maintain optimal comfort conditions.

Comfort in buildings Americans spend 87% of their time indoors [68], and since comfort conditions directly influence the productivity and well-being of building occupants [72], comfort is a crucial objective in the design and operation of building spaces and equipment. Comfort in indoor spaces depends on multiple factors, including temperature, humidity, air quality and lighting. It is important to note that comfort depends both on the design of the indoor space, for example the materials used for construction and on the proper operation and active control of the HVAC system and other elements such as blinds. Thermal comfort has been studied extensively and multiple models have been devised to measure it quantitatively, such as the predicted mean vote (PMV) and the predicted percentage of

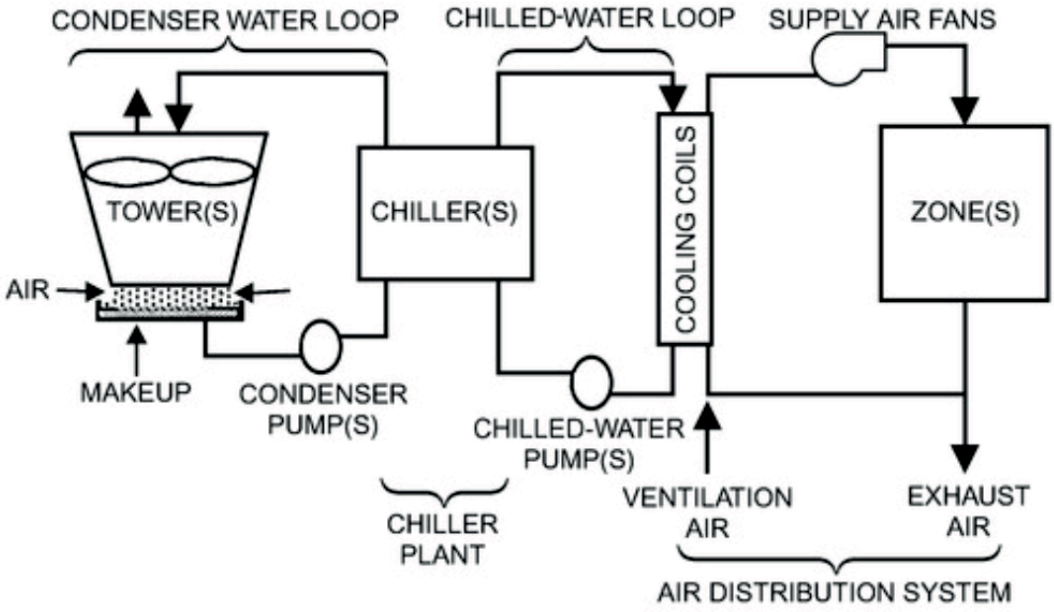

Figure 2.1 – Prototypical cooling system. From [2]

dissatisfied (PPD) [35], [103], relating temperature, humidity but also season to comfort. Some of these are discussed in more detail in Appendix B.

Energy cost Buildings are responsible for 37% of the total energy consumed in the European Union [109], one third of which concerns commercial buildings and the rest residential buildings. It is estimated that about 50% of the energy in buildings is consumed by the HVAC system. That represents a very large share of the total energy consumed worldwide and a great target for potential savings [154]. Policies have recently focused on setting new standards for building energy efficiency, such as the recent European Energy Performance of Buildings Directive [32], reflecting a global concern for improving energy efficiency of buildings. Accordingly, academic research has also focused more and more on energy efficiency of buildings, including the control sytems of buildings [74], [129].

2.1.2 A traditional HVAC system and its control

There exists a very large range of HVAC systems, but structural similarities exist, in particular in their overall organization. Large HVAC systems include a supply loop and a distribution loop. The heat or cold is generated in the supply loop in a boiler/chiller/heat pump. It is then transported to heating/cooling coils through a fluid loop (generally water). The heating/cooling coils transfer the heat/cold to the fluid (air or water) circulating in the distribution loop. The fluid of the distribution loop is in turn circulated to the zones and the heat/cold is delivered to the room through air exchangers or a radiant system. Figures 2.1 and 2.2 illustrate standard heating and cooling system architectures.

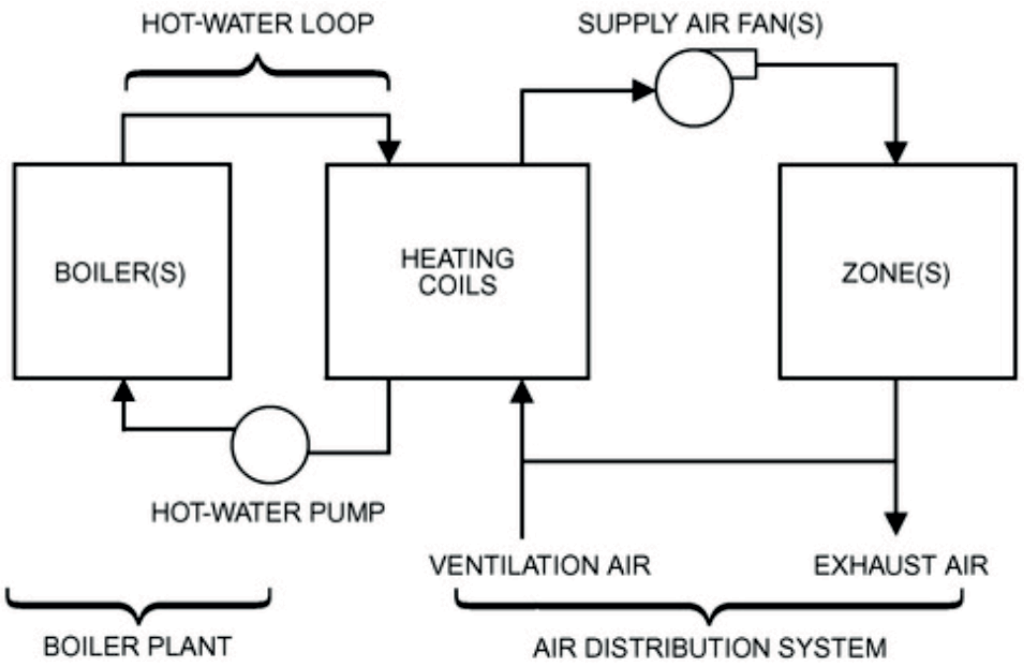

Figure 2.2 – Prototypical heating system. From [2]

The control systems also have typical configurations as reported in [2]:

HVAC systems are typically controlled using a two-level control structure. Lower-level local-loop control of a single set point is provided by an actuator. For example, the supply air temperature from a cooling coil is controlled by adjusting the opening of a valve that provides chilled water to the coil. The upper control level, also called supervisory control, specifies set points and other time-dependent modes of operation.

Control of a variable air volume (VAV) cooling system (Figure 2.1) responds to changes in building cooling requirements. As the cooling demand increases, the zone temperature rises as energy gains to the zone air increase. The zone controller responds to higher temperatures by increasing local flow of cool air by opening a damper. Opening a damper reduces static pressure in the primary supply duct, which causes the fan controller to create additional airflow. With greater airflow, the supply air temperature of the cooling coils increases, which causes the air handler feedback controller to increase the water flow by opening the cooling coil valves. This increases the chilled-water flow and heat transfer to the chilled water (i.e., the cooling demand).

The control of a hot-water heating system (Figure 2.2) is similar. As the heating demand increases, the zone temperature falls as energy gains to the zone air decrease. The zone controller responds to lower temperatures by opening a control valve and increasing the flow of hot water through the local reheat coil. Increasing water flow through the reheat coils reduces the temperature of the water returned to the boiler. With lower return water temperature, the supply water temperature drops, which causes the feedback controller to

increase the boiler firing rate to maintain the desired supply water temperature.

In Europe, it is fairly common to have water-based distribution loops with radiant heaters. Water is circulated to the rooms and heat exchange happens through radiation and convection between the radiators and the room air rather than direct air exchange. The control architecture in this type of system is similar to the one used in air-based systems.

Set points and operating modes for HVAC equipment can be adjusted by the supervisory layer to maximize overall operating efficiency. In modern buildings, the control is performed in a computerized energy management systems (EMS) that aims at reducing utility costs. Standard supervisory control uses a collection of rules to determine the best operating points for the system. This is referred to as rule based control (RBC). The design of the rules is based on knowledge of the system, experience and tuning. As: (1) the complexity of the system increases with the addition of extra equipment such as thermal storage, on site generation and shading control; and (2) the objectives of the control system are becoming increasingly complex, for example with peak shaving or optimal response to dynamic pricing, the complexity of rule-based controllers also increases [99]. Tuning may be impractical and RBC altogether inadequate for these complex objectives.

Numerous researchers focus on optimization-based strategies for energy-optimal control of buildings. Early works such as [18] have used offline optimization to improve the operation of the system, in this case the night setback strategy. [2] provides an extensive list of such optimized strategies that can then be used in the rule-based controller to improve operation. Recent years have shown a surge of interest in dynamic optimization and in particular model predictive control(MPC) for energy-optimal control of buildings. The framework of MPC is particularly suitable for building control due to its capability to handle constraints and to account for future weather, occupancy, and electricity price predictions in the control formulation.

2.1.3 MPC for Building Control

Building control has been identified early as a natural field for the application of MPC, due to various reasons, including its ability to handle constraints and complex objectives easily, the slow dynamics of buildings and the fact that stability is not the primary concern of building control. The use of Model Predictive Control has been explored extensively in the context of building control. Different objectives have been studied in the literature, such as total cost minimization [101], [84], [38], peak power reduction[105], [83], energy-optimal use of the building, and different types of demand response objectives [54], [148]. A variety of systems has been considered, including mixed-mode buildings [64], [133], storage systems [61], [85], [54], combined heat and power units [63] or passive solar systems [73].

It has been outlined that forecasts also play an important role, and have received special attention, in particular models for occupancy [108],[27] and the impact of weather on the building [107].

Specific efforts have been initiated in MPC theory to tackle building control problems, such as handling of periodic constraints [45] or stochastic MPC [107], [160]

It has been identified that MPC can help in understanding how to improve existing rule-based controllers. In [94], simplified operating rules are extracted from the results of the MPC simulations using data-mining procedures. Various factors influencing the energy saving potential of a building (utility rates, building mass, internal heat gains, efficiency of the HVAC system, and outside weather conditions) are studied in [60]. This study concludes that the factors affecting the energy use of a building do not necessarily influence its energy saving potential.

Summarizing the findings appearing throughout the literature, a few key advantages of predictive control for buildings are:

- The ability to utilize more information than classic techniques about the current and the future environment of the building when making control decisions: MPC offers a very natural way to feed forward information about weather, occupancy, price forecasts into the control scheme, and put it to best use thanks to the optimization problem formulation.

- The possibility to specify complex control objectives and constraints in an intuitive manner.

Experimental at-scale implementations have also been conducted. Of particular interest are the works [85], [86] where a hierarchical MPC controller is designed to improve the operation of the cooling system of the University of California, Merced campus buildings. The high-level MPC controller manages the energy conversion systems, including chillers, a cooling tower, pumps and takes the building as a load. A lower-level MPC layer takes care of the air handling units (AHU) and the variable air volume (VAV) boxes. An improvement of 19% of the average system COP is reported, resulting in significant savings. It lead to an improvement of the rule-based controller by 'imitation' of the optimal strategy deployed by the MPC controller. In other works, significant energy savings compared to the traditional rule-based controllers are reported in [110] and [71] for campus buildings in Europe, operated with reference tracking MPC controllers.

However, the key limiting factor to the deployment of MPC in buildings is usually the availability of a prediction model. An interesting contribution in this regard is [136] which reports that the identification, commissioning and installation costs for an MPC controller may in many cases outgrow its potential economic benefits. Therefore, efforts to facilitate the design of MPC controllers for building are still needed.

2.2 Building Simulation Tools

Various tools have been developed for building modeling, simulation and control design. Their strengths and weaknesses vary depending on the application. The most mature ones include Modelica, TRANSYS, ESPr, eQuest, and EnergyPlus [88]. Modelica is an equation-based modeling language that has a free open source building library which covers HVAC systems, multi-zone heat transfer and heat flow. It also enables real-time data exchange

with building automations systems. TRANSYS provides a transient simulation environment and is well suited for the detailed analysis of solar systems, HVAC systems, renewable generation, and co-generation systems. ESPr is based on a finite volume, conservation approach and is powerful for simulating scenarios in different operating and environmental conditions. eQuest is a comprehensive building energy simulation tool and supports complex geometries, and many HVAC configurations. EnergyPlus is a very detailed complete building energy simulation software and includes many simulation capabilities.

The main differences between these tools lie in their simulation capabilities, modeling approach, the way they handle interior and exterior surface convection, solar gain, data exchange and the additional software they support. See [24] and Table 2.1 in [88] for a detailed comparison of these tools.

2.2.1 EnergyPlus

EnergyPlus [25] is a detailed building energy simulation software developed by the U.S Department of Energy (DOE) for the simulation of building, HVAC, lighting, occupancy, ventilation, and other energy flows in a building. It is typically used by architects, engineers, and researchers and helps to optimize the building design for energy and water usage.

EnergyPlus is a combination of many modules working together to determine the heating or cooling energy requirement of a building. It include modules for shading computation, day lighting, window heat transfer, sky model, air loops simulation, zone equipment simulation, airflow network, and conduction transfer function. Each module simulates and determines its energy impact on the building and the HVAC system. The integrated simulation approach used in EnergyPlus means that all modules are simulated concurrently and a constant feedback between the modules ensures that a physically realistic solution is obtained.

Some of the key features of EnergyPlus include the integrated, simultaneous solution of the thermal zone conditions and HVAC system response, heat-balanced based solution of radiant and convective effects, sub-hourly user definable time steps for interaction between the thermal zone and the environment, combined heat and mass transfer models, illuminance and glare calculations, component-based HVAC supporting both standard and novel configurations, a large number of built-in HVAC and lighting control strategies, import and export of data with other engines for co-simulation, and generation of detailed output reports with user defined time-resolutions[1].

EnergyPlus takes as inputs building description data and weather data as structured ASCII text files. The core of the software is script based and does not have any official GUI or user interface. Third-party software has been developed, e.g., OpenStudio [53] to interface with EnergyPlus. Generally, EnergyPlus, like most of the other detailed building simulation software, is not considered an easy-to-use tool and requires experience.

One of the strengths of EnergyPlus is that it allows the simulation of different types of environments, building types, HVAC types and configurations, and external weather conditions. It also enables the simulation of renewable, e.g., PV's and co-generation units.

[1] https://energyplus.net/

Another advantage is the free availability of a validated database of standard building models of different types and locations provided by the Reference Buildings database of the U.S. DOE [146]. It includes models for offices, warehouse, retail stores, malls, schools, supermarkets, restaurants, hospitals, hotels, and apartment buildings. This database is representative of approximately 70% of all the commercial buildings in the U.S. and is a good resource to carry out simulations with a wide variety of buildings.

EnergyPlus building models are generally of good quality, and are considered to be a reasonable representation of buildings. Various works have experimentally tested and validated EnergyPlus models [1], [144], [93], [59]. However, EnergyPlus models, because of their complexity, are not suitable as prediction models in optimization based control design. Therefore, there is a need to develop a systematic modeling procedure to obtain simple, yet representative models which can be used for control design.

2.2.2 MLE+

MATLAB is one of the most popular development and prototyping environment for control design. It offers a flexibility much superior to specialized software such as EnergyPlus. MLE+ has been designed as a bridge that interfaces Matlab and EnergyPlus. As we will use MLE+ as the basis for the co-simulation interface of Openbuild, we give here a brief presentation of its scope.

MLE+ [11] is a MATLAB / SIMULINK toolbox for co-simulation with EnergyPlus. The toolbox provides an interface between EnergyPlus and MATLAB. It relies on BCVTB [156] to handle the communication of data between the two pieces of software. It is useful to carry out co-simulations where the building energy simulation is performed in EnergyPlus and the controller design and implementation is done in MATLAB. It also helps collecting data from EnergyPlus simulations for system identification or analysis purposes.

Using MLE+ requires the knowledge of EnergyPlus and involves manual processing for setting up the co-simulation which can be cumbersome when a large number of simulations is required.

2.3 Building Modeling

Building thermodynamic modeling can broadly be divided into three main categories - first principles physics-based (white-box), data-driven (black-box), and a combination of physics-based and data-driven (gray-box) modeling approaches [74], [3]. All these approaches have been studied in the literature and have their associated benefits and drawbacks.

First principles physics-based modeling methods [74], [3] involve constructing a detailed model of the building thermodynamics based on the principles of heat transfer through conduction, convection, and radiation. A Resistance-Capacitance (RC) network of nodes is constructed where each node represents the temperature in a specific zone, wall, surface, ceiling, or floor. The interconnection of nodes is defined by the physical geometry of the building. The model parameters (conduction, and convection coefficients, etc.,) are

usually obtained from the knowledge of the construction material and architectural details. Constructing these types of models is time consuming (especially for large buildings) and requires expert knowledge of the building thermodynamics. The dimension of the model can be quite large depending on the size of the building, whereas the quality of the model is generally good.

Data driven modeling [125] approaches use experimental input-output data to learn a dynamical model of the building thermodynamics. The advantage of this method is that it does not require any knowledge of building construction or geometry, but the internal states of the models obtained by this method lack any physical interpretation. The procedure can be applied to either the whole building or to a subsection of the building. Usually, a large data set is required to obtain models of reasonable accuracy which is difficult to obtain for an occupied building. Moreover, the identification data is also required to have a rich frequency content, which is difficult to obtain in a real building. Some authors have proposed to use the data from the energy simulation software, e.g., EnergyPlus. OpenStudio was used in [23] to perturb the EnergyPlus model and generate the experimental data which is then used to fit a reduced-order linear model. The results demonstrated a model which was accurate enough for control and was used in simulation to design an MPC controller. Generally, there is no systematic method to select the structure and order of the model and it might take several trial-and-error rounds to obtain a reasonable model.

Grey-box modeling or hybrid modeling [58] approaches first choose a model structure based on the physical knowledge of the building and use parameter estimation techniques to identify the model parameters. Using a physical model structure reduces the requirement of a large training data set, and can provide a better quality model compared to black-box methods. [19] proposes a transfer function based model with parameters constrained to satisfy a physical representation for energy flows in the building. The model parameters were identified using simulation data from TRANSYS and field data from a test site, resulting in a satisfactory model quality. [10] presented a Monte-Carlo simulations based method to estimate the model parameters. [111] used subspace identification with data generated from EnergyPlus and divided the building into smaller parts to make sure that the estimation algorithm could be applied with the available computational power, and combined the identified parts together to obtain the complete model. The resulting model was validated successfully. [88] proposed using a parameter adaptive building model with time-varying parameters in a RC model to capture the time varying impact of the internal and external disturbances on zone temperatures. The parameters were then estimated online using an extended Kalman filter.

Experimental results have also been reported in the literature. [165] identified a low-complexity data-based model and an RC model of an entire floor of Sutardja Dai Hall, an office building on the University of California, Berkeley campus. Experiments were conducted and semi-parametric regression was used for data based modeling. The comparison results showed that the RC model was more accurate, but both models performed well for closed-loop control. [137] obtained two models of a single zone test office using system identification and physical modeling approaches and both the models showed a reasonable performance in

predicting the room temperatures with the RC model being slightly more accurate at high frequencies. [147] used grey-box system identification methods to obtain a thermodynamic model for a building in Belgium for MPC operation.

All these methods are time consuming and often are difficult to generalize. At minima, the parameter estimation part of the modelling procedure needs needs to be repeated for every new building. Therefore, a systematic modeling approach is required which can be used with minimal effort to construct a good quality control oriented model.

Remark 2.1. Concurrently and independently to the development of OpenBuild, a similar effort was undertaken in the development of the BRCM toolbox [139]. This toolbox also helps to create discrete-time state-space (bi-)linear models for buildings using a physical modeling approach. The Toolbox is based on [138] and constructs a RC model of the building zones while the model parameters are provided by the user or can partly be obtained from EnergyPlus. The model validation with EnergyPlus shows a reasonable performance for the considered case. However, it does not provide input data compatible with the model for weather and usage description, and does not offer co-simulation capabilities. □

2.4 MPC for Building Control

This section provides an overview of the ingredients used in MPC for buildings. It serves as reference for the rest of the thesis.

2.4.1 Optimization Problem

We start from a standard MPC problem formulation:

$$\begin{aligned}
&\underset{\mathbf{x},\mathbf{u}}{\text{minimize}} && J(\mathbf{u}) && (2.1)\\
&\text{subject to} && x_{t+1} = f(x_t, u_t, d_t) && (2.2)\\
& && u_t \in \mathcal{U} && (2.3)\\
& && y_t = g(x_t) && (2.4)\\
& && y_t \in \mathcal{Y} && (2.5)\\
& && t = 0, \ldots, N-1 &&
\end{aligned}$$

where $\mathbf{u} = (u_0, u_1, \ldots, u_{N-1})$, $\mathbf{x}$ and $\mathbf{y}$ are the control, state and output sequence over the control horizon, respectively. The choice of the cost function (2.1) is discussed in section 2.4.4. Equations (2.2) and (2.4) embed the dynamics of the system and the effect of the disturbance and are discussed in section 2.4.2. Equation (2.3) gathers the input constraints and (2.5) represents the zone temperature constraints as discussed in section 2.4.3.

2.4.2 Model of the system

As we already mentioned, an MPC controller requires a model of the system. We usually consider discrete-time state-space models of the form:

$$\begin{aligned} x^+ &= f(x, u, d) \\ y &= g(x) \end{aligned} \tag{2.6}$$

where x denotes the state of the system, u the controlled input to the system, d the vector of disturbances affecting the system and y represents the output of the system. In the case of buildings the output is usually the temperature in different zones of the buildings. The inputs are the control variables of the HVAC system: depending on the type of HVAC, these inputs can be flow rates, supply temperatures, temperature setpoints, blind positions, or thermal power inputs, for example.

Buildings are affected by large disturbances coming from weather and internal gains, and it is crucial to model the effect of these disturbance in our model to have a good prediction quality. d typically regroups the effect of the outside temperature, sun irradiance, occupancy, and internal gains from equipment, lighting, etc.

We will see in Chapter 3 that the model in our approach is decoupled in two parts: the model for the thermodynamics of the building, which takes as inputs thermal power inputs to the zones and as outputs the temperatures inside the building, and the model of the HVAC system which is system dependent and takes as inputs the actual controlled inputs and outputs the resulting thermal flows to the rooms.

2.4.3 Constraints

One of the most advertised advantages of MPC is its natural ability to handle constraints on inputs and states of the problem. In the case of buildings, the constraint will typically include constraints on the inputs captured in (2.3) which model the operational limitations of the system, for example limits on power inputs, flow-rates, supply temperature, ... In addition, it is frequent to impose comfort constraints, captured in (2.5). We usually define a comfort range for the zone temperatures as $[T_{\text{ref}} - \beta, T_{\text{ref}} + \beta]$ where T_{ref} is the optimal temperature and β a parameter defining the size of the comfort range.

Notice that for commercial buildings, it is customary to relax the temperature during unoccupied hours in order to reduce the total energy consumption, a strategy referred to as night-time setbacks. In that case, the comfort range is extended during the night so that the constraint reads $y_t \in [T_{\text{ref}} - \beta_t, T_{\text{ref}} + \beta_t]$ with β_t a time-varying quantity.

2.4.4 Objective Function

Another advantage of MPC is the possibility to specify various types of objectives. Temperature tracking is rarely the objective of the control for buildings and quadratic costs are not common. Instead, economic performance is commonly specified as the objective of the problem. Assuming a relationship is known between the control inputs applied to the

Table 2.1 – Cost functions in MPC problem

Minimum energy	$J(u) = \sum_{t=0}^{N} e_t$
Minimum cost	$J(u) = \sum_{t=0}^{N} c_t e_t$
Peak charge	$J(u) = c_{\text{peak}} \max_{t \in [T_0, T_f]} p_t$

system and the amount of energy used (electricity or other), so that $e_t = h(u_t, x_t, d_t)$ with e_t the energy consumption at time step t, a minimum energy objective reads:

$$J(u) = \sum_{t=0}^{N} e_t$$

A minimum cost of energy objective is formulated as:

$$J(u) = \sum_{t=0}^{N} c_t e_t$$

with c_t the time-varying cost of energy. Buildings are often subject to differentiated tariffs so that c_t changes according to a schedule, with alternating periods of peak demand with high cost of energy and periods of low demand with lower cost of energy. In other cases, the price is dynamic, and changes continuously. In this case, the cost of energy might need to be forecast [4].

A typical objective is also to reduce peak demand over predefined periods of time, as specified by a lot of utility tariff plans. The cost can then include a term of the form:

$$J(u) = c_{\text{peak}} \max_{t \in [T_0, T_f]} p_t$$

with c_{peak} the cost of peak electricity consumption and p the power demand.

Table 2.1 recaps these classical costs.

Demand Response objectives can be formulated. Event-driven Demand Response sometimes requires pre-specified power decrease upon request. For example, [114] studies such a problem and uses the following cost function:

$$J = \sum_{t=0}^{N_{OC}-1} V_t^e - \delta_t V_t^{dr}$$

with $V_t^e = c_t^t e_t$ the cost of electricity consumption, $V_t^{dr} = c_t^d (B_{d,h} - p_{d,h})$, the payment from DR participation, where $B_{d,h}$ is the baseline consumption at time step t (day d, hour h) and c_t^d the payment for power reduction. The baseline consumption for an hour h is the average energy consumption during hour h over a set of previous days $\mathcal{S}_{d,h}$, and is given by:

$$B_{d,h} = \beta_{d,h} \frac{1}{|\mathcal{S}_{d,h}|} \sum_{j \in \mathcal{S}_{d,h}} p_{d-j,h},$$

where $\mathcal{S}_{d,h}$ is the set of days used to compute the baseline, $\beta_{d,h}$ is a weather correction factor. δ_k is the binary variable indicating the status of DR participation at time step k.

An objective mixing different costs can be chosen and it is possible to penalize deviations from optimal comfort using one of the metrics introduced in Appendix B. Even when not directly using comfort metrics in the cost, a soft-constrained formulation is often used. In that case, extra decision variables s_t referred to as slacks are introduced and the temperature constraints are transformed into $y \in [T_{\text{ref}} - \beta_t - s_t, T_{\text{ref}} + \beta_t + s_t]$ while the slacks are penalized in the cost so that:

$$J(u) = \ldots + \rho(s)$$

with ρ a loss function.

2.5 Summary

Looking back at the MPC problem formulation (2.1)-(2.4), we see that when considering a particular building for control, the challenge is to gather and compile all the information necessary to build up the elements of the MPC problem, namely, the system model, the disturbance inputs to the model and the constraints description. In particular, we have outlined in the literature review a lack of systematic approaches to construct building models that are *appropriate for control and optimization*.

We introduce the OpenBuild toolbox in the next chapter: one of the main functionality of the toolbox is to construct automatically the model of the building together with the disturbance inputs corresponding to the simulated usage and weather.

3 The OpenBuild Toolbox

3.1 Contribution

The primary objective of the OpenBuild toolbox is to facilitate the implementation, testing and validation of MPC controllers for buildings. It features the following novel elements:

- The OpenBuild toolbox enables the extraction of building models that are suitable for control and optimization purposes, based on available and standard building description data.

- The disturbance data affecting the building including weather, internal gains and occupants, is also extracted with the toolbox.

- Through Openbuild, users can access a large amount of data about existing buildings and realistic input data to simulate various occupancy, weather and usage scenarios. This is possible because OpenBuild works in combination with the popular simulation environment EnergyPlus.

- It facilitates the design of controllers and observers, in particular predictive control algorithms, and their validation through cosimulation with EnergyPlus, by integrating the cosimulation interface MLE+. The user only requires input data files in EnergyPlus input format to create building models, without knowledge of modeling or EnergyPlus, and can co-simulate controllers from MATLAB. Therefore, the toolbox is particularly suited for control engineers and researchers that want to prototype building controllers.

3.2 Structure of the Chapter

The rest of this chapter is organized as follows: Section 3.3 gives a very brief overview of the modeling principles used to derive the building thermodynamic models. Section 3.4 gives an overview of the components of the toolbox. Section 3.5 discusses the quality of the model extracted through OpenBuild. Section 3.6 gives a simple example that illustrates what a user needs to do to use the OpenBuild toolbox.

3.3 Thermodynamics model explanation

The goal of the modeling procedure is to obtain a model which is simple enough to be suitable for control (especially MPC), yet satisfactorily captures the dynamics of the building. A physical modeling approach is adopted. The following physical phenomena are modeled:

- Heat transfer through conduction
- Heat transfer through convection
- Long-wave radiation on all internal and external surfaces
- Internal gains (lighting, occupancy, equipment) on all internal surfaces
- Solar radiation on internal and external surfaces

We give in this section a brief overview of the modeling procedure, and refer the reader to Appendix A for a detailed description.

3.3.1 Modeling Fundamentals

The well-established RC modeling framework [138, 79] is used to model the thermodynamics of the building. It consists of representing the building as a set of thermal nodes in a graph where each node's temperature is assumed to be representative of the temperature of a physical portion of the building and the temperature dynamics of each node is described by a linear differential equation. A parallel with electrical circuits illustrates best the concepts: temperatures of the zone air and of the building elements are represented by the voltages at each node of the RC network. The heat fluxes between the nodes are equivalent to the currents between the nodes of the RC network. Coefficients of heat conduction between the nodes and convection between the zone air and the building surfaces are modeled by resistances in the RC network. The thermal capacity of the zone air and of the layers in the building surfaces are modeled by the capacitors. Long wave radiation from outside and between surfaces are also linearized and represented by resistances.

3.3.2 Model Parameters

The computation of the parameters in the RC model is carried out using both the input data file and the post processed EnergyPlus data (surface view factors, convection coefficients, etc.). The thermal capacities and the conduction coefficients in the RC model depend on the physical properties of the materials used in the building construction, as described in the building data file. The convection coefficients in the RC model depend on the material properties, but also on other external factors including weather conditions. In EnergyPlus, the computation of convection coefficients can be carried out using different algorithms (see [29], pp.64-74, 78-94), and yields time-varying convection coefficients. A constant time averaged coefficient is considered in the model extraction and is collected from the post-processed EnergyPlus data. The long-wave radiation from the external

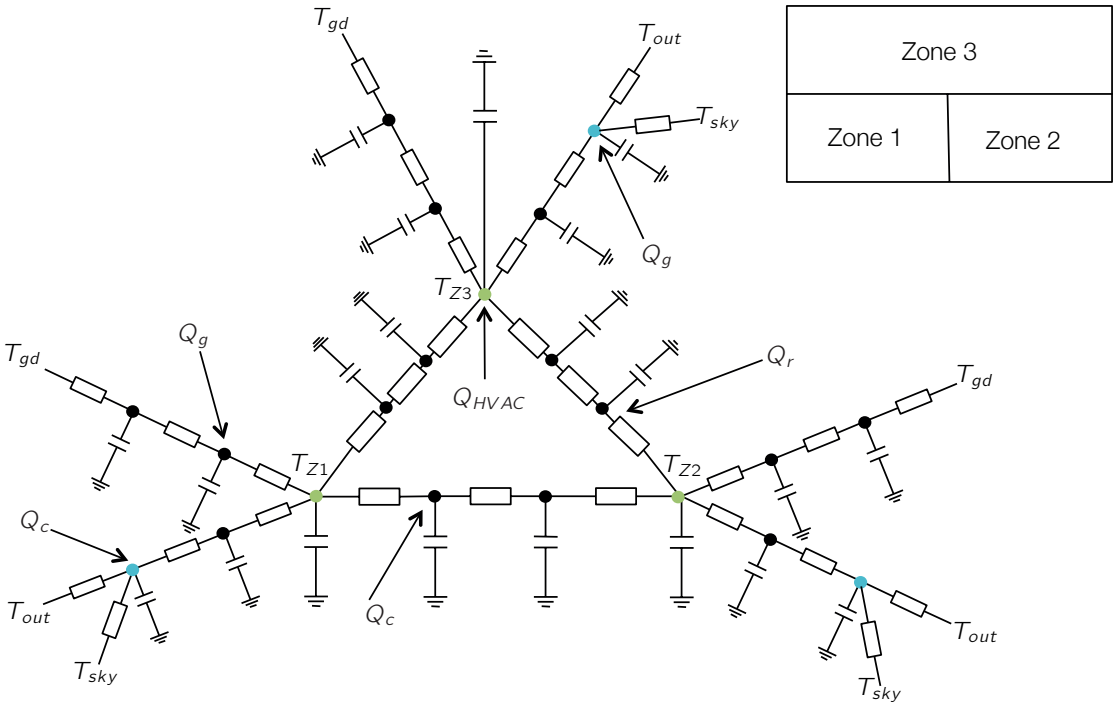

Figure 3.1 – Model Structure (green nodes: zone air, blue node: outside surfaces, black nodes: inside surfaces)

sources and between the internal surfaces of the building is characterized by a nonlinear function (see [29], pp. 76-77). This function is linearized, viewing factors are obtained from the post-processed EnergyPlus data and the physical properties of the construction material are obtained from the building data file. The solar radiation and the internal gains acting on the building surfaces are obtained from the post-processed EnergyPlus data and are applied to the corresponding nodes of the RC network. Lastly, EnergyPlus computes equivalent U-values capturing the overall heat transfer through windows, which are used by OpenBuild for window modeling. All model parameters are retreived from EnergyPlus input files or computations. In the absence of building description data, these parameters would need to be identified, which is beyond the scope of the Openbuild toolbox.

3.3.3 Model Structure

Figure 3.1 illustrates the construction of the RC structure created for a three zone building. Note that the actual node network created is more complex but is simplified here for illustration purposes. The following energy flux balance equation is applied at each node of the RC model:

$$C_n \frac{dT_n}{dt} = Q_c + Q_g + Q_r + Q_{\text{HVAC}}, \tag{3.1}$$

where C_n is the thermal capacity and T_n is the temperature of node n, respectively. The temperature T_n of each node represents the average of the temperature over a physical portion of the building. Q_c combines the heat fluxes acting on the node due to conduction and convection, Q_g is the flux from solar and internal gains, Q_r is the flux due to longwave radiation exchange, and Q_{HVAC} is the flux from HVAC acting on the node. Note that Q_c and Q_r depend on the temperature at other nodes of the network while Q_g represents thermal fluxes from the outside of the system. This equation for all nodes forms a set of linear differential equations. The windows are a special case in the model, since they are assumed to have no thermal capacity: they are modeled by a set of algebraic equations (see [29], pp. 225-231). For simplicity, we use a linearized version of these equations to obtain explicit expressions of the window surface temperatures and substitute it in the differential equations of the rest of the temperature nodes.
This procedure provides a continuous time linear state-space model of the building:

$$\begin{aligned} \dot{x} &= Ax + B_u u + B_d d \\ y &= Cx \end{aligned}$$

which is discretized at a desired time step to obtain a model of the form:

$$\begin{aligned} x_{k+1} &= Ax_k + B_u u_k + B_d d_k \\ y_k &= Cx_k \end{aligned} \tag{3.2}$$

where $x_k \in \mathbf{R}^n$ is the state vector (containing the temperatures of all the zones, surfaces, and internal nodes), $u_k \in \mathbf{R}^{n_u}$ is the control input (Q_{HVAC}), and $d_k \in \mathbf{R}^{n_d}$ is the weather (*e.g.*, outside temperature and solar gains) and internal gains disturbance vector. The predicting quality of the model resulting from the modeling approximations is discussed in Section 3.5.

Remark 3.1. The complete modeling procedure described in this section, including creating an RC network graph, computing of the model parameters, solving of algebraic equations and obtaining the linear model (3.2) is carried out automatically, taking as input only the building data description file and the weather description file. □

3.4 Code structure and simulation workflow

The main objective of OpenBuild is to enable the design and testing of advanced controllers, especially MPC controllers, in realistic simulation scenarios. It builds on the co-simulation interface MLE+ to provide control experts most of the tools and data required for controller design for buildings, as pictured in Figure 3.2. The OpenBuild toolbox helps to collect and construct these components, and streamlines their use in an integrated workflow.

Co-simulation is considered a valuable option for control design [155]. EnergyPlus is a widely used high-fidelity simulation environment, but it is not suited for complex controller design. Recent contributions [11] have enabled co-simulations between EnergyPlus and

Figure 3.2 – Dataflow in OpenBuild co-simulations

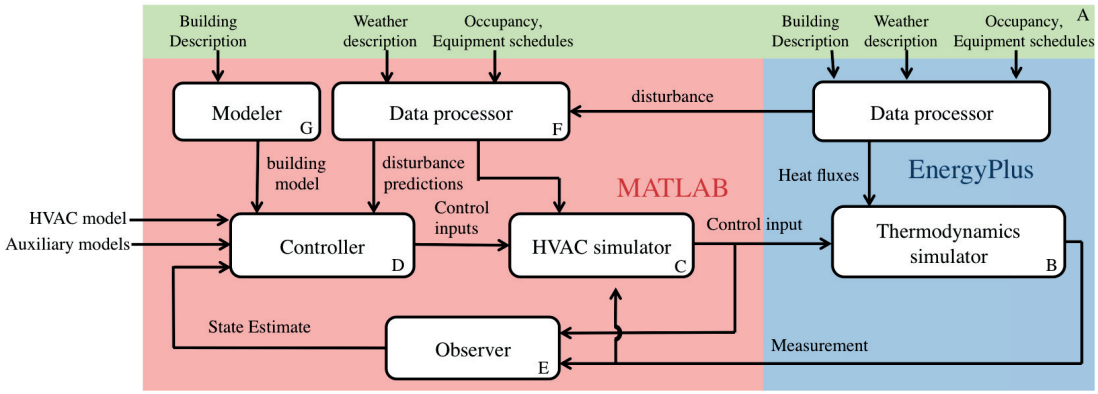

MATLAB, where the controller is designed and simulated in MATLAB. However, co-simulations require a number of other elements including building description data, description of weather, occupancy and usage of the building. MPC design requires models of the building and HVAC system suitable for optimization. Simulations also require the conversion of weather and occupancy data to the actual inputs of the models used for control. This section details each of these components as they are included in OpenBuild. Figure 3.2 summarizes the different modules of OpenBuild with letter labels referring to the following subsections.

3.4.1 Building and weather data (A)

EnergyPlus allows the direct use of existing description data for buildings, such as the DOE reference buildings dataset [146]. In addition, tools are available to help users to easily create new models for EnergyPlus [53]. Lastly, conversion from other building description formats is often possible. EnergyPlus input data files include schedules of occupancy, equipment, lights, etc. that OpenBuild can directly interpret.
EnergyPlus takes standard weather data files as input. Typical weather data for numerous locations is readily available. Moreover, using EnergyPlus utility programs, additional weather files can be created based on measured or forecast weather data, also reconstructing missing or corrupted data. This is useful to construct predictions of the weather disturbances for an MPC controller. For example, a database of weather forecasts has also been collected: it can be used to test controllers with realistic historical forecasts, which are not easily found.

3.4.2 Thermodynamics simulator (B)

EnergyPlus can be used as the simulator for the thermodynamics of the building. It is possible to control some variables in EnergyPlus through an external interface, and [11] provides ways to run co-simulations from MATLAB. However, two main difficulties arise: first the external interface lacks flexibility and requires knowledge of EnergyPlus and in some cases manual modifications of the files. Second, only specific variables are available

for external control, mostly setpoints for thermostats. For most systems in EnergyPlus, no direct control of the low-level actuators and variables is possible (valve and damper positions, massflows, etc.). This presents from testing low-level controllers for the HVAC system. However, setpoint control is in many cases more realistic than low-level control of components, since they are usually equipped with local controllers and the supervisory controller of the building only manipulates temperature and flowrate setpoints.

Therefore, to enable flexible HVAC simulation, OpenBuild typically uses EnergyPlus only for the thermodynamics of the building. From MATLAB's point of view, the inputs to the zones are heat fluxes to the rooms or surfaces of the building. This allows the decoupling of the simulation of the building and the HVAC. This is a reasonable setup since the thermodynamics of the building is mostly independent from the HVAC type.

Remark 3.2. The models generated by OpenBuild can also be used to simulate the building in MATLAB without co-simulation. □

3.4.3 HVAC simulator (C)

Modeling the HVAC is a complex task, which is very difficult to perform automatically. The complexity of the HVAC descriptions in EnergyPlus are high, at a level of detail which is not required for controller design. Most works from the literature report targeted case-by-case modeling efforts for the HVAC, which is very time-consuming. The models used in an MPC controller need to be simple enough for optimization purposes, which disqualifies EnergyPlus. This motivates the modeling of HVAC systems directly in MATLAB. The models should map the actual input (such as electric power input, valve and damper positions or fluid flows) to the heat fluxes into the different rooms and surfaces. A framework is proposed to specify new HVAC system models easily. Some simple HVAC models have been developed and include simple forced-air systems, thermally activated building systems, electric boilers, heat pumps, and blind controls. In addition to simulating the HVAC, the HVAC simulator also computes appropriate inputs to the external interface of EnergyPlus. Additional modules such as batteries or storage tanks can easily be added and simulated together with the building. Notice that HVAC components can still be simulated in EnergyPlus in co-simulation but that requires manual processing of the files and good knowledge of EnergyPlus inner workings.

3.4.4 Controller (D)

Good controllers are imperative for the efficient operation of a building. OpenBuild focuses on MPC controllers. The controllers use a model of the dynamics of the system and solve a constrained optimization problem to compute an optimal input sequence. The performance of MPC controller relies greatly on the quality of the model. OpenBuild can directly extract models for the thermodynamics of the building (*cf* Section 3.4.7) to facilitate the MPC setup. Section 2.4 details a typical MPC formulation for buildings.

3.4.5 Observer (E)

Full state information of the linear model is required for control with MPC, however it is not available from EnergyPlus (or in a real building). Observers are required to estimate the state of the building, HVAC system, and auxiliary systems attached to it. Observer design can be challenging because of model mismatch and disturbance issues. By combining an offset-free formulation [90] and Kalman filtering, good performance was generally achieved in our simulations. The Kalman filter is also designed using the model of the building. Examples of filters and controllers are available in the toolbox examples but tuning of the observers has been observed to have a significant impact on the quality of the estimation, therefore requiring a minimum effort from the user.

3.4.6 Data Processor (F)

Implementation of MPC controllers requires the prediction of the weather, including solar gains, occupancy, and other internal gains. Occupancy and equipment use are usually specified in the form of schedules directly in the EnergyPlus file. Weather data comes in separate files which list temperatures, humidity ratios, weather conditions, solar irradiance, etc. This data needs to be interpreted to evaluate the impact of the weather on the building, *e.g.* through geometric computations to calculate the effect of the sun on each surface. EnergyPlus performs these computations, which we can directly exploit in OpenBuild. OpenBuild uses EnergyPlus as a pre-processing engine for the model. From only the building and weather description, it automatically runs the appropriate components of EnergyPlus to extract the corresponding weather and internal gain data compatible with the models. This is a key feature of OpenBuild which facilitates simulation greatly by requiring minimum user input.

3.4.7 Modeler (G)

When running simulations, EnergyPlus uses standard input files, describing the geometry and construction of the building, the heating system and simulation parameters. Based on the information in these files, it computes other quantities for the simulation, such as equivalent U-values of windows, viewing factors of internal surfaces, etc. This processed data is given out as an output of the simulations with EnergyPlus. OpenBuild automatically generates a linear state-space model of the building thermodynamics based on the input data files and the processed data from EnergyPlus. This automatic model generator is the backbone of the OpenBuild toolbox.

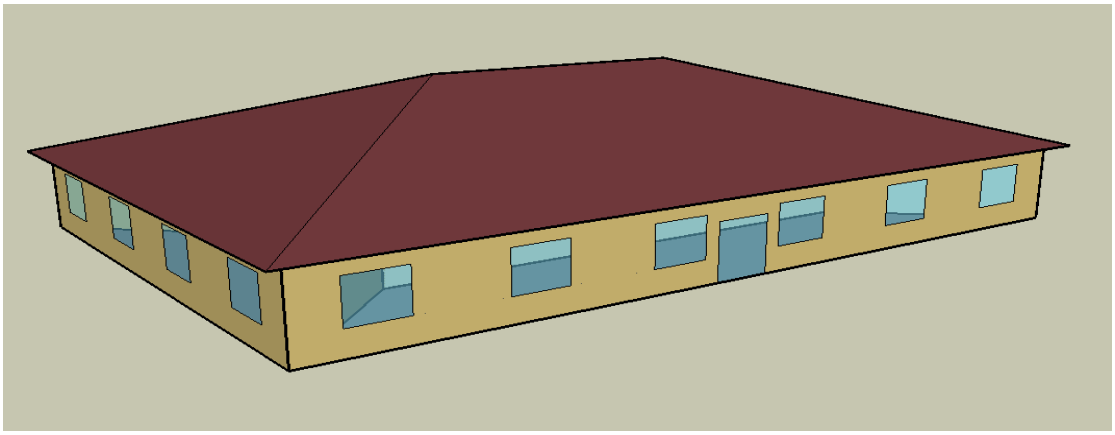

Figure 3.3 – Small Office

Table 3.1 – Characteristics of the Buildings

	Small Office	Warehouse
Floor Area (m^2)	511	4835
No. of floors	1	1
No. of zones	5	3
Window-to-wall ratio	21.2%	0.58%
Peak Occupancy (people/$100m^2$)	5.38	0.1
Exterior walls type	mass	metal
Roof type	attic	metal
Foundation Type	mass floor	mass floor

3.5 Validation of the building models

3.5.1 Data used for validation

One of the advantages of using EnergyPlus as the basis of our thermodynamic model extraction is the availability of a number of typical building models of different types from the Reference Building Database [146] of the U.S. DOE. The building models are in standard EnergyPlus input data format and come with typical schedules for occupancy, and internal gains (lighting, electrical equipment, etc.). The buildings comply with ASHRAE standards for energy efficiency.

We selected two building models - Small Office and Warehouse from this database for validating the quality of the models extracted using OpenBuild. The pictures of the two models are shown in Figure 3.3 and 3.4, and their characteristics are summarized in Table 3.1. These models together with their typical occupancy, internal gain patterns, and typical measurement year (TMY) weather data of Chicago are used for the validation experiments. Chicago has a large variation of temperatures over the year, allowing validating the models in both summer and winter conditions.

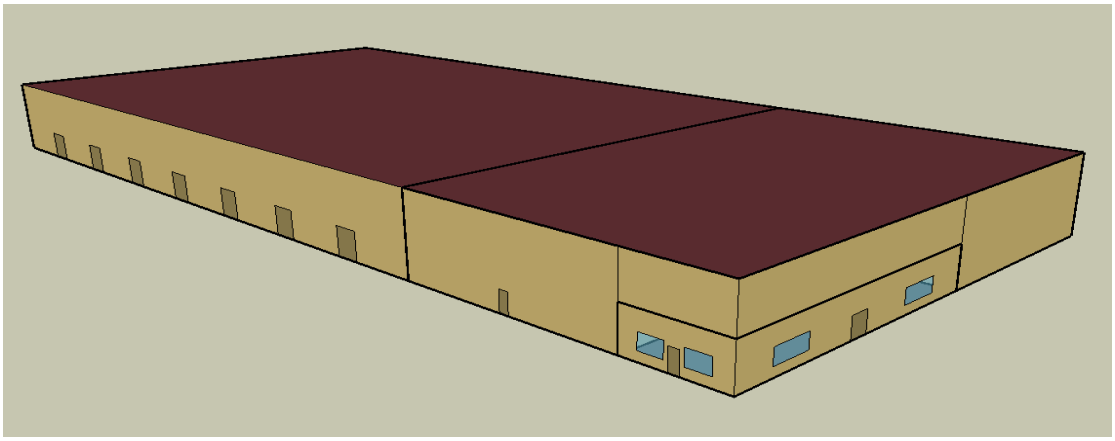

Figure 3.4 – Warehouse

3.5.2 Time-domain comparison

MPC based control schemes rely on the open-loop prediction models to generate the control inputs. We compare the time-domain prediction quality of the linear models with the original EnergyPlus models to evaluate the model quality. Two comparisons (open loop output comparison and and open loop input comparison) are performed.

Open loop Output comparison

The zone temperatures (output) of the two models are compared when excited with the same inputs. The EnergyPlus models are simulated using their default controllers with a sampling time of 15 minutes. The zone temperatures track specified setpoints according to the default schedules of the buildings. The thermal power input applied by the default controller in each zone of the building, and the associated disturbance input (occupancy, weather, etc.) are applied to the corresponding linear model in open loop. The zone temperature trajectories from both simulations are compared. The zone temperatures from the two simulations, for two of the zones of the small office model are shown in Figure 3.5 for a period of one week. The monthly RMSE for each building model is shown in Figure 3.6. The yearly maximum error, mean error, and RMSE for each building are reported in Table 3.2. The results show that the small office and the warehouse have a yearly RMSE of 1^oC, and 0.6^oC, respectively. It can be seen in Figure 3.6 that the RMSE is slightly higher in summer months for the office building due to the increased impact of the solar radiations. This effect is not seen in the warehouse model because it almost does not have windows. We emphasize that in this simulation the output temperature of the EnergyPlus model is the result of closed-loop control: it therefore appears very constant in simulation compared to the output of the linear model which is essentially an open loop profile. This is observed in Figure 3.5.

Open loop Input comparison

In this comparison, we aim to compare the thermal load of the model required to maintain the same output temperature. This more directly measures the predicting ability of the

	Small Office	Warehouse
RMSE (^oC)	1.02	0.638
Max. Error (^oC)	4.75	5.528
Mean Error (^oC)	0.569	-0.132

Table 3.2 – Statistics of the open-loop output (zone temperatures) comparison

	Small Office	Warehouse
RMSE (kW)	1.30	13.93
Normalized RMSE	0.0588	0.0273
Max. Error (kW)	9.04	45.68
Mean Error (kW)	0.675	6.477

Table 3.3 – Statistics of the open-loop input (total thermal power) comparison

model in terms of thermal power consumption. The EnergyPlus model is simulated with its default controller to track a reference temperature of $T_{\text{ref}} = 23^oC$. Next, an open-loop optimization problem is solved for each month with the linear model (3.2) to compute the trajectory of control input to achieve the same T_{ref} as output. The total thermal power input trajectories from the two simulations are compared. The two power trajectories for the small office model are shown in Figure 3.7 for a period of one week. The monthly normalized RMSE for each building model is shown in Figure 3.8. The power requirements of different buildings vary due to the difference in their sizes, therefore the RMSE of each building is normalized with respect to its peak thermal power consumption for comparison. The peak power consumption of the small office and the warehouse is $22kW$ and $510kW$, respectively. The yearly maximum error, mean error, RMSE, and the normalized RMSE for each building is reported in Table 3.3. The results show that the normalized RMSE values for the buildings are small. It can be seen in Figure 3.8 that the normalized RMSE has a similar trend as for the output comparison due to the effect of solar radiations. Overall, the models predict the thermal demand of the zones satisfactorily.

The two comparison results show that although the linear models have small errors compared to the EnergyPlus models, they still capture the thermodynamics of the buildings reasonably well, and are able to predict the thermal power requirements of the buildings in open loop.

3.5.3 MPC versus PID

Our intended use for the models is in optimal control applications. We have seen that the model captures the dynamics of the building quite satisfactorily but errors remain, in particular some steady-state drifts. We perform closed-loop simulations here to show how using the model generated with OpenBuild improves control. On one hand, a PI controller is designed for each zone in each building to provide good tracking performance. On the other hand, MPC controllers are also designed to track a reference temperature of $T_{\text{ref}} = 23^oC$. This second controller does not introduce integral action to compensate

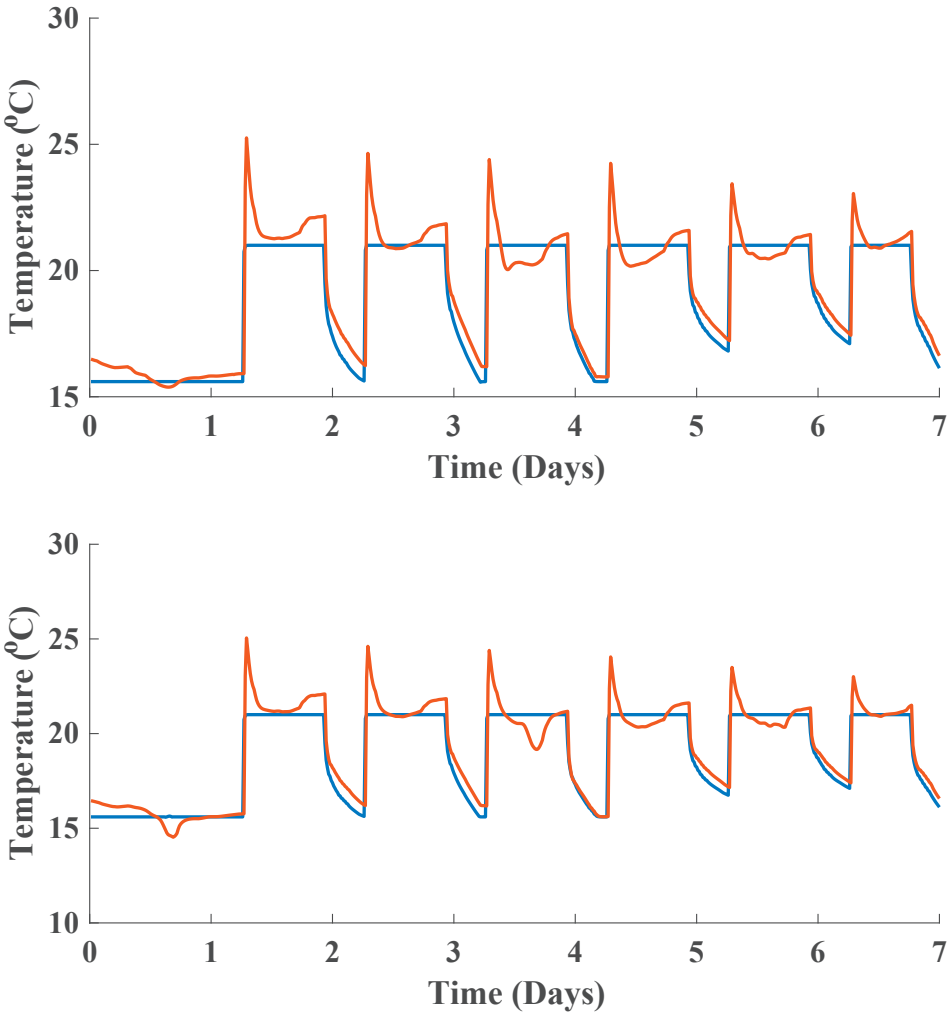

Figure 3.5 – Open loop output comparison: the same input is applied to both models and the output temperature are plotted here - Small Office (zone 1 (top), zone 2 (bottom): EnergyPlus - Blue, OpenBuild model - Red)

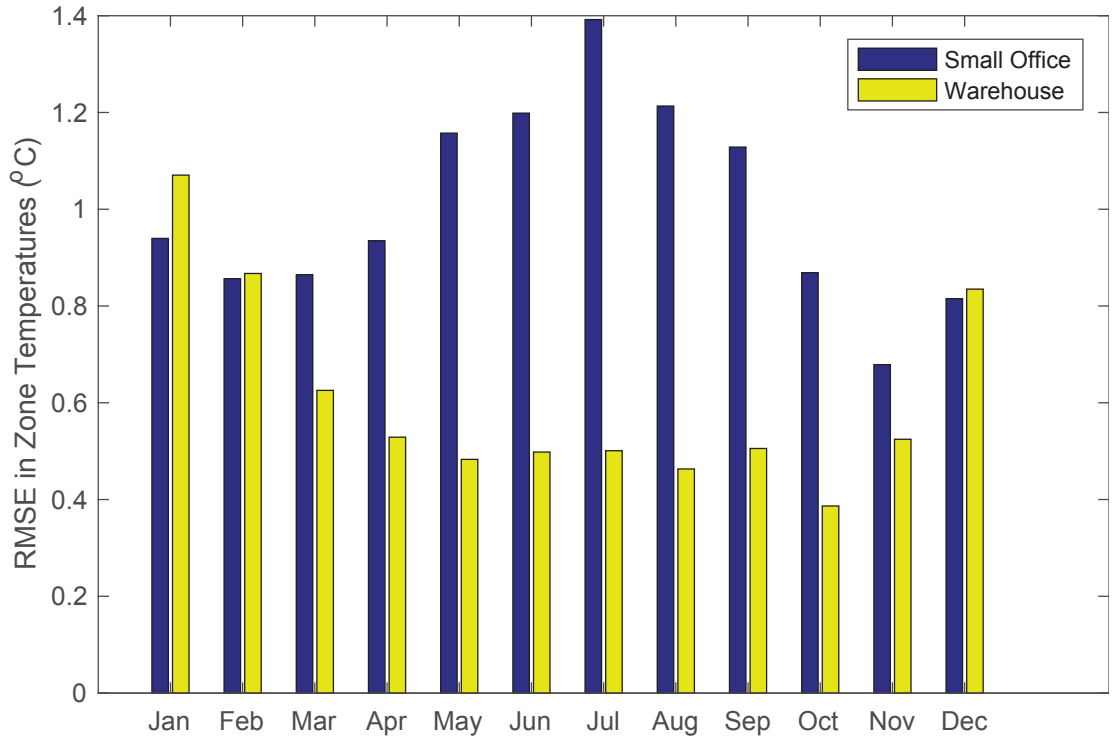

Figure 3.6 – Monthly open-loop zone temperature RMSE

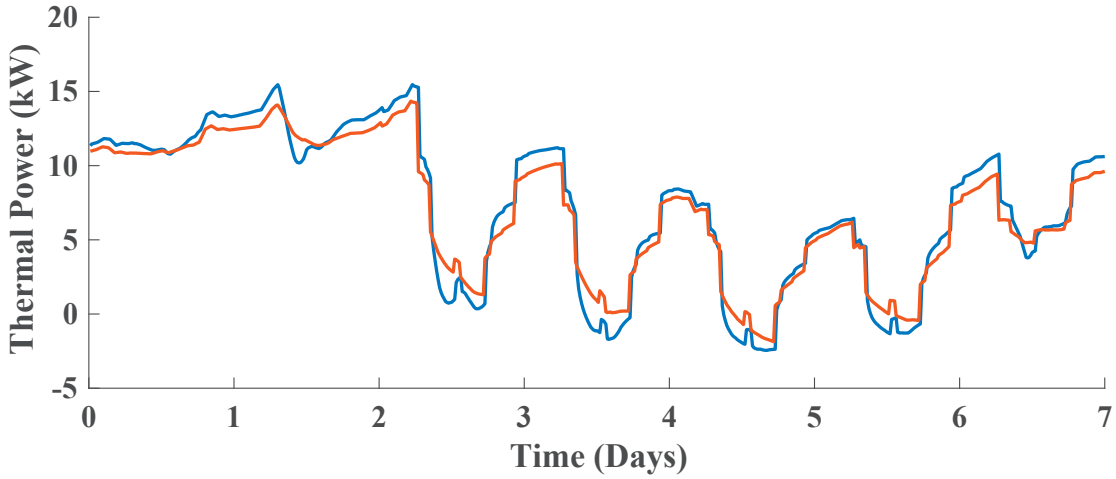

Figure 3.7 – Open loop input comparison - Small Office: EnergyPlus - Blue, OpenBuild model - Red)

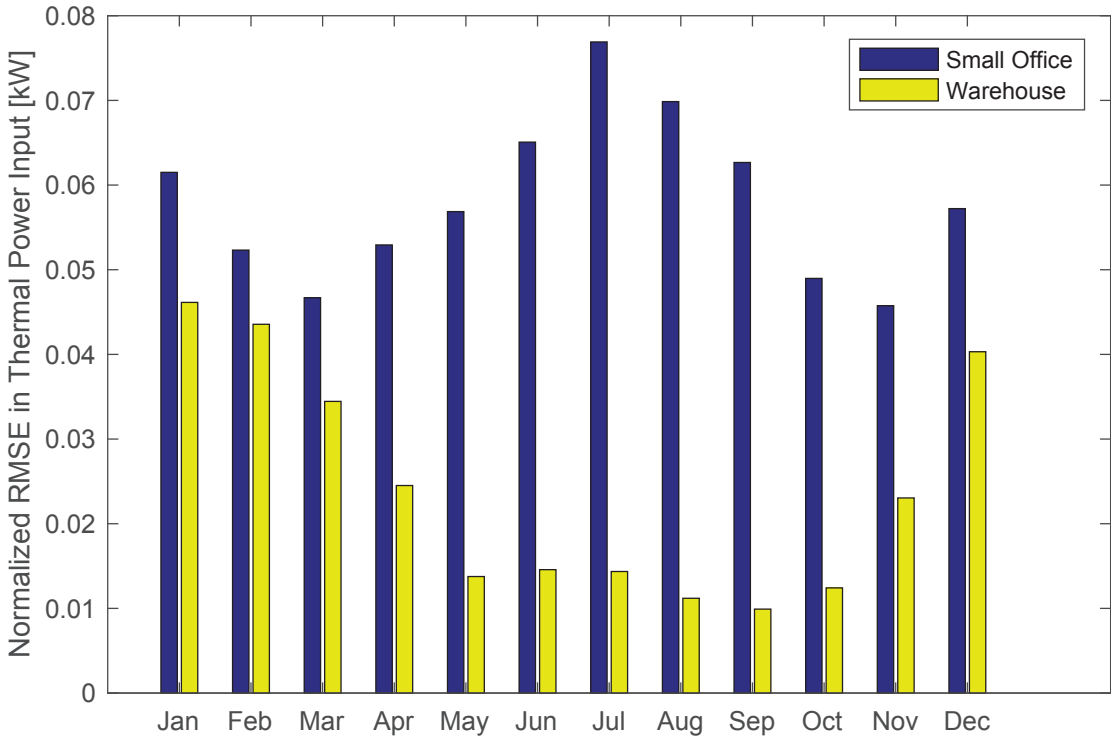

Figure 3.8 – Monthly open-loop total thermal power RMSE

for errors (coming from model mismatch for example). This can be mitigated by using a modified MPC controller where the model is augmented with a disturbance term affecting the system, and where the disturbance is estimated as part of the state estimation step. This third controller is referred to as the offset-free MPC (OFMPC) [91]. The output is augmented with a disturbance term so that $y = Cx + d$ and the disturbance vector d is estimated together with the state x. A Kalman filter is tuned to estimate the state of the system for both MPC controllers. The global tracking quality is measured by means of the yearly root mean square error and maximum tracking error and reported in Table 3.4. We can observe that MPC outperforms a well-tuned PI controller and in particular the offset-free MPC improves the tracking significantly in all cases. We see that a large part of the prediction error of the model can be offset by proper disturbance estimation, which validates our objective to use the model for MPC applications.

To evaluate the impact of the weather on the quality of the model, we also reported monthly RMSE for each building in Figures 3.9 and 3.10. We can observe a seasonal pattern. For the office building, the quality of tracking is slightly worse in summer. This is probably due to the fact that the effect of higher solar irradiance causes larger prediction errors of the models. The warehouse does not have windows so the effect of sun is less crucial. Notice that the OF MPC manages in the case of the warehouse to mitigate the error more consistently all year round, which suggests a more persistent type of disturbance that the estimation counteracts more easily.

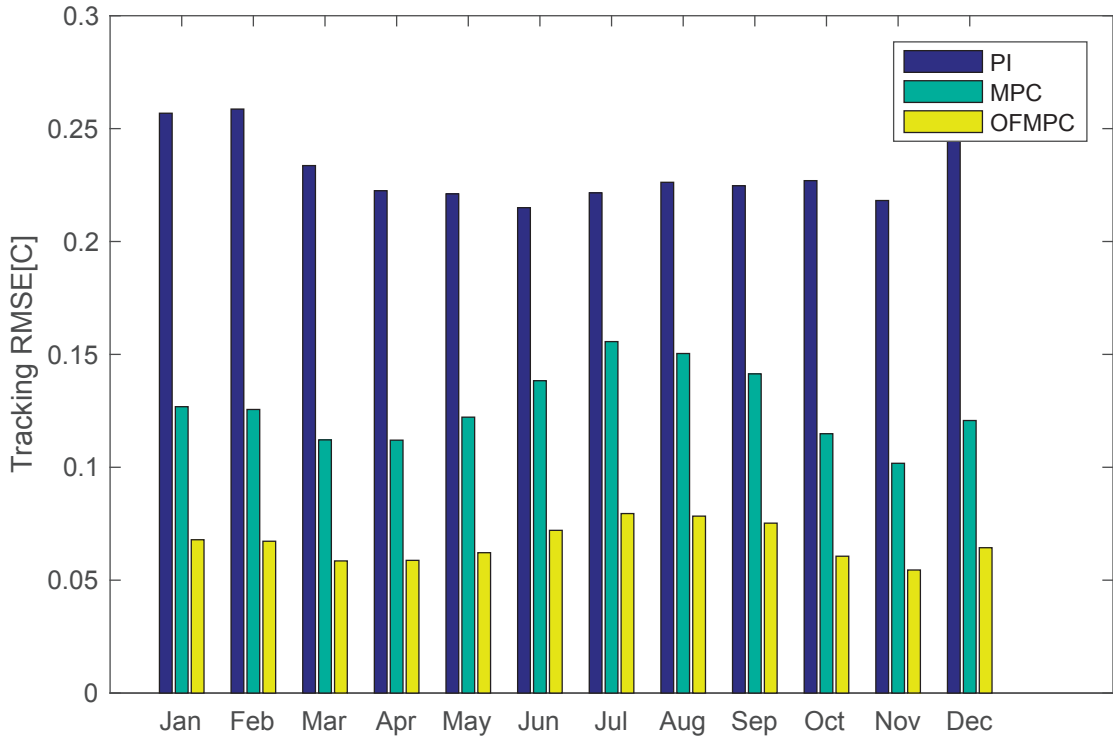

Figure 3.9 – Monthly tracking RMSE for the small Office

It would be possible to adapt the parameters of the model to different periods of the year but this was deemed unnecessary.

Remark 3.3. As OpenBuild relies on a physical modeling approach, the quality of the model obtained is dependent on the particular building considered. EnergyPlus includes a very large quantity of modules that model different aspects of the building. The presence or absence of certain types of object may affect the building model prediction quality as we have observed in our investigations. We have continuously updated the toolbox to be able to generate accurate models for more buildings[1], but this is still an ongoing effort as we have observed that some models may perform significantly worse at times, usually due to some

[1] see http://la.epfl.ch/openBuild for latest release

Table 3.4 – Yearly statistics of the comparison

		RMSE(^oC)	Max Error(^oC)
Small Office	PID	0.231	1.44
	MPC	0.128	1.04
	OFMPC	0.0671	0.55
Warehouse	PID	0.23	1.11
	MPC	0.18	0.67
	OFMPC	0.052	0.34

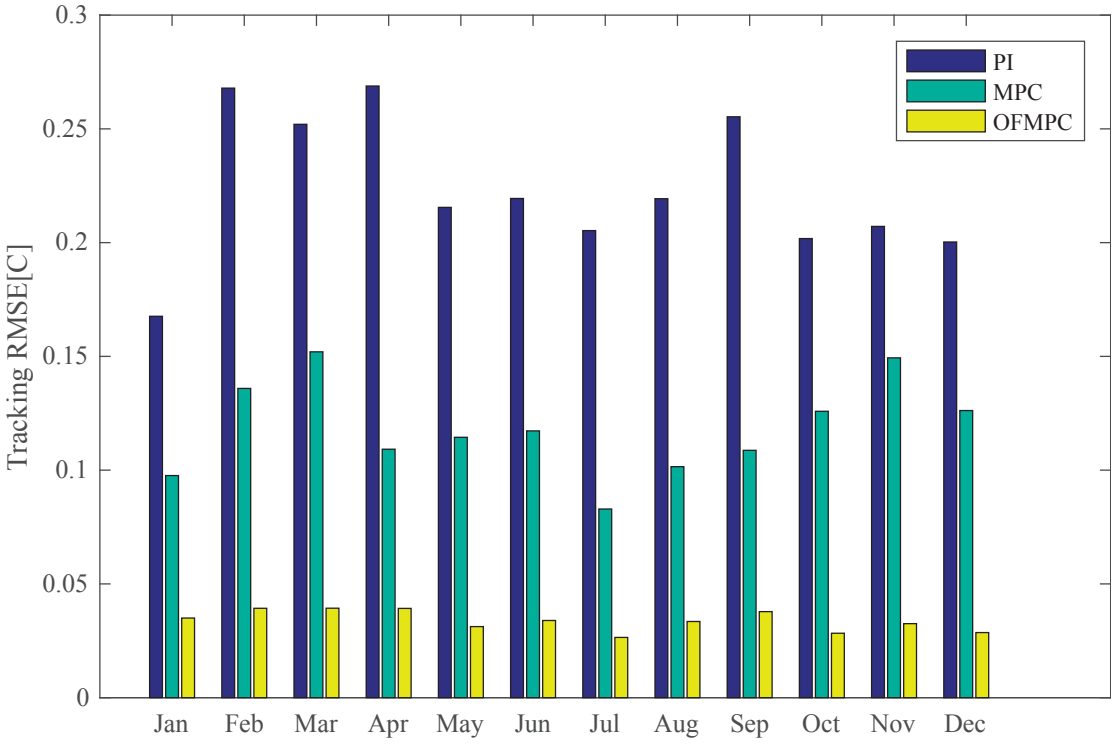

Figure 3.10 – Monthly tracking RMSE for the Warehouse

part of the model not being processed or modeled as intended. An important aspect in this regard in that through the cosimulation interface, it is possible to validate the quality of the model automatically by comparing simulations of the EnergyPlus model and the extracted model, as described earlier in this section. A short discussion about the use of OpenBuild for system identification is provided in the concluding chapter, in section 8.2.1 □

3.6 Example use of the OpenBuild toolbox

This section gives a step-by-step procedure to carry out a simulation study using OpenBuild, outlining how the toolbox helps the user performing the tasks easily. The study is purposefully simple and aims at illustrating how the OpenBuild toolbox can be used.

We consider a large twelve storey office building located in New York taken from the DOE Commercial Building Reference set [146]. The building has 19 zones served by a forced air heating and cooling system. We focus in this example on the use of a thermal storage for load shifting and minimization of the total cost of operation. We assume the building has a cold water tank which is supplied by an electrical heat pump. A step-by-step procedure to carry out this simulation using OpenBuild is given below

Step 1: A building object is initialized using as input the building data file and the weather data file. All required data is imported to MATLAB. During this process, EnergyPlus is first run once through OpenBuild and the processed data from the simulation is collected.

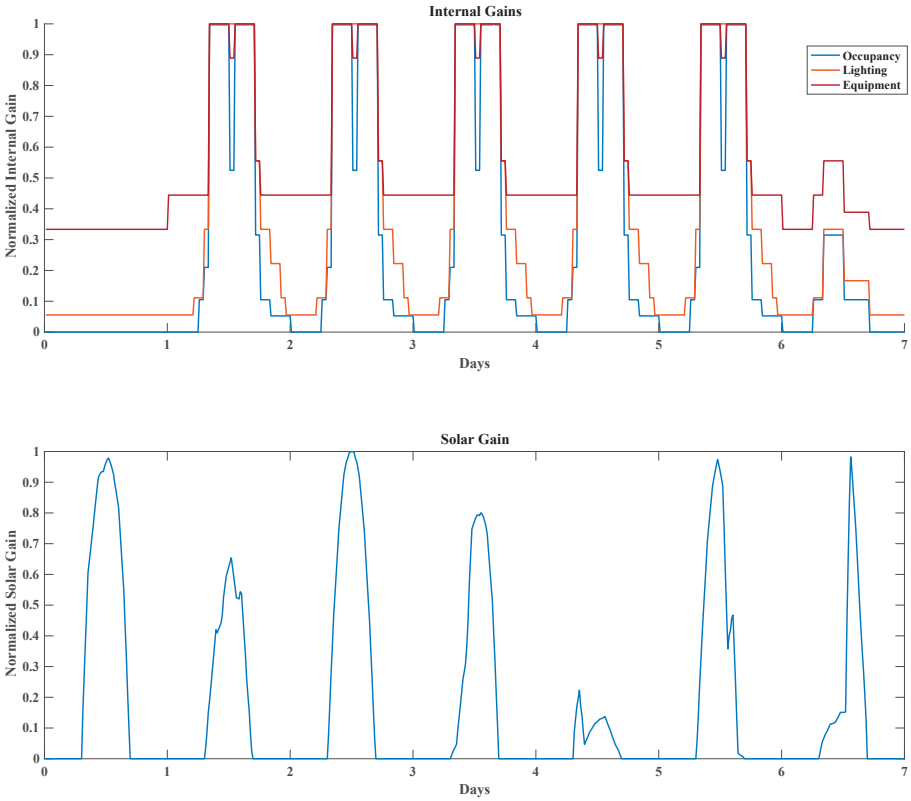

Figure 3.11 – Example of Internal and Solar Gains for an office building.

Step 2: The building data is used to automatically generate a linear state-space model of the form of equation (**??**). At this point the inputs to the model are heat fluxes to each zone. For simplicity, it is considered here that each zone is served by an individual air handling unit which controls the heat flux to the room. The total cooling load of the building is given by $q_{load} = \sum_{k=1}^{n_u} u_k$ where u_k is the heat power input to zone k.
Step 3: A simulation engine object is initialized. This object handles the communication between the different objects simulated, either in MATLAB or in EnergyPlus. EnergyPlus is added as a simulator for the thermodynamics.
Step 4: A cold water tank is modeled in MATLAB and added to the simulation engine object. The tank is assumed to be perfectly stirred and the heat pump has a fixed coefficient of performance. Therefore, the tank dynamics model takes a very simple form:

$$C_p V \dot{T}_{tk} = \alpha(T_r - T_{tk}) - \eta_c P_e + q_{load} \tag{3.3}$$

where T_{tk} is the temperature of the cold water tank which stands in a room with constant temperature T_r. C_p is the heat capacity of water, V is the volume of the tank, and α is a coefficient representing heat leakage out of the tank. η_c is the coefficient of performance of the heat pump (which we assume independent of the outside temperature in this case for simplicity) and P_e is the electrical power consumption of the heat pump. This model is created manually, and it is then added to the simulation engine automatically.
Step 5: This is the main step where user input is normally necessary. The user needs to implement a controller in MATLAB, possibly using the building model constructed by OpenBuild. In our case, the building model is discretized with a time-step of 30 minutes and is reduced using the Hankel-Norm based balanced truncation method. The resulting model is used as the prediction model along with the storage tank model in an MPC controller. The MPC controller is designed to minimize the total cost of operation in the presence of day-night electricity tariffs. An offset-free formulation [90] with soft comfort constraints is implemented. Night and weekend setbacks (time varying constraints) on the zone temperature are used (see Section 2.4). A prediction horizon of one day is considered. The following constraints are applied:

$$0 \leq P_e \leq P_{max} \tag{3.4}$$

$$u_{k,min} \leq u_k \leq u_{k,max} \tag{3.5}$$

$$T_{min} \leq T_{tk} \leq T_{max} \tag{3.6}$$

where P_{max}, $u_{k,min}$and $u_{k,max}$ are the maximum electrical power for the heat pump, and the minimum and maximal inputs, respectively. T_{min} and T_{max} represent minimum and maximal allowed temperatures in the storage tank.
Step 6: The models of the building and the storage are used to design the observer.
Step 7: Finally, the simulation engine runs the closed-loop simulation and the simulation data is saved. The simulation is run for a period of one week during the summer of 2012, using the real weather data of New York.

Figure 3.12 – Percentage decrease in the total cost with varying size of storage

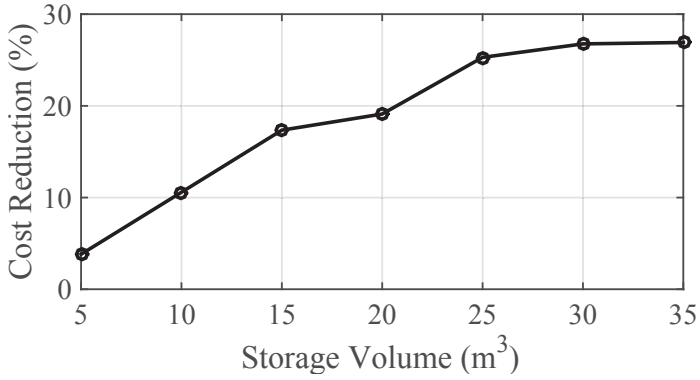

We refer to the OpenBuild manual [49] for a more comprehensive description of the toolbox use.

Remark 3.4. The data for weather, occupancy, and internal gains required to simulate the linear models is also extracted from the EnergyPlus simulation output using OpenBuild. A typical profile of occupancy patterns, solar gain, and internal gains for a period of one week is shown in Figure 3.11. □

Simulations are performed for different sizes of the storage tank and the total electricity consumption of the building over a period of one week is compared. The results are depicted in Figure 3.12. As seen in this figure, the percentage reduction in the total cost of electricity consumption compared to the case with no storage tank, increases with the size of the storage tank. This is due to the capability of the building to shift its electricity consumption to off-peak periods using the storage tank. The cumulative energy consumption over a period of one week for the case with no storage tank and with a $30m^3$ storage tank is shown in Figure 3.13. In this figure, the high tariff price periods have a shaded background. With the storage tank, the cumulative electrical energy consumption during the peak price periods is constant. Without storage the building consumes more electricity during the higher price periods, increasing the total cost of operation. We can see that the use of the storage does not allow to use less energy overall, but allows to shift energy use from periods of high price to periods of low price, hence reducing the total cost of energy.

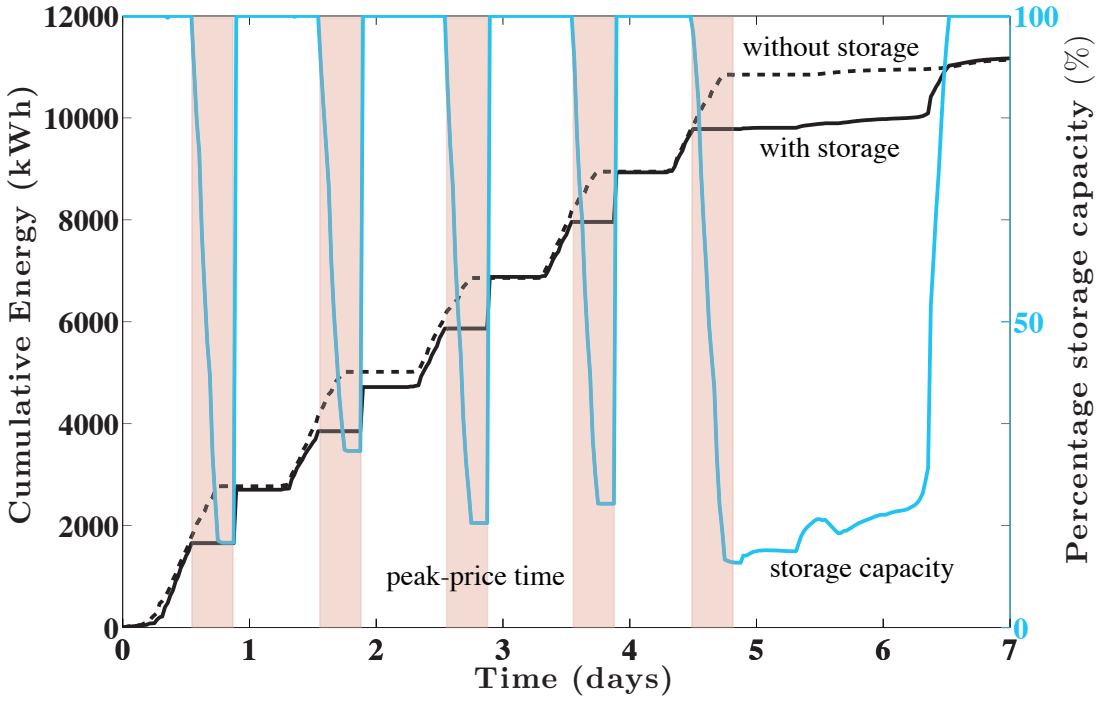

Figure 3.13 – Impact of storage ($30m^3$) on building's cumulative energy use

4 Use of the OpenBuild toolbox

OpenBuild has been developed to support our research and the research of our laboratory (Automatic Control Lab, EPFL) in general. OpenBuild is developed on open-source principles and is freely available for use of other labs and demonstrators, or for any entity or person interested in the operation and optimal control of buildings. OpenBuild has been proven in several contexts, and we present here all the contexts, to our knowledge, that OpenBuild has been utilized.

4.1 Research

OpenBuild research has been repeatedly used for different projects in our group to generate building models. The following papers have made use of data generated using OpenBuild:

- [114]: This paper studies the participation of buildings in the New-York system operator demand response program. Realistic data for an office building located in New York was generated using OpenBuild.
- [81]: An analysis of the participation of loads in the Swiss ancillary services market from the economic point of view.
- [112]: An extensive simulation of frequency regulation participation in Switzerland in the current market conditions.
- Theoretical papers [46], [15], and [134] include examples based on data from OpenBuild.
- OpenBuild has been used in combination with the *OpenBuildNet* software to perform grid scale simulation as reported in [102]

4.2 External Research

OpenBuild has also been used by other research laboratories for generating realistic building models. The following groups / projects have reported using OpenBuild:

- Energy Center, EPFL

- Simulation examples based on the data generated from OpenBuild have been used in the Ph.D. thesis [43].
- The toolbox has been reviewed in [36], [67], and the book [128].
- OpenBuild have also been reported to be used by other research laboratories for master projects, e.g., the Institute for Dynamics System and Control, ETH, Zurich, and by the Ruhr University Bochum.

4.3 Teaching

OpenBuild has been used for a number of teaching projects.

- The Eurotech winter/summer school, 'Energy Systems: From Physics to Systems' is a multidisciplinary two week course for PhD students covering a range of topics related to energy systems, including control. A mini-project on model predictive control for buildings was proposed and conducted by students participating to the school. The building description data was obtained using OpenBuild.
- One of the course projects for the master level class Model Predictive Control features energy-efficient control of buildings. The data for this project was extracted using OpenBuild
- A number of semester and master projects have aimed at extending capabilities of OpenBuild, or have used OpenBuild to generate data:
  - *Demand Response parametric study* by Hervé Tommasi, aimed at generating multiple building model using openbuild in order to study the most important building features that influence its ability to provide demand response to the grid.
  - *Modeling and control of a building with a battery storage system* by Victor Saadé . This project explored the control strategy for the PV + battery system that will be installed in the EPFL solar decathlon building. The thermal model of the building was obtained through OpenBuild using an EnergyPlus description file for the planned building.
  - *Semester project: Parameter Estimation of the thermal model of a building using OpenBuild and EnergyPlus* by Bertrand Buisson. This project was exploring the possibility to perform parameter identification for building modeling compared to standard system identification techniques. The basic idea of the project was to extract input data and a model structure from EnergyPlus through OpenBuild and perform system identification and parameter identification.
  - *Data-based weather prediction models for control* by Marlène Dollfus. This project aimed at mitigating the effect of weather prediction error by using a filtering/prediction strategy for the forecast error for the upcoming time slots

fusing forecast/local measurement and knowledge from past data. The effect of the strategy proposed was evaluated in a building control problem with data generated from OpenBuild.

– *Data-driven optimization for the Energy Bidding problem* by Tiago Morim. This project's goal is to explore different strategies to model the uncertainty in the uncertain energy regulation problem, in order to find the most effective way to use available samples of the uncertainty from historical data. The strategy was tested on an energy regulation problem for a building modeled through OpenBuild.

4.4 Other

The toolbox is available publicly online[1]. To date, it has been dowloaded more than 200 times.

[1] https://sourceforge.net/projects/openbuild/

Appendix

A Detailed modeling

In this section, a fully detailed description of the modeling procedure is given. The modeling procedure was largely inspired by the EnergyPlus modeling framework, but significant differences are detailed when necessary. The RC modeling framework is employed. The RC modeling framework simplifies the partial differential equations describing heat transfer using a lumped parameter equivalent circuit. A number of thermal nodes are placed and an equivalent thermal capacitance C_i is associated to each node. The thermal capacitance represents the thernal mass present at that node and depends on the mass and material describing that node. Nodes in the network are connected with thermal resistors that have an equivalent thermal resistance R_{ij}. This resistance models the potential for heat transfer between this nodes. Finally, a forcing term Q_i at each node represents extra contribution of heat transfer at that node and includes heat transfer through internal gains, from solar radiation, from the heating system, etc. For each node a differential equation describes the heat transfer and takes the from

$$C_i \dot{T}_i = \sum_{j \in \mathcal{N}_i} \frac{1}{R_{ij}} (T_j - T_i) + Q_i \tag{A.1}$$

where T_i is the temperature at node i in degree Celsius, C_i the thermal capacitance of node i in $J/^oC$, R_{ij} the thermal resistance between node i and j in $^oC/W$, $\mathcal{N}_i$ the set of nodes neighbouring i and Q_i the thermal forcing term in W. Note that despite being primarily designed to represent thermal conduction, thermal resistances simply induce a linear differential equation structure and can therefore be used to model any exchange phenomena that has a linear dependance on temperature difference, (that might be the case after linearization). We used thermal equivalent resistances to model thermal conduction, convection and longwave radiations, as detailed in the subsequent subsections.

A.1 Thermal node placement

Following recommendations and assumptions of EnergyPlus, one core assumption is that the building is divided in thermal zones. A thermal zone usually designates a part of the building served by a single terminal HVAC unit. The basic assumption concerning thermal zones is that the temperature is uniform in that zone (in other words the air in that zone

is "well-stirred"). Each thermal zone can therefore be represented by a single node on the thermal graph. The capacitance associated to that zone directly corresponds to the thermal capacitance of the air in the zone. Following [29], pp.7, the expression of the thermal capacitance is:

$$C = C_p \rho_{air} V * c_z \tag{A.2}$$

with V the volume of air in the zone and C_p the zone air specific heat. The density of air is taken as in standard conditions with $\rho_{air} = 1.204 kg/m^3$. At typical value of humidity ratio of 50% and temperature of 25^oC, an average value of the air specific heat of $1.02 kJ/kg^oC$ is taken. The computation of the volume is performed by EnergyPlus and collected from output data files. Finally, c_z is a zone multiplier and may be added in EnergyPlus for technical reason.

Next, nodes are placed in surfaces. To evaluate heat conduction inside surfaces, a state-space model approach is also used in EnergyPlus. As detailed in [29], pp.37, a number of nodes are placed across the surface, and conduction is modeled using lumped parameter values. Although the precision of the method grows with the number of nodes a good compromise was found positioning nodes at each interface between two materials inside the surface.

Each layer of the surface has a total thermal capacitance which is computed as $C = \rho C_p l A$ with A the surface in m^2, C_p the specific heat capacity of the material in J/kg^oC, l the width of the layer in m, and ρ the density of the material in kg/m^3. The conductive resistance between adjacent nodes is computed as $R = \frac{l}{kA}$ with k the thermal conductivity of the material in $W/^oCm$. By assumption the thermal capacitance of a node at the interface of layers i and j takes half of the total capacitance of layers i and j, so that $C = \frac{C_i + C_j}{2}$.

A.1.1 Special case of no mass materials

In EnergyPlus, some materials are specified as having no mass. They are treated slightly differently as per [29], pp.40-41. Two cases may occur:

- If the no-mass layer is stuck between two "massive" layers, then the previously proposed approach still works: the interface nodes will simply receive a zero mass contribution from both. If several no-mass layers are together, they are transformed into one equivalent no-mass layer first
- If the surface starts or ends with a no-mass layer, then the no-mass layer will be given the same properties as air.

A.1.2 Remarks on EnergyPlus conduction modeling

Two notable differences can be noted between our approach and EnergyPlus. The first is that EnergyPlus establishes a state-space model first with a number of nodes varying

between 6 and 18 per layer of material, which is much larger than in our cases. Using a large number of nodes is also possible in our case but would inflate the state-space size drastically, which was not deemed necessary considering the small benefit in terms of prediction quality. Secondly, EnergyPlus transforms the state-space model into a model that does not make explicit use of internal nodes temperatures. It is converted instead into a model that takes as inputs previously observed temperatures at the surfaces on the outside and inside faces of the surfaces. While this has the advantage of eliminating the need for an observer later on, the procedure to produce the CTF coefficient is reported to become unstable when the time step shrinks too much (see discussion in [29], pp.38). On the other hand, using state-space models is standard in control and well understood, which led us to keep that representation.

A.1.3 Particular cases of surfaces: adiabatic surfaces

Some surfaces are modeled using the adiabatic boundary condition. As detailed in [29], pp.93, Adiabatic boundary conditions are applied to two surface types in EnergyPlus: 1) Surfaces with adiabatic outside boundary conditions 2) Internal Mass objects. For both surface types, EnergyPlus will apply the same boundary conditions to each side of the construction so that there is no temperature difference across the surface. In this case, all heat transfer into the surface is a result of the dynamic response of the construction to varying inside boundary conditions. The surface will store and release heat only at the inside face of the surface (it is assumed that the outside face is not within the zone). Adiabatic boundary conditions are dealt with by short circuiting the inside face and outside face node of the surface considered. The heat balance at each point should not be applied directly. It should appear from the point of view of the outside face that energy comes from the inside face, but not the other way around.

A.1.4 Particular cases of surfaces: Ground connection

Some surfaces have a ground boundary condition. This appears in simulations where heat exchange with the ground can be quite significant especially for single story buildings. A temperature for the ground is computed as detailed in [28] on pp. 81. To achieve that, the outside face temperature node is forced to the ground temperature which becomes a new input to the building. Usually the ground temperature is quite consistent across the year but it can be recovered from the EnergyPlus run. Forcing the node to the ground temperature is like having a voltage source in the equivalent RC electrical network.

A.2 Convection

EnergyPlus proposes a number of models to take into account thermal convection from the surfaces to the air, one of which can be explicitly specified in the input file. Convection

takes a form similar to conduction.

$$Q_{conv} = h_c(T_a - T_s) \tag{A.3}$$

where T_a is the temperature of the air, T_s the temperature of the surface, and h_c a time-varying convection coefficient which is computed based on various factors (temperature in the room, humidity, etc), depending on the calculation method selected. Note that methods to compute inside and outside convection are different. See [29], pp.76-92 to learn more on the convection coefficient computation for inside convection and [29], pp.62-72 for outside surface convection. In our case, a time invariant average of the convection coefficient is extracted from simulation. Note that convection coefficients display typically a periodic pattern so different models could be learnt for daytime and nighttime for example, but a time invariant model was deemed more convenient and sufficiently accurate.

A.3 Internal longwave radiation

Internal longwave radiation describes the internal thermal exchange fluxes in the building between internal surfaces. It has been observed that this represents a significant part of the heat exchange in EnergyPlus and has therefore been modeled separately. As per [29], pp.74-75, the thermal longwave radiation exchange is governed by equation:

$$q_{i,j} = A_i F_{i,j}(T_i^4 - T_j^4) \tag{A.4}$$

with A_i the area of surface i, T temperatures in K and $F_{i,j}$ the 'scriptF' factor from surface i to j. ScriptF factors are exchange coefficient between pairs of surfaces and take into account all possible paths between these surfaces. For implementation in the model a linearization is taken around typical conditions.

A.4 External longwave radiation

The outside surface of the building also exchanges thermal radiation with the surrounding environment, namely the air, the sky and the ground. The total long wave radiation exchange hence takes the form, per [29], pp.57-59:

$$Q_{LWR} = \epsilon\sigma F_{gnd}(T_{gnd}^4 - T_s^4) + \epsilon\sigma F_{sky}(T_{sky}^4 - T_s^4) + \epsilon\sigma F_{air}(T_{air}^4 - T_s^4) \tag{A.5}$$

where ϵ is the long-wave emittance of the surface and is collected from input data, σ is the Stefan-Boltzmann constant and the F's are the view factor to air temperature, sky temperature and ground surface temperature respectively. As in EnergyPlus, air and ground surface temperature are taken to be the same. The expressions of the view factor are taken

to be:

$$
\begin{aligned}
F_{gnd} &= 0.5(1 - cos\phi) \\
F_{air} &= 0.5(1 - \beta)(1 + cos\phi) \\
F_{sky} &= 0.5\beta(1 + cos\phi) \\
\beta &= \sqrt{0.5(1 + cos\phi)}
\end{aligned}
$$

where ϕ is the tilt angle of the surface.

A similar linearization procedure is taken around average temperatures, as for internal convection. Note that the sky temperature then becomes an input to the model whereas it is not something directly measurable. EnergyPlus computes what the sky temperature is as a function of outdoor temperature, cloud coverage and humidity ratio. Value for the sky temperature is usually close but lower than outdoor temperature, especially in clear sky conditions. Note that some cooling systems exploit the fact that sky temperature is low by using a roof pool to cool down the water at night.

A.5 Solar heat gain rate

A large part of the gains affecting the system come from the sun. Detailed geometric computations are performed in EnergyPlus to compute the global horizontal and normal irradiance (GHI and NHI), as well as the resulting irradiance on each surface, outside and inside the building. Total solar radiation heat gain rate are available for every surface in the building and are collected and used as inputs to the model. While this has the benefit of leveraging the whole computational power of EnergyPlus, it adds a new input for every surface exposed to the sun in the building. Several improvements or alternatives could be brought to the model. The difficulty of modeling solar radiation is that their effect is time-varying (actually periodic with a period of one day and slow drift over the year), but linear if the input is taken as the normal horizontal irradiance. It has been observed that clustering all solar inputs in one yields a model which is too rough. The question is then if linear time-invariant model with a large number of inputs is more convenient than a linear time-varying model with a single input. A reasonable compromise can be to reduce the number of inputs to a few significant ones (mostly depending on the main directions of incidence. This would cause some inaccuracies, especially for indoor surfaces but would probably yield a good approximating model. A data driven approach was adopted to cluster disturbances that are very similar.

A.6 Internal gains

Different types of objects in EnergyPlus input files allow one to describe different types of internal gains in the rooms, including gains from electric equipment, lights, and people. Each piece of equipment produces a heat flux affecting the building, with a convective part (which directly affects the room air), a latent part (through evaporation, this part is

un-modeled in our building) and a radiative part. This split is described in the EnergyPlus object, and a schedule describes the total heating rate for that object. This processed data is used as inputs to our models. As described in [29], pp.1020, radiative gains are distributed on surfaces in proportion to the value of their surface absorbtance.

Remark A.1. Gains from people are specific in the sense that they depend on indoor conditions. It is a reasonable assumption that they are constant provided the zones are air conditioned. In addition, internal gains from people usually represent a relatively small share of internal gains. See [29], pp.1016-1020 for more details on internal gains computations. □

A.7 Windows

Windows are modeled in great detail in EnergyPlus as explained in [29], pp.217-233. Two modeling methods are employed. The first one models windows layer by layer, and is the one implemented in EnergyPlus. The second, simpler, reuses the layer-by-layer approach but converts first an arbitrary window performance into an equivalent single layer. OpenBuild uses the second method for its computation. the first step is to recover the equivalent U-value for that window. Following [29], pp.221-226, we have

$$\frac{1}{U} = R_{i,w} + R_{l,w} + R_{o,w}$$

where $R_{i,w}$ is the inner film resistance, $R_{o,w}$ the outer film resistance and $R_{l,w}$ the layer resistance, all in m^2K/W. From U all values can be computed using equations:

$$R_{i,w} = \begin{cases} \frac{1}{0.395073\ln(U)+6.949915} & \text{for } U < 5.85 \\ \frac{1}{1.788041U-2.886625} & \text{for } U \geq 5.85 \end{cases}$$

$$R_{o,w} = \frac{1}{0.025342U - 29.163853}$$

A two layer model of the window is used, in the same fashion as other surfaces. The layer resistance is used to specify the conduction between the two layers. Inside and outside convection coefficients are recovered from the EnergyPlus run average value. A different type of solar heat gain is affecting the window. It is computed in EnergyPlus under the name 'Surface Window Total Glazing Layers Absorbed Solar Radiation Rate' which is assumed to be spread between the two layers equally. The window layers obey the same type of differential equation that describe their temperature evolution, but the main difference with other walls is that they are assumed to have no thermal inertia. This transforms equation (A.1) in an algebraic equation by setting the left hand side part to zero. This algebraic equation allows to express the temperature of the window layers as a function of the temperature at the other nodes and the disturbance and substitute in the rest of the

differential equations.

$$C_{wall}\dot{T}_{wall} = A_{11}T_{wall} + A_{12}T_{windows} + B_1 u$$
$$0 = A_{21}T_{wall} + A_{22}T_{windows} + B_2 u$$

which gives $T_{windows} = -A_{22}^{-1}A_{21}T_{wall} - A_{22}^{-1}B_2 u$ and after substitution:

$$C_{wall}\dot{T}_{wall} = (A_{11} - A_{12}A_{22}^{-1}A_{21})T_{wall} + (B_1 - A_{12}A_{22}^{-1}B_2)u$$

A.8 Infiltration

Infiltration is described by some specific objects in the EnergyPlus input files. As detailed in [29], pp.360-361, infiltration describes any outdoor air that unintentionally enters the zones by way of infiltration (that is, not through mechanical ventilation). It is assumed to be instantaneously mixed with the zone air. The amount of energy that is exchanged between the zone and the outside air is described by the equation

$$Q_{\text{inf}} = \dot{m}C_{air}\rho_{air}(T_o - T_z) \tag{A.6}$$

where $\dot{m}$ is the mass flow rate exchange in m^3/s, C_{air} the thermal capacitance of air in $J/K/kg$, ρ_{air} the density of air in kg/m^3, T_o the outside temperature and T_z the zone temperature. According to the documentation, the mass flow rate is computed as

$$\dot{m} = I_{inf}F_{sch}(A + B|T_o - T_z| + Cv + Dv^2) \tag{A.7}$$

where I_{inf} is the design maximum flow rate, F_{sch} a scheduled value that controls the flow rate as a function of time, v the wind speed and A, B, $C$and D user-chosen coefficients. Default value in EnergyPlus is (1,0,0,0) so that the mass flow rate does not depend on outside conditions. Even in that case, the flow rate is usually time-varying. For convenience, we chose not to use a time-varying infiltration. Two options are available. The first introduces a new input to the model which is the energy exchange through infiltration. Values from the simulation can be used and should be relatively consistent if the indoor temperature is not too far from the simulation temperature. It also allows to cascade the system with a more detailed model for infiltration if desired. Otherwise, a constant mass flow rate needs to be fixed: the average flow rate in simulation can be used.

B Comfort Modeling

One of the most important objectives of building control is to maintain or improve occupants' comfort. Comfort is a human's perception of his environment, and therefore is difficult to measure. This perception of comfort is different for different people and might also vary for the same person at different times. Various measures of comfort have been reported in the literature, e.g., the Predicted Mean Vote (PMV), the Predicted Percentage of Dissatisfied (PPD), etc. PMV is based on the model developed by Fanger [35] and is the predicted mean point rated by a large group of people. It is based on heat balance equations and empirical data that rates how a person would feel about a thermal condition. PPD is a function of PMV and analytical equations have been developed for this relationship [22]. The analytical equations defining PMV and PPD are complicated and are a function of many parameters, e.g., operative temperature, relative humidity, air velocity, metabolic activity, and clothing resistance, etc. Therefore, it makes them difficult to use for control design.

Another similar, but slightly simpler measure developed by ASHRAE via a logistic regression analysis performed on the data collected in the ASHRAE RP-884 database is called ASHRAE Likelihood of Dissatisfied (ALD) [22] and is defined in literature as

$$ALD(T) = \frac{e^{0.008T^2+0.406T-3.050}}{1+e^{0.008T^2+0.406T-3.050}} \in [0.05, 1.00) \tag{B.1}$$

where $T = |T_{zone} - T_{comfort}|$, T_{zone} is the zone temperature, and $T_{comfort}$ is the optimal comfort temperature. Unlike, PMV and PPD, ALD is only a function of the absolute difference between the zone temperature and the optimal comfort temperature.

All these measures are for a specific building zone and for a specific point in time. A measure called Long-term Percentage of Dissatisfied (LPD) has been proposed for an average value of comfort throughout the building [22]. It accounts for the hourly-predicted ALD calculated for each zone and is weighted by the number of people inside the zone, and over time and is given as

$$LPD(ALD) = \frac{\sum_{t=1}^{T}\sum_{z=1}^{Z}(p_{t,z}ALD_{t,z})}{\sum_{t=1}^{T}\sum_{z=1}^{Z}(p_{t,z})} \tag{B.2}$$

where $ALD_{t,z}$ and $p_{t,z}$ are the ALD and normalized occupancy of the zone z at time t.

Although ALD is only a function of zone temperatures and is simpler than PMV and PPD, it is still difficult to use for control design because it is non-linear. In most of the MPC based control design found in the literature, the comfort is usually defined by a bound of temperatures around the optimal comfort temperature resulting in convex constraints for the MPC optimization problem. However, ALD together with LPD can easily be used in the post-processing to evaluate the occupants' comfort.

Part II Robust tracking commitment

5 Robust tracking commitment

We introduce in this chapter the robust tracking commitment problem. After stating a formal description of the problem, we briefly relate it to the main application that motivated its formulation, the reserve provision problem. In Section 5.2, we review some relevant literature before exposing the main results in Section 5.3. We present situations where the robust tracking commitment problem can be solved tractably for large problem instances in Section 5.4. We introduce a few extensions to the main problem formulation in Section 5.5. Next an example of reserve provision by a building illustrates the applicability of the approach in Section 5.7.1 while Section 5.7.2 develops the concept of virtual battery. Finally, Section 5.8 develops ideas to extend the finite horizon guarantees obtained earlier to the infinite horizon case.

The key ideas of this chapter were first published in [46] whose content was refined and extended to write the manuscript [15] in collaboration with Altuğ Bitlislioğlu to form the content of Sections 5.3, 5.4, 5.5 and 5.7.1. Section 5.8.2 is mostly extracted from [46], while Sections 5.7.2 and 5.8 are original in this thesis. Part of the content of [15] on a possible distributed implementation of the robust commitment problem is left out of the thesis since it is due to my colleague Altuğ Bitlislioğlu.

Notation

We introduce the mathematical notation employed in the rest of the chapter. $\mathbb{R}^n$ denotes the Euclidean space of dimension n, $\mathbb{Z}$ denotes the set of integers, and $\mathbb{N}$ denotes the set of nonnegative integers. For two integers $i \in \mathbb{Z}$ and $j \in \mathbb{Z}$ such that $i < j$, let $\mathbb{Z}_{[i,j]} := \{i, i+1, \dots, j\}$. I_n denotes the identity matrix of dimension n, T_n the lower unit triangular matrix and $\otimes$ denotes the Kronecker product. The notation $\prod$ is used to described the cartesian product of multiple sets. For a matrix $\mathbf{M} \in \mathbb{R}^{n \times m}$, an integer $i \in \mathbb{Z}_{[1,n]}$ and a set $\mathcal{J} \subseteq \mathbb{Z}_{[1,m]}$, $\mathbf{M}(i, \mathcal{J})$ indicates the set of components that belong to the ith row and to columns whose indices belong to $\mathcal{J}$. For a set $\mathcal{Q} \subseteq \mathbb{R}^n \times \mathbb{R}^m$, the orthogonal projection operator is defined as $\mathrm{Proj}_x(\mathcal{Q}) := \{x \in \mathbb{R}^n | \ \exists y \in \mathbb{R}^m, (x, y) \in \mathcal{Q}\}$. Given two functions $f : \mathbb{R}^n \to \mathbb{R}^l$ and $g : \mathbb{R}^m \to \mathbb{R}^n$, $f \circ g : \mathbb{R}^m \to \mathbb{R}^l$ denotes the composition of f and g , such that $f \circ g(x) = f(g(x))$. We use a bold font to denote sequences over time: for example $\boldsymbol{u} = (u_0, \dots, u_{N-1})$. The horizon is omitted when it follows from the context.

5.1 Motivation and Formalization

Consider a system described by the state-space difference equation:

$$\begin{aligned} x^+ &= f(x, u, \xi) \\ y &= g(x, u, \xi) \end{aligned} \tag{5.1}$$

where $x \in \mathbb{R}^{n_x}$ denotes the state of the system, $u \in \mathbb{R}^{n_u}$ the controlled input to the system and $\xi \in \mathbb{R}^{n_\xi}$ a disturbance affecting the system. We call ξ the disturbance, but let us keep in mind that it is a placeholder for any uncontrolled signal such as dynamic perturbation to the system or external request signals. $y \in \mathbb{R}^{n_y}$ represents some output of interest for the system. In addition, the system is subject to constraints:

$$x_t \in X_t, \quad u_t \in U_t, \quad y_t \in Y_t \tag{5.2}$$

Remark 5.1. We will usually use $y_t \in Y_t$ to specify tracking constraints. We will therefore sometimes refer to these constraints as the tracking constraints, in opposition to the 'regular' state constraints $x_t \in X_t$. □

When the system is in state x_0 at time 0, the input sequence $\boldsymbol{u} = (u_0, \dots, u_{N-1})$ is applied, and the disturbance sequence $\boldsymbol{\xi} = (\xi_0, \dots, \xi_{N-1})$ is observed, the state at time i is denoted by $\phi_i(x_0, \boldsymbol{u}, \boldsymbol{\xi})$, and the resulting sequence of states $(\phi_1(x_0, \boldsymbol{u}, \boldsymbol{\xi}), \dots, \phi_N(x_0, \boldsymbol{u}, \boldsymbol{\xi}))$ by $\boldsymbol{\phi}(x_0, \boldsymbol{u}, \boldsymbol{\xi})$.

We state the *robust tracking commitment problem* next:

Problem 5.2 (Robust Tracking Commitment)**.** Let N be a fixed horizon. Given an initial condition x_0, find a set $\Xi \subset \mathbb{R}^{Nn_\xi}$ and a control policy $\boldsymbol{\pi}$ with $\pi_i : \Xi \to \mathbb{R}^{n_u}$ for $i \in \mathbb{Z}_{[0,N-1]}$ such that:

$$\forall \boldsymbol{\xi} \in \Xi,\ \boldsymbol{\phi}(x_0, \boldsymbol{\pi}(\boldsymbol{\xi}), \boldsymbol{\xi}) \in \mathcal{X},\ \boldsymbol{\pi}(\boldsymbol{\xi}) \in \mathcal{U},\ \mathbf{y} \in \mathcal{Y} \tag{5.3}$$

and

$$\boldsymbol{\pi} \in \mathcal{F} \tag{5.4}$$

where $\mathcal{U} = \prod_{t=0}^{N-1} U_t$, $\mathcal{X} = \prod_{t=1}^{N} X_t$, $\mathcal{Y} = \prod_{t=0}^{N-1} Y_t$ and $\mathcal{F}$ a set of functions ■

$\mathcal{F}$ can be used to enforce structural constraints on the control policy such as causality. If such a Ξ and $\boldsymbol{\pi}$ can be found, then we say that Ξ is (N-step) admissible for system (5.1) with respect to the requirements $\mathcal{F}$.

We can assume without restriction that the policy $\boldsymbol{\pi}$ depends on $\boldsymbol{\xi}$ only rather than $\boldsymbol{\xi}$ and the state x. Indeed, the state at time t can be inferred from the sequence of disturbance ξ affecting the system and control inputs applied up to time $t-1$. See for example [52] for a discussion on the equivalence of state sequence policies and disturbance sequence policies under appropriate assumption. Finally, note that we are looking for a set Ξ in $\mathbb{R}^{Nn_\xi}$ which implicitly mean that ξ can be time-dependent and time-correlated.

This problem formulation is general, but in order to make the discussion more concrete, we present next the *reserve provision problem* in order to show why we are interested in this problem.

Example 5.3 (Reserve provision Problem). Suppose we have an energy system connected to the power grid with a model of the form (5.1), where x describes the states of the system (for example the temperatures in a building), u the control input to the system (for example the setpoints of the heating system). We are interested in the power consumption of the system over the next day, starting from the current initial condition x_0. Assume that the power grid operator sends a power consumption request ξ at a pre-determined frequency that the system should follow. We can define y as the tracking error which can take the form $y = g(x, u) - \xi$ where $g(x, u)$ is a model of the power consumption as a function of the state and input to the system. We want to satisfy operating constraints captured by X_t and U_t while maintaining a small power consumption tracking error (for example $\|y\| \leq e_{\max}$).

We want to solve problem 5.2, where Ξ captures the set of power consumption trajectories that can be tracked by the system, Depending if the power consumption request is communicated in advance or on the fly, the control policy $\boldsymbol{\pi}$ needs to satisfy different constraints captured by $\mathcal{F}$.

A practical instance of this problem is the so-called frequency regulation problem, which is described in greater detail in Part III. □

Our goal is to explore the space of admissible sets Ξ and find a good candidate that satisfies desired properties. Possible desired properties include:

Volume In the case of the reserve provision problem, the system operator may offer a payment for the flexibility the system can offer. A large set Ξ is naturally more valuable than a small one, hence is rewarded with a higher payment.

Simplicity In the case of the reserve provision problem, the system operator or an aggregator may collect admissible power consumption trajectory sets from a large number of loads and generators, which it will use to determine an optimal reserve dispatch by solving another large scale optimization problem involving the set representations. In this case, a simple description of the sets is preferable. It may also be beneficial to be able to interpret easily the characteristics of Ξ. An attractive idea is for example to characterize an energy system as an equivalent 'virtual battery', meaning that it can store and release energy in the same way as a lossless battery would. From the point of view of power consumption, that allows describing the system using two intuitive parameters: a power rating and a storage limit, and hence conceal the complexity of the system. We will revisit the concept of virtual battery in subsection 5.7.2.

Structure Similarly, structural properties such as convexity may be required in order to use Ξ in another layer of optimization.

The particularity of our approach that distinguishes it from more standard robust reachability analysis is that we are not interested in certifying a particular disturbance set

Ξ, but we want in some sense to optimize over candidate sets. That requires specific instruments that will be presented in the next sections.

Example 5.4. Consider a linear system:

$$x^+ = Ax + B(u + \xi)$$

subject to additive input disturbance and subject to constraints $x \in X$. Solving Problem 5.2 certifies that the system is robust to input disturbances in Ξ over a N step horizon. From this, we can see that Problem 5.2 can serve as an analysis tool to look at the robustness of systems. □

5.1.1 Special cases of Problem (5.2)

This problem formulation is general and covers some classical control problems. By exploring here the connection of problem (5.2) to classical problems, we can get inspiration on how to solve it.

If Ξ is fixed and $\boldsymbol{\pi}$ is restricted to not depend on $\boldsymbol{\xi}$, then problem 5.2 becomes a N-step robust reachability question and is equivalent to showing that:

$$\exists \mathbf{u} \in \mathcal{U} : \forall \boldsymbol{\xi} \in \Xi,\ \boldsymbol{\phi}(x_0, \mathbf{u}, \boldsymbol{\xi}) \in \mathcal{X},\ \mathbf{y} \in \mathcal{Y} \tag{5.5}$$

We define now the set of input and disturbance that satisfies all constraints over an $N-$step horizon:

$$\mathcal{Q}(x_0) := \{(\boldsymbol{u}, \boldsymbol{\xi}) \mid \boldsymbol{\phi}(x_0, \boldsymbol{u}, \boldsymbol{\xi}) \in \mathcal{X},\ \boldsymbol{u} \in \mathcal{U},\ \boldsymbol{y} \in \mathcal{Y}\} \tag{5.6}$$

In (5.5), the input sequence $\boldsymbol{u}$ is the same for every sequence $\boldsymbol{\xi}$. On the other extreme, if a different control trajectory $\mathbf{u}$ can be chosen for each trajectory $\boldsymbol{\xi}$ in Ξ, then the question is whether:

$$\forall \boldsymbol{\xi} \in \Xi,\ \exists \mathbf{u} \in \mathcal{U} : \boldsymbol{\phi}(x_0, \boldsymbol{u}, \boldsymbol{\xi}) \in \mathcal{X},\ \mathbf{y} \in \mathcal{Y} \tag{5.7}$$

This case can be interpreted geometrically as explained in the following lemma:

Lemma 5.5. *Equation* (5.7) *is equivalent to*

$$\Xi \subseteq Proj_{\boldsymbol{\xi}}(\mathcal{Q}(x_0)) \tag{5.8}$$

where $Proj_{\boldsymbol{\xi}}(\mathcal{Q}(x_0))$ *denotes the projection of the set* $\mathcal{Q}(x_0)$ *onto the* $\boldsymbol{\xi}$*-subspace.*

Proof. : The proof directly follows from the definition of the projection operator and of $\mathcal{Q}(x_0)$. $\Xi \subseteq \text{Proj}_{\boldsymbol{\xi}}(\mathcal{Q})$ means that $\forall \boldsymbol{\xi} \in \Xi,\ \exists \boldsymbol{u} : (\boldsymbol{u}, \boldsymbol{\xi}) \in \mathcal{Q}(x_0)$, *i.e.* $\forall \boldsymbol{\xi} \in \Xi,\ \exists \boldsymbol{u} : \boldsymbol{u} \in \mathcal{U},\ \boldsymbol{\phi}(x_0, \boldsymbol{u}, \boldsymbol{\xi}) \in \mathcal{X},\ \boldsymbol{y} \in \mathcal{Y}$, that is Equation (5.7) holds. □

5.1.2 On the notion of maximum size uncertainty sets

A natural question is whether there exists a maximal size uncertainty set $\Xi_{\max}$ that contains all possible admissible uncertainty sets. In other words, the question is if two sets Ξ_1 and Ξ_2 are admissible, then is $\Xi_1 \cup \Xi_2$ also admissible?

It turns out that it depends on $\mathcal{F}$. In the case that $\mathcal{F}$ is $\mathbb{R}^{Nn_\xi} \to \mathbb{R}^{Nn_u}$, that is there are no restriction on the policy, referring back to Lemma 5.5, we saw that admissibility in this case is equivalent to the set inclusions $\Xi_1, \Xi_2 \subseteq \text{Proj}_{\boldsymbol{\xi}}(\mathcal{Q}(x_0))$, which directly leads to $\Xi_1 \cup \Xi_2 \subseteq \text{Proj}_{\boldsymbol{\xi}}(\mathcal{Q}(x_0))$, that is $\Xi_1 \cup \Xi_2$ is admissible. In this case, the maximum admissible is exactly $\text{Proj}_{\boldsymbol{\xi}}(\mathcal{Q}(x_0))$. Even if that case, it can be beneficial to look for a 'lightweight' approximation since the projection may be very complex to compute: even in the case where $\mathcal{Q}(x_0)$ is a polyhedron, computing its projection can have very high complexity if the dimension of the space is large [66].

In the case of the open-loop robust reachability case (Equation (5.5)), the union of admissible sets is not necessarily admissible. For example, it may be the case that Ξ_1 is admissible with a control input $\boldsymbol{u}_1$ and Ξ_2 with $\boldsymbol{u}_2$, but in general $\mathbf{u}_1 \neq \mathbf{u}_2$ and there exists no single input for which $\Xi_1 \cup \Xi_2$ is admissible. In general, there is no maximum size uncertainty set.

5.2 Relation to existing literature

The idea of looking into the modulation of uncertainty sets and representing complex feasibility sets with simpler sets sits at the crossroads of output tracking, invariance, reachability analysis, multi-stage programming, (semi-infinite) optimization, and model reduction. It therefore connects to a large body of literature. This section aims at highlighting the connections of that idea with other topics, and present the most relevant literature therein.

5.2.1 Model predictive control

Finite horizon robust control for linear systems is well established in the model predictive control (MPC) literature [95, 118]. The robust and stochastic MPC literature often considers systems subject to additive disturbance and linear dynamics, for example:

$$x^+ = Ax + Bu + w \tag{5.9}$$

and subject to polytopic constraints on state and inputs, $x \in X$, $u \in U$. A time-invariant disturbance is usually considered so that $\forall t \geq 0, w_t \in W$ and one looks for a feasible policy to maintain the system within the constraints at all time.

Problem 5.6. Find a state-feedback policy π such that, given $x_0 \in X$:

$$\forall w_t \in W,\ x_t \in X, u_t = \pi(x_t) \in U, \text{ with } x_{t+1} = Ax_t + Bu_t + w_t,\ \forall t \geq 0 \tag{5.10}$$

■

It has been proven that using a policy π in the disturbance sequence is equivalent to using a policy in the state [52]. Similarities between this problem and Problem 5.2 where w plays the role of ξ are apparent. A number of solutions have been proposed [96, 117, 120, 52]. They rely on the usual characteristics of MPC to solve the problem:

- Approximate the infinite horizon with a finite horizon problem and repeat the procedure in a receding horizon fashion
- Drive the state to a terminal state appropriately chosen to ensure recursive feasibility
- Parametrize the control policy to make sure the problem is computationally tractable

In particular, the so-called affine disturbance feedback MPC [52] is instrumental in the results we will develop, we therefore give a brief summary of its results here. It proposes to use an affine policy in the uncertainty, so that $u_t = \sum_{i<t} M_{t,i} w_i + d_t$, or in stacked notation:

$$\boldsymbol{u} = \boldsymbol{M}\boldsymbol{w} + \boldsymbol{d} \tag{5.11}$$

where $\boldsymbol{M}$ is chosen strictly lower block-triangular as a result of causality requirements. In addition, the state at the end of the horizon is restricted to lie in a terminal set $\mathbb{X}_f$.

The following optimization problem is solved at each iteration:

$$\begin{aligned} \text{minimize} \quad & V_N(\mathbf{M}, \mathbf{d}) \\ \text{subject to} \quad & \forall i \in \mathbb{Z}_{[0,N-1]} \\ & \forall \boldsymbol{w} \in W^N \\ & \phi_i(x, \boldsymbol{u}, \boldsymbol{w}) \in X \\ & \phi_N(x, \boldsymbol{u}, \boldsymbol{w}) \in \mathbb{X}_f \\ & u_i \in U \\ & \boldsymbol{u} = \boldsymbol{M}\boldsymbol{w} + \boldsymbol{d} \end{aligned} \tag{5.12}$$

Through an appropriate choice of V_N and $\mathbb{X}_f$, it is shown that Problem (5.12) is recursively feasible and this controller is input to state stable. If X, U, $\mathbb{X}_f$ are all described as polyhedra in inequality form, the solution to (5.12) implies solving a quadratic program subject to robust linear constraints, which under some assumptions on the set W can be transformed into a convex program which allows solving it efficiently even in large dimensions.

5.2.2 Invariance

One ingredient of MPC is the use of invariant or robust invariant sets. Background information is provided in Section C.1, we review it here in connection with Problem 5.2.

A set $\mathbb{X}_f$ is robust controlled invariant for system $x^+ = f(x, u, w)$ with constraints $x \in X$ and $u \in U$ and subject to disturbance $w \in W$ if (see Definition C.3):

$$\mathbb{X}_f \subseteq X \text{ and } \forall x \in \mathbb{X}_f, \exists u \in U : \forall w \in W,\ f(x, u, w) \in \mathbb{X}_f$$

If $\mathbb{X}_f$ in problem (5.12) is chosen as a robust controlled invariant set, then solving this problem in closed loop results in an infinite horizon robustly feasible system, which solves (5.10). The feasible region of the problem actually is a robust invariant set. Therefore, robust MPC can be seen as the way to substitute intractable offline computation with repeated tractable online computations.

Note that knowing a robust invariant set $\mathbb{X}_f$ already solves Problem (5.10). Indeed, from any point in $\mathbb{X}_f$, it is then enough to find a control action $u \in U$ that keeps the system inside $\mathbb{X}_f$ for any value of $\xi \in \Xi$. We know that such a control action exists by definition of a robust controlled invariant set. Using robust MPC allows extending the robust feasible region with respect to $\mathbb{X}_f$.

It is customary to look either for large invariant sets or 'maximal' invariant sets, or small invariant set, depending on the context. Methods have been proposed to compute maximal invariant sets, starting from [42] for autonomous systems, but are usually only applicable in small dimensions. An interesting contribution is [116], where robust invariant sets are computed based on an affine disturbance feedback policy. It displays similarities with our approach in the sense that it optimizes over sets through transformations and Minkowski sums. Considering a disturbance set Ξ, the key idea is that if a sequence of control policies can be found that will shrink the disturbance set after k steps, a robust control invariant set can be inferred. Some heuristics are also provided to maximize or minimize the size of the robust controlled invariant set. The advantage is that the resulting algorithm solves a convex program which scales nicely with the size of the system. The drawback is that it is relatively tricky to optimize the robust invariant set since it is only indirectly related to the control policy. Despite considering a fixed uncertainty set, this contribution showcases affine disturbance feedback for invariance computation together.

5.2.3 Infinite, semi-infinite and robust programming

Notice that Problem (5.12) includes an infinite number of constraints, indexed by $\boldsymbol{w}$. Such a problem is referred to in the literature as a semi-infinite problem [135]. The most general form of that type of problem is:

$$\begin{aligned} \text{minimize} \quad & f(x) \\ \text{subject to} \quad & x \in M \end{aligned} \tag{5.13}$$

with:

$$M := \{x | g(x, \xi) \leq 0 \, \forall \xi \in \Xi(x)\}$$

The problem is called generalized semi-infinite program when the the set Ξ depends on the decision variable x (rigorously speaking, $\Xi : \mathbb{R}^n \rightrightarrows \mathbb{R}^m$ is then a set-valued mapping). It is a standard semi-infinite program if Ξ does not depend on x. An infinite program is a program where the decision space is infinite dimensional, for example if we optimize over control policies. This type of problem has been extensively studied in the literature. See [135] for a recent literature review on the topic.

Semi-infinite programs are very general and perhaps the bridging gap between all the topics introduced so far. Indeed it is easy to see that most problems presented so far can be cast as semi-infinite programs.

Problem (5.13) can be rewritten:

$$\begin{aligned} \text{minimize} \quad & f(x) \\ \text{subject to} \quad & \max_{\xi \in \Xi(x)} g(x, \xi) \leq 0 \end{aligned} \tag{5.14}$$

where the maximization over ξ is called the inner or lower problem. Semi-infinite programs are in general difficult to solve. Citing [135]:

> The main computational problem in semi-infinite optimization is that the lower level problem has to be solved to global optimality, even if only a stationary point of the upper level problem is sought.

In other words, there is no way to go around global optimization for the lower level problem, which limits drastically the size of problem that can be solved.

Robust programming is closely related to semi-infinite programming and is the discipline that studies optimization problem with some of the parameters being not exactly known, but for which a set containing this uncertain parameter is available. It gives rise to inequalities of the form:

$$h(x, \xi) \leq 0 \ \forall \xi \in \Xi$$

The robust programming literature has mostly focused on computational complexity, mostly by identifying instances of the problem that can be converted to convex finite dimensional programs and therefore are tractable in medium to large dimensions [8, 9]. These are of particular interest for us since multi-stage problems tend to be plagued by large dimensions very quickly. A description of the main results of interest is provided in Appendix C.3 and will be referred to in the following developments, when they have been used in this work.

5.2.4 Tracking

Another related problem is the one of *output regulation*, which deals with the capability of a system to track a reference trajectory that is generated by an external dynamical system [37]. In the finite horizon framework, the external system serves as a generator for

the reference trajectory set. Most of the work in output regulation deals with asymptotic tracking guarantees [37], [91]. Similarly, for systems subject to additive disturbances, the authors of [76] show robust convergence to a neighborhood of a fixed reference that is allowed to change occasionally. Our aim differs in that we want to guarantee tracking at all times over a fixed horizon. Therefore, similar to [34], we are not looking for asymptotic guarantees. In this direction, the authors of [26] utilize robust invariant sets to guarantee tracking with specified error bounds during and after the finite prediction horizon. The guarantees are sought for a given reference generator under the assumption that there exists a feasible solution to the problem. However, none of the aforementioned works consider the problem of modulating the uncertainty set while solving the control problem.

5.2.5 Recent developments in system flexibility modeling in the literature

The recent surge of interest in Demand Response and advanced interaction between loads and the power grid have triggered numerous contributions in the domain of the modeling of system flexibility, some of which have independently developed ideas that are close to the ones developed in this chapter. We give a detailed description of the works that have come to our attention in that domain and underline the main differences and similarities that these works have with our own.

Using robust MPC is an established idea, including in the context of power grids, such as in the recent work [153], where the authors allocate reserves while considering temporal correlation of the demand-generation forecast and assuming the forecast error to belong to a polytopic set defined over a finite prediction horizon. Considering temporal correlation for uncertainty modeling is also found out to be beneficial in the context of the multistage economic dispatch problem [80]. In both those works the uncertainty set is however fixed a priori.

To the best of our knowledge, the first article that attempted to describe the flexibility of a system in a synthetic way is [87]. In this work, upward and downward flexibility as well as nominal consumption are simultaneously computed in a min-max robust MPC formulation. The method however considers a single actuator and the solution is not robust to any possible value of the tracking request in the same sense than in our work.

[152] and [5] consider aggregation of several subsystems to track a reference signal and optimize maximum up-down limits on the reference, however the robust formulation is again limited either to single dedicated actuators or predetermined schemes that distribute the required change in the total power consumption among actuators. [158] considers disturbance sets that are norm balls and optimizes over linear mappings to modify the disturbance set utilizing dual norm formulations. This work was derived independently from ours and also features the key idea of reformulating the commitment problem as a standard robust optimization problem, also introduced in our work [46]. It was extended in [159], which reframes the problem in a more general context by introducing the idea of robust optimization problem with 'adjustable' uncertainty sets. It does not include the extensive discussion on time correlation and information structure, but includes interesting

developments on cases where the uncertainty sets are chosen as mapped from a space of larger dimension, a case which is not explicitly covered in the manuscript [15]. Another similar work is [149], where the authors propose optimizing over a linear map to be applied to a polytopic reference set that represents energy constraints in frequency regulation signals.

Other works have tackled similar problems in more specific contexts. [57] and [162] propose aggregation methods for characterizing the power consumption flexibility of a collection of thermostatically controlled loads (TCLs). This can be considered as a particular case of the commitment problem and can be addressed with the methodology proposed in this chapter. Another related work is [100] where the problem of serving a set of time constrained load requests (such as electric vehicle charging) is tackled. Sufficient conditions are given for a supply profile to be able to serve the loads and a dispatch strategy is proposed. This work differs from ours by considering a continuous time formulation and exploiting the specific structure of the problem to derive a solution.

A number of recent contributions are also closely related to the ones already mentioned and prove that the idea of flexibility modeling is gaining momentum [7, 161, 89].

5.3 Main results

This section presents the main results developed to solve Problem 5.2. The core idea is to recast this problem into another similar problem where the uncertainty set is fixed. We also examine in detail how to ensure causality.

5.3.1 Information structure of control policies

Causality is an important characteristics of multi-stage programs and should be considered with care, especially considering that the system in our case might be subject to heterogeneous sources of uncertainty which are observed at different times. We formalize here the requirements on the control policy. We have to account for the fact that the uncertain exogenous signals are revealed partially to the controller as time progresses. Generally speaking, any decision variable u_k might depend on a subset of the uncertainty vector $\boldsymbol{\xi}$ and only on this subset. To make this claim more precise, the concept of the information structure of a function f is introduced. The presentation follows concepts from Section 14.2 of [8] but adopts a different formulation.

Definition 5.7. Let $\mathcal{I}$ be a subset of $\mathbb{Z}_{[1,n]}$, and

$$\mathcal{F}(\mathcal{I}) = \{f : \mathbb{R}^n \to \mathbb{R} \mid \forall x, \hat{x} \in \mathbb{R}^n,\ x_{\mathcal{I}} = \hat{x}_{\mathcal{I}} \Rightarrow f(x) = f(\hat{x})\} \tag{5.15}$$

where $x_{\mathcal{I}}$ denotes the entries of x defined by the indices of $\mathcal{I}$.
Let $\mathcal{I} = (\mathcal{I}_k)_{k \in \mathbb{Z}_{[1,m]}}$ be a collection of index subsets and

$$\mathcal{F}(\mathcal{I}) = \{f : \mathbb{R}^n \to \mathbb{R}^m,\ f_k \in \mathcal{F}(\mathcal{I}_k)\ \forall k \in \mathbb{Z}_{[1,m]}\} \tag{5.16}$$

If $f \in \mathcal{F}(\mathcal{I})$, then we refer to $\mathcal{I}$ as the information structure of f. ■

Loosely speaking, $\mathcal{F}(\mathcal{I})$ denotes the set of real-valued functions that depend only on the input indexed in $\mathcal{I}$. For functions with multiple outputs, the information structure is defined output-wise. $\mathcal{I}$ summarizes the information structure of the function f: the k^{th} component of f depends only on inputs indexed in $\mathcal{I}_k$. For example, in the robust multi-stage control setting considered here, a typical requirement of the control policy will be non-anticipativity which states that the current control action can depend on observations made in the past; in our notation, this fact translates to: for each stage, every control action can depend on past measurements, so that $\pi_k \in \mathcal{F}(\mathcal{I}_k)$ with $\mathcal{I}_k \in \mathbb{Z}_{[1,k-1]}$. Notice here a small abuse of notation in the sense that π_k is a function with values in $\mathbb{R}^{n_u}$, and by $\pi_k \in \mathcal{F}(\mathcal{I}_k)$ we mean that every component of π_k is in $\mathcal{F}(\mathcal{I}_k)$.

Example 5.8. An open-loop policy does not depend on the realization of the uncertainty, so that it has information structure $\mathcal{I}_k = \emptyset$ for all k. Conversely, if control action can be adjusted assuming full knowledge of $\boldsymbol{\xi}$, then the information structure is $\mathcal{I}_k = \mathbb{Z}_{[1,N]}$ for all k. □

In the following, we sometimes depict information structures using a matrix notation where the k^{th} row of the matrix represents the indicator vector of $\mathcal{I}_k$ (1 if the element belongs to $\mathcal{I}_k$, 0 otherwise).

5.3.2 Set admissibility

Following the ideas introduced in Section 5.1, we introduce the following definitions:

Given a set Ξ, we define the set of all admissible control policies mapping from disturbance sequences to input sequences:

$$\Delta(\Xi) := \left\{ \boldsymbol{\pi} : \Xi \to \mathbb{R}^{Nn_u} \mid \forall \boldsymbol{\xi} \in \Xi,\ (\boldsymbol{\pi}(\boldsymbol{\xi}), \boldsymbol{\xi}) \in \mathcal{Q}(x_0) \right\} \tag{5.17}$$

where we recall that $\mathcal{Q}$ is defined as:

$$\mathcal{Q}(x_0) := \{(\boldsymbol{u}, \boldsymbol{\xi}) \mid \boldsymbol{\phi}(x_0, \boldsymbol{u}, \boldsymbol{\xi}) \in \mathcal{X},\ \boldsymbol{u} \in \mathcal{U},\ \boldsymbol{y} \in \mathcal{Y}\} \tag{5.18}$$

The argument x_0 was dropped in the definition of Δ for notational simplicity. We are now ready to introduce the main concept.

Definition 5.9. The set $\Xi \subset \mathbb{R}^{Nn_\xi}$ is *admissible* for system (5.1) in state x_0 with respect to the information structure $\mathcal{I}$ if

$$\mathcal{F}(\mathcal{I}) \cap \Delta(\Xi) \neq \emptyset\,. \tag{5.19}$$

■

Based on Definition 5.9, we can write the family of admissible uncertainty sets for

tracking with respect to a given information structure

$$\Omega = \left\{ \Xi \subset \mathbb{R}^{Nn_\xi} \mid \exists \boldsymbol{\pi} \in \mathcal{F}(\mathcal{I}) \cap \Delta(\Xi) \right\} \tag{5.20}$$

Remark 5.10. We consider here a finite horizon N, but let us note that these definitions conceptually extend to the infinite horizon case. □

First we tackle the problem of simply finding a N-step admissible reference set, without attaching any cost function to the problem. The robust tracking commitment problem 5.2 can be written as:

$$\text{find } \Xi : \Xi \in \Omega \tag{5.21}$$

For a fixed uncertainty set, admissibility can be verified by searching over control policies. However it is not obvious how to search over possible admissible sets and corresponding control policies simultaneously. In order to treat the problem with a unified methodology, we will characterize admissible sets mappings of an initial uncertainty set $\hat{\Xi}$ by a modifier function. The advantage of this approach will be evident in the following section 5.4, when we formulate computationally tractable methods for evaluating the admissibility of uncertainty sets for tracking, utilizing parameterized function based techniques available in the robust optimization literature.

5.3.3 Implicit modulation of uncertainty sets

Let us formalize the modulation of uncertainty sets by modifier functions. We first define the *uncertainty modifier* function $\boldsymbol{\nu} : \mathbb{R}^{Nn_\xi} \to \mathbb{R}^{Nn_\xi}$, which is assumed to be bijective and used for reshaping a given uncertainty set.

$$\boldsymbol{\nu}(\hat{\Xi}) = \{\boldsymbol{\nu}(\boldsymbol{\xi}) : \boldsymbol{\xi} \in \hat{\Xi}\} \tag{5.22}$$

In the following, we will show that we can evaluate the admissibility of the set $\Xi = \boldsymbol{\nu}(\hat{\Xi})$ via conditions on the composite function $\hat{\boldsymbol{\pi}} = \boldsymbol{\pi} \circ \boldsymbol{\nu}$ that is applied to the initial set $\hat{\Xi}$, as depicted in Figure 5.1. This allows us to fix an initial uncertainty set $\hat{\Xi}$, embed the modifier function into the control policy and implicitly modulate uncertainty sets and control policies simultaneously. To this end we introduce the following lemma:

Lemma 5.11. *Let $\boldsymbol{\nu} : \mathbb{R}^{Nn_\xi} \to \mathbb{R}^{Nn_\xi}$, be a bijection and $\hat{\Xi}$ be a compact set with non-empty interior . The set $\Xi := \boldsymbol{\nu}(\hat{\Xi})$ is N-step admissible for tracking by system* (5.1) *in state x_0 with respect to the information structure $\mathcal{I}$ if and only if*

$$\exists \hat{\boldsymbol{\pi}} \in \Delta_{\boldsymbol{\nu}}(\hat{\Xi}) : \hat{\boldsymbol{\pi}} \circ \boldsymbol{\nu}^{-1} \in \mathcal{F}(\mathcal{I}) \tag{5.23}$$

where $\Delta_{\boldsymbol{\nu}}$ is defined as

$$\Delta_{\boldsymbol{\nu}}(\hat{\Xi}) := \{\boldsymbol{\pi} : \forall \boldsymbol{\xi} \in \hat{\Xi},\ (\boldsymbol{\pi}(\boldsymbol{\xi}), \boldsymbol{\nu}(\boldsymbol{\xi})) \in \mathcal{Q}\} \tag{5.24}$$

Proof. : Suppose $\hat{\boldsymbol{\pi}} \in \Delta_{\boldsymbol{\nu}}(\hat{\Xi})$ and $\hat{\boldsymbol{\pi}} \circ \boldsymbol{\nu}^{-1} \in \mathcal{F}(\mathcal{I})$. Then we have

$$\forall \hat{\boldsymbol{\xi}} \in \hat{\Xi},\ (\hat{\boldsymbol{\pi}}(\hat{\boldsymbol{\xi}}), \boldsymbol{\nu}(\hat{\boldsymbol{\xi}})) \in \mathcal{Q} \tag{5.25}$$

Let $\boldsymbol{\xi} := \boldsymbol{\nu}(\hat{\boldsymbol{\xi}})$. Since $\boldsymbol{\nu}$ is bijective, we have $\hat{\boldsymbol{\xi}} = \boldsymbol{\nu}^{-1}(\boldsymbol{\xi})$. Therefore (5.25) is equivalent to

$$\begin{aligned} &\forall \boldsymbol{\nu}^{-1}(\boldsymbol{\xi}) \in \hat{\Xi},\ (\hat{\boldsymbol{\pi}} \circ \boldsymbol{\nu}^{-1}(\boldsymbol{\xi}), \boldsymbol{\nu} \circ \boldsymbol{\nu}^{-1}(\boldsymbol{\xi})) \in \mathcal{Q} \\ \Leftrightarrow &\forall \boldsymbol{\xi} \in \boldsymbol{\nu}(\hat{\Xi}),\ (\hat{\boldsymbol{\pi}} \circ \boldsymbol{\nu}^{-1}(\boldsymbol{\xi}), \boldsymbol{\xi}) \in \mathcal{Q} \\ \Leftrightarrow &\forall \boldsymbol{\xi} \in \Xi,\ (\boldsymbol{\pi}(\boldsymbol{\xi}), \boldsymbol{\xi}) \in \mathcal{Q} \text{ with } \boldsymbol{\pi} = \hat{\boldsymbol{\pi}} \circ \boldsymbol{\nu}^{-1} \\ \Leftrightarrow &\boldsymbol{\pi} \in \Delta(\Xi) \end{aligned} \tag{5.26}$$

Moreover, we have that $\boldsymbol{\pi} = \hat{\boldsymbol{\pi}} \circ \boldsymbol{\nu}^{-1} \in \mathcal{F}(\mathcal{I})$ by bijectivity of $\boldsymbol{\nu}$. This concludes that Ξ is causally admissible for tracking according to Definition 5.9. The reverse direction follows from the equivalence of all steps.

□

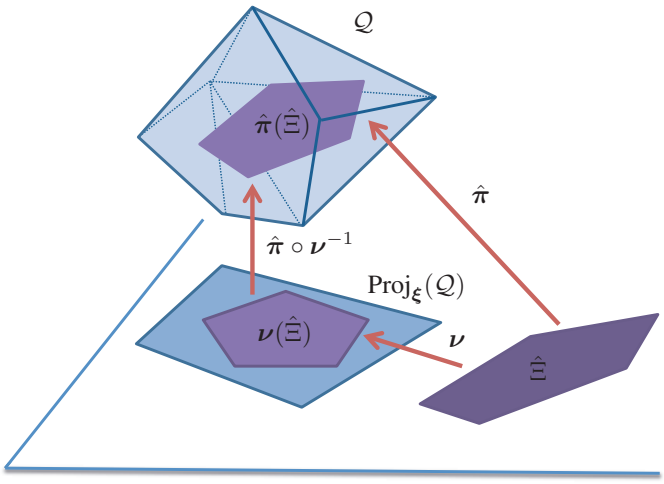

Figure 5.1 – Conceptual sketch of the relationships between uncertainty sets and applied functions. The initial uncertainty set $\hat{\Xi}$ is not necessarily a subset of the projection of $\mathcal{Q}$, therefore might not be admissible according to Lemma 5.5. However once we find a feasible lifting of this set into $\mathcal{Q}$, we can take its projection as an admissible uncertainty set, which is given by $\Xi = \boldsymbol{\nu}(\hat{\Xi})$. The corresponding admissible control policy can be obtained by letting $\boldsymbol{\pi} = \hat{\boldsymbol{\pi}} \circ \boldsymbol{\nu}^{-1}$.

Remark 5.12. Since the modifier function $\boldsymbol{\nu}$ is an arbitrary bijection, we do not lose generality when we consider uncertainty sets that can be characterized as the image of a given initial compact set $\hat{\Xi}$ with non-empty interior, under $\boldsymbol{\nu}$. □

According to Lemma 5.11 we can write an equivalent formulation of the family of

admissible sets for a given initial set $\hat{\Xi}$

$$\Omega = \left\{ \Xi \subset \mathbb{R}^{Nn_\xi} \middle| \; \exists \boldsymbol{\nu}, \hat{\boldsymbol{\pi}} : \Xi = \boldsymbol{\nu}(\hat{\Xi}), \hat{\boldsymbol{\pi}} \in \Delta_{\boldsymbol{\nu}}(\hat{\Xi}), \hat{\boldsymbol{\pi}} \circ \boldsymbol{\nu}^{-1} \in \mathcal{F}(\mathcal{I}) \right\} \tag{5.27}$$

Figure 5.1 illustrates the relationship between the policies and the set in the case of the full information. When we look for a N-step admissible set that belongs to Ω, the description (5.27) allows us to implicitly manipulate uncertainty sets and control policies simultaneously to verify admissibility, as will be seen in Section 5.3.4. However, while searching for a modifier function $\boldsymbol{\nu}$, the condition $\hat{\boldsymbol{\pi}} \circ \boldsymbol{\nu}^{-1} \in \mathcal{F}(\mathcal{I})$ is difficult to evaluate since it is a condition on a composite function that involves the inverse of $\boldsymbol{\nu}$. In the following, we will propose a simple sufficient condition directly on $\boldsymbol{\nu}$, that is easy to evaluate and ensures causal admissibility of the modified uncertainty set. We start by splitting the causality conditions of the composite function $\hat{\boldsymbol{\pi}} \circ \boldsymbol{\nu}^{-1}$.

Lemma 5.13. *Let $(\mathcal{I}_k)_{k \in \mathbb{Z}_{[1,m]}}$ be a set of information structures and $f : \mathbb{R}^n \longrightarrow \mathbb{R}$. If for all k, $f \in \mathcal{F}(\mathcal{I}_k)$ then $f \in \mathcal{F}(\bigcap_k \mathcal{I}_k)$.*

The proof of Lemma 5.13, as well as other technical proofs in this section are grouped in Appendix D.2. The results will be briefly discussed in this section and the reader is referred to Appendix D.2 for more details. Lemma 5.13 states an intuitive fact, that is if the output of a function f depends only on inputs indexed by $\mathcal{I}_1$ and $\mathcal{I}_2$, then it actually depends only on inputs indexed by their intersection. This directly motivates the next lemma.

Lemma 5.14. *Let $\boldsymbol{g} : \mathbb{R}^n \to \mathbb{R}^n$, be a bijection. Given an information structure $\mathcal{I} = (\mathcal{I}_k)_{k \in \mathbb{Z}_{[1,n]}}$, define $\hat{\mathcal{I}} = (\hat{\mathcal{I}}_j)_{j \in \mathbb{Z}_{[1,n]}}$ as:*

$$\hat{\mathcal{I}}_j = \bigcap_{\{i | j \in \mathcal{I}_i\}} \mathcal{I}_i \tag{5.28}$$

The following equivalence holds

$$\forall \boldsymbol{f} \in \mathcal{F}(\mathcal{I}), \boldsymbol{f} \circ \boldsymbol{g} \in \mathcal{F}(\mathcal{I}) \iff \boldsymbol{g} \in \mathcal{F}(\hat{\mathcal{I}}) \tag{5.29}$$

Equation (5.28) characterizes a set of functions which do not change the information structure of $\boldsymbol{f}$. Loosely speaking, it states that if $\boldsymbol{f}_i$ depends on x_j then $\boldsymbol{g}_j$ should not depend on anything that $\boldsymbol{f}_i$ does not depend on. Notice that $\hat{\mathcal{I}}_j$ is always nonempty and in particular it contains j. This reflects the fact that a 'diagonal' mapping (where $\boldsymbol{g}_j$ depends only on j for all j in $\mathbb{Z}_{[0,N-1]}$) does not change the information structure of any function it is composed with. for example, for linear functions it means that multiplying by a diagonal matrix always preserves the sparsity pattern.

In Figure 5.2, the information structure $\hat{\mathcal{I}}$ for different information structures $\mathcal{I}$ are presented. The k^{th} row of the matrix represents the indicator vector of $\mathcal{I}_k$. These matrices can be thought of as sparsity patterns in the case where the control policies are linear. The

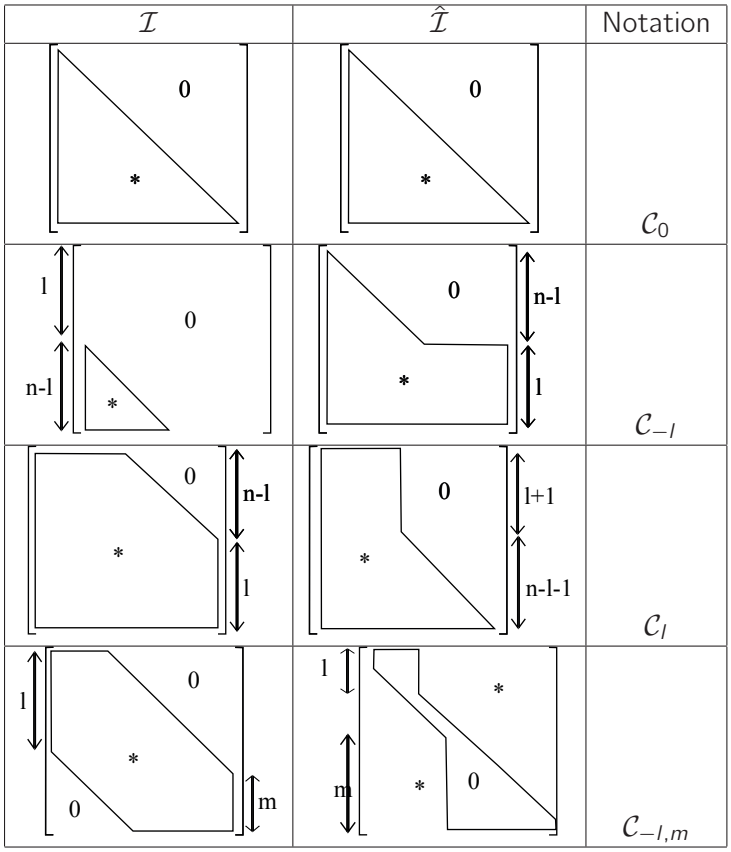

Figure 5.2 – For given information structures, the corresponding information structure of the uncertainty modifier function

first column shows the sparsity pattern of the control policy $\boldsymbol{\pi}$ and the second column the corresponding sparsity-preserving sparsity pattern. In other words, multiplying the matrix from the first column by the matrix from the second column will result in the same sparsity pattern. This directly helps us select control policies and modifier functions such that their composition will still respect the required information structure. For example, as would be expected, the first row of Figure 5.2 tells us that a lower triangular control policy composed with a lower triangular modifier will still be lower triangular. However more complex features in $\mathcal{I}$, such as delays and forecasting, result in non-trivial sparsity patterns for $\hat{\mathcal{I}}$.

5.3.4 Sufficient conditions for causal admissibility of modified uncertainty sets

In view of Lemma 5.11, simultaneous optimization over $\boldsymbol{\pi}$ and $\boldsymbol{\nu}$ would be beneficial for searching admissible uncertainty sets. Lemma 5.14 is instrumental in proving that from a control policy $\hat{\boldsymbol{\pi}}$ defined on $\hat{\Xi}$ and an invertible mapping $\boldsymbol{\nu}$, a control policy defined on $\boldsymbol{\nu}(\hat{\Xi})$ which has the desired information structure can be recovered. Indeed, $\hat{\boldsymbol{\pi}} \in \mathcal{F}(\mathcal{I})$ and $\boldsymbol{\nu}^{-1} \in \mathcal{F}(\hat{\mathcal{I}})$ ensures that $\hat{\boldsymbol{\pi}} \circ \boldsymbol{\nu}^{-1}$ defined on $\boldsymbol{\nu}(\hat{\Xi})$ belongs to $\mathcal{F}(\mathcal{I})$ according to the

lemma.

However, conditions on $\boldsymbol{\nu}^{-1}$ are inconvenient since the aim is to optimize directly over $\boldsymbol{\nu}$. Sufficient conditions on $\boldsymbol{\nu}$ are sought to replace the condition $\boldsymbol{\nu}^{-1} \in \mathcal{F}(\hat{\mathcal{I}})$. Unfortunately, a certain information structure for $\boldsymbol{\nu}^{-1}$ does not usually result in a specific information structure for $\boldsymbol{\nu}$. In particular, a sparse information structure for $\boldsymbol{\nu}^{-1}$ does not generally result in a sparse information structure for $\boldsymbol{\nu}$. For example, the inverse of a causal function is not generally causal. The following lemma gives sufficient conditions on $\boldsymbol{\nu}$.

Lemma 5.15. *Suppose $\boldsymbol{\nu} : \mathbb{R}^n \longrightarrow \mathbb{R}^n$ is a continuous bijection of $\mathbb{R}^n$ and $\boldsymbol{\nu} \in \mathcal{F}(\hat{\mathcal{I}})$ as defined by equation* (5.28)*. Define $\mathcal{G} = \{\boldsymbol{f} \circ \boldsymbol{\nu} \mid \boldsymbol{f} \in \mathcal{F}(\mathcal{I})\}$. We have*

$$\mathcal{G} = \mathcal{F}(\mathcal{I})$$

Under mild assumptions, Lemma 5.15 states that composing $\boldsymbol{f} \in \mathcal{F}(\mathcal{I})$ with $\boldsymbol{\nu}$ results in a function with the same information structure.

Corollary 5.16. *Given an information structure $\mathcal{I}$ and $\hat{\mathcal{I}}$ as defined in equation* (5.28)*, if $\boldsymbol{\nu}$ is a continuous bijection and $\boldsymbol{\nu} \in \mathcal{F}(\hat{\mathcal{I}})$, then $\boldsymbol{\nu}^{-1} \in \mathcal{F}(\hat{\mathcal{I}})$.*

Proof. According to Lemma 5.15, $\mathcal{F}(\mathcal{I}) = \{\boldsymbol{f} \circ \boldsymbol{\nu}^{-1} \mid \boldsymbol{f} \in \mathcal{G}\} = \{\boldsymbol{f} \circ \boldsymbol{\nu}^{-1} \mid \boldsymbol{f} \in \mathcal{F}(\mathcal{I})\}$. Hence, for any $\boldsymbol{f} \in \mathcal{F}(\mathcal{I})$, it holds that $\boldsymbol{f} \circ \boldsymbol{\nu}^{-1} \in \mathcal{F}(\mathcal{I})$. The fact that $\boldsymbol{\nu}^{-1} \in \mathcal{F}(\hat{\mathcal{I}})$ follows from Lemma 5.14. □

Theorem 5.17. *Let $\boldsymbol{\nu} : \mathbb{R}^{Nn_\xi} \to \mathbb{R}^{Nn_\xi}$, be a continuous bijection and $\mathcal{I}$ an information structure, $\hat{\mathcal{I}}$ defined by equation* (5.28) *and $\Delta_{\boldsymbol{\nu}}$ in equation* (5.24)*. $\boldsymbol{\nu}(\hat{\Xi})$ is causally admissible for tracking with respect to the information structure $\mathcal{I}$ if*

$$\begin{aligned} &\mathcal{F}(\mathcal{I}) \cap \Delta_{\boldsymbol{\nu}}(\hat{\Xi}) \neq \emptyset \\ &\boldsymbol{\nu} \in \mathcal{F}(\hat{\mathcal{I}}) \end{aligned} \tag{5.30}$$

Proof. Suppose there exists $\hat{\boldsymbol{\pi}} \in \mathcal{F}(\mathcal{I}) \cap \Delta_{\boldsymbol{\nu}}(\hat{\Xi})$. Since $\boldsymbol{\nu}$ is a continuous bijection, $\boldsymbol{\nu} \in \mathcal{F}(\hat{\mathcal{I}})$ implies that $\boldsymbol{\nu}^{-1} \in \mathcal{F}(\hat{\mathcal{I}})$ by Corollary 5.16. Lemma 5.14 in turn ensures that $\hat{\boldsymbol{\pi}} \circ \boldsymbol{\nu}^{-1} \in \mathcal{F}(\mathcal{I})$. Finally, application of Lemma 5.11 concludes the proof. □

Theorem 5.17 provides sufficient conditions for causal admissibility of an uncertainty set for tracking. We can define the family of admissible sets that comply with these sufficient conditions as

$$\tilde{\Omega}(\hat{\Xi}) = \left\{ \Xi \subset \mathbb{R}^{Nn_\xi} \;\middle|\; \begin{array}{l} \exists \boldsymbol{\nu}, \hat{\boldsymbol{\pi}} \\ \Xi = \boldsymbol{\nu}(\hat{\Xi}),\ \boldsymbol{\nu} \in \mathcal{F}(\hat{\mathcal{I}}) \\ \hat{\boldsymbol{\pi}} \in \mathcal{F}(\mathcal{I}) \cap \Delta_{\boldsymbol{\nu}}(\hat{\Xi}) \end{array} \right\} \tag{5.31}$$

For the definition of $\tilde{\Omega}$ we have replaced the condition $\hat{\boldsymbol{\pi}} \circ \boldsymbol{\nu}^{-1} \in \mathcal{F}(\mathcal{I})$ with the sufficient but simpler conditions $\hat{\boldsymbol{\pi}} \in \mathcal{F}(\mathcal{I})$ and $\boldsymbol{\nu} \in \mathcal{F}(\hat{\mathcal{I}})$. Therefore $\tilde{\Omega}$ is a restriction of the original

family of admissible sets Ω.

$$\tilde{\Omega}(\hat{\Xi}) \subseteq \Omega \tag{5.32}$$

The restriction will depend on the initial set $\hat{\Xi}$ and thus the argument of $\tilde{\Omega}$ is added to reflect this fact. However, this restriction leads to tractable formulations based on the available robust programming literature, as we will show in the next section.

Finally, we write the *modified causal admissibility* problem that is based on sufficient conditions (5.30) as

$$\text{find } \Xi : \Xi \in \tilde{\Omega} \tag{5.33}$$

5.4 Tractable approximations

The problem formulation (5.33) allows us to search over uncertainty sets implicitly by means of modifier functions. However, the problem is still difficult in its general form, due to the infinite dimension of the search space and the infinite number of constraints. Therefore we will look for finite dimensional and tractable approximations of the tracking commitment problem in order to solve it efficiently.

Using the definitions of $\tilde{\Omega}$ and $\Delta_{\boldsymbol{\nu}}$, we can rewrite the modified robust tracking commitment problem as

$$\begin{aligned} \text{find} \quad & \hat{\boldsymbol{\pi}}, \boldsymbol{\nu} \\ \text{subject to} \quad & \forall \hat{\boldsymbol{\xi}} \in \hat{\Xi} \\ & (\hat{\boldsymbol{\pi}}(\hat{\boldsymbol{\xi}}), \boldsymbol{\nu}(\hat{\boldsymbol{\xi}})) \in \mathcal{Q} \\ & \hat{\boldsymbol{\pi}} \in \mathcal{F}(\mathcal{I}) \\ & \boldsymbol{\nu} \in \mathcal{F}(\hat{\mathcal{I}}) \ . \end{aligned} \tag{5.34}$$

Note that (5.34) is an *adjustable robust optimization* (ARO) problem [8]. In the standard form of ARO, the uncertainty set is fixed, whereas the tracking commitment problem requires optimization over possible uncertainty sets. Through manipulation of the problem as discussed above, we have replaced the need to optimize over the uncertainty set by the optimization of the modulation policy $\boldsymbol{\nu}$, therefore casting the robust tracking commitment problem into the standard ARO framework, because the uncertainty modifier $\boldsymbol{\nu}$ can also be treated as a decision rule.

5.4.1 Linear policy and modifier functions

Tractable adjustable robust programming methods presented in [8] are applicable to robust linear optimization problems. To utilize them, the following assumption is made:

Assumption 5.18. The system is linear and described by:

$$\begin{aligned} x^+ &= Ax + B_u u + B_\xi \xi \\ y &= Cx + D_u u + D_\xi \xi \end{aligned} \tag{5.35}$$

with constrained state and inputs $(x_t, u_t) \in X_t \times U_t \subset \mathbb{R}^{n_x} \times \mathbb{R}^{n_u}$, disturbance $\xi \in \mathbb{R}^{n_\xi}$ and output $y \in \mathbb{R}^{n_y}$. The sets X_t and U_t are assumed to be bounded polytopes. ■

Following Assumption 5.18, the feasibility set $\mathcal{Q}$ also becomes polytopic and can be written as

$$\mathcal{Q} = \{(\boldsymbol{u}, \boldsymbol{\xi}) \mid H\boldsymbol{u} + Q\boldsymbol{\xi} \leqslant q\}$$

For the derivation of Q, H, and q see appendix D.1. This polytopic description of the feasibility set allows the treatment of the modified robust tracking commitment problem (5.34) in the uncertain linear optimization framework.

Until this point, we have not made any strong assumptions on the families of uncertainty sets, policy and modifier functions. Results of section 5.3.4 apply to generic functions and sets. Therefore, the sufficient conditions in (5.31) can be used to verify causal admissibility of any uncertainty set, using generic policies and modifier functions. In the following, we present restrictions on the family of uncertainty sets, control policies and modifier functions that allow the verification of causal admissibility of the uncertainty set in a computationally tractable manner.

The following assumption applies for the uncertainty set:

Assumption 5.19. The uncertainty sets under consideration are representable by intersections of convex cones as

$$\hat{\Xi} = \left\{\boldsymbol{\xi} \mid F_i\boldsymbol{\xi} + f_i \in \mathbf{K}_i,\ i \in \mathbb{Z}_{[1,m]}\right\} \tag{5.36}$$

where the cone $\mathbf{K}_i$ is proper (closed, convex with non-empty interior). ■

In this section we build our formulation on the results of [8] which shows that restricting the search space of policies to linear (or affine) functions leads to finite dimensional and tractable formulations.

Let us define the linear versions of the control policy and the uncertainty modifier

$$\hat{\boldsymbol{\pi}}_{lin}(\boldsymbol{\xi}) := \hat{\mathbf{M}}\boldsymbol{\xi} + \hat{\mathbf{m}}, \quad \boldsymbol{\nu}_{lin}(\boldsymbol{\xi}) = \mathbf{L}\boldsymbol{\xi} + \boldsymbol{l} \tag{5.37}$$

where $\hat{\mathbf{M}} \in \mathbb{R}^{Nn_u \times Nn_\xi}$ and $\mathbf{L} \in \mathbb{R}^{Nn_\xi \times Nn_\xi}$ is invertible. We can describe the causality conditions by constraints on $\hat{\mathbf{M}}$ and $\mathbf{L}$

$$\begin{aligned} &\hat{\mathbf{M}}(k, \mathbb{Z}_{[1,Nn_\xi]} \backslash \mathcal{I}_k) = 0, \quad k \in \mathbb{Z}_{[1,N]} \quad &&\Leftrightarrow \hat{\boldsymbol{\pi}}_{lin} \in \mathcal{F}(\mathcal{I}) \\ &\mathbf{L}(k, \mathbb{Z}_{[1,Nn_\xi]} \backslash \hat{\mathcal{I}}_k) = 0, \quad k \in \mathbb{Z}_{[1,N]} \quad &&\Leftrightarrow \boldsymbol{\nu}_{lin} \in \mathcal{F}(\hat{\mathcal{I}}) \end{aligned} \tag{5.38}$$

Note that the constraints (5.38) impose that the elements of $\hat{\mathbf{M}}$ and $\mathbf{L}$ multiplying the elements of the uncertain variable which are not included in the information structure at step k to be zero, thus enforcing causality of the linear functions $\hat{\boldsymbol{\pi}}_{lin}$ and $\boldsymbol{\nu}_{lin}$ with respect to $\mathcal{F}(\mathcal{I})$ and $\mathcal{F}(\hat{\mathcal{I}})$, respectively.

Let us now formulate the set admissibility problem (5.34) with linear policies given in (5.37) and conic uncertainty sets described by (5.36).

$$\begin{aligned} \text{find} \quad & \hat{\mathbf{M}}, \mathbf{L}, \hat{\mathbf{m}}, \boldsymbol{l} \\ \text{subject to} \quad & \forall \hat{\boldsymbol{\xi}} : F_i \hat{\boldsymbol{\xi}} + f_i \in \mathbf{K}_i, \quad i \in \mathbb{Z}_{[1,m]} \\ & H(\hat{\mathbf{M}}\hat{\boldsymbol{\xi}} + \hat{\mathbf{m}}) + Q(\mathbf{L}\hat{\boldsymbol{\xi}} + \boldsymbol{l}) \leqslant q \\ & (\hat{\mathbf{M}}, \mathbf{L}) \text{ satisfies (5.38)} \end{aligned} \tag{5.39}$$

The invertibility condition on $\mathbf{L}$ is not explicitly enforced. Invertibility can be checked a posteriori when solving (5.39). In general, an appropriate choice of cost function results in invertible matrices. Once the problem is solved, a feasible solution $(\hat{\mathbf{M}}, \mathbf{L}, \hat{\mathbf{m}}, \boldsymbol{l})$ can be used to construct the uncertainty set that is causally admissible for tracking and the corresponding control policies:

$$\Xi = \mathbf{L}\hat{\Xi} + \boldsymbol{l}, \quad \boldsymbol{\pi}(\boldsymbol{\xi}) = \mathbf{M}\boldsymbol{\xi} + \mathbf{m}, \quad \mathbf{M} = \hat{\mathbf{M}}\mathbf{L}^{-1}, \quad \boldsymbol{m} = \hat{\mathbf{m}} - \hat{\mathbf{M}}\boldsymbol{L}^{-1}\boldsymbol{l} \tag{5.40}$$

To recover a tractable formulation of (5.39), the worst case realizations of the uncertainty can be considered by enforcing the constraint; $\max_{\hat{\boldsymbol{\xi}} \in \hat{\Xi}} \left\{ H\mathbf{M}\hat{\boldsymbol{\xi}} + Q\mathbf{L}\hat{\boldsymbol{\xi}} \right\} \leqslant q - H\hat{\mathbf{m}} - Q\boldsymbol{l}$ where the maximization is meant row-wise. As reviewed in Section C.3, one can replace the maximization by dualizing this maximization problem. Thereafter, it is not necessary to solve the *min* problem, since existence of a feasible dual variable is sufficient. Therefore, the original semi-infinite constraint under uncertainty can be transformed into a finite dimensional constraint on the dual variables. It reformulates as:

$$\begin{aligned} \text{find} \quad & \mathbf{Z}, \hat{\mathbf{M}}, \mathbf{L}, \hat{\mathbf{m}}, \boldsymbol{l} \\ \text{subject to} \quad & \mathbf{Z}_i^T \in \mathbf{K}_i^*, \ i \in \mathbb{Z}_{[1,m]} \\ & \sum_{i=1}^{m} \mathbf{Z}_i f_i \leqslant q - H\hat{\mathbf{m}} - Q\boldsymbol{l} \\ & \sum_{i=1}^{m} \mathbf{Z}_i F_i = -\left(H\hat{\mathbf{M}} + Q\mathbf{L}\right) \\ & (\hat{\mathbf{M}}, \mathbf{L}) \text{ satisfies (5.38)} \end{aligned} \tag{5.41}$$

where the dual vectors are stacked in matrices $\boldsymbol{Z}_i$. The dual reformulation for the tracking commitment problem (5.39) is convex in linear control policies parametrized by $\hat{\mathbf{M}}$, $\hat{\mathbf{m}}$ and linear uncertainty modifiers parametrized by $\mathbf{L}$, $\boldsymbol{l}$. Therefore, when the sets $\mathbf{K}_i$ are polyhedral, second order or semi-definite cones, the problem formulation (5.41) allows tractable computations of feasible reference sets admissible with respect to the information

structure $\mathcal{I}$, by system (5.35). Table 5.1 gives a summary of problem complexity in case of most common uncertainty sets for the reference and disturbance.

Ξ	Dual reformulation
$F\boldsymbol{\xi} \leqslant f$	LP
$F\boldsymbol{\xi} + f : \|\boldsymbol{r}\|_2 \leqslant 1$	SOCP
$F\boldsymbol{\xi} + f \in \mathcal{S}_+$	SDP

Table 5.1 – Optimization type for (5.41), depending on the type of uncertainty set. Note that the polytopic representation also covers 1 and ∞ norm balls. An extended table is discussed in [51]

.

5.5 Extensions of the robust tracking commitment problem

5.5.1 Nonlinear policy and uncertainty modifiers

The formulation (5.41) is restricted to affine functions, but in certain cases it is possible to deal with nonlinear policies (or modifier functions) in a computationally tractable manner. The key principle, introduced in [8] and studied in greater detail in [41] is to consider a modified uncertainty set which is the image of the original uncertainty under a nonlinear lifting. If the lifted uncertainty set or its convex hull can be represented in the conic form of (5.36), the machinery of linear policies and modifier functions can be applied. An extensive list of tractable instances is given in [41] and an example is described in Appendix C.3. The combination of the nonlinear lifting and linear policy and modifiers results in a nonlinear policy and modifier function.

Consider again the constraints:

$$H\boldsymbol{\pi}(\boldsymbol{\xi}) + Q\boldsymbol{\nu}(\boldsymbol{\xi}) \leqslant q, \quad \forall \boldsymbol{\xi} \in \Xi \tag{5.42}$$

We define the lifted uncertainty variable, and the corresponding uncertainty set as

$$\mathcal{Z} := \{\boldsymbol{\zeta} = \Lambda(\boldsymbol{\xi}), \mid \boldsymbol{\xi} \in \Xi\} \tag{5.43}$$

with $\Lambda : \mathbb{R}^k \longrightarrow \mathbb{R}^{k'}$ a nonlinear lifting operator. Following [41], we may require that there exists a retraction operator ρ such that $\rho \circ \Lambda = I_k$, the identity operator. This ensures that the lifted policy subsumes the linear policy and therefore if there exists a linear policy satisfying constraints then there also exists a nonlinear one of that form. This implies that $k' \geq k$ and Λ is injective. We can now choose the policy and modifier functions under the form:

$$\boldsymbol{\pi}(\boldsymbol{\xi}) = \tilde{\mathbf{M}}\boldsymbol{\zeta} + \hat{\mathbf{m}} = \tilde{\mathbf{M}}\Lambda(\boldsymbol{\xi}) + \hat{\mathbf{m}} \text{ and } \boldsymbol{\nu}(\boldsymbol{\xi}) = \tilde{\mathbf{L}}\boldsymbol{\zeta} + \mathbf{l} = \tilde{\mathbf{L}}\Lambda(\boldsymbol{\xi}) + \mathbf{l} \tag{5.44}$$

and the objective is then to find $\tilde{\mathbf{M}}$, $\tilde{\mathbf{L}}$, $\hat{\mathbf{m}}$ and $\mathbf{I}$ such that:

$$H\tilde{\mathbf{M}}\boldsymbol{\zeta} + Q\tilde{\mathbf{L}}\boldsymbol{\zeta} \leqslant q - H\hat{\mathbf{m}} - Q\boldsymbol{I}, \quad \forall \boldsymbol{\zeta} \in \operatorname{conv}(\mathcal{Z}) \tag{5.45}$$

As discussed in Appendix C.3, if the convex hull of $\mathcal{Z}$ can be recast in the form of (5.36), then a tractable robust counterpart can be formulated.

5.5.2 Modulating the tracking error set

We start by making the following observation: The parameter q in Problem (5.41) enters the problem linearly. This implies that it can be freely optimized. This can prove useful to relate the size of the constraint set to the size or magnitude of the uncertainty.

Example 5.20. Consider a simple input tracking problem. Suppose ξ is a reference signal to be tracked by the inputs. Say that:

$$y = c_u^\top u - \xi$$

and $Y = \{y \mid Sy \leq h\}$. Suppose we are looking for scalings of a normalized uncertainty that can be tracked, so that $\boldsymbol{\xi} = \lambda\hat{\boldsymbol{\xi}}$ with λ a scalar. It might be useful to also parametrize Y such that $h = \hat{h}\lambda$ so that the allowed tracking error is proportional to the magnitude of the scaling. In turn h enters linearly in q so the convex nature of the problem is conserved. This situation exactly arises in the case of secondary frequency control since the tracking error allowed is defined as a fixed percentage of the accepted bid, see section 7.4 for the detailed implementation on an example. □

This also allows one to implement soft constraints on the system, which is typical in MPC problems to ensure feasibility.

5.5.3 Optimal tracking commitment

As mentioned earlier, the set admissibility (5.21) is a feasibility problem. On the other hand, the optimal set admissibility problem looks into minimizing a cost function.

$$\underset{\boldsymbol{\pi} \in \mathcal{F}(\mathcal{I}) \cap \Delta(\Xi)}{\text{minimize}} \; J(\boldsymbol{\pi}, \Xi) \tag{5.46}$$

Relying on the tractable formulation with linear control policies and uncertainty modifiers (5.39), we can solve a tractable version of the robust tracking commitment problem 7.2.

$$\begin{aligned} \text{minimize} \quad & J(\boldsymbol{u}, \mathbf{L}) \\ \text{subject to} \quad & \forall \hat{\boldsymbol{\xi}} : F\hat{\boldsymbol{\xi}} + f \in \mathbf{K} \\ & H\hat{\mathbf{M}}\hat{\boldsymbol{\xi}} + Q\mathbf{L}\hat{\boldsymbol{\xi}} \leqslant q - H\hat{\mathbf{m}} - Q\boldsymbol{I} \\ & (\hat{\mathbf{M}}, \mathbf{L}) \text{ satisfies (5.38)} \end{aligned} \tag{5.47}$$

For notational simplicity, the uncertainty set is described by a single conic set here, but they can also be defined as the intersection of several conic sets as in (5.36). The dependency of the cost function on $\mathbf{L}$ captures the fact that the cost might depend on the transformation applied to the uncertainty set. Typically, a large uncertainty set may be rewarded. For example, following the simple observation that:

$$\text{Vol}(\mathbf{L}\hat{\Xi} + \mathbf{l}) = \det(\mathbf{L})\text{Vol}(\hat{\Xi})$$

where Vol denotes the volume of a set, we see that we can try to maximize the determinant of L to maximize the volume of the modified uncertainty set. Using appropriate manipulations, the problem remains convex. Another proxy can be to maximize the trace of $\mathbf{L}$ which also favor 'large' uncertainty sets[159].

With a suitable cost function, the optimal commitment problem (5.47) can be solved. Natural cost functions would usually depend on the realization of the uncertainty, that is $J = J(\boldsymbol{u}, \boldsymbol{\xi}, \mathbf{L}) = J(\boldsymbol{\xi}, \mathbf{L})$ since $\boldsymbol{u}$ is a function of $\boldsymbol{\xi}$. It is typical then to consider either an expected cost:

$$\bar{J} = \mathbb{E}_{\boldsymbol{\xi}}\left[J(\boldsymbol{\xi}^{(i)}, \mathbf{L})\right] \tag{5.48}$$

for which a sample average approximation can be taken as:

$$\bar{J} = \frac{1}{N_s}\sum_{i=1}^{N_s} J(\boldsymbol{\xi}^{(i)}, \mathbf{L}) \tag{5.49}$$

where the $\boldsymbol{\xi}^{(i)}$'s are i.i.d. samples of the uncertainty. This requires either availability of previously observed samples or some probabilistic information on $\boldsymbol{\xi}$. Another approach is to use a worst case approach, by transforming the problem into:

$$\begin{aligned} \text{minimize} \quad & \gamma \\ \text{subject to} \quad & \forall \hat{\boldsymbol{\xi}} : F\boldsymbol{\xi} + f \in \mathbf{K} \\ & H\hat{\mathbf{M}}\hat{\boldsymbol{\xi}} + Q\mathbf{L}\hat{\boldsymbol{\xi}} \leqslant q - H\hat{\mathbf{m}} - Q\boldsymbol{l} \\ & J(\boldsymbol{\xi}, \boldsymbol{L}) \leqslant \gamma \\ & (\hat{\mathbf{M}}, \mathbf{L}) \text{ satisfies (5.38)} \end{aligned} \tag{5.50}$$

Now depending on the nature of J, the robust constraint $J(\hat{\boldsymbol{\xi}}, L) \leqslant \gamma \; \forall \hat{\boldsymbol{\xi}} \in \Xi$ can be converted to a tractable form. In particular, if J is linear in $\hat{\boldsymbol{\xi}}$, then that constraint can be dealt with as discussed in Section 5.4.1.

5.6 Discussion about the modeling assumptions and the use of robust programming

Our aim is to solve an uncertain multi-stage optimization problem. We use here a robust programming approach by restricting the uncertainty to belong to a set for which constraints need to be satisfied. Another common approach to solve this type of problem are stochastic programming methods [130], regrouping a number of methods whose common denominator is to use a probabilistic description of the uncertainty. Similarly to robust programming methods, stochastic programming methods require assumptions to solve the problem efficiently. They often use realizations of the uncertainty, available under the form of samples. One of the most common way of solving such problems is to form a so-called scenario tree, a structure taking into account the causality requirement of the problem. The complexity of the scenario grows exponentially when the horizon increases, which is impractical for our purposes due to the large horizon we are faced with. A possible simplification is to reduce the number of time stages to two.

The work [33] includes a comparison between a robust programming approach as presented in this manuscript and a two-stage stochastic programming approximation. It highlights that the stochastic version is less conservative than the robust one, a typical observation. However, we have also observed that depending on the problem, the two-stage approximation is too optimistic: in particular, in the case of the intraday market it results is an unrealistic behavior of the controller.

Note that even in the robust programming case, the choice of the set in which the uncertainty lies is implicitly associated to some probabilistic guarantees [92]. Finally, the robust approach only applies to the constraints, while the cost can still be treated in a probabilistic fashion, as briefly discussed in section 5.5.3.

5.7 Applications

In this section, we will illustrate the methods and concepts put forward above on an example of a building providing ancillary services to the grid.

5.7.1 Power tracking with a building

Let us look at the problem of power consumption tracking with a building. Let us assume that the building needs to declare two quantities ahead of time: its baseline power consumption and the flexibility in power consumption around this baseline it can accommodate. For that, it has to provide one number λ called the *capacity bid* that represents the maximum positive or negative power consumption deviation the building is willing to support. For example, if $\lambda = 10$kW, it means it could be required to increase (or decrease) its power consumption by 10 kW for the period of commitment. We assume that the building receives its power consumption deviation request in real-time. At the time it receives the signal, the building controller needs to make sure it adjusts its power consumption by the amount requested

with respect to the pre-declared baseline. We assume that the building can change its power consumption much faster than the sampling time of the robust tracking commitment problem, so that response can be assumed immediate. Deviations in the power consumption tracking are allowed within an error margin proportional to the bid. For details on frequency control, the reader is referred to [142] and the extensive discussion in Part III.

Notice that the robust tracking method we just described is particularly suited for this application. Indeed, all possible requests can be represented by a reference set $\mathcal{R}$, that the building operator can modify (essentially in this case, scale up or down depending on the value of λ). An optimal set size can be computed provided that an appropriate cost function is chosen as will be demonstrated next. By choosing y defined in equation (5.1) to be the total power consumption of the building and X and U to represent the operating constraints of the building, we can formulate this problem as a robust tracking commitment problem.

We consider an office building with three controlled zones served by individual air handling units that we assume can control the heat fluxes to the zones. A linear state-space model of the building was extracted and validated against EnergyPlus simulation data using the toolbox OpenBuild, whose working principles are detailed in Part I. One week of typical summer weather for the city of Chicago is used in this study. The model of the building is a model of the form (5.70) with state dimension $n_x = 10$ and input dimension $n_u = 3$. The input vector u represents the thermal power input power to the zones (which is negative since it is cooling season). In this study, y is a scalar that represents the total electricity consumption so that $y_k = \alpha \sum_{i=1}^{n_u} |u_i|$ with α the electric to thermal conversion factor. For simplicity, a linear relationship is assumed here but a more detailed model could be used depending on the heating system, provided it is linearized. The peak thermal cooling load of the building is 45kW for the summer period. The input constraint set U specifies maximum and minimum cooling levels in the rooms so that $u_{i,\min} \leq u_i \leq u_{i,\max} = 0$ for each thermal zone input, reflecting the sizing of the equipment. The state constraints X specifies temperature zones in the constraints so that the temperature is maintained between 20°C and 25°C.

The uncertainty is divided in two parts, so that $\xi = (w^\top; r^\top)^\top$ with w the disturbance affecting the system and capturing the effect of internal gains, solar radiations and outdoor temperature and r the tracking reference. Accordingly, the uncertainty takes the form:

$$\Xi = \mathcal{W} \times \mathcal{R}$$

The decision process goes as follows: at time $t_0 = 0$, the building starts in initial condition x_0. The tracking period starts at time t_1 and ends at time t_2, therefore leaving a 'preparation' period for the building controller from t_0 to t_1. The building controller computes a baseline consumption $\mathbf{p}_{\text{nom}}$ and up-down regulation limits around this baseline. Up-down regulation bids result in a 'box' uncertainty set. We therefore fix the basic uncertainty shape as the

unit box:

$$\hat{\mathcal{R}}_{box} = \{\boldsymbol{r} \,|\, \|\boldsymbol{r}\|_\infty \leq 1\} \tag{5.51}$$

For the external disturbance from weather and internal gains, the disturbance set is defined as follows

$$\mathcal{W} = \{\boldsymbol{w}_{\text{nom}} + \boldsymbol{w}_{\text{stoch}} \,|\, \boldsymbol{w}_{\text{stoch,i}}^T Q_i \boldsymbol{w}_{\text{stoch,i}} \leq 1,\ i = 1, 2, 3\} \tag{5.52}$$

As such, $\mathcal{W}$ is the direct product of three 'uncorrelated' ellipsoidal uncertainty sets so that $\mathcal{W} = \mathcal{W}_{\text{sun}} \times \mathcal{W}_{\text{gains}} \times \mathcal{W}_{\text{temp}}$. $\boldsymbol{w}_{\text{nom}}$ is the nominal prediction of the uncertainty over the prediction horizon and the three ellipsoids represent confidence sets that should cover a reasonable part of the possible outcomes for the disturbance. The choice of the Q_i's determines the size of the set $\mathcal{W}$ and should be done so that $\mathcal{W}$ contains the actual weather realization with a high confidence (see , *e.g.* [92]). Generally speaking, the selection of good uncertainty sets in classical robust optimization are a subject of active research [14] and fall outside the scope of the present work, but notice that rather than fixing the uncertainty $\mathcal{W}$, the method proposed in this work could also be used to optimize for $\mathcal{W}$ as well and by doing so, evaluate how much prediction error in the weather and the internal gains can be accommodated.
Finally we have $\hat{\Xi} = \hat{\mathcal{R}} \times \mathcal{W}$.

We consider here an affine controller and modifier function as in (5.37). Assuming that the flexibility needs to be constant over the tracking period as is for example required in the Swiss flexibility market (see details in Part III), we have to restrict the modifier function to a uniform scaling of the uncertainty set (that is, time-varying flexibility is not allowed). For clarity we keep the description of the uncertainty split between the reference to track and the external disturbance, so that: $\boldsymbol{\xi} = (\boldsymbol{r}, \boldsymbol{w})$ and $\boldsymbol{\nu} = (\boldsymbol{\nu}_{\mathcal{R}}, \boldsymbol{\nu}_{\mathcal{W}})$. We assume the weather uncertainty is unknown at the time of the decision whereas the reference is revealed as it needs to be tracked: this results in an information structure that is depicted in Figure 5.3. We see that the modifier function could theoretically modify the uncertainty set so as to "mix" the external disturbance and the reference. In this application, it would not have physical sense so it is preferable to keep a block diagonal structure for the modifier's information structure. The disturbance uncertainty set is fixed a priori while the reference set can be modified. Furthermore, in the case that the reference set is a fixed up/down box along the horizon then the reference tracking set can only be scaled uniformly so that the modifier function will reduce to the simpler form:

$$\mathbf{L} = \begin{pmatrix} \lambda I_N & 0_{N,Nn_w} \\ 0_{Nn_w,N} & I_{Nn_w} \end{pmatrix} \tag{5.53}$$

Notice that enforcing (5.53) implicitly enforces the requirement that $\boldsymbol{\nu} \in \hat{\mathcal{I}}$. The description of the uncertainty set $\hat{\Xi} = \hat{\mathcal{R}} \times \mathcal{W}$ can easily be put into the form of equation (5.36) since it is the Cartesian product of a polyhedron with three ellipsoids.

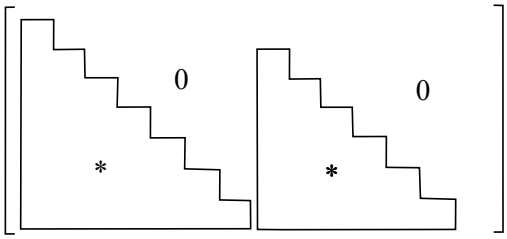

(a) $\mathcal{I}$

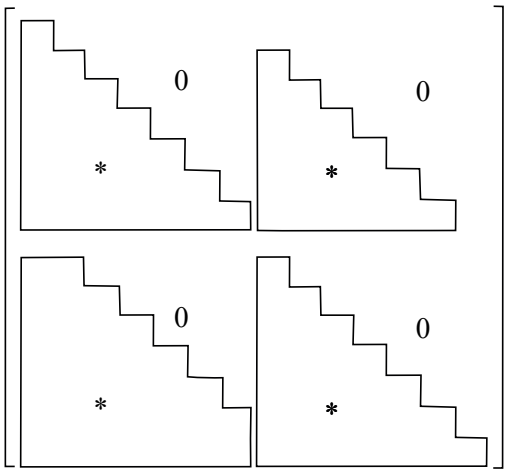

(b) $\hat{\mathcal{I}}$

Figure 5.3 – Information structure for the example. (a) shows that decisions at time step t can depend on the reference up to time t and disturbance up to time $t-1$. (b) is the resulting information structure for the modifier function.

We assume that a payment proportional to the bid is made to the reserve provider, and the energy is also paid for, yielding the cost function $J = \mathbf{c}_\mathsf{e}{}^\top \mathbf{p}_\mathsf{nom} - c_\mathsf{flex}\lambda$ where $\mathbf{c}_\mathsf{e}$ is the vector of time-varying prices of electricity, $\mathbf{p}_\mathsf{nom}$ is the baseline consumption and c_flex is the unit reward price of the power tracking commitment (hence promising to track $\pm$1kW for the commitment period is rewarded at the price c_flex).

The tracking error is sized proportionally to the tracking requirement so that tracking errors amounting up to 10% of the maximum tracking requirement are allowed. This yields:

$$y \in Y := \{\boldsymbol{e} \mid \|\boldsymbol{e}\|_\infty \leqslant 0.1\lambda\}$$

which results in a tractable reformulation as described in section 5.5.2.

A horizon of one day with a time step of one hour is considered. For the sake of illustration, we take $c_e^t << c_\mathsf{flex}$ in order to favor participation in the tracking commitment. The problem solved is a second-order cone problem with 200,000 non-zero variables and 900 second-order cone constraints. Solving time on a 2.7GHz i-Core 7 platform was 7 seconds. The optimal value of λ is 5.4, meaning that the building can offer a 5.4kW up/down power tracking capacity for a period of 10 hours. This represents 8% of the peak cooling power

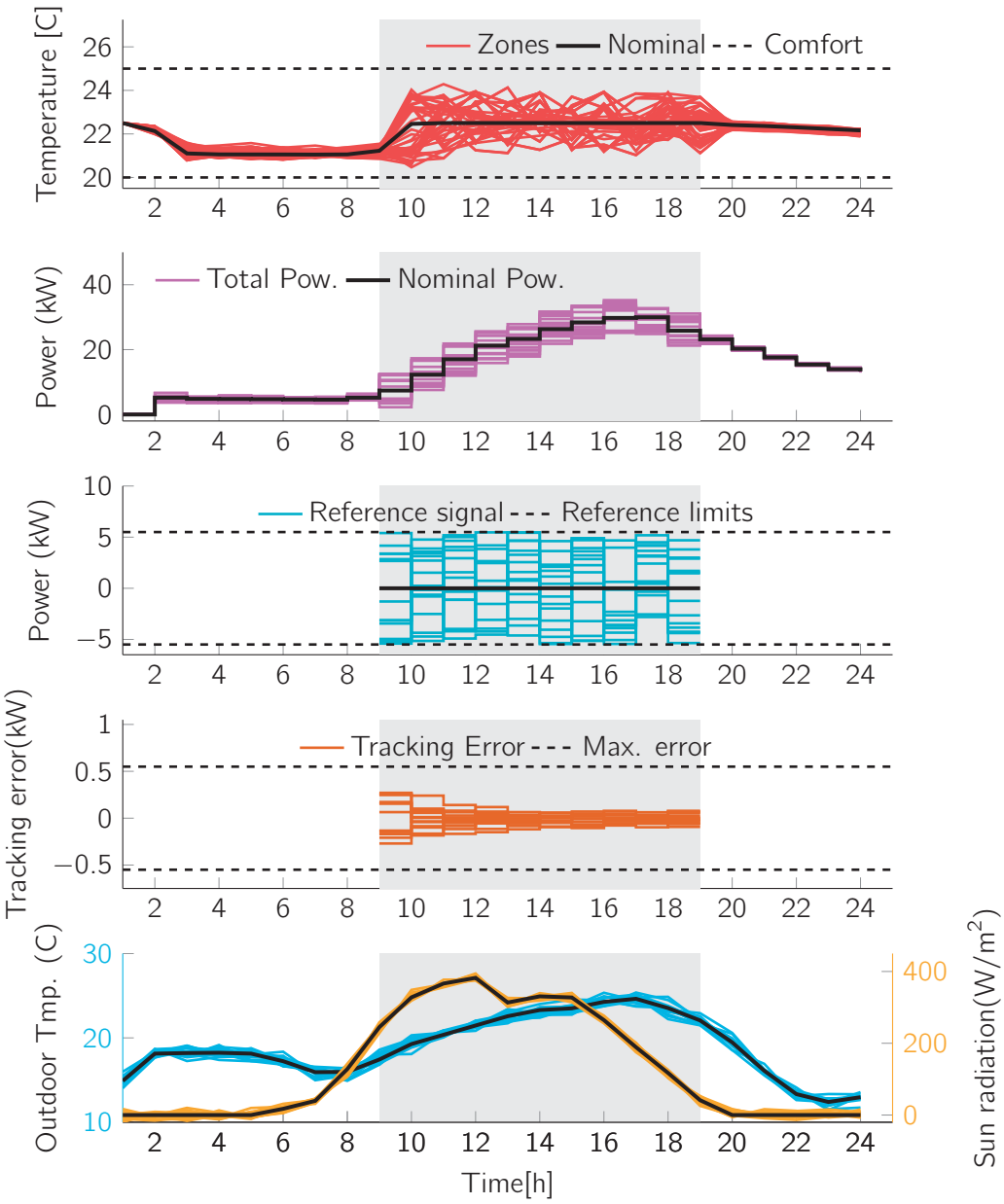

Figure 5.4 – Trajectories for different weather and reference scenarios in the optimized uncertainty set. Shaded region is the tracking commitment period. Black lines show the 'nominal' scenario where the reference is zero and the weather takes its predicted value. From top to bottom: temperature in zones, total power consumption, tracking reference, tracking error, and weather scenarios.

and 36% of the average power consumption for that day.

Figure 5.4 shows the trajectories generated in response to randomly generated weather and reference signals inside the uncertainty sets. In each of the plots, the shaded band shows the reference tracking times. The different plots show the average temperature in the building as well as in individual zones, the total power consumption in the building, the requested power consumption to be tracked on top of the nominal consumption, and the tracking error. It can be observed that in the nominal case, the power consumption increases during the day to compensate for the higher solar radiation and outside temperature as shown in the bottom plot. Therefore, the baseline consumption varies during the day to maintain the temperature at the nominal value of 22.5 ^{o}C. In addition, it is seen how the temperature and power consumption changes in response to varying tracking requests (depicted in the middle plot). As a result of the requested increase or decrease of the power consumption, the temperature respectively drops or rises in the rooms, within the prescribed comfort constraints.

5.7.2 Influence of the integral constraint in the uncertainty set and the 'virtual battery' concept

In the previous example, we impose that the building be able to offer up or down regulation for a long period of time, which can be limiting for loads. In this section, we propose a way of mitigating this issue by using time-correlated (meaning the constraint describing the set couple different time stages) reference sets with integral constraints that capture more accurately the capabilities of the load. Let us consider an uncertainty set of the form:

$$\hat{\mathcal{R}}_{batt} = \left\{ \mathbf{r} \;\middle|\; \begin{array}{ll} s_0 = \dfrac{s_{\max}}{2} & \\ 0 \leq s_t \leq s_{\max}, & \forall t \in \mathbb{Z}_{[1,N]} \\ s_{t+1} = s_t + r_t & \forall t \in \mathbb{Z}_{[1,N]} \\ -p_{\max} \leq r_t \leq p_{\max} & \forall t \in \mathbb{Z}_{[1,N]} \end{array} \right\} \tag{5.54}$$

By analogy with the feasible set of a simplified battery model, we will refer to this uncertainty set as the 'battery' reference set, where s represents the state of charge of the battery. Notice that contrary to the box reference set, the battery reference set is time-correlated.

We respectively consider a box reference set (5.51) and a battery reference set (5.54) and compute the maximum bid that can be offered. Notice that the design of the battery reference set requires the choice of a value for the integral constraint limit $s_{\max}$ and the maximum power $p_{\max}$. We can first fix $p_{\max} = 1$ without loss of generality since we will be scaling the set. We assume for now that $s_{\max} = 5.6$kWh, which is then the capacity to power ratio of the battery.

To study the influence of the integral limit in the reference set, the tracking bid is evaluated as a function of the duration of the tracking commitment. A preparation time of 8 hours without tracking is kept in order to cancel the effect of the initial condition.

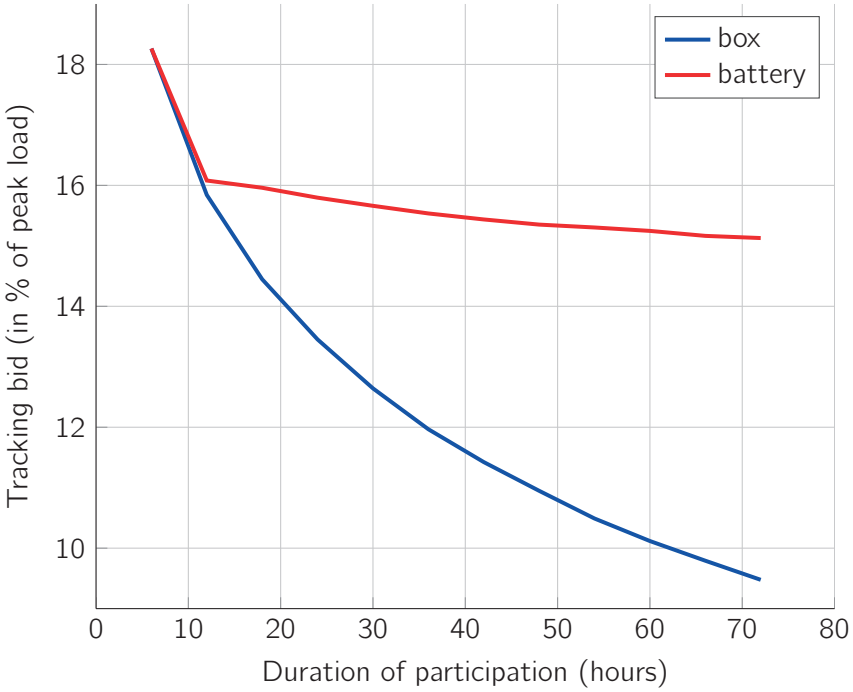

Figure 5.5 – Tracking capacity bid versus duration of participation for box and battery reference set

The weather is considered known perfectly in advance in this case to rule out other factors of uncertainty in the computation. Beyond 66 hours, the computational burden becomes prohibitive. The maximum bids for the battery and the box uncertainty sets are reported on Figure 5.5. We can observe that, beyond 12h of consecutive participation, introducing an integral limit for the tracking commitment allows increasing the tracking bid, and more so as the duration of participation time increases. Thanks to the integral constraints, situations of long lasting positive or negative tracking requests are ruled out, thus relieving the tracking requirements on the building, and leading to less conservative solutions.

This problem corresponds to the 'virtual battery' idea briefly mentioned in Section 5.1. Knowing the values of the scaling λ^* and baseline $\mathbf{p}_{\text{nom}}$ computed, we can conclude that the building can act (in terms of power consumption) like an ideal battery described by parameters $(\lambda^*; \lambda^* s_{\max})$. Therefore, it makes sense to say that the building is a virtual battery.

The virtual battery is described with two parameters (plus the baseline), and the parameter pair above is just one possible battery that the building can behave like. It is instructive to look at all possible parameter pairs that describe what the building can do. For that, we can again exploit our method as follows. First let us notice that:

$$\mathcal{R}_{batt} = \mathcal{R}_{box}(p_{\max}) \bigcap \mathcal{R}_{soc}(s_{\max}) \tag{5.55}$$

with:

$$\mathcal{R}_{box}(p_{\max}) := \{\boldsymbol{r} \,|\, \|\boldsymbol{r}\|_\infty \leq p_{\max}\} = p_{\max}\mathcal{R}_{box}(1)$$

and

$$\mathcal{R}_{soc}(s_{\max}) := \{\boldsymbol{r} \,|\, \|T_N\boldsymbol{r}\|_\infty \leq \frac{s_{\max}}{2}\} = s_{\max}\mathcal{R}_{soc}(1)$$

and T_N the unit lower triangular matrix that maps a power profile into the corresponding state of charge trajectory.

If we consider a horizon of tracking N, it holds that $\mathcal{R}_{box}(p_{\max}) \subseteq \mathcal{R}_{soc}(s_{\max})$ if $p_{\max} < \frac{s_{\max}}{2N}$ and conversely that $\mathcal{R}_{soc}(s_{\max}) \subseteq \mathcal{R}_{box}(p_{\max})$ if $s_{\max} < p_{\max}$. In addition, it is straightforward to see that if the load can behave like the battery $(p_{\max}, s_{\max})$ then it can also behave like the battery $(\alpha p_{\max}, \alpha s_{\max})$ for any $\alpha \in [0, 1]$. Therefore, we can fix one of these two parameters and find the largest scaling of the resulting battery the system is equivalent to. For example, let us fix the value of $p_{\max}$ to 1 and grid values of $s_{\max}$ between $p_{\max}$ and $2Np_{\max}$.

Using the notation $\mathcal{R}_{batt} = \{\boldsymbol{r} | F\boldsymbol{r} + f(s_{\max}, p_{\max}) \geq 0\}$ with:

$$F = -\begin{bmatrix} I_N \\ T_N \end{bmatrix} \otimes \begin{bmatrix} 1 \\ -1 \end{bmatrix} \text{ and } f(s_{\max}, p_{\max}) = \begin{bmatrix} \mathbf{1}_{2n} \otimes p_{\max} \\ \mathbf{1}_{2n} \otimes \frac{s_{\max}}{2} \end{bmatrix}$$

We solve:

$$\begin{aligned} \text{maximize} \quad & \lambda \\ \text{subject to} \quad & \mathbf{Z}^T \geq 0 \\ & \mathbf{Z}f(1, s_{\max}) \leqslant q - H\hat{\mathbf{m}} - Q\boldsymbol{l} \\ & \mathbf{Z}F = -\left(H\hat{\mathbf{M}} + Q\mathbf{L}\right) \\ & (\hat{\mathbf{M}}, \mathbf{L}) \text{ satisfies (5.38)} \\ & \boldsymbol{L} = \lambda I_N \end{aligned} \tag{5.56}$$

This is a parametric linear program where the constraint matrix depends on $s_{\max}$. In general, this type of parametric linear program is quite difficult to analyze and the optimal value function is a piecewise rational function of the parameter vector [39]. Using the particular structure of this problem, we can push the analysis further. Noting that $f(1, s_{\max}) = vs_{\max}$ with v a column vector, we can rewrite the inequality as:

$$\mathbf{Z}v \leq \frac{1}{s_{\max}}(q - H\hat{\mathbf{m}} - Q\boldsymbol{l})$$

for any $s_{\max} > 0$. Introducing $\tilde{\mathbf{m}} \leftarrow \frac{\hat{\mathbf{m}}}{s_{\max}}$ and $\tilde{\mathbf{l}} \leftarrow \frac{\mathbf{l}}{s_{\max}}$, the problem now takes the form of a more standard parametric LP with the right hand side of the constraint affine in $\theta = \frac{1}{s_{\max}}$.

We then know that the optimal solution is a piecewise-affine function of θ. In fact,

for $s_{\max} \leq p_{\max}$, we have that $\mathcal{B}_{batt} = \mathcal{B}_{soc}(s_{\max}) = s_{\max}\mathcal{B}_{soc}(1)$ and $\lambda^*(s_{\max}) = \frac{\lambda^*(1)}{s_{\max}}$. Similarly, if $s_{\max} \geq 2Np_{\max}$, then $\mathcal{B}_{batt} = \mathcal{B}_{box}(1)$ and therefore $\lambda^*(s_{\max}) = \lambda^*(2N)$. We report in Figure 5.6 the value of the optimal value function as a function of $s_{\max}$.

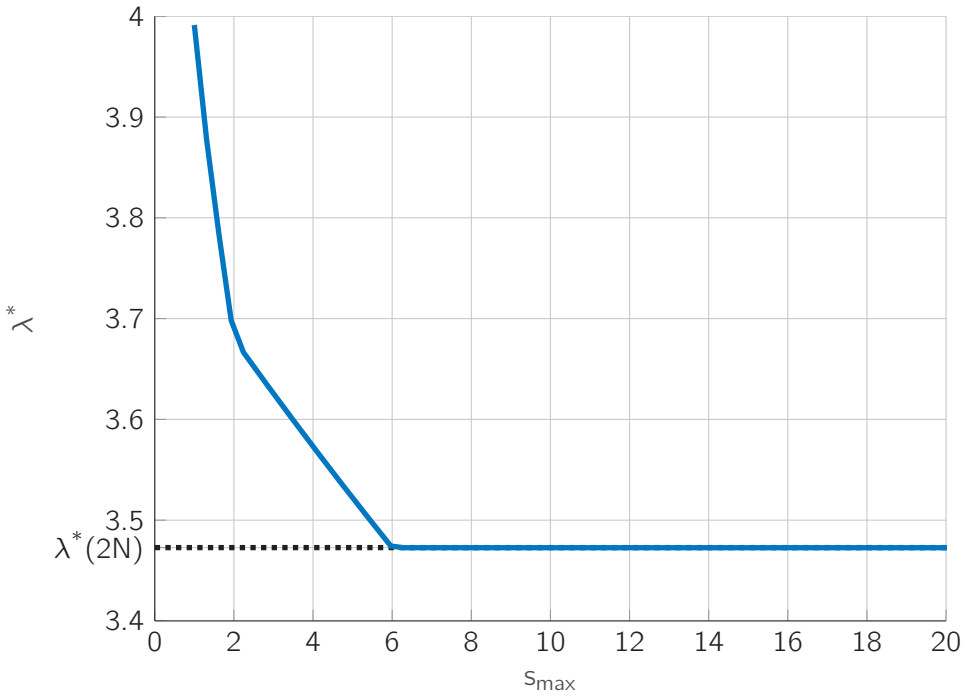

Figure 5.6 – Maximum admissible battery scaling as a function of the state of charge limit

From these values we can reconstruct the parameters of all batteries that are admissible for the system. To do so, we can use the previous curve and compute the values of the parameters corresponding to the maximum scaling of each battery. For a battery of parameter $(1, s_{\max})$, the maximum admissible scaling $\lambda^*(s_{\max})$ was computed which yields the battery parameters $(\lambda^*(s_{\max}), \lambda^*(s_{\max})s_{\max})$. Since $\lambda^*(s_{\max})$ was piecewise-affine in $\frac{1}{s_{\max}}$, then $\lambda^*(s_{\max}).s_{\max}$ is a piecewise-affine function of $s_{\max}$. Consequently, the Pareto curve of the maximum admisssible parameter pairs takes a piecewise affine form, as is suggested by Figure 5.7, which depicts the parameters pairs of all causally admissible virtual batteries.

5.8 Infinite Horizon guarantees

So far we have looked at finite horizon problems. However, we have no guarantees about what happens beyond the horizon N. Ideally, we would like to be able to solve:

Problem 5.21. Given an initial condition x_0, find a set Ξ indexed by $\mathbb{N}$ and a control policy $\boldsymbol{\pi}$ with $\pi_t : \Xi \to \mathbb{R}^{n_u}$ for $t \geq 0$ such that:

$$\forall \boldsymbol{\xi} \in \Xi,\ \phi_t(x_0, \boldsymbol{\pi}(\boldsymbol{\xi}), \boldsymbol{\xi}) \in X_t,\ \pi_t(\boldsymbol{\xi}) \in U_t,\ y_t \in Y_t,\ \forall t \geq 0 \tag{5.57}$$

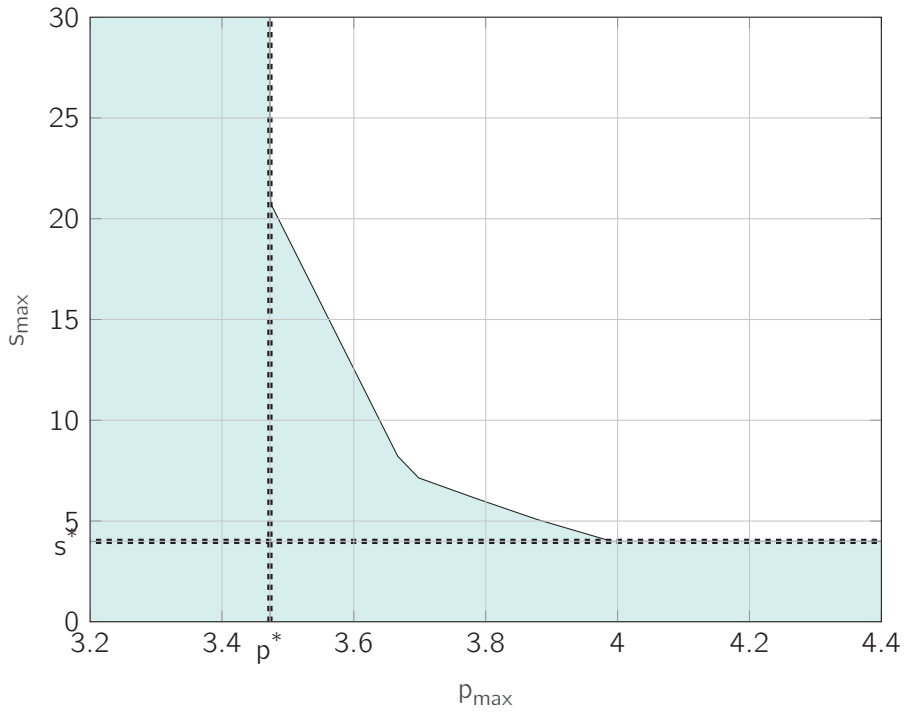

Figure 5.7 – The shaded region shows all battery parameter pairs that define a causally admissible battery reference set for the building over horizon N. p^* are s^* are the parameters the smallest box and 'soc' box causally admissible, respectively.

and

$$\boldsymbol{\pi} \in \mathcal{F} \tag{5.58}$$

■

Notice that Ξ then becomes infinite dimensional (indexed over time). Proving infinite horizon tracking may prove significantly more involved, especially if we are still trying to optimize over the set Ξ. In the most general case, Ξ will be time-correlated. For example, the idea of the virtual battery discussed in section 5.7.2 can be extended to the infinite horizon case by considering the reference set:

$$\Xi = \left\{ \mathbf{r} \;\middle|\; \begin{array}{ll} s_0 = \dfrac{s_{\max}}{2} & \\ 0 \leq s_t \leq s_{\max}, & \forall t \in \mathbb{N} \\ s_{t+1} = s_t + r_t & \forall t \in \mathbb{N} \\ -1 \leq r_t \leq 1 & \forall t \in \mathbb{N} \end{array} \right\} \tag{5.59}$$

Even when Ξ is fixed, there is no known efficient way to solve this problem, because of the time invariance and correlation of the problem. Additional assumptions are needed.

Guaranteeing infinite horizon feasibility is a classical concern in MPC, as we discussed in section 5.2.1. The usual way to handle this type of problem is to solve the problem on a finite horizon while imposing terminal constraints. By solving the problem repeatedly with a receding horizon, the existence of an infinite horizon policy is guaranteed provided the problem can be solved for the initial condition. To follow the same approach, the following assumption is required:

Assumption 5.22 (Time-invariance after N step)**.**

$$\forall t \geq N,\, Y_t = Y,\, U_t = U,\, X_t = X,\, \Xi = \Xi_{:N-1} \times R^{\mathbb{N}} \tag{5.60}$$

where $R \subseteq \mathbb{R}^{n_\xi}$ and $\Xi_{:N-1} \subseteq \mathbb{R}^{Nn_\xi}$. ■

Assumption 5.22 states that the problem becomes time-invariant after a finite time horizon N. The uncertainty set may still be time-correlated over the first N steps.

At time step 0, we propose to solve the following problem:

$$\begin{aligned} \text{find} \quad & \boldsymbol{\pi},\, \Xi_{:N-1} \\ \text{such that} \quad & \forall i = 0, \dots, N-1 \\ & \forall \boldsymbol{\xi} \in \Xi_{:N-1} \\ & \phi_i(x, \boldsymbol{u}, \boldsymbol{\xi}) \in X_i \\ & \phi_N(x, \boldsymbol{u}, \boldsymbol{\xi}) \in \mathbb{X}_f \\ & u_i = \pi_i(\boldsymbol{\xi}) \in U_i \\ & \boldsymbol{\pi} \in \mathcal{F} \end{aligned} \tag{5.61}$$

The choice of $\mathbb{X}_f$ will be discussed next.

Remark 5.23. Problem (5.61) is identical to the robust tracking commitment problem 5.2, with the addition of the terminal constraint $\phi_N(x, \mathbf{u}, \boldsymbol{\xi}) \in \mathbb{X}_f$. If $\mathbb{X}_f$ is a polytope, then, the developments of Sections 5.3 and 5.4 can still be followed and the uncertainty set can still be optimized tractably. □

Note that if control decisions at time step t can depend on disturbance up to time $t-1$ (ie $\boldsymbol{\pi} \in \mathcal{C}_{-1}$), we retrieve a problem close to a classical robust MPC problem. We then need $\mathbb{X}_f$ to be a robust controlled invariant set, as discussed in section 5.2.1.

Lemma 5.24. *Under assumption 5.22, if $\mathbb{X}_f$ is a robust controlled invariant set for system* (5.1) *subject to constraints $u \in U$, $x \in X$, $y \in Y$ with disturbance $\xi \in R$, solving problem* (5.61) *with $\mathcal{F} = \mathcal{C}_{-1}$ guarantees the existence of a solution to problem 5.21 with $\Xi = \Xi_{:N-1} \times R^{\mathbb{N}}$.*

Proof. It follows directly from the definition of a robust controlled invariant set together with the assumption of time invariance of the problem after horizon N. □

In the case where decisions at time step t can depend on disturbance up to time t (ie $\boldsymbol{\pi} \in \mathcal{C}_0$), then another type of invariant set is required:

Definition 5.25. A set $\mathbb{X}_f$ is invariant for tracking in set R for system (5.1) subject to state, input and output constraints X, U and Y when:

$$\forall x \in \mathbb{X}_f,\ \forall \xi \in R,\ \exists u \in U :\ f(x,u,\xi) \in \mathbb{X}_f,\ g(x,u,\xi) \in Y \text{ and } \mathbb{X}_f \subseteq X \tag{5.62}$$

■

In contrast to most of the literature where it is assumed that the control input is chosen before the disturbance affecting the system is revealed, in the case of robust tracking, the disturbance is revealed prior to the choice of the control decision. This type of problem is studied in [6] where multi-stage max-min problems are studied and solved using a dynamic programming approach. We call invariant set for this type of situation invariant set for tracking. Invariant sets for tracking are discussed in [115].

Lemma 5.26. *Under assumption 5.22, if $\mathbb{X}_f$ is as an invariant set for tracking in set R for system* (5.1) *subject to constraints $u \in U$, $x \in X$, $y \in Y$, solving problem* (5.61) *with $\mathcal{F} = \mathcal{C}_0$ guarantees the existence of a solution to problem 5.21 with $\Xi = \Xi_{:N-1} \times R^{\mathbb{N}}$.*

Proof. It follows directly from the definition of an invariant set for tracking together with the assumption of time invariance of the problem after horizon N. □

The two previous lemmas allow to solve the infinite horizon problem by looking at a finite horizon problem.

5.8.1 Computation of maximal invariant sets for tracking

The computation of invariant sets is usually difficult. The computation of robust controlled invariant sets have been studied in [116, 121] and their use in the context of tracking in [26].

We give here few results pertaining to the computation of invariant sets for tracking that complement the results from [115].

Let us denote for any ξ, $\mathbb{X}_\infty(\xi)$ the maximal controlled invariant set for the system $x^+ = f(x,u,\xi), y = g(x,u,\xi)$ where ξ is fixed and known and $X_\infty(R)$ the maximal invariant set for tracking for system (5.1). The following holds:

Lemma 5.27. $\mathbb{X}_\infty(R) \subseteq \bigcap_{\xi \in R} \mathbb{X}_\infty(\xi)$

Proof. Let us first prove that there exists a maximal invariant set for tracking. If $\mathbb{X}_1$ and $\mathbb{X}_2$ satisfy (5.62), then it is easy to see that $\mathbb{X}_1 \cup \mathbb{X}_2 \subseteq X$ and for $x \in \mathbb{X}_1 \cup \mathbb{X}_2$, then either $x \in \mathbb{X}_1$ and we can see that there exists $u \in U$ such that $f(x,u,\xi) \in \mathbb{X}_f, g(x,u,\xi) \in Y$ by (5.62) applied to $\mathbb{X}_1$, or $x \in \mathbb{X}_2$ and the same holds by (5.62) applied to $\mathbb{X}_2$. Finally, this means that $\mathbb{X}_1 \cup \mathbb{X}_2$ is also an invariant set for tracking in set R for (5.1).

Now, let us prove that $\mathbb{X}_\infty(R) \subseteq \bigcap_{\xi \in R} \mathbb{X}_\infty(\xi)$, *i.e.* that for any $\xi \in R, \mathbb{X}_\infty(R) \subseteq \mathbb{X}_\infty(\xi)$. Consider $\xi \in R$. By (5.62), $\forall x \in \mathbb{X}_\infty(R),\ \exists u \in U :\ f(x,u,\xi) \in \mathbb{X}_\infty(R),\ g(x,u,\xi) \in Y$ and $\mathbb{X}_\infty(R) \subseteq X$, therefore $\mathbb{X}_\infty(R)$ is an invariant set for the affine system $x^+ = f(x,u,\xi), y = g(x,u,\xi)$, and it follows that $\mathbb{X}_\infty(R) \subseteq \mathbb{X}_\infty(\xi)$. □

The converse inclusion is not true, that is, in general $\bigcap_{\xi\in R}\mathbb{X}_\infty(\xi) \not\subseteq \mathbb{X}_\infty(R)$, as illustrated by the following example:

Example 5.28. Consider the system $x^+ = -1.1x + u + \xi$ subject to the constraints $x \in [-5, 5]$, $u \in [-0.2, 0.2]$ and $R = [0.1; -0.1]$. In this simple case, it is easy to see that $\mathbb{X}_\infty(0.2) = [-2.9048, 3.0952]$, and $\mathbb{X}_\infty(-0.2) = [-3.0952, 2.9048]$, and consequently, $\bigcap_{\xi\in R}\mathbb{X}_\infty(\xi) = [-2.9048, 2.9048]$.

However, it is easily seen also that $\mathbb{X}_\infty(R) = [-1, 1]$ which is much smaller than $\bigcap_{\xi\in R}\mathbb{X}_\infty(\xi)$.

Actually, the reason that $\bigcap_{\xi\in R}\mathbb{X}_\infty(\xi) \not\subseteq \mathbb{X}_\infty(R)$ is that being in the intersection of the $\mathbb{X}_\infty(\xi)$ guarantees that the state can be maintained in any $\mathbb{X}_\infty(\xi)$ but not necessarily in their intersection. □

Consequently, it is not enough to be able to compute control-invariant sets to compute invariant set for tracking and a variant of the procedure described in Section C.1 is needed.

For that, a new pre-set operation needs to be defined, as the tracking pre-set:

$$\mathrm{pre}^R_{\mathrm{trk}}(\mathbb{X}) := \{x | \forall \xi \in R, \exists u \in U,\ f(x, u, \xi) \in \mathbb{X}, g(x, u, \xi) \in Y\} \tag{5.63}$$

where the subscript trk denotes the fact that this is a tracking pre-set where the input u can be different for each value of the tracking reference ξ. We can readily see that:

$$\mathrm{pre}^R_{\mathrm{trk}}(\mathbb{X}) = \bigcap_{\xi\in\Xi} \mathrm{pre}_\xi(\mathbb{X}) \tag{5.64}$$

where the notation pre_ξ denotes the preset for system $x^+ = f(x, u, \xi)$ is defined as:

$$\mathrm{pre}_\xi(\mathbb{X}) := \{x | \exists u \in U,\ f(x, u, \xi) \in \mathbb{X}, g(x, u, \xi) \in Y\} \tag{5.65}$$

Now, the Algorithm 1 on page 95 is valid to compute the maximal invariant set for tracking, provided the pre-set operation is replaced as specified by (5.63).

Lemma 5.29. *Under the assumption that U is convex, f is control and disturbance affine ($f(x, u, \xi) = f(x) + g(x)u + h(x)\xi$) and R is polytopic, then the tracking pre-set of a convex set $\mathbb{X}$ can be computed as:*

$$\mathrm{pre}^R_{trk}(\mathbb{X}) = \bigcap_{\xi\in\mathrm{vert}(R)} \mathrm{pre}_\xi(\mathbb{X}) \tag{5.66}$$

where $\mathrm{vert}(R)$ *denotes the set of vertices of R*

Proof. Since $\mathrm{vert}(R) \subseteq R$, it holds that $\bigcap_{\xi\in R}\mathrm{pre}_\xi(\mathbb{X}) \subseteq \bigcap_{\xi\in\mathrm{vert}(R)}\mathrm{pre}_\xi(\mathbb{X})$.

Now, let $x \in \bigcap_{\xi\in\mathrm{vert}(R)}\mathrm{pre}_\xi(\mathbb{X})$. That means that for every vertex $\xi^{(i)}$ of R, there exist a $u^{(i)} \in U$ such that $f(x, u^{(i)}, \xi^{(i)}) \in \mathbb{X}$. Consider any $\xi \in R$. ξ can be written as a convex combination of the vertices of R, so that $\bar{\xi} = \sum_i \lambda^{(i)}\xi^{(i)}$ with $\sum_i \lambda_i = 1$ and $\lambda_i \geq 0\,\forall i$. We know that by convexity of U, $\bar{u} = \sum_i \lambda_i u^{(i)} \in U$ and $f(x, \bar{u}, \bar{\xi}) = \sum_i \lambda^{(i)} f(x, u^{(i)}, \xi^{(i)}) \in \mathbb{X}$

by convexity of $\mathbb{X}$. This proves that $x \in \text{pre}_{\bar{R}}(\mathbb{X})$ for all x so that $x \in \bigcap_{\xi \in R} \text{pre}_\xi(\mathbb{X})$. Hence, $\bigcap_{\xi \in \text{vert}(R)} \text{pre}_\xi(\mathbb{X}) \subseteq \bigcap_{\xi \in R} \text{pre}_\xi(\mathbb{X})$ which concludes the proof. □

Furthermore, under the same assumption, together with the convexity of the constraint set X, we have that the maximal invariant set for tracking is convex [115]. Armed with lemma 5.29, we can now compute invariant sets for tracking using 'usual' pre-set computation for affine systems, using a finite number of points, provided we can enumerate the vertices of the set R. This is particularly convenient when the reference has small dimension: it is the case in the reserve provision case where the reference has dimension one and therefore R has only two vertices.

Example 5.30. We compute the maximal invariant set for tracking for a linear system. We consider one of the room of the LADR experimental setup, as described in the next part in Section 7.3.2. Around an operating point, we would like to compute the maximum invariant set for tracking for a reference set R. The system has dimension 2 and we fix $R = [-r_{\max}; r_{\max}]$, we compute the maximal invariant set for tracking with output constraints $y = Cx \in [T_{\text{ref}} - \beta; T_{\text{ref}} + \beta]$, input constraints $u \in [0; P_{\max}]$ and tracking constraints $u - r \in [-\epsilon, \epsilon]$. By applying Algorithm 1 on page 95 adapted to the tracking case, we depict the result in Figure 5.8. In this instance, $T_{\text{ref}} = 23^o\text{C}$, $\beta = 2^o\text{C}$ and $r_{\max} = 0.27kW$. The computation assumes that the system is at steady state with an outside temperature of 0^oC and no sun.

□

5.8.2 An implicit characterization of control-invariant sets for tracking

The explicit computation of maximal invariant set for tracking as described in the previous section is only possible for small system dimensions. It is useful to have an implicit description of invariant sets. We make the following assumption:

Assumption 5.31. We consider the system

$$\begin{aligned} x^+ &= Ax + Bu \\ y &= Cx + D_u u + D_\xi \xi \end{aligned} \tag{5.67}$$

In addition, the tracking constraints are only active until time step N, or in other words $Y_t = \mathbb{R}^{n_y} \, \forall t \geq N$ ■

This assumption is tailored to the reserve provision context, where the system is subject to operational constraints captured in U and X and needs to commit reserves for tracking on a predefined period of time, and therefore has practical relevance.

Under assumption 5.31, we propose a solution that does not rely on the (often expensive) explicit computation of an invariant set. We introduce an implicitly defined terminal condition, which ensures infinite horizon feasibility. We follow the idea of [75], by enforcing that x_N is a feasible steady state of the system.

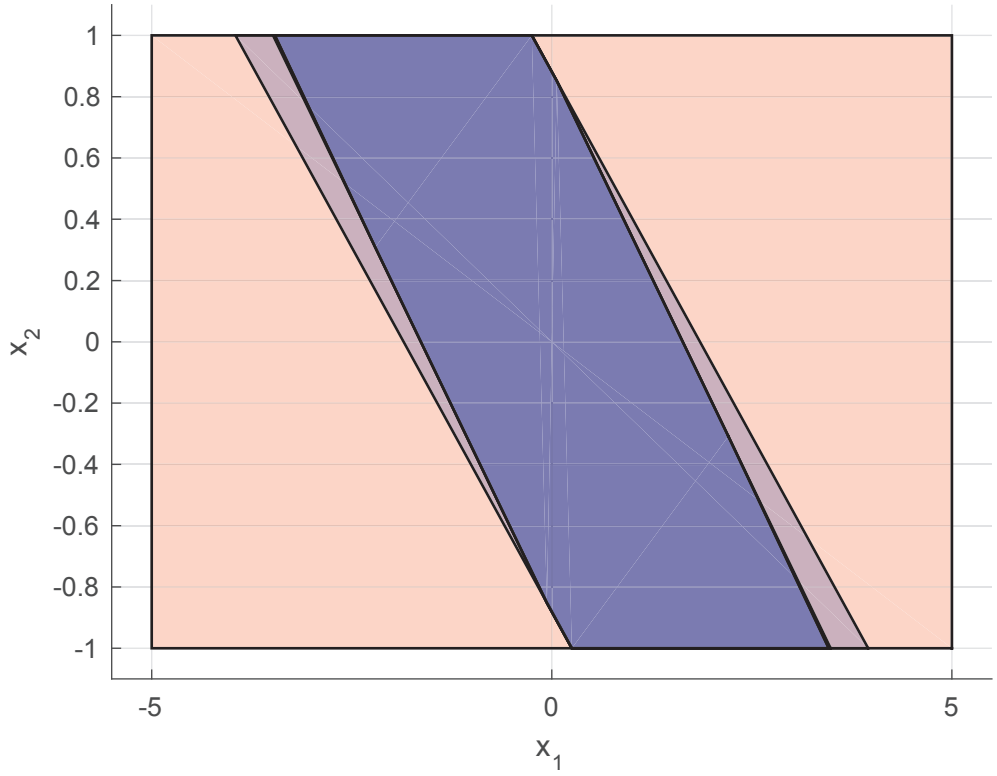

Figure 5.8 – The red region shows the state constraint set and the blue polyhedral regions depict the successive iterations of the algorithm computing the maximal invariant set for tracking for the system (4 iterations to termination)

It is easy to see that the set:

$$\mathbb{X}_{ss} = \{x \,|\, \exists u \in U : \; x = Ax + Bu \text{ and } x \in X\} \tag{5.68}$$

is an control-invariant set for the system.

Now, let us examine how to solve Problem 5.21 with $\mathbb{X}_f = \mathbb{X}_{ss}$ under assumption 5.31 and affine policies. We also define u_N as an affine function of the reference, so that $u_N = M_{ss}\boldsymbol{\xi} + m_{ss}$.

The equations $x_N \in X$ and $u_N \in U$ are additional robust inequalities and can be dealt with according to the developments of Section 5.4.1. The steady-state condition $x_N = Ax_N + Bu_N$ then remains. We have that x_N is an affine function of $\boldsymbol{\xi}$:

$$x_N = \bar{A}x_0 + \bar{B}\mathbf{M}\boldsymbol{\xi} + \bar{B}\boldsymbol{m}, \tag{5.69}$$

where $\bar{A} := A^N$, $\bar{B} := \begin{bmatrix} A^{N-1}B & \cdots & AB & B \end{bmatrix}$. The steady-state equation from (5.68)

yields:

$$\bar{A}x_0 + \bar{B}\mathbf{M}\boldsymbol{\xi} + \bar{B}\boldsymbol{m} = A(\bar{A}x_0 + \bar{B}\mathbf{M}\boldsymbol{\xi} + \bar{B}\boldsymbol{m}) + B(M_{ss}\boldsymbol{\xi} + m_{ss}) \quad \forall \boldsymbol{\xi} \in \Xi \tag{5.70}$$

If Ξ is full dimensional, then a necessary and sufficient for (5.70) is:

$$\begin{aligned} \bar{A}x_0 + \bar{B}\boldsymbol{m} &= A\bar{A}x_0 + A\bar{B}\boldsymbol{m} + Bm_{ss} \\ \bar{B}\boldsymbol{M} &= A\bar{B}\boldsymbol{M} + BM_{ss} \end{aligned}$$

which are linear equality constraints in the decision variables. We can simply augment the problem (5.41) with these to ensure infinite horizon constraint satisfaction.

Remark 5.32. In some applications, such as building control, it is preferable to keep the system in a periodic steady state, due to the periodic nature of the disturbances and constraints. The developments above directly extend to this case. □

5.8.3 Remarks on a receding horizon implementation

Once a set $\Xi_{:N-1}$ has been found by solving problem (5.61), we then assume it is fixed during operation. As in MPC, we will solve a similar problem in receding horizon where the uncertainty set is fixed. The only major concern is the time correlation in $\Xi_{:N-1}$. At time step t, we will have observed disturbance up to time $t-1$, denoted $\boldsymbol{\xi}_{0:t-1}$ (depending on the assumption on the information structure). As as consequence, we will solve a problem of the form:

$$\begin{aligned} \text{find} \quad & \boldsymbol{\pi} \\ \text{such that} \quad & \forall i \in \mathbb{Z}_{[t,t+N-1]} \\ & \forall \boldsymbol{\xi} \in \Xi(\boldsymbol{\xi}_{0:t-1}) \\ & \phi_i(x, \boldsymbol{u}, \boldsymbol{\xi}) \in X_i \\ & \phi_N(x, \boldsymbol{u}, \boldsymbol{\xi}) \in \mathbb{X}_f \\ & u_i = \pi_i(\boldsymbol{\xi}) \in U_i \\ & \boldsymbol{\pi} \in \mathcal{F} \end{aligned} \tag{5.71}$$

where $\Xi(\boldsymbol{\xi}_{0:t-1})$ is the set of all disturbances that can be observed over the next N steps and are consistent with the set Ξ optimized at the first iteration, more precisely:

$$\begin{aligned} &\Xi(\boldsymbol{\xi}_{0:t-1}) := R^N \text{ if } t \geq N \\ &\Xi(\boldsymbol{\xi}_{0:t-1}) := \left\{ (\xi_t, \dots, \xi_{t+N-1}) \;\middle|\; \begin{array}{l} (\boldsymbol{\xi}_{0:t-1}, \xi_t, \dots, \xi_{N-1}) \in \Xi_{:N-1} \\ \xi_i \in R \text{ for } N \leq t \leq t+N-1 \end{array} \right\} \text{ if } t < N \end{aligned} \tag{5.72}$$

Application of this receding horizon policy solves (5.61), i.e. ensures infintie horizon tracking in Ξ.

Remark 5.33. We can imagine re-optimizing the disturbance set while solving the receding

horizon problem. If a solution was found at the first iteration, problem (5.61) could be solved in receding horizon and would be recursively feasible, under some mild assumptions. Roughly speaking, the parametrization of the set at iteration $t+1$ should include the tail of the set obtained at iteration t. □

5.9 Summary and conclusion

We have formulated the robust tracking commitment problem in order to tackle the problem of reserve provision. It consists of a robust reachability problem where we also attempt to optimize over the uncertainty set. We propose to optimize the uncertainty set by defining it as the image of a fixed uncertainty set by a modifier function. By embedding the modifier function into the control policy, we show how to recover a more classical semi-infinite optimization problem, for which tractable instances are known. One particularity of our problem is that the uncertainty may be heterogeneous and observed at different time instants. This requires particular attention and motivated the introduction of information structures. Sufficient conditions were derived to ensure appropriate constraints on the policies in order to respect the information availability when taking decisions.

The method proposed is illustrated on a reserve provision problem, which also leads to the concept of virtual battery as a proxy to describe a load from the point of view of the electric power consumption flexibility. Finally, some solutions are provided in order to extend some of the ideas developed to the infinite horizon case, under specific assumptions.

In the next part, one of the objectives is to demonstrate the applicability and relevance of the approach developed in this chapter in a realistic experimental testbed.

Appendix

C Technical background

This appendix provides common definitions, and results used in this manuscript. For most of the results, references are provided for proofs.

C.1 Invariance

Invariance is a fundamental problem in control, and bears connection to many sub-fields of control theory.

Definition C.1. A set $\mathbb{X}_f$ is control-invariant for system $x^+ = f(x,u)$ with constraints $x \in X$ and $u \in U$ if:

$$\mathbb{X}_f \subseteq X \text{ and } \forall x \in \mathbb{X}_f, \exists u \in U : \; f(x,u) \in \mathbb{X}_f$$

■

A useful characterization of control-invariant sets uses the notion of pre-set defined as:

$$\begin{aligned} \text{pre}(\mathbb{X}) &:= \{x | \exists u \in U : f(x,u) \in \mathbb{X}\} = \text{Proj}_x \bar{\mathcal{Q}} \\ &\text{with } \bar{\mathcal{Q}} := \{(x,u) \,|\, f(x,u) \in \mathbb{X},\; u \in U\} \end{aligned} \tag{C.1}$$

and Proj_x denotes the projection on the x-subspace.

Lemma C.2. *A set $\mathbb{X}_f$ is control-invariant for system $x^+ = f(x,u)$ with constraints $x \in X$ and $u \in U$ if and only if:*

$$\mathbb{X}_f \in X \text{ and } \mathbb{X}_f \subseteq \text{pre}(\mathbb{X}_f)$$

Notice that if $\mathbb{X}_1$ and $\mathbb{X}_2$ are control-invariant then it is straightforward to see that $\mathbb{X}_1 \cup \mathbb{X}_2$ also is control-invariant. From that follows the existence of a 'maximal' control-invariant set that contains all control-invariant sets for the system. Computing this maximal control-invariant set is of particular interest since it represents all controllable states under the constraints. Unfortunately, computing maximal control-invariant sets is notoriously difficult. A method was proposed in [42] for autonomous systems but can be easily generalized to controlled systems. We give here a summary of the method.

Algorithm 1 Algorithm to compute maximal control-invariant set

$O_i \leftarrow X$
loop
  $O_{i+1} \leftarrow O_i \cap \text{pre}(O_i)$
  if $O_{i+1} = O_i$ **then**
    return $O_\infty = O_i$
  end if
end loop

Actual implementation of this algorithm requires the ability to compute the pre-set of a set, which involves the computation of intersection of sets and projections. Software packages are available to perform these operations such as [62], but they are computationally intensive and it is usually only possible to apply algorithm 1 in restricted dimensions, even for sets of simple form such as polytopes.

The definitions above extend to system subject to uncontrolled disturbances.

Definition C.3. A set $\mathbb{X}_f$ is robust controlled invariant for system $x^+ = f(x, u, \xi)$ subject to disturbance $\xi \in \Xi$ with constraints $x \in X$ and $u \in U$ if:

$$\mathbb{X}_f \subseteq X \text{ and } \forall x \in \mathbb{X}_f, \exists u \in U : \forall \xi \in \Xi,\ f(x, u, \xi) \in \mathbb{X}_f$$

■

The notion of maximal robust controlled invariant set can also be defined, as well as the equivalent of the pre-set for system subject to disturbances as:

$$\text{pre}^{\Xi}(\mathbb{X}) := \{x | \exists u \in U : \forall \xi \in \Xi,\ f(x, u, \xi) \in \mathbb{X}\} \tag{C.2}$$

Note that the characterization C.2 and the conceptual algorithm 1 extend to this case by simply replacing the pre-set definition by the robust pre-set one. Maximal robust controlled invariant sets can still be computed using this algorithm but complications arise very quickly. For example, as discussed in [119], pre-sets for linear system subject to state-dependent disturbance can be nonconvex, which complicates the problem drastically. An extension of the classic algorithm is proposed for a subclass of piecewise-affine systems, but complexity grows very quickly.

A detailed overview on set invariance is given in [16].

C.2 Farkas lemma

Farkas lemma is widely used in convex analysis.

Lemma C.4. *[166] Let $A \in \mathbb{R}^{m \times n}$ and $b \in \mathbb{R}^m$. Exactly one of the two systems:*

$$\{x \mid Ax = b,\ x \geq 0\} \text{ and } \left\{y \mid A^\top y \leq 0,\ b^\top y > 0\right\}$$

is feasible.

Another variant of the lemma reads:

Lemma C.5. *[166] Let $A \in \mathbb{R}^{m\times n}$, $b \in \mathbb{R}^m$, $a_0 \in \mathbb{R}^m$ and $b_0 \in \mathbb{R}$. Assume the polytope $\mathcal{P} = \{x \mid Ax \leq b, \}$ is nonempty. Then, $a_0^T x \leq b_0$ holds for all $x \in \mathcal{P}$ if and only if there exists $z \geq 0$ a row vector such that $zA = a_0$ and $zb \leq b_0$.*

Extending this to polytopic inclusion, we have that $\mathcal{P} \subseteq \{x \mid Cx \leq d, \}$ with $C \in \mathbb{R}^{p\times n}$ and $d \in \mathbb{R}^p$ if and only if there exists $Z \in \mathbb{R}^{n\times p}$ such that $Z \geq 0$, $ZA = C$ and $Zb \leq d$.

C.3 Robust Optimization

We present here the main results we will use that pertain to robust linear programming, following a presentation close to [8].

Let us introduce the following robust linear constraint:

$$c^\top \xi \leq b \quad \forall \xi \in \Xi \tag{C.3}$$

with

$$\Xi = \left\{\xi \mid F_i\xi + f_i \in \mathbf{K}_i,\ i \in \mathbb{Z}_{[1,m]}\right\} \tag{C.4}$$

where each $\mathbf{K}_i$ is a closed convex cone with nonempty interior. Note that, the considered class of uncertainty sets is quite extensive, as it allows the description of well known cones such as the non-negative orthant, the Lorentz cone and the positive semi-definite cone as well as their intersections and products.

Equation (C.3) is equivalent to

$$\max_{\xi\in\Xi} c^\top \xi \leq b \tag{C.5}$$

By dualizing the maximization problem using conic duality, introducing vector Lagrange multiplier vector $z_i \in \mathbf{K}_i^*$ the dual cone of $\mathbf{K}_i$, inequality (C.3) is equivalent to:

$$\begin{aligned} \exists z_i \in \mathbf{K}_i^* : \sum_i z_i^\top F_i &= -c^\top \\ \sum_i z_i^\top f_i &\leq b \end{aligned} \tag{C.6}$$

(C.6) is called the dual reformulation of (C.3). It consists of a finite number of convex inequalities and linear equalities, and only a limited number of extra variables have been introduced. For the proof, we refer the reader to [8], Theorem 1.3.4.

Extensions to this result have been studied in [8] and [41]. Assuming that the uncertainty set takes the form:

$$\Xi = \{\Lambda(\zeta) \,|\, \xi \in \Xi\} \tag{C.7}$$

with $\Lambda : \mathbb{R}^k \longrightarrow \mathbb{R}^{k'}$ a nonlinear lifting operator. If Ξ or its convex hull, denoted convh(Ξ), can be represented in conic form (C.4), then a dual reformulation like (C.6) can be formed. This is particularly useful to use nonlinear policies in the uncertainty. A list of tractable cases has been identified in the robust programming literature including quadratic lifting for ellipsoidal uncertainty sets, piecewise linear continuous lifting with box uncertainty sets, polynomial lifting with box uncertainty sets. The reader is referred to [8] and [41] for more details. Other works such as [13] propose mixed-integer reformulations for other types of lifting operators.

As an example of a tractable robust program with a lifted uncertainty set, we briefly summarize results from [8] showing that quadratic liftings can be handled with ellipsoidal uncertainty sets. Consider the ellipsoidal uncertainty set:

$$\Xi = \{\Lambda(\zeta) \mid \|\mathcal{T}\zeta\|_2 \leqslant 1\} \tag{C.8}$$

with $\mathcal{T}$ an invertible matrix and:

$$\Lambda(\zeta) = \begin{bmatrix} 1 & \zeta^T \\ \zeta & \zeta\zeta^T \end{bmatrix} \tag{C.9}$$

That is $\xi = \Lambda(\zeta)$ contains all products of components of ζ and therefore can be used to model quadratic policies in ζ. As shown in [8], the convex hull of the lifted uncertainty set Ξ is given by:

$$\text{convh}(\Xi) = \left\{ \xi = \begin{bmatrix} 1 & \zeta^T \\ \zeta & W \end{bmatrix} \;\middle|\; \xi \succeq 0,\ \text{tr}(\mathcal{T}W\mathcal{T}^T) \leqslant 1 \right\} \tag{C.10}$$

where $\xi \succeq 0$ means that ξ is a symmetric positive semi-definite matrix. This representation can be put in the standard conic form of (C.4), and therefore allows a tractable dual reformulation like (C.6). As an application example, in [164], the authors use quadratic liftings to find the largest volume inner approximations of polytope projections.

D Proofs and Derivations

D.1 Polytopic description of the feasibility set $\mathcal{Q}$

The dense form of the system equations (5.35), which describes the evolution of the system for N steps, is given by

$$\boldsymbol{x} = \mathbf{A}x_0 + \mathbf{B}_u\boldsymbol{u} + \mathbf{B}_\xi\boldsymbol{\xi}$$
$$\boldsymbol{y} = \mathbf{C}\boldsymbol{x} + \mathbf{D}_u\boldsymbol{u} + +\mathbf{D}_\xi\boldsymbol{\xi}$$

The matrices $\mathbf{A} \in \mathbb{R}^{Nn_x \times n_x}$, $\mathbf{B}_u \in \mathbb{R}^{Nn_x \times Nn_u}$, $\mathbf{B}_\xi \in \mathbb{R}^{Nn_x \times Nn_\xi}$, $\mathbf{C} \in \mathbb{R}^{Nn_y \times Nn_x}$, $\mathbf{D}_u \in \mathbb{R}^{Nn_y \times Nn_u}$ and $\mathbf{D}_\xi \in \mathbb{R}^{Nn_y \times Nn_\xi}$are defined as:

$$\mathbf{A} := \begin{bmatrix} A \\ A^2 \\ \vdots \\ A^N \end{bmatrix},\ \mathbf{B}_u = \mathbf{E} \otimes B_u,\ \mathbf{B}_\xi = \mathbf{E} \otimes B_\xi,\ \mathbf{C} := [I_N \otimes C\ \ \mathbf{0}],\ \mathbf{D} := I_N \otimes D$$

with

$$\mathbf{E} := \begin{bmatrix} I_{n_x} & 0 & \cdots & \vdots \\ A & I_{n_x} & \cdots & \vdots \\ \vdots & \vdots & \ddots & \vdots \\ A^{N-1} & A^{N-2} & \cdots & I_{n_x} \end{bmatrix}$$

The polytopic state, input and output constraint sets can be described as:

$$\mathcal{X} := \{\boldsymbol{\phi} \in \mathbb{R}^{Nn_x} : \mathbf{F}_x\boldsymbol{\phi} \leqslant \mathbf{f}_x\}$$
$$\mathcal{U} := \{\boldsymbol{u} \in \mathbb{R}^{Nn_u} : \mathbf{F}_u\boldsymbol{u} \leqslant \mathbf{f}_u\}$$
$$\mathcal{Y} := \{\boldsymbol{y} \in \mathbb{R}^{Nn_y} : \mathbf{F}_y\boldsymbol{y} \leqslant \mathbf{f}_y\}$$

The feasibility set $\mathcal{Q}$ also becomes polytopic and can be written as:

$$\mathcal{Q} = \{(\boldsymbol{u}, \boldsymbol{\xi}) \mid H\boldsymbol{u} + Q\boldsymbol{\xi} \leqslant q\}$$

with:

$$H := \begin{bmatrix} \mathbf{F}_x\mathbf{B}_u \\ \mathbf{F}_u \\ \mathbf{F}_y(\mathbf{C}\mathbf{B}_u + \mathbf{D}_u) \end{bmatrix}, \quad Q = \begin{bmatrix} \mathbf{F}_x\mathbf{B}_\xi \\ \mathbf{0} \\ \mathbf{F}_y(\mathbf{C}\mathbf{B}_\xi + \mathbf{D}_\xi) \end{bmatrix}, \quad q = \begin{bmatrix} \mathbf{f}_x - \mathbf{F}_x\mathbf{A}x_0 \\ \mathbf{f}_u \\ \mathbf{f}_y - \mathbf{F}_y\mathbf{C}\mathbf{A}x_0 \end{bmatrix}$$

where $\mathbf{0}$'s are matrices of zeros with proper dimensions.

D.2 Proofs for theorems of Section 5.3.1

Notation: Given a set of indices $\mathcal{J}$, let $\bar{\mathcal{J}}$ be the complementary of $\mathcal{J}$ in $\mathbb{Z}_{[1,n]}$. Denote m the cardinality of $\mathcal{J}$. As $x_\mathcal{J}$ denotes the entries of x indexed by $\mathcal{J}$, $\boldsymbol{\nu}_\mathcal{J}$ denotes the function from $\mathbb{R}^n$ into $\mathbb{R}^m$ formed by the outputs of $\boldsymbol{\nu}$ indexed by $\mathcal{J}$. Given $\mathcal{J}$, we also overload notation and denote $\boldsymbol{\nu}(x_\mathcal{J}, x_{\bar{\mathcal{J}}})$ to make explicit the respective dependency of $\boldsymbol{\nu}$ on $x_\mathcal{J}$ and $x_{\bar{\mathcal{J}}}$. Accordingly, denote $\boldsymbol{\nu}(x_\mathcal{J}, .)$ the restriction of $\boldsymbol{\nu}$ to $\{x_\mathcal{J}\} \times \mathbb{R}^{n-m}$.

Proof of Lemma 5.13. Consider two information structures $\mathcal{I}_1$ and $\mathcal{I}_2$. Suppose $f \in \mathcal{F}(\mathcal{I}_1), \mathcal{F}(\mathcal{I}_2)$. Let x, x' be such that $x_{\mathcal{I}_1\cap\mathcal{I}_2} = x'_{\mathcal{I}_1\cap\mathcal{I}_2}$. Choose y such that $y_{\mathcal{I}_1} = x_{\mathcal{I}_1}$ and $y_{\mathcal{I}_2} = x'_{\mathcal{I}_2}$ (this is possible because $x_{\mathcal{I}_1\cap\mathcal{I}_2} = x'_{\mathcal{I}_1\cap\mathcal{I}_2}$). Since $f \in \mathcal{F}(\mathcal{I}_1)$, we have that $f(x) = f(y)$. Similarly, $f \in \mathcal{F}(\mathcal{I}_2)$ implies that $f(x') = f(y)$. Together this gives $f(x) = f(y) = f(x')$ for all x, x' such that $x_{\mathcal{I}_1\cap\mathcal{I}_2} = x'_{\mathcal{I}_1\cap\mathcal{I}_2}$ *i.e.* $f \in \mathcal{F}(\mathcal{I}_1 \cap \mathcal{I}_2)$. Noticing that $\bigcap_k \mathcal{I}_k = \mathcal{I}_1 \cap (\bigcap_{k\neq 1} \mathcal{I}_k)$, it is straightforward to extend the argument above to the intersection of finitely many information structures. □

Proof of Lemma 5.14. By convention, $\hat{\mathcal{I}}_k = \mathbb{Z}_{[1,n]}$ if $\{i | k \in \mathcal{I}_i\}$ is empty.
Direction $\Longleftarrow$: Assume $\boldsymbol{g} \in \mathcal{F}(\hat{\mathcal{I}})$. Consider $(x, \hat{x})$ such that $x_{\mathcal{I}_j} = x'_{\mathcal{I}_j}$ and $\boldsymbol{f} \in \mathcal{F}(\mathcal{I})$. Let us prove that $\boldsymbol{f} \circ \boldsymbol{g}(x) = \boldsymbol{f} \circ \boldsymbol{g}(x')$. Let us denote $y = \boldsymbol{g}(x)$ and $y' = \boldsymbol{g}(x')$. Let us consider any $k \in \mathcal{I}_j$. Then according to equation (5.28), we have $\hat{\mathcal{I}}_k \subseteq \mathcal{I}_j$ and hence $x_{\hat{\mathcal{I}}_k} = x'_{\hat{\mathcal{I}}_k}$. In turn this implies $y_k = y'_k$ by definition of $\mathcal{F}(\hat{\mathcal{I}})$. Since this holds for all $k \in \mathcal{I}_j$, it holds that $y_{\mathcal{I}_j} = y'_{\mathcal{I}_j}$ and therefore $\boldsymbol{f} \circ \boldsymbol{g}(x) = \boldsymbol{f}(y) = \boldsymbol{f}(y') = \boldsymbol{f} \circ \boldsymbol{g}(x')$ since $\boldsymbol{f} \in \mathcal{F}(\mathcal{I})$.
Direction $\Longrightarrow$: Assume $\boldsymbol{g} \notin \mathcal{F}(\hat{\mathcal{I}})$. There exists an index j such that $g_j \notin \mathcal{F}(\hat{\mathcal{I}}_j)$. Since $\hat{\mathcal{I}}_j = \bigcap_{\{i|j\in\mathcal{I}_i\}} \mathcal{I}_i$ we can use Lemma 5.13 to conclude that there exists i such that $g_j \notin \mathcal{F}(\mathcal{I}_i)$ and $j \in \mathcal{I}_i$. (The intersection is non-empty since if it was then $\hat{\mathcal{I}}_j = \mathbb{Z}_{[1,n]}$, which contradicts the possibility that $g_j(x) \neq g_j(x')$). Then there exist x and x' such that $x_{\mathcal{I}_i} = x'_{\mathcal{I}_i}$ and $g_j(x) \neq g_j(x')$. Consider the function $\boldsymbol{f}$ defined as follows: $\forall k \neq i$, f_k is identically 0. This trivially implies $f_k \in \mathcal{F}(\mathcal{I}_k)$ no matter what $\mathcal{I}$ is. Define f_i as:

$$\begin{cases} f_i(y) = 1 \text{ if } y_j = g_j(x') \\ f_i(y) = 0 \text{ otherwise} \end{cases}$$

Consider y, y' such that $y_{\mathcal{I}_i} = y'_{\mathcal{I}_i}$. Since $j \in \mathcal{I}_i$, we have $y_j = y'_j$ and hence $f_i(y) = f_i(y')$. Therefore $f_i \in \mathcal{F}(\mathcal{I}_i)$ and $\boldsymbol{f} \in \mathcal{F}(\mathcal{I})$. However, $f_i \circ \boldsymbol{g}(x) = 0$ and $f_i \circ \boldsymbol{g}(x') = 1$ by definition of f_i. Putting everything together, we can conclude that $x_{\mathcal{I}_i} = x'_{\mathcal{I}_i}$ and $\boldsymbol{f} \circ \boldsymbol{g}(x) \neq \boldsymbol{f} \circ \boldsymbol{g}(x')$, therefore $\boldsymbol{f} \circ \boldsymbol{g} \notin \mathcal{F}(\mathcal{I})$. □

Proof of Lemma 5.15. $\mathcal{G} \subseteq \mathcal{F}(\mathcal{I})$: It directly follows from Lemma 5.14.

$\mathcal{F}(\mathcal{I}) \subseteq \mathcal{G}$: Consider $\boldsymbol{g} \in \mathcal{F}(\mathcal{I})$. Showing that there exists $\boldsymbol{f} \in \mathcal{F}(\mathcal{I})$ such that $\boldsymbol{g} = \boldsymbol{f} \circ \boldsymbol{\nu}$ is equivalent to showing that $\boldsymbol{f} = \boldsymbol{g} \circ \boldsymbol{\nu}^{-1} \in \mathcal{F}(\mathcal{I})$ ($\boldsymbol{\nu}$ is a bijection). It is done by contradiction. Suppose $\boldsymbol{f} \notin \mathcal{F}(\mathcal{I})$. This means that for some k, $f_k \notin \mathcal{F}(\mathcal{I}_k)$. To lighten notation, let $\mathcal{I}_k = \mathcal{J}$. There exist y, y' such that $y_{\mathcal{J}} = y'_{\mathcal{J}}$ and $f_k(y) \neq f_k(y')$. By definition of $\hat{\mathcal{I}}$, $\boldsymbol{\nu}_{\mathcal{J}}$ cannot depend on elements of $\bar{\mathcal{J}}$, *i.e.* $x_{\mathcal{J}} = x'_{\mathcal{J}} \implies \boldsymbol{\nu}_{\mathcal{J}}(x) = \boldsymbol{\nu}_{\mathcal{J}}(x')$. Fix $x \in \mathbb{R}^n$. We divide the remainder of the proof in intermediate steps for clarity.

Bijectivity of $\boldsymbol{\nu}_{\mathcal{J}}(., x_{\bar{\mathcal{J}}})$: Notice that $\boldsymbol{\nu}_{\bar{\mathcal{J}}}(x_{\mathcal{J}}, .)$ is injective in $\mathbb{R}^{n-m}$ since $\boldsymbol{\nu}$ is injective. Denoting $V(x_{\mathcal{J}}) = \boldsymbol{\nu}_{\bar{\mathcal{J}}}(x_{\mathcal{J}}, \mathbb{R}^{n-m})$, by continuity of $\boldsymbol{\nu}$, $V(x_{\mathcal{J}})$ is an open set. By injectivity of $\boldsymbol{\nu}$, if $\boldsymbol{\nu}_{\mathcal{J}}(x) = \boldsymbol{\nu}_{\mathcal{J}}(x')$ with $x_{\mathcal{J}} \neq x'_{\mathcal{J}}$, then $V(x)$ and $V(x')$ are disjoint. By surjectivity of $\boldsymbol{\nu}$, it also holds that $\cup_{\{x'_{\mathcal{J}} | \boldsymbol{\nu}_{\mathcal{J}}(x_{\mathcal{J}}, x_{\bar{\mathcal{J}}}) = \boldsymbol{\nu}_{\mathcal{J}}(x'_{\mathcal{J}}, x_{\bar{\mathcal{J}}})\}} V(x'_{\mathcal{J}}) = \mathbb{R}^{n-m}$. Since $\mathbb{R}^{n-m}$ is connected, it cannot be covered by a non-trivial union of disjoint open sets, which implies that $\{x'_{\mathcal{J}} | \boldsymbol{\nu}_{\mathcal{J}}(x_{\mathcal{J}}, x_{\bar{\mathcal{J}}}) = \boldsymbol{\nu}_{\mathcal{J}}(x'_{\mathcal{J}}, x_{\bar{\mathcal{J}}})\}$ is reduced to $\{x_{\mathcal{J}}\}$, which in other words means injectivity of $\boldsymbol{\nu}_{\mathcal{J}}(., x_{\bar{\mathcal{J}}})$.
Surjectivity of $\boldsymbol{\nu}_{\mathcal{J}}(., x_{\bar{\mathcal{J}}})$ directly follows from the surjectivity of $\boldsymbol{\nu}$. Indeed, $\forall y \in \mathbb{R}^m$ there exist x' such that $\boldsymbol{\nu}_{\mathcal{J}}(x') = y$. Then $\boldsymbol{\nu}_{\mathcal{J}}(x'_{\mathcal{J}}, x_{\bar{\mathcal{J}}}) = y$. Together, this proves the bijectivity of $\boldsymbol{\nu}_{\mathcal{J}}(., x_{\bar{\mathcal{J}}})$ for all $x_{\bar{\mathcal{J}}}$.

Bijectivity of $\boldsymbol{\nu}_{\bar{\mathcal{J}}}(x_{\mathcal{J}}, .)$: Injectivity directly follows from the injectivity of $\boldsymbol{\nu}$. For $x_{\mathcal{J}}$ fixed, by injectivity of $\boldsymbol{\nu}_{\mathcal{J}}(., x_{\bar{\mathcal{J}}})$ there does not exist any other $x'_{\mathcal{J}}$ such that $\boldsymbol{\nu}_{\mathcal{J}}(x_{\mathcal{J}}, x_{\bar{\mathcal{J}}}) = \boldsymbol{\nu}_{\mathcal{J}}(x'_{\mathcal{J}}, x_{\bar{\mathcal{J}}})$. Therefore, surjectivity of $\boldsymbol{\nu}$ implies that $\boldsymbol{\nu}_{\bar{\mathcal{J}}}(x_{\mathcal{J}}, \mathbb{R}^{n-m}) = \mathbb{R}^{n-m}$, *i.e.* surjectivity of $\boldsymbol{\nu}_{\bar{\mathcal{J}}}(x_{\mathcal{J}}, .)$.

Contradiction : Consider $x_{\mathcal{J}}$ such that $\boldsymbol{\nu}_{\mathcal{J}}(x_{\mathcal{J}}, x_{\bar{\mathcal{J}}}) = y_{\mathcal{J}}$. Bijectivity of $\boldsymbol{\nu}_{\mathcal{J}}(., , x_{\bar{\mathcal{J}}})$ ensures its existence. In turn, bijectivity of $\boldsymbol{\nu}_{\bar{\mathcal{J}}}(x_{\mathcal{J}}, .)$ ensures that there exists $x_{\bar{\mathcal{J}}}, x'_{\bar{\mathcal{J}}}$ such that $\boldsymbol{\nu}_{\bar{\mathcal{J}}}(x_{\mathcal{J}}, x_{\bar{\mathcal{J}}}) = y_{\bar{\mathcal{J}}}$ and $\boldsymbol{\nu}_{\bar{\mathcal{J}}}(x_{\mathcal{J}}, x'_{\bar{\mathcal{J}}}) = y'_{\bar{\mathcal{J}}}$. Combining the results above gives $\boldsymbol{\nu}(x_{\mathcal{J}}, x_{\bar{\mathcal{J}}}) = y$ and $\boldsymbol{\nu}(x_{\mathcal{J}}, x'_{\bar{\mathcal{J}}}) = y'$. Then, $g_k(x) = f_k \circ \boldsymbol{\nu}(x) = f_k(y)$ and similarly $g_k(x') = f_k \circ \boldsymbol{\nu}(x') = f_k(y')$. Finally, this shows that $g_k(x) \neq g_k(x')$ which implies $g_k \notin \mathcal{F}(\mathcal{I}_k)$. this contradicts the assumption that $\boldsymbol{g} \in \mathcal{F}(\mathcal{I})$. Finally, this confirms that $\boldsymbol{f} \in \mathcal{F}(\mathcal{I})$. □

Part III

Experiments with Laboratoire d'Automatique Demand Response

6 Introduction and literature review

6.1 Introduction

Following the developments of the previous part, an experimental demonstration of this work has been planned has led to the definition and implementation of the Laboratoire d'Automatique Demand Response Testbed (LADR). The platform was designed to serve as a validator for building control methods developed in the lab and has been built by a group of students including myself, Faran Qureshi, Altuğ Bitlislioğlu and Luca Fabietti. All important aspect of the platform development are briefly described in this chapter. A stronger emphasis is put on aspects that I personally contributed most to.

The first part of this chapter introduces the terminology and the literature related to the experimental implementation of ancillary services and Demand Response, in particular using building HVAC systems.

6.2 State of the art and nomenclature

6.2.1 Overview and terminology

This subsection introduces some common terminology, and delineates traditional categorizations coming under the umbrella of demand-side management. There is a large array of services that loads can provide to the power grid. From the point of view of control, they mostly differ by the timescales involved, both in terms of the duration of the service provided and the time response required to offer these. Slow services, on timescales ranging from hours to days, include peak shaving, energy dispatch, *etc.*The mechanisms of activation of the loads are usually classified in two categories: direct load control and price-based control. In the former, the authority organizing the service directly controls the resource or sends commands to the system. In the latter, the operator of the service sends an incentive to the resource, most of the time under the form of a price, and the participants

choose to react to the price signal by adapting their power consumption how they see fit. Historically, both types of systems have coexisted in energy markets. The dominant trend is that services on slow timescales are price-based, and often procured in financial markets. The best known example is the bulk energy market, structured in the form of day-ahead and intraday markets. On the other hand, services on fast time scales usually require some form of direct load control. Indeed, fast and precise actuation does not easily accomodate mechanisms based on price since automating response to such signals is not straightforward. Citing [20]:

> We will not consider price response as a mechanism for achieving fully responsive nondisruptive control for several reasons. First, electricity markets do not presently clear on time scales faster than 5 min. Consequently, price signals are not used for fast services such as regulation and spinning reserve on the supply side. (We note that the 5-min threshold between price-based and nonprice-based load response dates back at least as far as the seminal work of Schweppe et al. in 1980 [47]). Second, having direct control over loads increases the system operator's ability to predict the loads' responses (though price response forecasts certainly are possible) and provides third-party aggregators certainty over how much capacity they can bid into ancillary service markets [43]. Finally, customers, especially small ones, may be disinterested in (or incapable of) identifying their own demand curve (i.e., instantaneous quantity responsiveness as a function of real-time price) if their objective is to receive a service that is a function of energy use over time (e.g., thermal comfort) rather than instantaneous consumption.

For example, secondary frequency control usually takes the form of a power consumption tracking task, a direct form of control.

The literature also studies the adequacy of specific types of devices for providing grid services. Particular features of appliances make them more or less apt for providing the service needed. Characteristics of interest include rated power, ramp rates, continuous or on/off nature of the power consumption, time constants, ability to store energy, communication requirements, *etc.*Most commonly studied resources to provide grid services are batteries, plugin hybrid electric vehicles (PHEVs)[145], Thermal Controllable Loads (TCLs)[70], which include fridges, electric boilers, heat pumps. Building heating, ventilation and air conditioning equipment (HVAC)[55] are also studied but are somewhat different since they might combine different equipment with various characteristics. The reference [106] gives guidelines to decide what type of service a particular resource could be suitable for, and discusses the aforementioned type of systems. [163] outlines the peculiariry of commercial HVAC systems:

> The tested demand side resources can be categorized into three groups: (1) Energy storage. It includes storage for electricity (e.g., battery and flywheel) and thermal storage (e.g., water heater and ceramic storage). (2) Heating systems

> (e.g., electric boilers and resistance heaters). (3) Independent systems with variable frequency drives (e.g., wastewater treatment pumps). However, these tested systems are all independent systems (i.e., there are no interdependencies with other related systems when providing frequency regulation(FR)). Therefore, these systems do not require sophisticated controls and are easy to implement. The commercial building HVAC systems; however, have many interdependent subsystems and many forms of capacity limits to manage when providing FR.

Note that loads considered for grid services are usually small to medium size and therefore this calls for an aggregation scheme, which is another major direction in the literature [40, 44]. The goal of aggregation is to harvest the potential of a large number of loads and control these loads simultaneously to provide the service required. Literature on aggregation looks at combining a large number of identical or similar loads, but can also look into combining completely heterogeneous loads to benefit from different types of resources. Literature on finding interesting synergies between different types of providers is relatively scarce, but represents a promising avenue of research. An interesting example in this regard is the business model of the swiss company *Tiko*[1], the only company to date that offers secondary frequency control service in the Swiss market with residential loads. *Tiko* controls a population of heat pumps and electric boilers whose start and stop times can be shifted during the night, in order follow the power consumption requests. The main source of revenue of *Tiko* comes from a contractual agreement with hydroelectric dam operators that wish to participate in secondary control. Participation in secondary frequency control requires some level of energy production from the dams, which they wish to obviate during nighttime. It is hence advantageous for them to have *Tiko* provide the baseline and tracking service during the night while they cover it during daytime.

6.2.2 Ancillary services with loads

In this section, we focus specifically on provision of ancillary services with loads. Frequency regulation mechanisms take different forms in different regions but mostly rely on the same underlying principles. Different works across the control, building systems and power systems communities deal with the use of demand side resources for frequency regulation. We outline here the most significant works from our point of view and identify common trends and challenges that have been discussed in the literature and support our research directions. As discussed in [20], one of the challenges of demand side resources for frequency regulation is that the loads are (in most cases) not primarily aimed at providing this service and must therefore make sure that they maintain an appropriate quality of service while providing frequency regulation to the grid. Citing [20]

> The primary characteristic of load control that distinguishes it from conventional generation-based approaches is that it must deliver a reliable resource to

[1] https://tiko.ch/

> the power system while simultaneously maintaining a level of service commensurate with customer expectations. These two objectives are often in competition, and one of the greatest technical challenges to the competitiveness of engaging loads in power system services is to develop approaches that balance these objectives [1].

Modeling of the operating constraints of loads can prove challenging, especially in the case of buildings where multiple subsystems are interacting. A widely observed characteristic is the limited storage capacity of loads, meaning that their ability to store or release energy over extended periods of time is constrained by physical limitations. The most obvious example of that is an electric battery (or other types of storage technologies), where the energy storage capacity is a defining characteristic and contributes largely to the price of the device (the reader is referred to [65] for estimates of price of batteries as a function of power rating and storage capacity). Similarly, it is quite natural to also think of thermal systems as storage systems where the difference between the thermal state of the system with respect to a desired state reflects an energy state of charge (for example, the temperature of the water in a reservoir). The work [56] actually models a population of TCLs with a single state battery model. It gives upper-bounding and lower-bounding 'equivalent' batteries for the feasible set of the population of TCLs.

The limited capacity storage has early been identified as an obstacle for the integration of loads in regulation provision, despite their superior capabilities in terms of tracking (they usually can support higher ramp rates than traditional generation). Citing the FERC order 755:

> The commission finds that the current frequency regulation compensation practices of RTOs and ISOs result in rates that are unjust, unreasonable, and unduly discriminatory or preferential. Specifically, current compensation methods for regulation service in RTO and ISO markets fail to acknowledge the inherently greater amount of frequency regulation service being provided by faster-ramping resources. In addition, certain practices of some RTOs and ISOs result in economically inefficient economic dispatch of frequency regulation resources.

As explained in [163], the FERC has imposed a pay-for-performance criterion to the power operators. The Pennsylvania-New Jersey-Maryland Interconnection (PJM) has for example chosen to decompose its regulation signal in two components, one favouring slow ramping units (regA) and another fast ramping units (regD), to increase penetration of storage systems and demand-side resources in the market. This measure has directly favoured the penetration of load-side resources in regulation procurement and propelled PJM as a leader in that domain.

6.2.3 Ancillary services with buildings

The procurement of regulation services to the grid with building systems has attracted increasing attention in research, as some markets are opening up to consumers. Two main focuses can be found in the literature. A number of theoretical papers have focused on the formal computation of the reserve size that can be offered by a resource or a pool of reserves. A detailed review of these works is done in part II, see in particular Section 5.2.5. These works do not necessarily restrict the analysis to buildings, but they often take as examples building systems. We review here experimental and 'realistic' simulation works focusing on building HVAC system control and discussing practical challenges related to their implementation.

[163] proposes two methods to inject the regulation signal in either the fan duct pressure or the zone temperature setpoint (which indirectly influences the consumption of the fan). Detailed simulation is performed and the interaction between components is analyzed. Results show that the setpoint modulation works better despite a more sluggish response. [141] showcases the control of the variable speed compressor of a commercial HVAC chiller. Control of the system is achieved through manipulation of the cooling water setpoint temperature. The regulation signal is filtered in order to achieve energy neutrality over a 10 minute average. Despite this, the performance of the tracking controller is good enough to meet the requirements of PJM for the tracking signal regD, which is designed for energy neutrality over longer periods of time. In this study, only the chiller power consumption was monitored, so the effect of this strategy on the overall power consumption is not measured, but potential side effects are discussed in [140]. It is identified that the variation of the chiller load will induce transient variations in the coefficient of performance of the equipment but that can be dealt with with a properly tuned controller. The average COP on the other hand will remain the same, therefore not deteriorating the overall performance of the system. Moreover, induced variations in the pump power consumption should be minimal while the fan will be impacted more significantly, with some delay making it more difficult to compensate for. [78] studies the use of fans for frequency regulation. It is demonstrated that fans offer a satisfactory performance for power modulation in the frequency band $[(1/10\text{min}; 1/30\text{sec})]$. The frequency band is limited in that way to ensure that the effect on occupants is limited and that the fan modulation does not impact the chillers. A common difficulty arising in these works is the difficulty to model short term changes in the power consumption of the full HVAC system, in particular the interaction between different components. In addition, in the absence of a model of the effect of the modulation on the zone temperature, a choice is made to keep the impact on the zone temperature minimal, which then reduces the ability to exploit the thermal storage of the building itself. Only the inertia of the heating system itself is exploited, which may be very small and therefore does not allow to cover for deviations whose frequency content is larger than 10 minutes.

Recent works [151] and [150] explore frequency regulation on an experimental testbed: the testbed is equipped with a central cooling system and a VAV box. A three level control architecture is used: a scheduler determines the reserve capacity for the next day, an MPC

controller is used for supply air temperature control and a tracking controller is used to control the fans at high speed and provide the regulation. Such a hierarchical controller structure is necessary due to the interacting timescales. The scheduler solves a nonlinear robust optimization problem by considering the extreme cases of the uncertainty. On the intermediate level, an MPC controller makes sure to choose the supply air mass flow rate appropriately by solving a problem similar to the scheduling problem but with fixed reserves. A low-level switched controller controls the fan speed, based on the characteristic curve of the fan and fine adjustments made through a proportional integral controller. Details of the results and implementation is given in [151].

6.3 Motivation and goals

Based on the previous literature overview, common characteristics and issues appear in relation to ancillary services provision with buildings:

- Slow and fast interacting timescales
- Determination of a baseline consumption
- Significant modeling effort

While going through these aspects, we will see how they relate to our work and how we are set to tackle them in our own experimental work.

6.3.1 Slow and fast interacting timescales

While the provision of ancillary services is a service that requires fast responses of the providers and continuous service, the market is cleared on a slow timescale: the fastest timescale is below the second, whereas the ancillary services market is usually cleared on a daily basis (even weekly in the current Swiss regulation). This has a number of consequences that guide the design of controllers for ancillary services. First of all, a hierarchical structure of the controller appears natural. A basic architecture requires at least two layers: A reserve scheduler runs at a slow frequency and decides the amount of reserve to engage for the upcoming time period (say one day), and possibly the baseline power consumption. In the lower layer, a fast controller chooses the inputs of the heating system in order to meet the tracking requirement in real time. A two-level architecture is sufficient for model-free methods, such as in [78]. Schematically, a heuristic method can be used to determine the regulation capacity offered at the upper level and the fast controller modulates the equipment inputs to provide tracking. This is particularly appropriate if a single piece of equipment equipment is used to provide the tracking, such as the fan in [78]. On the other hand, it has several drawbacks: designing a good fast controller for a complex system with multiple interacting subsystems (as is typical for an HVAC system) is difficult. The fast timescale makes the recourse to optimal control difficult and the fast controller would typically take the form of a simple PI-tracking controller which could lead the system away

from optimal operation. Even in the case of a single actuator or equipment providing the tracking service, it might be that the scheduler needs to take conservative margins in order to ensure that the fast controller does not violate operational constraints while tracking.

We propose to use a three layer architecture in our work in [33] and [47] (cf figure 7.10). The reserve scheduler remains unchanged, but a second layer that we call optimal planning is added in order to update the plan of operation at a frequency of 15 minutes, and passes down setpoints to the lower level controller around which to operate. In a three-level architecture, the upper (regulation scheduling) layer still decides the amount of regulation provided based on current state and forecasts for the system. A tracking controller still operates at the fastest timescale to adapt the power consumption in real time. An additional layer operates at an intermediate timescale (typically 15 minutes). This layer has the opportunity to reschedule the operating point of the system based on updated forecasts and can accommodate a model-based controller to achieve optimal operation. We will see that the middle layer can for example naturally take care of baseline rescheduling through intraday market trades.

6.3.2 The baseline consumption

A central issue of having loads participate in DR is the concept of a baseline power consumption. The baseline power consumption should intuitively be the power consumption a unit would have experienced if it was not providing a particular DR service. Supposing the service consists of changing the power consumption of a power unit over time, it is necessary to know with respect to what power consumption the tracking performance should be measured. Depending on the type of service provided, the precision and speed required and the particular market, different approaches are adopted. The most unambiguous solution is to have the unit announce in advance what its power consumption would be if no regulation service is provided, a scenario sometimes referred to as 'full dispatchability' [132]. While being clearly defined, this method is not always applied because:

- It increases the operational burden of participation: units have to commit their baseline consumption on a regular basis, which also typically needs to be automated.
- The predictability of units may not be total, in particular it may rely on other uncertain factors such as weather. In this case, the unit should include an additional margin in order to be able to accommodate for its own uncertainty. In addition, small systems are typically subject to larger uncertainties, at least proportionally to their size. If combining a large number of small units together helps reducing their associated uncertainty, it can be expected that the errors on the individual predictions are correlated, especially when they depend on exogeneous information such as weather forecasts.

In our experiments, we have considered that the baseline is announced in advance as a result of energy purchases on the intraday and day-ahead markets. This choice was made for the following reasons:

- It is the rule for participation to ancillary services in Switzerland, as of now. The largest difference that was introduced in our simulation and experiment of secondary frequency control is that the bidding is performed on a daily basis instead of a weekly basis due to the unpredictability of loads on such a long timescale. It is expected that this particular rule of the market will be made more flexible in coming years.

- This rule is relatively stringent and requires a good predictability of the unit. Success in implementing this rule suggests that compliance with more 'relaxed' regulatory frameworks should be easily achievable

Nevertheless, other approaches have been proposed and implemented. As was discussed in detail in our work [113], demand response programs adopt a more flexible approach in order to limit overall complexity. Rules to compute the baseline consumption a posteriori are sometimes provided. As an example, The New-York ISO day-ahead demand response program proposes to compute the baseline based on the power consumption of previous 'similar' days preceding a demand response event participation. The California Edison ISO also takes into account the temperature prediction the day preceding the participation day in the computation of its DR baseline rule.

For frequency regulation, several methods relying on timescale separation have been proposed and experimented. Works [141] and [78] propose to track signals whose bandwidth is pre-limited through filtering. Only fast frequencies are considered for tracking. The baseline is then computed a posteriori by filtering the final power consumption keeping only frequencies lower than the lowest of the tracking signal. While this does not correspond to the actual market rules, these works are based on the PJM ancillary services market where the baseline consumption is the result of the real-time market clearing which is difficult to emulate. In [163], the baseline is computed online as the output of a slow controller that chooses the cooling water setpoint so that the chiller works at a favorable coefficient of performance. The baseline is therefore decided online. The treshold of 10 minutes was chosen so as to keep the baseline close to the level decided by the slower controller and hence maintain a good coefficient of performance, as well as to limit the impact of this control on the other components in the system. Interestingly, it is reported that despite having to filter the regulation signal, a sufficient quality of tracking was achieved according to the PJM tracking quality criteria.

Finally, a related topic to the one of the baseline consumption is metering which goes far beyond the scope of this work. We will simply report here our assumptions without discussing extensively their practical implications. It is assumed that a unit participating in a given service is equipped with its own metering unit. This means that if the unit considered is the heating system of a building, it is metered separately from the rest of the building electric consumption. This is assumed for simplicity and is often not too restrictive since the rest of the power consumption could possibly be predicted quite accurately. A corollary assumption to this one is that the unit considered should be independent of other neighboring systems. This implies that the totality of the heating system should typically

be considered if it includes interacting subsystems. This particular topic is the subject of extended discussion in [141], [77], [163], among others.

6.4 The Swiss energy market

The experiments performed on the LADR platform considers the regulations of the Swiss ancillary service market. We give here an overview of ancillary services and in particular of the Swiss AS market, both from the technical and financial point of view to introduce the reader who is not familiar with these concepts. The references [142, 126, 122] have been used to write this section.

Energy in Switzerland is traded day-ahead in the European integrated wholesale market, EPEX SPOT, grouping France, Germany, Britain, Switzerland, Austria, Belgium, the Netherlands and Luxembourg. EPEX manages the trading of energy and cross border exchanges between countries. In each country, the Transmission System Operator (TSO) is responsible for the safe operation of the system and the delivery of energy according to plan. In Switzerland, the TSO is SwissGrid.

Energy is traded on the day-ahead market for each hourly slot everyday for the following day. Bids are collected from participants until 12:00 on day D for each hourly slot on day D+1. Following market clearing, EPEX publishes the index of prices for the next day. Following that publication, one hour or 15 minute slots can be traded on the intraday market. Each hour, 15-minute periods or block of hours can be traded until 60 minutes before delivery. Starting at 3pm on the current day, all hours of the following day can be traded. Starting at 4pm on the current day, all 15-minute periods of the following day can be traded.

That covers the energy trading part but does not suffice to ensure proper operation of the grid since power consumption and generation cannot be predicted perfectly and forecasting errors will cause discrepancies between real-time and scheduled operation. The power consumption and generation need to be balanced very quickly in order to maintain safe operating conditions for the transmission system. To cover imbalances, the TSO contracts a number of resources for different services called *ancillary services* (AS). [122] reviews technical characteristics of ancillary services across different European markets while the companion paper [123] focuses on the economic aspects.

Frequency control is one of the categories of ancillary services, and is designed to maintain the frequency of the system at the nominal 50 Hz. The deviation of the frequency is precisely a measure of the imbalance between production and consumption across the network, so that a frequency below 50 Hz indicates a production shortage and a frequency above 50 Hz indicates a production surplus. Frequency control is divided into three categories, namely primary, secondary and tertiary frequency control, for which we give a description focused on the Swiss case. The reference [30] gives a detailed overview of ancillary services in North America and Europe.

6.4.1 Primary frequency control

For a steady-state frequency deviation δf from the nominal frequency, a generator participating in primary control will change its generation by δP. The droop of the generator, which is the gain of the feedback loop in the primary frequency controller, is then defined as:

$$s_G = -(\delta f / f_n)/(\delta P / P_n) \tag{6.1}$$

where P_n is the nominal output power. Primary control is in essence a decentralized proportional control scheme that relies on the measurement of the frequency available everywhere. To avoid jittering, the droop control is only active when the frequency deviation comes out of an insensitivity band ($\pm$20mHz in Switzerland). Primary frequency control should be fully active after 30 seconds at most according to European regulations. Primary reserve in Switzerland should be fully active when the frequency deviation reaches $\pm$200mHz. On average, a total of $\pm$74MW of primary reserve is contracted in Switzerland at an average price of 15 CHF/MW/h (2016 average, total of 100 million CHF annual payments).

6.4.2 Secondary frequency control

Secondary frequency control introduces the integral control action necessary to bring the frequency back to the nominal 50Hz and balance cross-border energy exchanges. Swissgrid runs a central controller to compute a control signal called the *area generation control* signal (AGC). This signal is dispatched at a one second rate to secondary frequency control providers that are supposed to adapt their power consumption according to the AGC. If the AGC is positive, they should increase their power generation (or decrease their power consumption) accordingly and conversely. SwissGrid requires symmetric bids for secondary frequency control so that providers need to indifferently be able to increase or decrease their power consumption/generation. In the prequalification test for secondary frequency control in Switzerland, a tracking error of 5% of the bid is allowed with a delay of at most 20 sec.

A total of $\pm$396 MW of secondary reserve is contracted for Switzerland all year round. The total cost for secondary reserve is 90 million CHF annually, which corresponds to an average price of 40CHF/MW/h of up/down regulation offered (2016 averages).The empirical distribution of the AGC signal computed by Swissgrid over the years 2014 and 2015 is reported in Figure 6.1. An interesting observation is that most of the time, the AGC signal is close to zero, which means that the tracking request is very small compared to the highest possible value it may take.

6.4.3 Tertiary frequency control

Tertiary frequency is the slowest form of frequency control. Tertiary control is used for the relief of the secondary control reserve in order to restore a sufficient secondary control volume. The tertiary control reserve is necessary for adjusting major, persistent control deviations, in

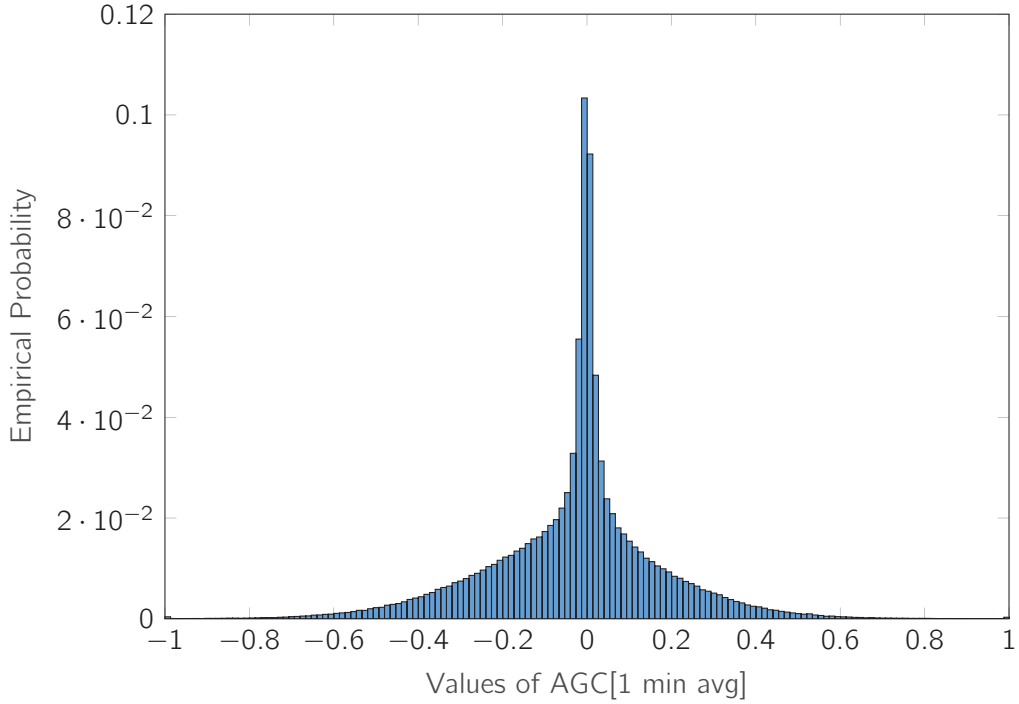

Figure 6.1 – Empirical PDF of the 1-minute averaged AGC signal. Values are normalized between -1 and 1 for minimum and maximum power requests. [Courtesy of SwissGrid]

particular after production outages or unexpectedly long-lasting load changes. Activation is effected by the Swissgrid dispatcher by means of special electronically transmitted messages to the providers, who must then intervene in power plant production to ensure the supply of tertiary control power within 15 minutes. Therefore, tertiary frequency control is less automatized than other levels of frequency control.

In Switzerland, tertiary control bid for negative and positive power are separated. SwissGrid uses on average 530MW of positive reserve at an average price of 2CHF/MWh and 350MW of negative power reserve at an average price of 2.5CHF/MWh (averages for 2016).

7 Frequency control with the LADR platform following the Swiss market regulations

7.1 Contribution and structure of the chapter

The contribution of this chapter is two-fold:

- It supports the developments of Part II in two main ways:
  - It provides another example of how the theory developed is applicable to a realistic problem, namely the provision of ancillary services with a building heating system. We will see that the problem naturally formulates as a robust tracking commitment problem.
  - It provides experimental evidence that the method developed to characterize the load's power consumption flexibility works well. We will see that a significant flexibility could be provided by our system while always respecting the operational constraints of the system, as well as as maintaining a good level of comfort.
- It provides elements of response regarding the aspects discussed in Section 6.3 in the previous chapter:
  - Regarding the interacting timescales, we provide evidence that a three-level control architecture helps the system to reach a good level of performance.
  - Regarding the baseline consumption, it shows that a controllable load can achieve full dispatchability, using a model based approach inspired by MPC, and more since it offers extra flexibility. However, we will see that the amount of time that the baseline needs to be declared ahead of delivery of the demand response service is a key factor for exploiting the flexibility of the system.

We report in this chapter on a group of experiments conducted during the winter season 2015-2016. We detail in section 7.4 how these experiments extended our previous work as well as existing works in the literature.

The rest of the chapter is structured as follows: Section 7.2 presents the LADR experimental platform, Section 7.3 presents the identification procedure of the LADR platform to built the model used in our MPC problem setups. Section 7.4 presents the control architecture employed in our experiments while Section 7.6 reports on the experimental results from secondary frequency control provision with the LADR platform. Finally, Section 7.7 offers an experimental validation of the concept of virtual battery.

7.2 The LADR platform

7.2.1 Scope and objectives

The LADR platform was designed for fast deployment of building heating control algorithms developed in the laboratory. The following desired characteristics have been listed for the system:

- Availability of an electricity based heating/cooling systems
- Possibility to emulate other type of heating systems/ Flexible control of the heating systems
- Possibility to control the actuation at a fast rate for regulation type experiments
- Monitoring of the heating system, in particular the electric power consumption at a fast rate.
- Accurate and fast control of the system, especially regarding its power consumption.
- Control of heating systems in realistic conditions, subject to large unmeasured disturbance (live office)

The following constraints have also influenced the orientation of the project

- EPFL does not allow the installation of cooling systems in the offices.
- No thermal power input measurement is availalble at a fine grain level for the existing water radiator system.
- A minimally invasive system is preferable due to the fact that occupied offices are used so installation should be fast and seamless.

In accordance with these requirements, a modified electric heater has been developed by Altuğ Bitlislioğlu to allow for fast variation of the power input to the heater. More details are provided in section 7.2.3. The electric heaters were chosen because they combine the following characteristics: (1) Modelling electric heaters is simple (2) It is possible to measure their power consumption directly (3) They are highly responsive elements which allows varying their power consumption very quickly. This is a key element to offer frequency

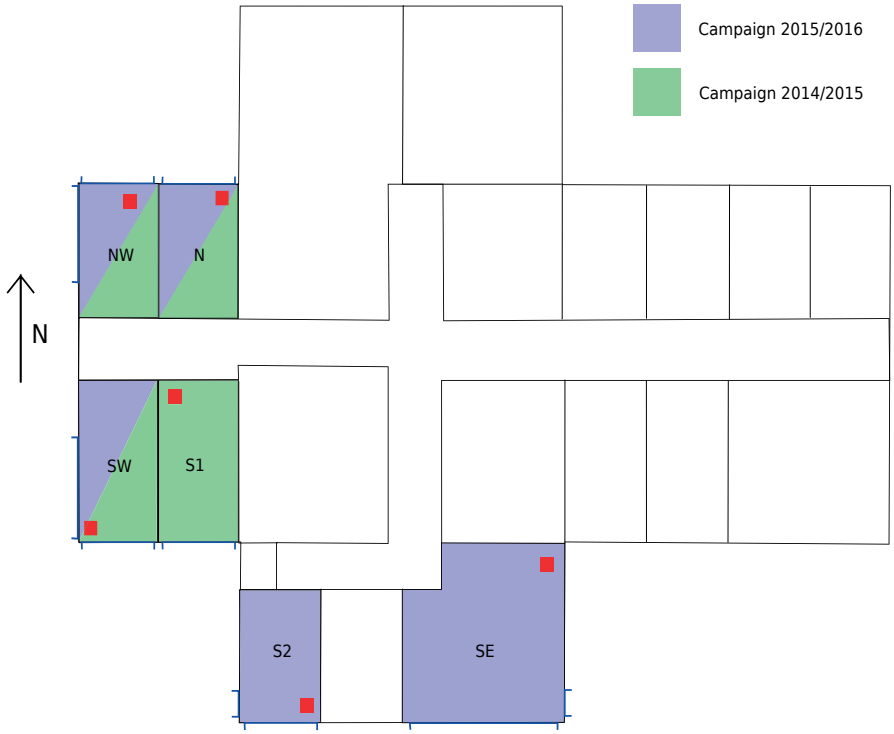

Figure 7.1 – Floor map of the laboratory. The colored rooms represents the space used for the experiments during the two field campaigns. Red box indicate the position of the heaters and blue lines indicate fenestration areas.

regulation services as fast continuous control is required; (4) Electric heating represents a significant share of the heating provision in Switzerland. Recent federal statistics indicate the presence of a quarter million electric-based heating units accounting for 4% of the total Swiss electricity consumption [104].

Two campaigns of experiments have been performed during the winter season of 2014-2015 and 2015-2016. Field campaigns have been performed in different sets of offices as detailed on Figure 7.1. Four rooms have been used during the first field campaign and five during the second one. Offices are labeled according to their exposure to the sun. Rooms NW, N, SW and S are individual offices. Room SE is a shared office occupied by six PhD students.

7.2.2 Main milestones of the LADR platform

Below are the dates detailing the design and main implementation steps of the LADR platform:

- **Summer 2014:** Definition of the LADR platform
- **September/October 2014:** Development of the LADR electric unit [Altuğ Bitlislioğlu]

- **November 2014:** The LA offices are equipped with Z-wave wireless sensors and radiator actuators. [Luca Fabietti/Tomasz Gorecki/Faran Qureshi]
- **December 2014 to January 2015**: Identification experiments in LADR offices. Identification of thermal input to temperature models. [Tomasz Gorecki/Faran Qureshi]
- **February to April 2015:** First experimental campaign: Basic control tests, and nighttime AGC tracking experiments. [Tomasz Gorecki/Luca Fabietti/Faran Qureshi]
- **Summer 2015:** Preparation of the publication on the first experimental phase, submission of the LADR first experimental paper: [33]
- **Autumn 2015:** Update of the communication infrastructure to YARP[Altuğ Bitlislioğlu]. Large refurbishment of the control code for reusability.
- **November 2015 to February 2016:** Second identification campaign: new offices, multi-input identification with weather inputs. [Tomasz Gorecki/Faran Qureshi]
- **January to April 2016:** Second experimental campaign. Full day experiments in occupied offices of AGC tracking with intraday participation. Study of the trade-off between comfort and available flexibility in the offices. [Tomasz Gorecki/Luca Fabietti/Faran Qureshi]
- **Summer 2016:** Preparation and submission of second experimental paper on the LADR results [47].
- **Autumn 2016:** Preparation of the LADR for the following season. Adaptation for autonomous operation over multiple days. Preparation of the platform for experiments in coordination with the battery from the DESL laboratory.[Luca Fabietti/Tomasz Gorecki]
- **Winter 2016-2017:** Dispatchable feeder + controllable building experiments. [Luca Fabietti/Tomasz Gorecki]

7.2.3 Hardware

The rooms have been equipped with wireless sensors for temperature, humidity, presence and light. Remote control Z-wave based valve have been installed on the existing radiators in order to switch them off during experiments. Modified fan-based electric heaters have been added to the controlled rooms. The heaters are rated at 1900 Watts at 230 Volts. The heaters are normally equipped with a thermostat and a switch to adjust the level of heating between three distinct levels. In order to be able to modulate their power consumption continuously, the heaters were customized with additional hardware that allows pulse-width modulation (PWM) at 4 Hz. They are equipped with micro computers and solid state relays in order to control their power consumption at a one second resolution. Z-wave plug

sensors have been added to the plugs to collect aggregate power consumption data at a second resolution, and as failsafe devices to be able to disconnect the system automatically in case of failure.

7.2.4 Software

Figure 7.2 summarizes the software and communication infrastructure. All the Z-wave based sensors are monitored through the software Indigo Domotics[1] that provides an API to poll and communicate with the sensors. Weather data is collected in real-time from Wunderground[2] weather stations online through the WeatherSnoop[3] plugin of Indigo. Communication with the heaters is custom designed. A major upgrade was performed for the second campaign and is briefly reviewed here. The YARP communication library [97] has been used to handle the low-level communication layer. The YARP node library developed in the laboratory is used to define the notion of node in a communication network. Interfaces to MATLAB and Python allow to support code on different platforms. The controllers of the heaters are implemented in Python and expose the heater as node on the network. The central controller is run in MATLAB on a separate workstation. All the data is collected in a centralized location on a web server designed with the Python framework Django. Weather forecasts are obtained through different web services on a regular basis.

7.3 Identification

In absence of building data, an approach based on system identification was used. OpenBuild could have been used to extract a structure of the model but considering the rooms are equipped with independent heating units, it appeared quickly that the coupling betweeen neighboring rooms was weak so that it was neglected and a separate model was identified for each room. This made system identification manageable. In the first campaign, simple models had been identified, taking as inputs the thermal power inputs to the heaters and as outputs the room temperatures. The performance of this model was sufficient for nighttime experiments with no excitation from the sun.

For the second campaign, an extended model was identified, taking into account the effect of the sun and outside temperature on the rooms. Linear black box identification was used. The MATLAB system identification toolbox was used to compute the model parameters.

7.3.1 Solar radiation modeling and forecasting

We know that the effect of the sun on the room is going to be time-varying due to the movement of the sun in the sky during the day. In order to be able to identify linear time-invariant models, the direct or horizontal radiation may not be sufficiently representative of

[1] https://www.indigodomo.com/
[2] https://www.wunderground.com/
[3] http://www.tee-boy.com/

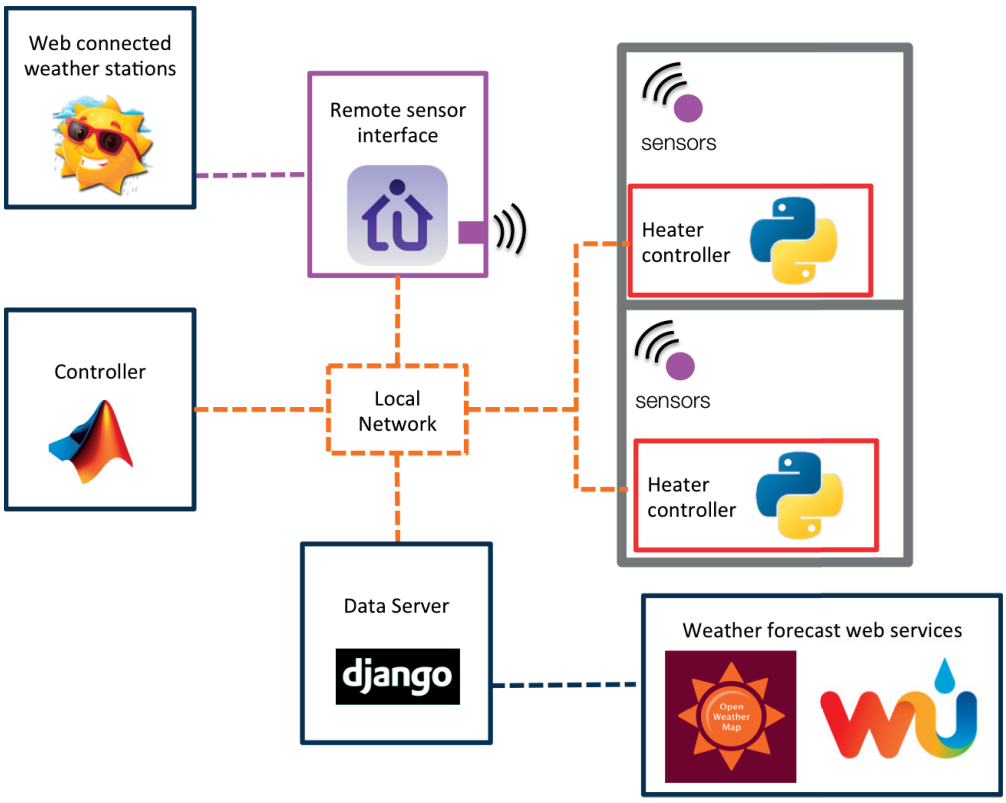

Figure 7.2 – Structure of the communication network.

the impact of the sun on particular rooms depending on their orientations. In order to get a better approximation, each room was identified taking as input the resulting radiation level on surfaces facing the main orientation of the room. Total solar radiation on every main cardinal directions is computed and the one giving the most satisfactory fit for the identification was kept for each room. The best input for room NW was total radiation on west facing surface, for rooms SW and S2 and SE, the the total radiation on south facing surfaces is used. Room N was identified without sun input since they did not significantly bring improvement to the predicting capability of the model.

Notice that the resulting solar irradiance on different surfaces is not directly measured and must be inferred from total horizontal irradiance, time of day and year, etc. A simple inference method was developed combining different available models and is reviewed here.

First notice that the total solar radiation on any surface is decomposed in a direct part (resulting from sun rays hitting directly the surface) and a diffuse part resulting from the diffusion of sun light by the clouds and the atmosphere.

$$I_{\text{tot}} = I_{\text{dir}} + I_{\text{diff}} \tag{7.1}$$

where I_{tot} is the total solar irradiance on a surface, I_{diff} is the total diffuse irradiance and I_{dir} the total direct irradiance. All solar irradiances are measured in W/m^2. A simple model for

diffuse radiation assumes that the diffuse radiation is uniformly contributed from the totality of the sky dome. The amount of diffuse solar radiation a surface receives is therefore a function of the fraction of sky it sees, and hence only depends on its tilt. As an example, the amount of diffuse radiation is maximum for an horizontal surface, and the total amount of diffuse irradiance received by a vertical surface is half of that maximum. We denote by $I_{\text{diff}}^{\text{hor}}$ and $I_{\text{diff}}^{\text{vert}}$ the diffuse irradiance received by horizontal surfaces and vertical surfaces respectively. It holds that $I_{\text{diff}}^{\text{hor}} = 2I_{\text{diff}}^{\text{vert}}$.
On the other hand, direct radiation depends on the relative orientation of the surface and the position of the sun in the sky. Figure 7.3 indicates how the position of the sun is described. The position of the sun can be computed as a function of location (longitude, latitude, elevation) and UTC time following reference [124]. A third party implementation in MATLAB [69] was used to compute elevation and Azimuth angles.

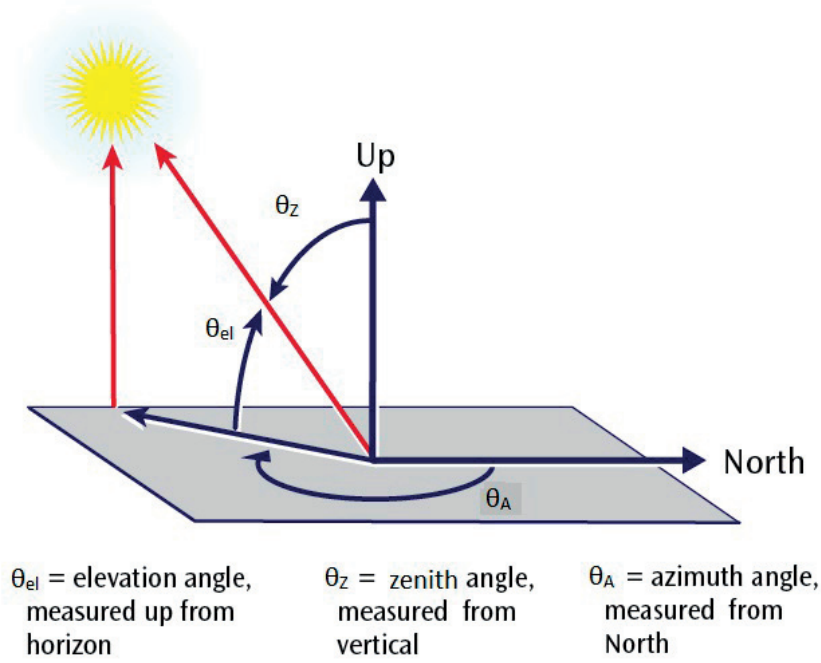

Figure 7.3 – Angles describing the sun position. Image courtesy of Sandia National Laboratory https://pvpmc.sandia.gov/modeling-steps/1-weather-design-inputs/sun-position/.

The amount of direct normal radiation (solar radiation on surface facing the sun) is related to the horizontal direct radiation by the equation:

$$I_{\text{dir}}^{\text{hor}} = I_{\text{dir}}^{\text{norm}} \sin(\theta_{\text{el}}) \tag{7.2}$$

For a surface of tilt angle α_{tilt} (computed like the elevation angle θ_{el}, so that a vertical surface has tilt angle 0 and an horizontal one has tilt 90^o) and orientation angle α_o

(computed like the azimuth angle θ_A so that a surface facing north has orientation angle 0 and one facing east has orientation angle 90^o), the relation between direct normal solar radiation and direct solar radiation on that surface is given by:

$$I_{dir} = I_{dir}^{norm} \cos(\theta_{el} - \alpha_{tilt}) \cos(\theta_A - \alpha_o) \tag{7.3}$$

For forecasts, the value of the total horizontal radiation is not usually available. The only information available is often a qualitative description of the weather (such as clear, scattered clouds, overcast...). The website openweathermap.org offers quantitative forecast for the cloud cover, in percentage of sky covered with clouds. From this data, the average horizontal radiation can be computed using the Zhuang-Huang Solar model [29], [157].

$$I = \frac{1}{k}.\left[I_0.\sin(h)(c_0 + c_1.CC + c_2.CC^2 + c_4.\phi + c_5.V_w\right] + d \tag{7.4}$$

where: I = estimated solar radiation [W/m^2]
I_0 = global solar constant = 1355W/m^2
CC = cloud cover [tenths]
V_w = wind speed [m/s]
ϕ = relative humidity [%]
$c_0, c_1, c_2, c_4, c_5, d$ = regression coefficients, given in [29], pp138-139.

The fraction of diffuse radiation on an horizontal surface $f_c = \frac{I_{dir}}{I_{tot}}$ also needs to be estimated. We know that if the cloud cover is total then $f_c = 1$. In clear sky conditions, a simplified model can be used to compute the total direct and diffuse horizontal radiation as:

$$\begin{aligned} I_{dir}^{hor} &= I_0 \sin(\theta_{el}) t^m \\ I_{diff}^{hor} &= 0.3 I_0 \sin(\theta_{el})(1 - t^m) \end{aligned} \tag{7.5}$$

where $t = 0.75$ is the average transmittance of the atmosphere and $m = \frac{p}{101.3}\sin(\theta_{el})$ with p the air pressure in kPa. In turn, the fraction of diffuse radiation on an horizontal surface can be deducted. This fraction is valid for a cloud cover of 0. It is then assumed that f_c is an affine function of cloud cover and is interpolated from the values at $CC = 0$ and $CC = 10$.

To summarize: to compute the total solar radiation on a surface for forecasting, (1) the forecast for cloud cover is recovered; (2) Equation (7.5) is used to compute the diffuse fraction of radiation on an horizontal surface and the total horizontal radiation using equation (7.3); (3) From these the horizontal diffuse and direct radiations are computed and the direct, diffuse and total solar radiation on the surface are calculated by means of equations (7.1), (7.4) and (7.2)

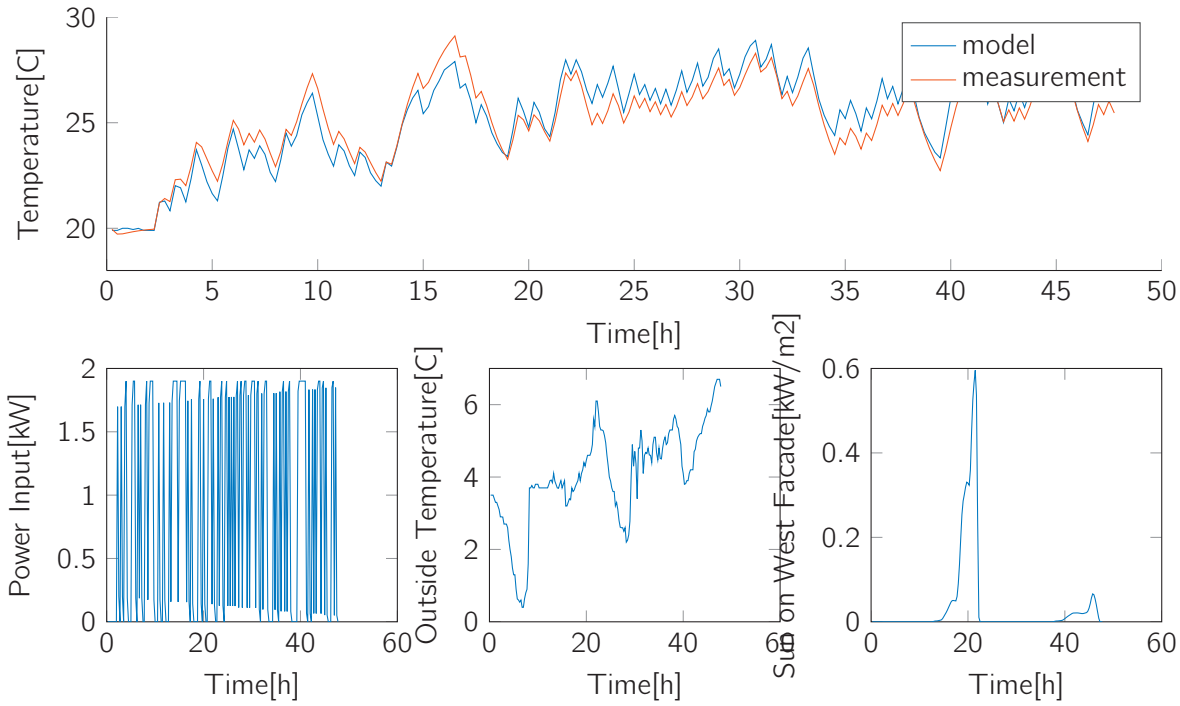

Figure 7.4 – Validation over one of the experiments for Room NW

7.3.2 Identification

A series of experiments has been conducted to collect data for identification. To minimize the effect of unmeasured disturbances, all experiments have been performed during nighttime and week-ends/holidays. The controllable inputs of the heater have been controlled using pseudo random binary sequences or step tests over long periods of time. A total of 12 experiments has been used for identification, with a few days worth of data for each room. For each room, an autoregressive model with exogeneous inputs was identified.

$$A(z^{-1})y(t) = B_1(z^{-1})q(t-1) + B_2(z^{-1})T_o(t-1) + B_3(z^{-1})q_{\text{sun}}(t-1) + e(t) \quad (7.6)$$

where $A(z^{-1})$, $B_1(z^{-1})$, $B_2(z^{-1})$ and $B_3(z^{-1})$ are polynomials of the delay operator z^{-1} and $e(t)$ a white noise disturbance, q the input from the heat input, T_o the outside temperature, y the room temperature and q_{sun} the sun irradiance input for the room. Note that due to the absence of measurement relative to occupancy, its influence is not explicitly modeled and will be considered as a disturbance. It was found that a model of second order for the dynamics and first order for the inputs was sufficient. Each model had an average fit[4] on experiments used for identification of 70% to 90 % depending on the room. Figures 7.4, 7.5, 7.6, 7.7, 7.8 show validation plots for each model identified.

[4] matlab fit computed as one minus the normalized root mean square prediction error

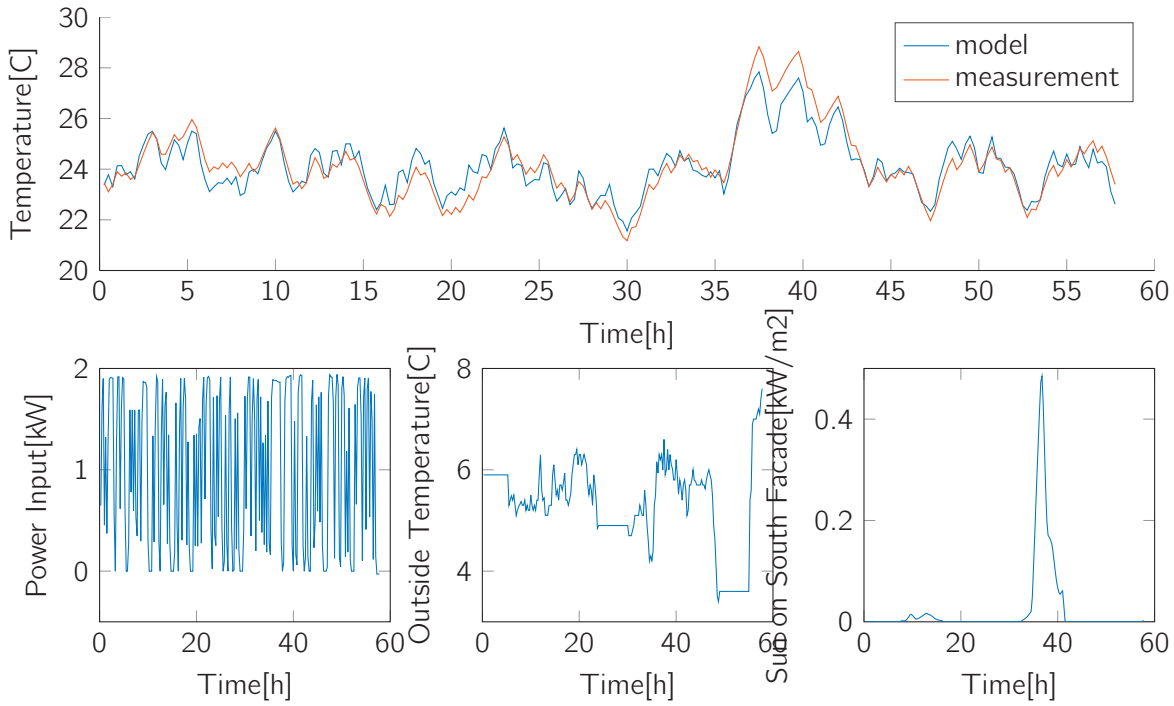

Figure 7.5 – Validation over one of the experiments for Room SW

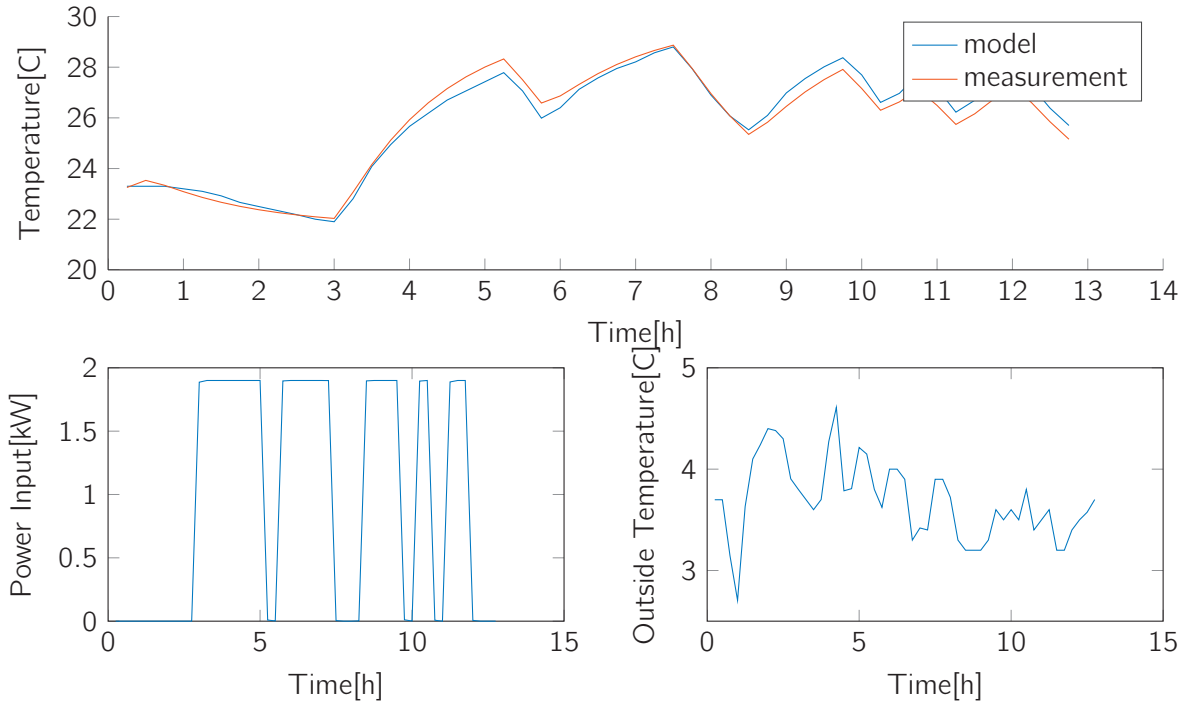

Figure 7.6 – Validation over one of the experiments for Room N

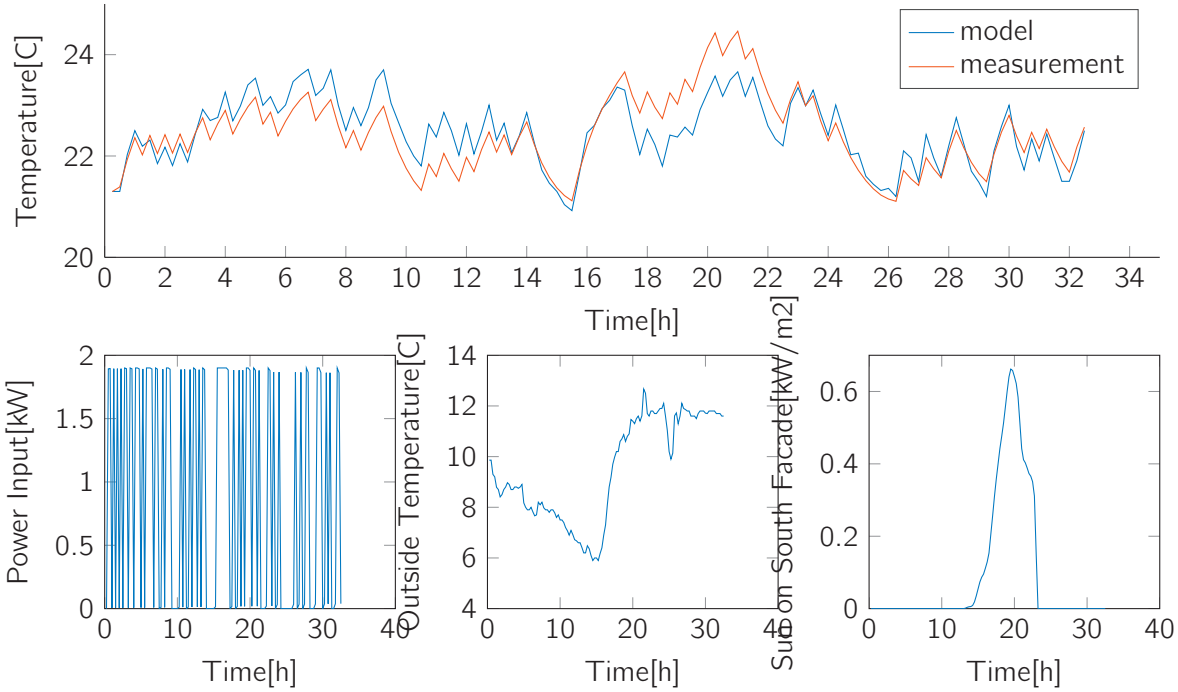

Figure 7.7 – Validation over one of the experiments for Room SE

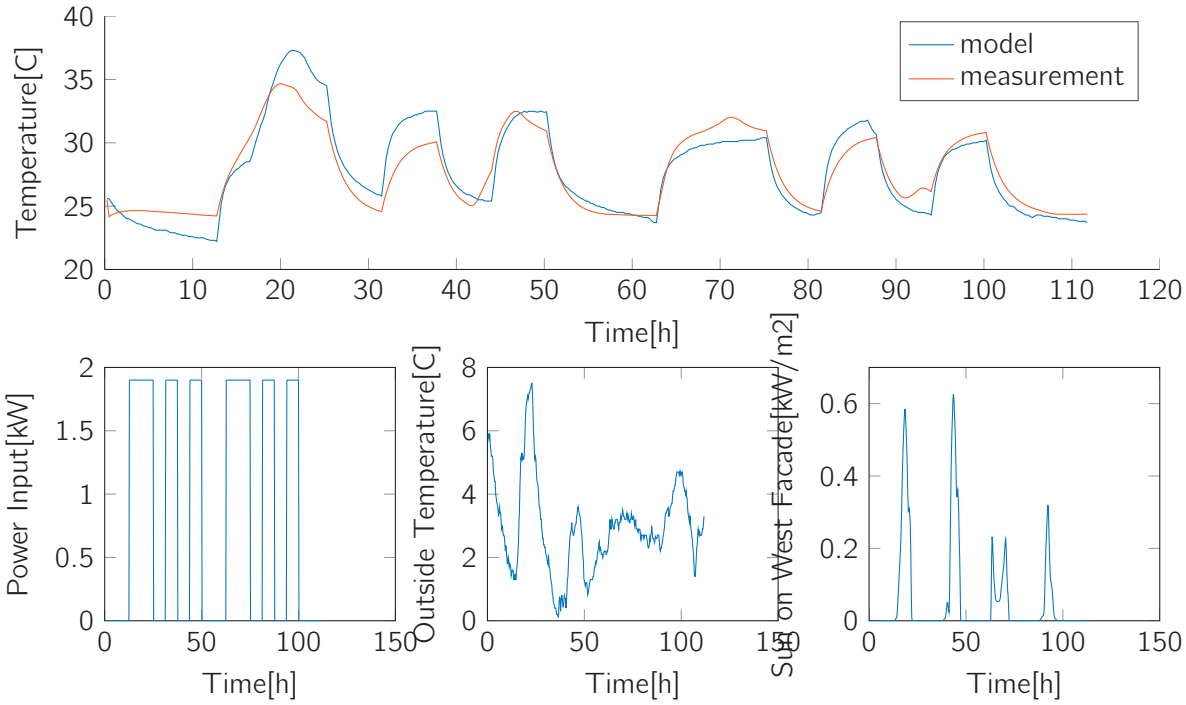

Figure 7.8 – Validation over one of the experiments for Room S2

Room	NW	SW	S2	SE	N
Gain from input to Temperature [C/(kW)]	5.5	5.7	4	1.6	4.3
Gain from Outside Temperature to Temperature[C/C]	0.2	0.2	0.05	0.15	0.1
Gain from Sun to Temperature[C/(kW/m^2)]	3.6	11	2.3	9.3	NA
Slow Time constant[h]	1.4	2.5	1	2.2	1.4
Fast Time constant[h]	0.15	0.13	0.07	0.04	0.16
Rise Time for step response[h]	3	5.25	4.75	2	3
Equivalent U-value [W/m2/K]	1.28	1.21	0.15	1.46	1.35

Table 7.1 – Parameters of the models identified. The rise time is the 10 to 90 % rise time for a step response

7.3.3 Model characteristics

We discuss here the most important characteristics of the models identified. They give an idea of the storage capacity of the building.

The identified model reveals the main characteristics of the building: the impact of the sun on the rooms is significant: static gains from solar inputs to temperature range from 3 to 11^oC/(kW/m^2) depending on the room. Note that the daily peak horizontal irradiance will range around 0.7 to 1kW/m^2 during sunny winter days. The effect of outdoor temperature is milder with static gains ranging from 0.1 to 0.2$^oC/^oC$(outside).

Two dominant time constants are identified for each room: one fast time constant ranging between 5 and 10 minutes and one slow time constant ranging between 1 and 2.5 hours. This can be interpreted as follows: the faster time constant corresponds to the air thermal mass that can be heated directly with our heating system. The slower time constant corresponds to the heavier thermal mass of the building. This second mode is the one that the controller will try to utilize to store energy in the system over a few hours. The 10 to 90 % rise time for a step response ranges between 2 and 3 hours.

Finally, the bode plots of the systems identified are reported in Figure 7.9. As expected the system is passive (there is no resonance in the system),

From the model of the system, we can estimate the amount of power needed to maintain the inner temperature at a fixed level T_1, when the outdoor temperature is at another fixed level T_2. Dividing this power by $T_1 - T_2$ and the area of outside envelope for each room we get a rough estimate of the equivalent average U-value of the envelope of the building. Values obtained range between 1 and 1.5W/m2/K. The U-value characterizes the thermal conductance of materials or surfaces through conduction and convection. In our case, we get an aggregate value that also includes gain through infiltration. Moreover, we neglect the presence of internal gains in the room, so the number would appear smaller than it really is. However, internal gains should be quite limited since identification experiments were performed without occupants. For comparison, high-quality double glazing has a U-value of about 2 W/m2/K. The notable exception is room S2 which has a much lower apparent U-value: that can be explained by the fact that this room is subject to more significant internal gains due to the presence of numerous computer servers and a lower window to

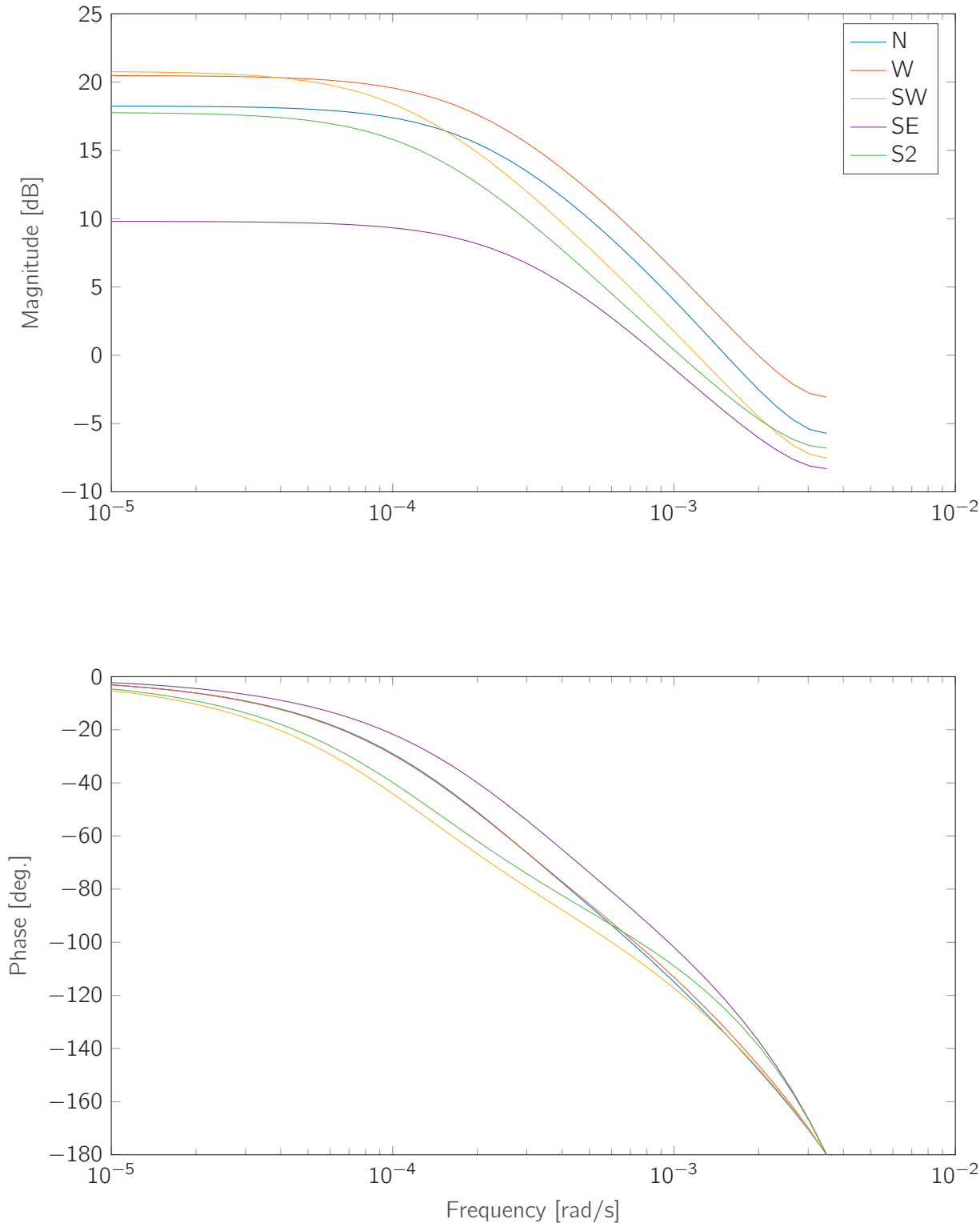

Figure 7.9 – Frequency response of the identified models

wall ratio. Subsequently this room was not used in experiments due to the fact that it almost does not need any heating. The U-values suggest that the insulation quality of the envelope is neither exceptionally high (which was not expected since the construction is old), nor very low. In that sense, the building can be considered relatively representative of not-so-recent office buildings in Switzerland.

7.4 Predictive control of the heaters

This section reports the control design approach and is mainly taken from the publication [47]. The main overarching theme of the experimental work was to demonstrate how to optimally use the thermodynamic storage of commercial buildings to offer frequency regulation services to the grid. The contribution of the second campaign with respect to our previous work [33] was twofold: first, we provide a method to determine the amount of regulation that can be provided taking into account the possibility to adjust power consumption on the intraday market. Second, we show how to optimally trade regulation commitment and comfort in the building during real-time operations.

The experimental demonstration extends existing experimental works presented in the literature in the following ways:

- The method proposed is in full accordance with the Swiss regulation for secondary frequency control. In particular, the baseline consumption is determined a priori as a result of the day-ahead market trades. Any modification of the baseline during the day respects the current rules of the intraday market.
- Modeling of the influence of outside temperature and the sun was performed for these offices. Weather forecasts were incorporated in the optimization to improve the previously proposed method.
- Experiments have been performed over extended periods of time (18 to 24h) in occupied offices. Experiments were successful despite large uncertainties in weather prediction and occupation and, therefore, demonstrate the robustness of the approach.

7.4.1 Control Structure

We consider a power consumer offering secondary frequency service. According to the Swiss market regulations, a tailored control architecture is proposed. A schematic of the controller structure is provided in Figure 7.10.

Table 7.2 reports the nomenclature for the following sections. The reserve scheduler decides on the capacity bid γ and the baseline purchased on the day-ahead market $\bar{p}_{i|DA}$ for each time slot i of the following day. Subsequently it can readjust its power baseline up to one hour in advance on the intraday market by placing an order $\bar{p}_{i|i-\delta}$ at time $i-\delta$ for each time slot i. For simplicity, we assume that all intraday adjustments are made at time $i-\delta$, the closing time for intraday transaction for time slot i. The final baseline is $\bar{p}_i = \bar{p}_{i|DA} + \bar{p}_{i|i-\delta}$. During the operation, a normalized AGC signal a_t (we use t to denote

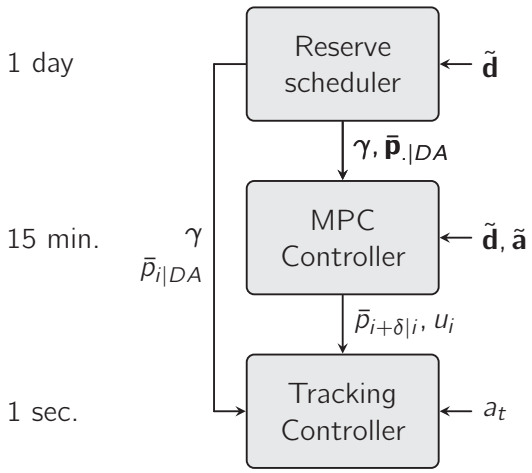

Figure 7.10 – Architecture of the control system for tracking service procurement with participation in the intraday market. See Table 7.2 for the definitions of symbols.

Symbol	Description
γ	Capacity bid
$\bar{p}_{i\|DA}$	Day-ahead baseline purchase
$\bar{p}_{i\|i-\delta}$	Intraday transaction performed at time $i-\delta$ for baseline at time i
$\bar{p}_i$	Baseline Power Consumption after intraday
δ	Minimum lag for intraday transactions
y_i	Outputs (Zone Temperatures)
ϵ_i	Tracking error
p_i	Total Power Consumption
u_i	Control action
d_i	Weather disturbance at time i
$\tilde{\mathbf{d}}$	Weather forecast
a_i	Normalized AGC signal at time i
$\tilde{\mathbf{a}}$	AGC forecast

Table 7.2 – Control architecture nomenclature.

the fastest time step while we keep i for the 15 minute time step) is scaled by the bid γ and dispatched at a rate of one second for tracking to the building, which has to adapt its power consumption such that:

$$|\epsilon_t| = |p_t - \bar{p}_t - \gamma a_t| \leq \alpha\gamma \tag{7.7}$$

where ϵ_t is the tracking error. Note that the tracking error is allowed to scale in proportion to the capacity bid with a factor α, in accordance with tracking regulation requirements as per [143]. It is readily seen that the problem has multiple timescales interacting: when deciding the capacity bid and day-ahead purchase, a prediction over a minimum of one day is required, while during operation, the tracking signal is received at a one second rate. Similarly to [151] and [33], the control architecture proposed is therefore hierarchical with three interacting layers as depicted in Figure 7.10:

- The reserve scheduler commits the capacity bid for the next time period (one day) and buys energy on the day-ahead market. At the start of each day, it computes a capacity bid using the current estimate of the state of the system and up-to-date weather forecasts. As a result of this computation, the bid γ and day-ahead purchases $\bar{\mathbf{p}}_{.|DA}$ are committed. It is important to notice that the scheduler already takes into account the possibility to adjust the baseline later on on the intraday market, as will be detailed in Section 7.4.3.

- A Model Predictive Controller (MPC) operates at a fifteen minute timestep: its purpose is two-fold: compute adjustments to the baseline using the intraday market, and recompute optimal inputs for the heating systems based on updated forecasts. As a result, an intraday trade is placed to adjust the baseline one hour ahead for a value $\bar{p}_{i+\delta|i}$. The inputs to the system for the upcoming time slot u_i are passed down to the fast controller.

- A fast controller modulates the power consumption of the HVAC at a fast rate (consistent with the tracking rules) to provide the tracking service. Based on the current received value of the AGC a_t and the committed baseline $\bar{p}_t$, the power input of the HVAC is controlled to meet the tracking requirement.

Assumption 7.1. The intraday markets are assumed to be liquid, meaning that it is always possible to sell or purchase energy according to the market clearing regulations. ■

While this assumption cannot be verified directly, intraday market data we have examined suggests that a large amount of energy is traded on the intraday market, especially just before the final clearing, one hour before delivery, for most hours of the year. In addition, liquidity on the intraday market is increasing every year.

In addition to experiments carried out during the day in occupied offices and for extended periods of time, the main difference in the formulation with our previous work [33] is the possibility to readjust the baseline in the intraday market. We will see that this feature is

paramount to the robustness of the scheme. As was outlined in the introduction, demand-side resources are subject to sustained prediction errors that hinder the ability to predict accurately their power consumption on long time horizons. Therefore, the possibility to partly reschedule baseline is fundamental. We will see that the intraday market allows us to successfully meet the combined competing objectives of maintaining comfort and providing accurate frequency regulation. Clearly, this statement depends on the predictive power of our models, but the experiments demonstrate that for our system, which is affected by large uncertainties, the statement holds, which is a significant improvement over our preliminary work, where the level of uncertainty was smaller since experiments were conducted at nighttime.

7.4.2 System Modeling

As discussed in Section 7.3.2, each room was identified with a model of the form of (7.6).

We transformed and combined the models from input-output form to state-space form as:

$$\begin{aligned} x_{i+1} &= Ax_i + B_u u_i + B_d d_i \\ y_i &= Cx_i \end{aligned} \tag{7.8}$$

where x denotes the state of the system. The control input to the system is the pulse-width modulation ratios sent to the heaters denoted u. Therefore $u \in [0, 1]$. A pulse-width ratio directly results in an electric power consumption $p = uP_{\text{max}}$. Finally, the heaters being resistive elements, the power consumption directly translates into a thermal power input to the room q, so that $q = p = uP_{\text{max}}$. Knowing the model of the system and the operational constraints, we can formulate the set of all feasible input trajectories that the building can follow while respecting constraints. It takes the following form:

$$\mathcal{U}(\bar{x}, \tilde{\mathbf{d}}) = \left\{ \mathbf{u} \;\middle|\; \begin{array}{l} x_{i+1} = Ax_i + B_u u_i + B_d \tilde{d}_i \\ y_i = Cx_i \\ |y_i - T_{\text{ref}}| \leq \beta \\ u_i \in \mathbb{U} = [0, 1]^{n_u} \\ x_0 = \bar{x}, \\ \forall i = 0, \ldots, N-1, \end{array} \right\} \tag{7.9}$$

where N is the horizon covering the participation period, T_{ref} the optimal temperature and β a parameter controlling the allowed comfort level deviation from optimum. Notice that this set depends on the initial condition $\bar{x}$ and a forecast for the disturbance $\tilde{\mathbf{d}}$.

7.4.3 Reserve scheduling

The reserve scheduler computes two quantities: a baseline energy consumption for the next day $\bar{\mathbf{p}}_{\cdot|\text{DA}}$, and a capacity bid, γ. Conceptually, the computed capacity bid should be chosen considering the following:

- For a given capacity bid, the controller needs to schedule the baseline consumption in such a way that regardless of the AGC signal it receives, it can shift its power consumption by that amount and still satisfy operational constraints.

- The building operator receives a payment for the "flexibility" he offers which is proportional to the bid. On the other hand, it also pays for baseline power. Intuitively, in the absence of local controllable generation, a higher bid also requires a higher baseline (since the building needs to be able to decrease its consumption by larger amounts). Therefore, there is a financial trade-off between bid and baseline. [112] develops how this trade-off depends on the ratio between the price of energy and the reward for flexibility. If the reward for flexibility is high enough, maximizing the bid we can offer will be optimal. For the sake of demonstration, we assume that it is the case.

The computation of the bid was done in accordance with the theory developed in Chapter 5. Assuming that a nominal bid of $\gamma = 1kW$ restricts possible AGC realizations to lie in the nominal set $\hat{\Xi}$, then once the bid and baseline have been fixed, the system is subject to the following tracking constraints:

$$|\epsilon_i| = |p_i - a_i| \leq \alpha\gamma \quad \forall \mathbf{a} \in \nu(\hat{\Xi}) := \gamma\hat{\Xi} + \bar{\boldsymbol{p}} \tag{7.10}$$

This is a robust constraint where the uncertainty set is modulated. We can therefore formulate a robust tracking commitment problem that fits the developments of Chapter 5 as we will see next.

Modeling of the AGC signal

The set $\hat{\Xi}$ still needs to be characterized. Remembering explanations of Section 6.4.2, we have in principle:

$$\hat{\Xi} = \{\mathbf{a} \mid \|\mathbf{a}\|_\infty \leq 1\} \tag{7.11}$$

However, we have also seen that the AGC tends to be very much concentrated around 0. This is a piece of information we can utilize to restrict the set further. Using principles of statistical inference, we can see that using a much more restricted set allows one to increase the bid offered significantly at the expense of only a small sacrifice in terms of guarantees. The design of uncertainty set for robust optimization is an active field of research and different approaches have been proposed, see [14], [92], [21] and references therein.

We define the set:

$$\hat{\Xi} := \left\{ \mathbf{a} = \sum_{j=1}^{N_s} \lambda^{(j)} \mathbf{a}^{(j)} \middle| \sum_j \lambda^{(j)} = 1, \lambda^{(j)} \geq 0 \right\} \tag{7.12}$$

where the $\mathbf{a}^{(j)}$'s are previously observed realizations of the uncertainty from years 2013 and

2014 (courtesy of Swissgrid). In other words, $\hat{\Xi}$ is the convex hull of a set of previously observed realizations of the uncertainty.

The key idea is that if the controller is able to handle values of the AGC that have been observed in the past it should perform well for new realizations due to the consistency of the AGC over time.

Computation of the bid

We solve the following problem:

Problem 7.2 (Reserve Scheduling Problem)**.**

$$
\begin{aligned}
\text{minimize} \quad & J \\
\text{s.t.} \quad & \forall \mathbf{a} \in \gamma \hat{\Xi} + \bar{\mathbf{p}}, && (7.13)\\
\text{(Building Contraints)} \quad & \mathbf{u} \in \mathcal{U}(x_0, \tilde{\mathbf{d}}), && (7.14)\\
\text{(Recourse policies)} \quad & \mathbf{u} = \pi(\mathbf{a}), && (7.15)\\
& \bar{\mathbf{p}}_{.|.-\delta} = \kappa(\mathbf{a}), && (7.16)\\
\text{(Power Consumption)} \quad & \mathbf{p} = h(\mathbf{u}), && (7.17)\\
\text{(Power tracking)} \quad & \|\boldsymbol{\epsilon}\|_\infty = \|\mathbf{p} - \mathbf{a}\|_\infty \leq \alpha\gamma && (7.18)\\
\text{(Baseline Power)} \quad & \bar{\mathbf{p}} = \bar{\mathbf{p}}_{.|.-\delta} + \bar{\mathbf{p}}_{.|DA} && (7.19)
\end{aligned}
$$

■

The decision variables are the capacity bid γ, the day-ahead baseline consumption $\bar{\mathbf{p}}_{.|DA}$, and the control policies π and κ satisfying causality requirements such that $\kappa \in \mathcal{C}_{-\delta}$ and $\pi \in \mathcal{C}_0$ reusing the notation introduced in Table 5.2 on page 68.

x_0 and $\tilde{\mathbf{d}}$ are data of the problem and represent the initial condition of the system and the prediction for the disturbances affecting the system, namely the weather and internal gains.

Since the constraints as described in (7.9) are polytopic, assumption 5.18 is satisfied. Similarly, the uncertainty set as described in (7.12) admits a conic representation so that assumption 5.19 is satisfied. Affine policies can be used to parametrize π and κ and obtain a tractable version of Problem 7.2:

$$\pi(\mathbf{a}) = \mathbf{M}\mathbf{a} + \mathbf{m} \text{ and } \kappa(\mathbf{a}) = \mathbf{N}\mathbf{a} + \mathbf{n}$$

To ensure causality, appropriate constraint on $\mathbf{M}$ and $\mathbf{N}$ are imposed so that $\kappa \in \mathcal{C}_{-\delta}$ and $u \in \mathcal{C}_0$. Namely, we impose that:

$$
\begin{aligned}
M_{i,j} &= 0 \text{ for } j > i \\
N_{i,j} &= 0 \text{ for } j > i - \delta
\end{aligned}
$$

Cost function

The payment for regulation capacity offers a per-unit reward c_{reg}. Energy is bought at a unit price c_e. The cost function takes the form:

$$J(\bar{p}, \gamma) = c_e \sum_{i=1}^{N} \bar{p}_i - c_{\text{reg}} \gamma$$

In the context of the experiment, we aimed at demonstrating the total flexibility of the buildings, and therefore we assume that $c_{reg} >> c_e$ so that 'maximum' capacity is offered.

Remark 7.3. The actual disturbance $\mathbf{d}$ is not known exactly at the time the problem is solved, only a forecast is available. Conceptually, it could be treated exactly like $\mathbf{a}$ and the solution of the problem could be robustified against forecast errors, for which data is readily available (at least for weather). The control decision would then become a function of the disturbance, *i.e.* $u = \pi(\mathbf{a}, \mathbf{d})$. In the optimization, we assume the disturbance will take its nominal value and the control decision is a function of the AGC signal only. The reasons for this are: 1) a simple static-gain analysis on the identified model of the building suggests that the relative impact of a forecast error for the weather disturbance is at least five times smaller than for the AGC signal, 2) forecasts are typically good enough on short timespans like one day 3) not modeling the exogenous disturbance as uncertain variables drastically reduces the controller complexity and 4) experimental results show that the impact of forecast errors on comfort violations is not substantial (please refer to Section 7.6, Table 7.4). □

7.4.4 Closed loop control

This section details the two lower-level layers of the control architecture. Once the capacity bid has been computed together with the baseline, the task of the controller is to satisfy the tracking constraint while making sure that operational constraints are simultaneously met.

MPC controller

We propose to use a predictive controller to maintain comfort. The controller relies on the assumption that being at maximum comfort also maximizes the flexibility. It is approximately the case if the maximum comfort temperature is chosen as the center of the comfort constraint range and uncertainty is symmetric (that is positive and negative AGC are equally likely). The steps of the MPC controller algorithm are:

1. Collect most updated current forecast for weather $\tilde{\mathbf{d}}$. This forecast is recovered from different web services. See section 7.6.1 for more details on the weather prediction.

2. Form a forecast $\tilde{\mathbf{a}}$ for the average of the AGC over the next few hours sampled at 15 minutes. It has been shown in [82] that the AGC is a time-correlated signal, at least up to two hours ahead. A predictor for the AGC over the prediction horizon is used:

it exploits the time-correlation properties of the AGC over short timescales to predict ahead.

3. Solve the following MPC problem

$$\begin{aligned} \text{minimize} \quad & \|\mathbf{y} - T_{\text{ref}}\|^2 \\ \text{s.t.} \quad & \forall j \in \mathbb{Z}_{[i,i+N-1]} \\ & x_{j+1} = Ax_j + B_u u_j + B_d \tilde{d}_j \\ & \mathbf{u} \in \mathcal{U}(x_i, \tilde{\mathbf{d}}) \\ & \|\tilde{\boldsymbol{\epsilon}}\|_\infty \leq \alpha\gamma \\ & \text{with } \tilde{\epsilon}_j = p_j - \bar{p}_j - \gamma \tilde{a}_j \end{aligned} \tag{7.20}$$

where the decision variables in this problem are $\mathbf{u}$, and $\bar{p}_{j|j-\delta}$ for $j \geq i+\delta$. γ, $\bar{\mathbf{p}}$ and $\bar{p}_{i|i-\delta}$ for $i < t+\delta$ are fixed in that problem, and come respectively from the reserve scheduling problem and previous iterations of the MPC controller. The controller aims at maintaining the temperature in the middle of the comfort range for the nominal predictions of the AGC and the disturbance acting on the system. The assumption underlying this choice is that the middle of the comfort range corresponds to a state of high flexibility. Note that the controller is free to adjust the baseline after a delay of δ conformly to the rules of the market. Note also that a robust multi-stage problem could also be solved at this level, where robust tracking constraints are enforced, but this simplified formulation has provided satisfying performance, for a much lighter computational cost.

4. Place an order on the intraday market to buy $\bar{p}^\star_{i+\delta|i}$, the intraday market trade computed in Problem 7.20. This effectively adjusts the baseline for timeslot $i+\delta$. Pass down the computed control input $u^\star_t$ to the tracking controller. Go back to step 1) at the next iteration.

Tracking controller

The tracking controller receives the AGC signal a_t each second and chooses the control input to the radiators. The tracking constraint reads $\|p_t - \bar{p}_t - \gamma a_t\| \leq \alpha\gamma$. Upon receipt of the optimal control action $u^\star$ from the MPC controller, the lower level controller computes the power input share going to zone k as $\nu^k = \frac{u^{\star k}}{\|u^\star\|}$, where u^k denotes the input to zone k. Using the current value of the AGC, the control input $u^k = \nu^k(\bar{p} + \gamma a)/P_{\text{max}}$ is computed. This value is capped between 0 and 1 to give the actual input to the heater, which is applied. It is easily seen that this strategy ensure exact tracking as long as the value of u^k is between 0 and 1. The optimal dispatch $u^\star$ was computed using a forecast for the AGC: as long as the forecast is not widely different from the actual realization, the value of u^k is close to the optimal value $u^\star$ computed at the upper level. Note that if the forecast of the AGC over the each 15 minute period was correct at the MPC level, then the temperature

prediction was also correct. This is due to the fact that the thermal system is essentially a low-pass filter and fast variation of the AGC will not affect the output of the system. They can therefore be disregarded in the MPC problem.

7.5 Relationship between control authority and uncertainty mitigation

One of the objectives of the controller is to absorb the uncertainty coming from the AGC signal. That basically consists in disturbance rejection. It should come as no surprise that an increase in control authority will result in a higher ability to reject disturbances. That is for example the case in Problem 7.2. If the minimum delay for intraday adjustments decreases, the control authority increases through relaxed constraints on the recourse matrix **N**: this results in a lower optimal value for the problem. For example, we elaborate on this concept by quantifying the trade-off between control authority and uncertainty mitigation by looking at the effect of the intraday market on the AGC signal.

Mitigating the effect of the AGC through intraday trades

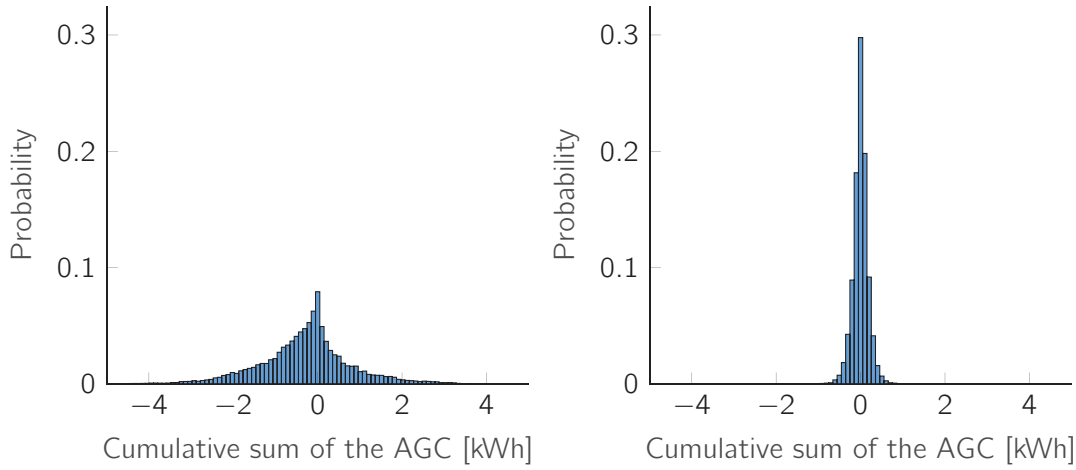

(a) AGC tracking without participation in the intraday market.

(b) Using the intraday market

Figure 7.11 – Empirical probability histogram of cumulative sum of the AGC signal over a one-day period (two years of data). The values of the cumulative sum are given as kWh per kW of capacity offered. Left plot shows the histogram for the 'day-ahead filtered' AGC and right plot the 'intraday-filtered' AGC.

In problem 7.2, the intraday market is used to mitigate the uncertainty of the AGC. In the following, we refer to the integral of the AGC as the energy request. If the energy request reaches a large positive or negative value, it means that the AGC was consistently positive or negative over extended periods of time. AGC signals with the highest energy requests are the most problematic to handle since they require the system to store or release

significant amounts of energy. This can cause two types of issues: (1) the limited energy storage capacity of the system might not support such a request, leading for example to constraint violations; (2) the system operates away from its optimal operating point which might degrade the performance of the equipment. Through the use of intraday trades, it is possible to reset the energy request close to zero by applying an appropriate filtering strategy, as discussed in [82]. The filtering strategy consists of measuring the current energy request of the sum of the AGC and previous trades on the intraday market, then purchasing the negative of that quantity on the intraday market for time slot $t + \delta$. This strategy attempts to reset the energy request of the AGC to zero at every timestep, but is affected by the delay of one hour caused by the clearing of the market. A 'filtered' AGC signal is obtained that way as the sum of the actual AGC and the intraday trades. This filtering strategy is a heuristic to maintain the state of charge of the AGC close to zero.

We emphasize that this filtering strategy is not used in problem 7.2, but simply illustrates how the intraday market can be used in order to maintain the AGC state of charge closer to zero. Instead, in problem 7.2, the recourse decision matrix $\mathbf{N}$ exactly embeds such a filtering strategy to readjust the baseline through intraday trades taking into account the state of charge of the AGC but also other factors such as forecasts for weather and current state of the system.

Figure 7.11 shows how the energy request histogram is transformed by applying the heuristic filtering strategy described above. Both the worst-case energy request and its 95^{th} percentile are divided by a factor larger than two. This shows that the energy storage capacity of the physical system needed is greatly reduced if we resort to the intraday market to offset its 'state of charge'. It is noticeable that the use of the intraday market reduces the variance of the energy request and brings the storage requirement typically around one kWh per kW of capacity offered against three to four times more when doing only day-ahead purchases.

7.6 Simulation and Experimental study

7.6.1 Experiments

In this section, we present a series of experiments that have been performed in the period from December 2015 to April 2016.

Each experiment extends over a period comprised between 18 and 24 hours. Experiments differ in two ways:

- Half of the experiments are performed as described in Sections 7.4.4 and 7.4.3, with the building controller computing a bid for tracking and purchasing energy in the day-ahead and intraday market. In the other half, it is assumed that the building cannot trade energy on the intraday market: therefore its baseline is entirely purchased day ahead and it has no opportunity to reschedule it. The aim is to highlight the effect of the intraday market in the ability of the building to successfully provide regulation. In practice, no intraday trades can be enforced by simply setting variables

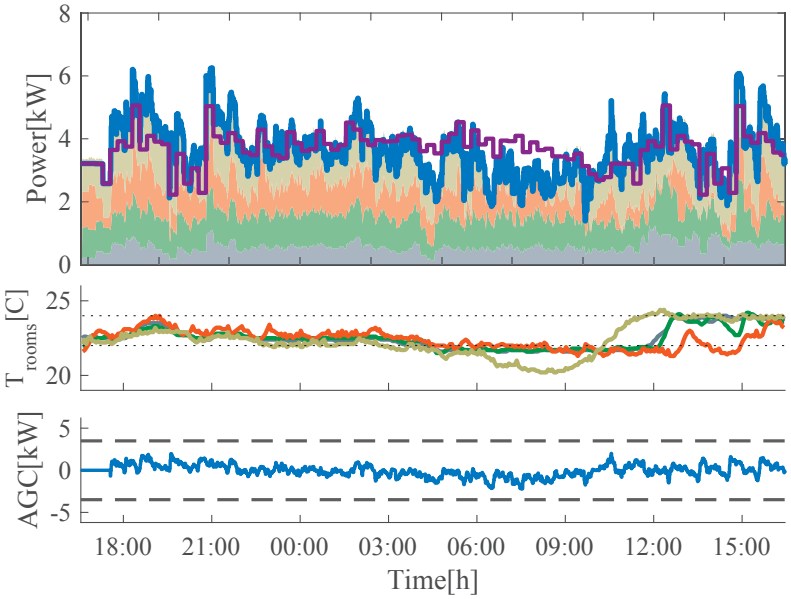

(a) AGC tracking without participation in the intraday market.

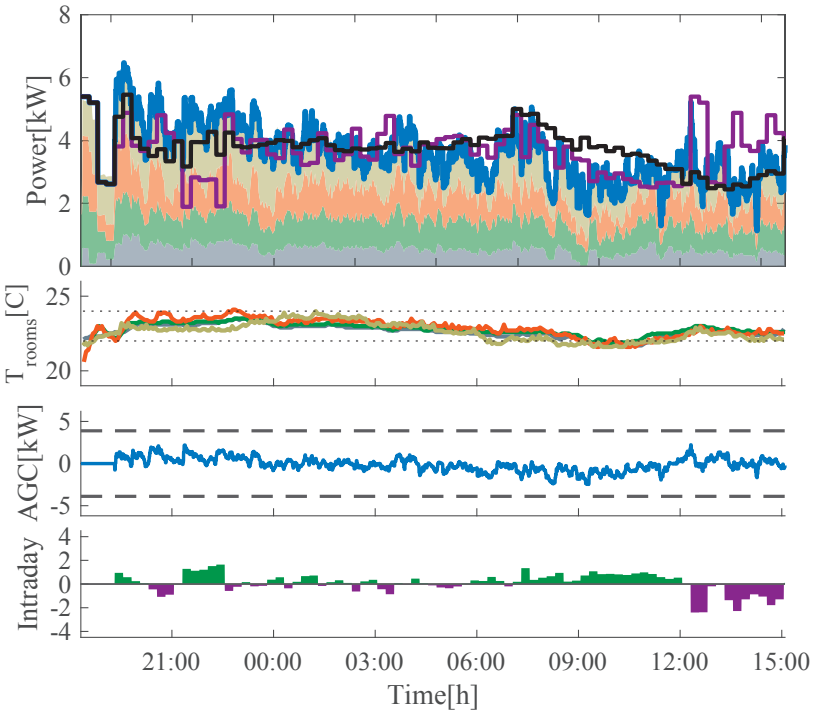

(b) AGC tracking with baseline readjustments in the intraday market.

Figure 7.12 – Two experiments of AGC tracking. The same AGC signal is used in both. Upper: Power distribution across the four zones. Baseline applied energy consumption (solid black line) advertised at time of bidding for subfigure (a) and the baseline after intraday transactions in subfigure (b). The original baseline (day-ahead) in the intraday scheme is also displayed (purple solid line). The blue line represents the total power to be tracked. Middle Up: Temperature variation for different zones. Each color corresponds to the measured temperature in each zone. Middle down: AGC signal variation and capacity bid. Lower: Transaction on the intraday market. Positive transactions (buy) in green and negative transactions in pink.

Parameter	Values
P_{max}	1.9kW
α	0.05
T_{ref}	23 ^oC
β	0.5; 1; 1.5; 2^oC
N_1	96 (1 day)
N_2	24 (6 hours)
N_s	200

Table 7.3 – Parameters of the simulation and experiments

$\mathbf{p}_{.|.+\delta}$ in the bidding problem to zero a priori.

- For each case (with and without intraday tracking), experiments have been conducted with different comfort ranges of ± 0.5, ± 1, ± 1.5 and $\pm 2^oC$ respectively around the comfort temperature $T_{\text{ref}} = 23^oC$ for all rooms. This allows exploring the trade-off between comfort and the ability of the building to provide regulation services. Varying the temperature comfort range is a simple way to control the comfort level.

Table 7.3 compiles the values of the parameters used in the simulation and experiments. The sampling time of the model in Problem 7.2 and the controller (7.20) is 15 minutes. A selection of representative previously observed AGC signals has been used in the different experiments. Realizations of the AGC with large energy requests have been included since they should illustrate best the influence of the intraday market.

A complete report on the experiments is found in Section E. One pair of experiments has been selectively reported in Figure 7.12 to illustrate how the use of the intraday can be beneficial. In Figure 7.12(a), the baseline was fixed at the beginning of the experiment. At around 7 am, due to errors in forecasts and a request for reducing power consumption (negative AGC), the controller ends up in a situation where it has to violate lower temperature constraints for at least one room since its 'budget' for power consumption is too low. The controller then takes a few hours to completely recover. Experiment 7.12(b) was performed in similar conditions but with the possibility to resort to the intraday market trades. Notice that the initial baseline schedule (purple line) is very close to the one for the first experiment, and the AGC test signal is the same in both experiments. It can be seen that from the moment the temperature starts to drop around 6am the controller anticipates the risk of constraint violation and purchases extra baseline for the upcoming hours, which eventually avoids constraint violation around 10am, when all temperatures reach the lower value of the constraints. Besides, by explicitly modelling the fact that the baseline could be readjusted, the optimal capacity computed in that case was larger by about 20%. A detailed discussion on all experiments is reported in appendix E.

We will next support the claim that what is observed in that particular experiment should be observable on average across all experiments and is characteristic of the difference between the two control schemes. Figure 7.13 aims at quantifying the trade-off between capacity offered and comfort. The capacity is reported as the percentage of the total power

installed that could be offered as up/down regulation. Comfort is computed using the *ASHRAE likelihood of dissatisfaction (ALD)* (see appendix B for more details). Experiments have been grouped in pairs for readability where each pair was performed in similar conditions (close weather, same AGC signal, and comfort constraints). In each pair, the round marker represents the result of the experiment when using intraday trades and the square marker the one without having intraday transactions. The first observation is that, in similar conditions, experiments using the intraday market always resulted in higher capacity bids and higher comfort.

Ultimately, each color of experiment corresponds to a different level of constraint tightening β from $\pm 0.5^oC$ in red to $\pm 2^oC$ in green. As expected, as the constraints are relaxed, higher bids for regulation can be offered, and result in lower average comfort.

7.6.2 Simulations

A series of simulations were also performed to compare with the experiments. The weather recorded for 60 different days during winter 2015 was used for simulations. For each weather scenario, the optimal bid is computed for 5 different levels of comfort tightening (the same as in the experiment plus $\pm 0.25^oC$, depicted in dark blue). The optimal computed controller was applied for 9 representative scenarios of the AGC. The resulting level of comfort was computed and reported in Figure 7.13. The conclusion derived from the experiments are confirmed and can be summarized as follows:

- Trading energy on the intraday market to readjust the baseline allows to offer higher capacity bids and improve comfort while offering regulation.

- Comfort level and regulation capability can be traded off, for example by relaxing the temperature constraints. The more the relaxation, the lower the comfort and the higher the bid.

Secondly, it can be seen that experimental results are consistent with the simulations in the sense that computed bids are almost identical while comfort levels are close. Experiments (especially when constraints are very tight), tend to display lower comfort with respect to the simulations. This is expected since simulations assume perfect predictions and perfect measurements, which of course is not the case in experiments.

Another conclusion seems to appear through the simulation results: for a given constraint level, the use of the intraday market increases the capacity offer, but also mitigates the variance of the comfort with respect to weather scenarios and AGC signals.

To illustrate the extent to which the intraday market is used, we report in Table 7.4 the statistics of the experiments. The total energy consumption, total net and absolute amount of intraday trades, as well as total day-ahead energy purchased, are reported. For the simulation columns, the number are averages over simulations performed with the same set of experiments as for Figure 7.13, with an extended test set for the AGC scenarios. For the experiments, averages over the 10 experiments of Figure 7.13 are reported.

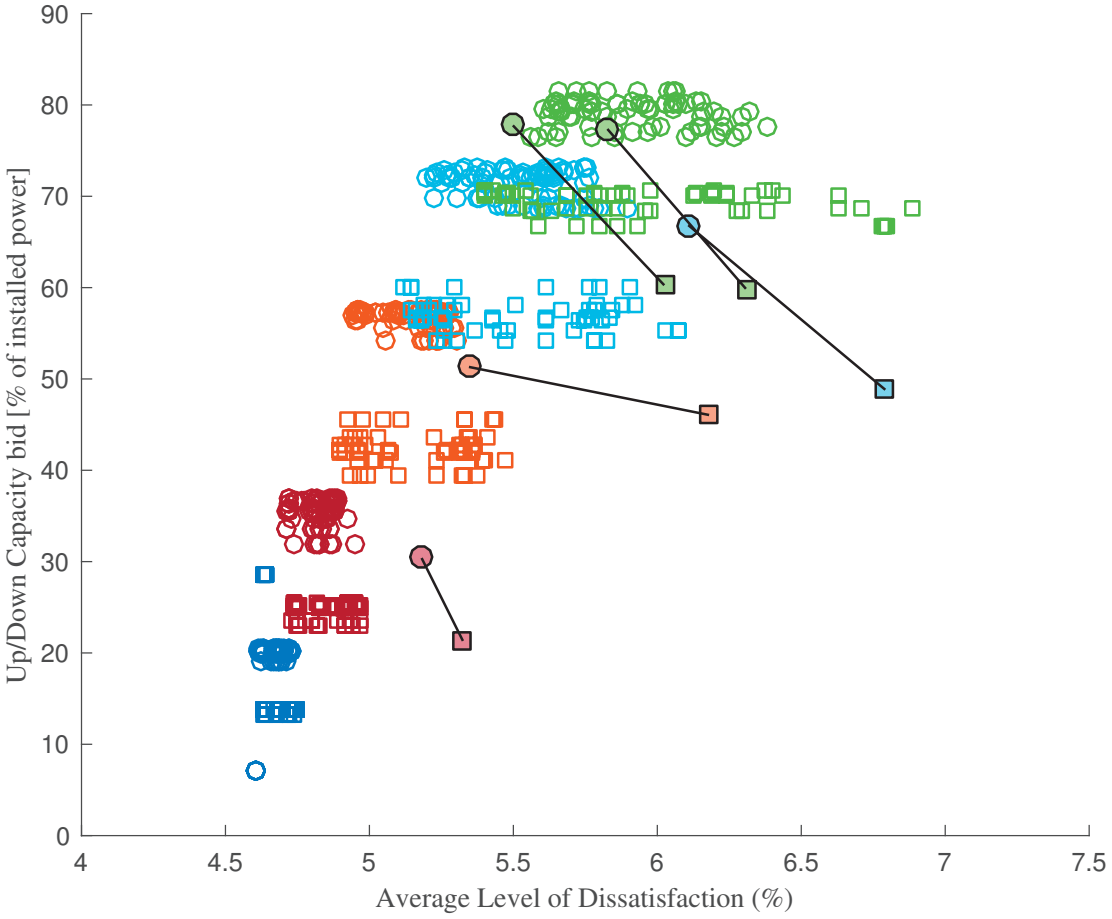

Figure 7.13 – Tracking capacity bid versus comfort achieved in closed-loop experiments and simulation . Colors correspond to different levels of constraint tightening (dark blue for $\pm 0.25^oC$, red for $\pm 0.5^oC$, orange for $\pm 1^oC$, light blue for $\pm 1.5^oC$, green for $\pm 2^oC$). White face markers correspond to simulation instances and colored ones to experiments. Circles correspond to experiments with intraday trades and squares to experiments without intraday trades. Desired improvement direction is to the top left

Quantity (in kWh/h)	Simulation (intraday)	Simulation (no intraday)	Experiment (intraday)	Experiment (no intraday)
Total Consumption	3.2	3.3	4.1	3.8
Day Ahead Purchases	3.3	3.3	3.6	3.8
Net Intraday Purchases	-0.1	0	0.5	0
Absolute Intraday Purchases	1	0	0.8	0
Avg Constraint Violation (^{o}C)	0	0	0.026	0.047

Table 7.4 – Statistics of the experiments. Numbers reported are normalized by the length of the experiments, yielding an average hourly consumption. The last line reports the constraint violation, averaged over rooms and time, in degrees Celsius.

Remark 7.4. When offering tracking, the total power consumption naturally depends on the AGC request. A set of simulations with a controller that tracks the reference temperature T_{ref} in every zone was conducted. The resulting power consumption has been compared to the one of the controller performing AGC tracking, but assuming that the AGC request is zero. The power consumptions differ by only 1% on average, which suggests that in the absence of an AGC request, the controller would perform almost identically to a controller maximizing comfort. Roughly speaking, that follows from the fact that maximum flexibility is available at the optimal comfort level when the temperature is in the middle of the temperature constraints if positive or negative requests are equally likely (which is the case regarding the AGC) □

The following observations are in order:

- The volume of intraday trades (sum of the absolute value of intraday trades) amounts to about 25% of the total power consumption, both in simulations and experiments. This demonstrates that the closed loop controller described in Section 7.4.4 is not trying to overact on the intraday market to maintain the temperature in the comfort range.

- In simulations, the net intraday energy trades are quite small on average: this means that intraday trades tend to cancel out over time, leaving a net intraday purchase below 5 % of the total power consumption.

- In the experiments, intraday trades are consistently positive at around 10 % of the total power consumption. This means that the algorithm tends to underestimate the needed power consumption slightly. Besides the fact that the number of experiments is not statistically significant, it is difficult to identify a single factor explaining this phenomenon: errors in weather forecasts, bias in the AGC signal received, model mismatch and unexpected disturbances will together contribute to these prediction errors. Note that if a consistent bias was confirmed over a more extensive set of experiments, it should be possible to eliminate it by, e.g., readjusting the prediction model. In general, it should be expected that prediction errors cannot be completely eliminated.

- In experiments, the average amount of constraint violation is almost divided by two when resorting to intraday trades. This confirms the observations made based on Figure 7.12 and can be explained simply: in the case where the baseline cannot be readjusted, the control authority available after the baseline has been fixed is relatively limited, whereas it is significantly increased when intraday trades are available. Therefore in the latter case, the controller is able to reject disturbances more efficiently and therefore mitigate constraint violations and increase average comfort, despite the fact that the regulation capacity offered is even larger. A by-product of this is that the controller is then less sensitive to forecast and model prediction errors. This directly relates to the discussion of Section 7.5.

Finally, based on these remarks, we emphasize that the strength of our approach is that the closed loop controller is able to overcome prediction errors and unexpected disturbance more successfully when resorting to baseline readjustments. That is very important because disturbances and errors cannot be avoided entirely in real-world applications. Conversely, it also means that for a fixed level of performance of the controller, the quality of models and forecast can be smaller when the baseline can be readjusted.

7.6.3 Discussion

Practical relevance and relations to other work

This work demonstrates how the inherent storage in a building can be used in order to offer significant flexibility at a controlled level of occupant discomfort. Combining our findings with those of other works considering commercial HVAC systems suggests some directions for practical implementation of regulation with commercial buildings. The works [141] and [78] have shown experimentally that frequency regulation could technically be provided by variable speed drive chillers and fans. However, they limit the frequency band supported by pre-filtering the regulation signal within a frequency band between 30 seconds and 10 minutes. By limiting the impact of the controls on the inside temperature as much as possible, only the inertia in the HVAC system is used, and this inertia is quite small in the absence of a storage system. Effectively, the inertia of the building system itself remains unused. By modeling the thermal dynamics of the building, our work demonstrated that a robust strategy could be used to exploit the inertia in the building heated space successfully and, hence, extend the frequency range of the service.

An interesting research direction could be to combine both concepts. On one side, the inertia of the HVAC could be exploited to absorb the fastest frequencies, for example by changing the duct pressure setpoint [78]. On the other hand, thermal power demand of the indoor space could be used to absorb slower frequencies. This requires the modeling of the response of the room temperature to changes in thermal power input, which has been demonstrated in our work. In general, a model of the effect of changes in the thermal power demand on the electricity power consumption needs to be found, but for slower timescales only, which mitigates the issue of modeling the interactions of all the components on fast timescales. The difficulty of this task is system dependent.

Need for fast actuation

Realistic HVAC systems also have a limit in terms of how fast they can vary their power consumption. Previous work on chillers and fans suggest that frequencies faster than 30 sec can pose operational issues for the equipment. To improve the quality of tracking, it might be needed to attach to the system a fast storage element such as an electric battery. Because of the high cost of battery capacity, the operation should try to limit the capacity needed for the control task, and therefore absorb only the fastest frequencies with the battery. Figure 7.14 gives the size of the battery needed to absorb the high frequency part

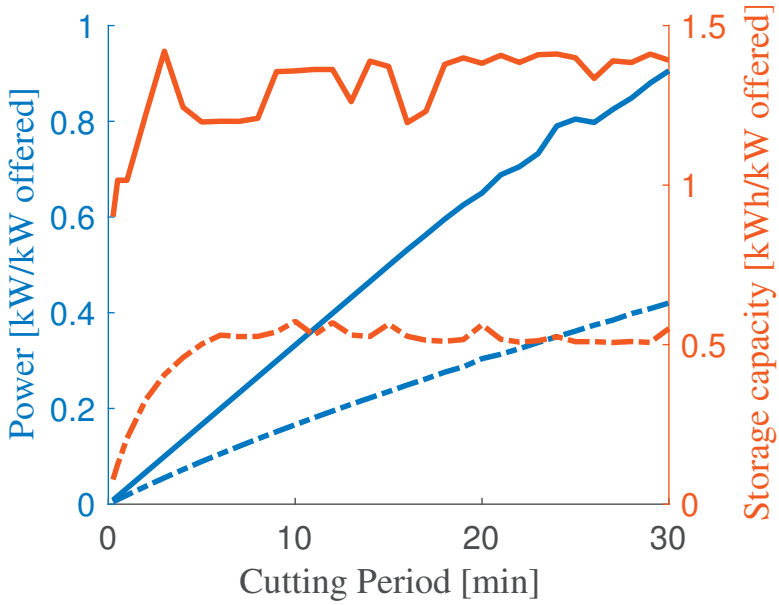

Figure 7.14 – Characteristics of the battery needed to absorb the fastest frequency in the AGC. Power ratings are in blue and energy storage capacity in red. Solid line is the worst case over one year, and dashed line the value needed to cover 99% of the signal. Values are computed for a 1 kW tracking capacity. The cutting period is the period corresponding to the highest frequency that the battery needs to track.

of the AGC as a function of the filtering frequency.

7.7 Validation of the virtual battery concept

In order to illustrate the concept of the virtual battery, an experiment was designed to highlight how the building can act as an energy storage resource. Once more, Problem 7.2 was solved with the difference that the reference set is chosen as in Equation (5.54), *i.e.* :

$$\hat{\Xi} = \left\{ \boldsymbol{a} \;\middle|\; \begin{array}{ll} s_0 = \dfrac{s_{max}}{2} & \\ 0 \leq s_t \leq s_{max}, & \forall t \in \mathbb{Z}_{[1,N]} \\ s_{t+1} = s_t + a_t & \forall t \in \mathbb{Z}_{[1,N]} \\ -1 \leq a_t \leq 1 & \forall t \in \mathbb{Z}_{[1,N]} \end{array} \right\} \tag{7.21}$$

with $s_{max} = 2.5kWh$. Excluding intraday trades in order to preserve the physical interpretability, we compute the maximum scaling of $\hat{\Xi}$ that the system can handle. Then, we run the experiment as described in Section 7.4.4. The signal extracted from $\hat{\Xi}$ is chosen such that the 'battery' reference discharges initially, then recharges entirely and discharges again finally, in alternating periods of five hours. The tracking signal is depicted in Figure 7.15 in the bottom subplot.

As a result, we observe in the middle subplot of Figure 7.15 that the temperature drops when the reference signal is negative and rises when it is positive. It is interesting to notice how most of the range of the temperature constraints is explored going from the 'discharged' state to the 'charged' state, which suggests that the scaling of the battery selected is neither too conservative (which would result in a small exploration) or too large (which would result in constraint violation). we can simply notice that temperatures are slightly shifted down compared to the center of the comfort range. This is due in part to the initial condition which happened to be quite low at the beginning of the experiment and was not fully canceled after the first hour. That causes some small constraint violation in one of the rooms and some extra slack in the higher range of temperature when the reference is consistently positive. We recall that the baseline in that case was not readjusted during the experiment, therefore there was no opportunity to cancel that shift by an positive readjustment of the baseline.

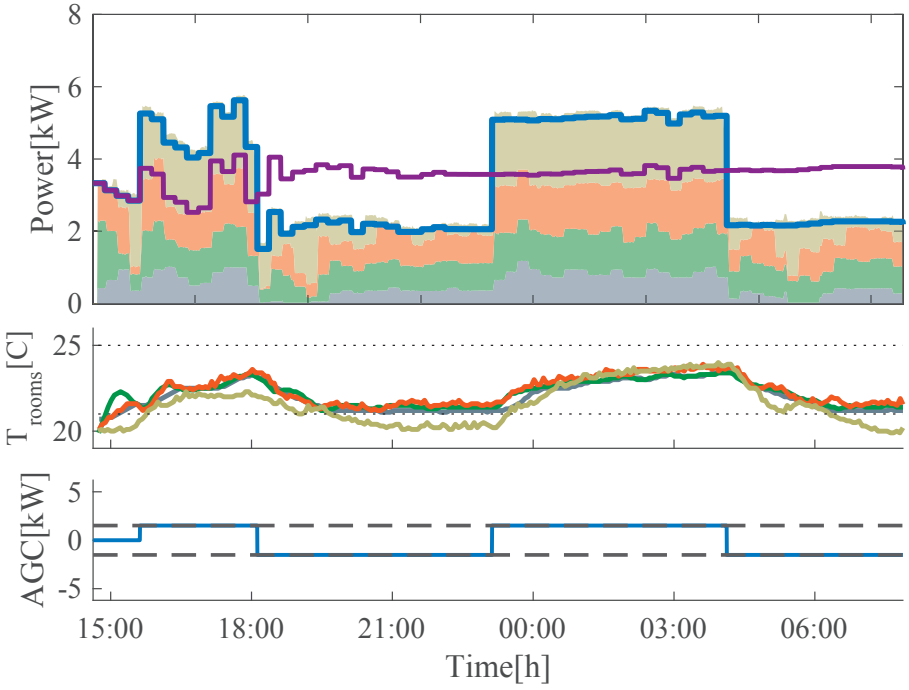

Figure 7.15 – Virtual battery validation

Appendix

E Full report of the experimental campaign

We report in this appendix the time plots for all the experiments reported in Figure 7.13 and discussed in the section 7.6.1. The experiments are grouped in pairs, so that each pair of experiments is performed with the same comfort constraint range in similar weather conditions and in most cases with the same realization of the AGC signal. They only differ in the fact that in the first experiment, the baseline was fixed day-ahead, and in the second it was adjusted on the intraday market with a one hour delay. In each plot, the top graph reports the electric power used in each room with stacked shaded colors. In purple the final baseline consumption is reported, and in blue the final total power consumption (that is the sum of the baseline and the scaled AGC signal). The second graph reports the temperature in the four rooms, as well as the comfort range in dotted lines. The third plot reports the scaled AGC signal and the bounds on the maximum AGC that the system can receive (in other words the capacity) in dashed lines. Finally, the last plot of the second graph reports the intraday trades for the experiment. Green is used for positive transactions (energy bought) and purple for negative transactions (energy sold).

The experiments reported in Figure E.1 have already been discussed in Section 7.6.1.

Figure E.2 reports the results of the experiments when the temperature constraints were the most stringent (only $\pm 0.5^o$C). Accordingly, the bid is reduced and despite a relatively large positive excursion of the AGC signal in positive values, we can see that the temperature increases, but always within bounds. It can be also observed how the intraday purchases correlate with the AGC values, with a streak of negative purchases after the AGC takes positive values.

Figure E.3 reports experiments with constraints of $\pm 1.5^o$C. Most noticeable here is that in the intraday case, the initial condition for the building is particularly low, and the controller resorts to large positive purchases to compensate for that initial mismatch. Overall, the intraday purchases remain positive despite large positive excursions of the AGC signal. This shows that the intraday purchases are performed not only in accordance to the AGC values, but also in response to the current state of the system and estimated disturbance affecting it.

In the case of the experiments of Figure E.4, it is quite clear how in the case of no intraday, the temperature rises in relation to the values of the AGC: negative initially, and positive at the end of the experiment leading to a drop and a rise of the temperature around

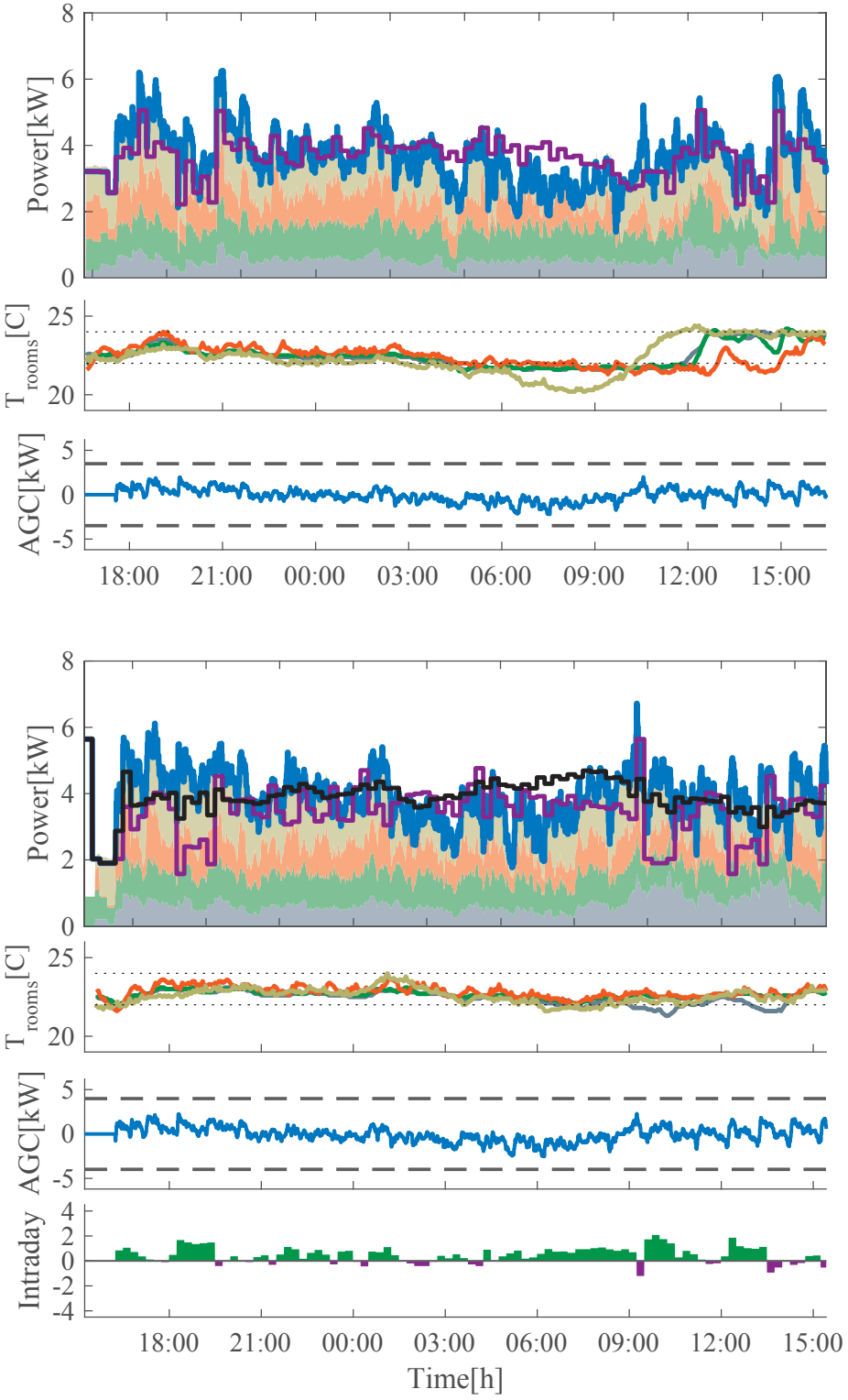

Figure E.1 – Experiments from 26/02/2016, no intraday (top) and 27/02/2016, intraday(bottom). $\beta = 1^{o}$C. Capacities: $\pm$3.5 and $\pm$3.9kW

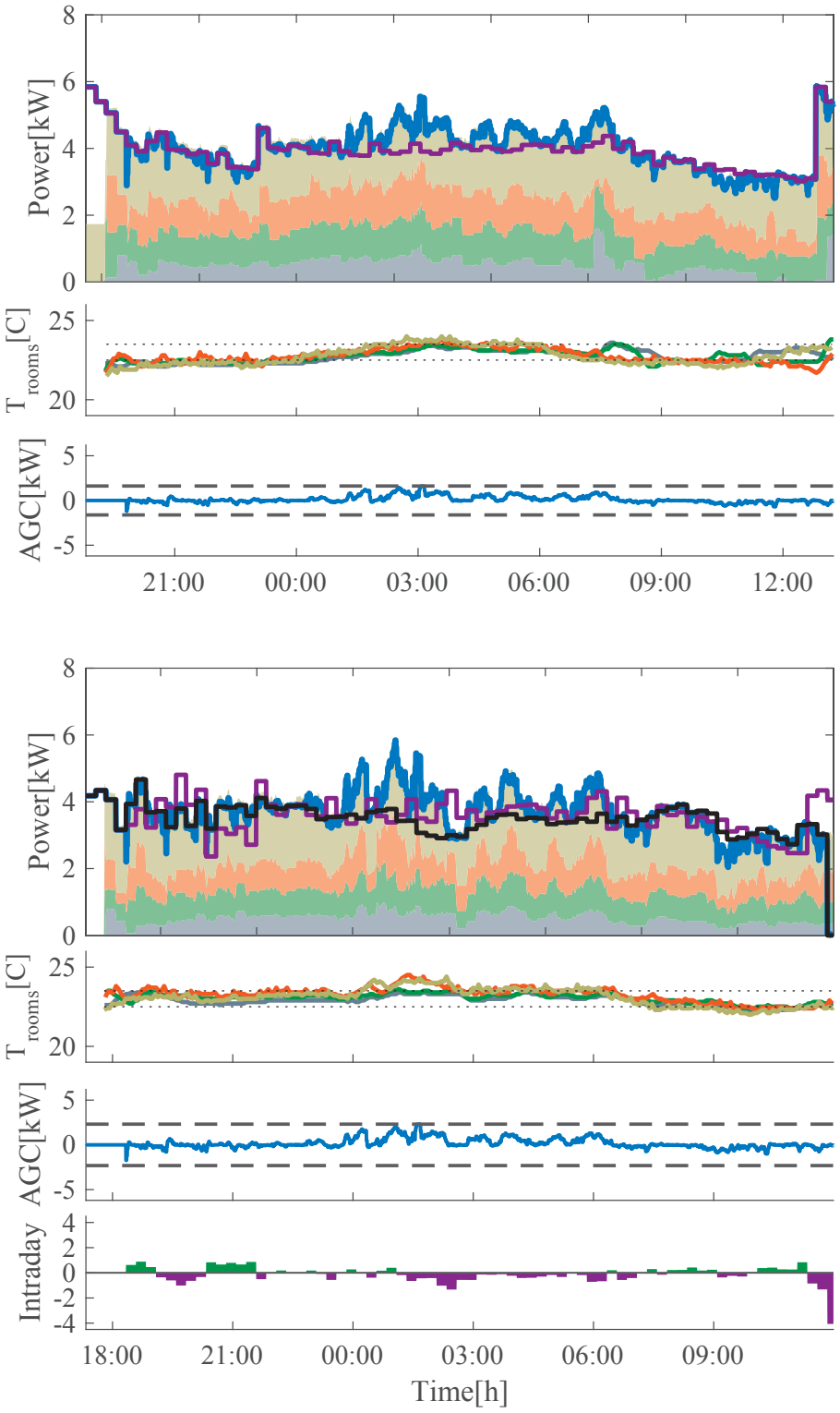

Figure E.2 – Experiments from 02/03/2016, no intraday (top) and 28/02/2016, intraday(bottom). $\beta = 0.5°C$. Capacities: ± 1.6 and ± 2.3kW

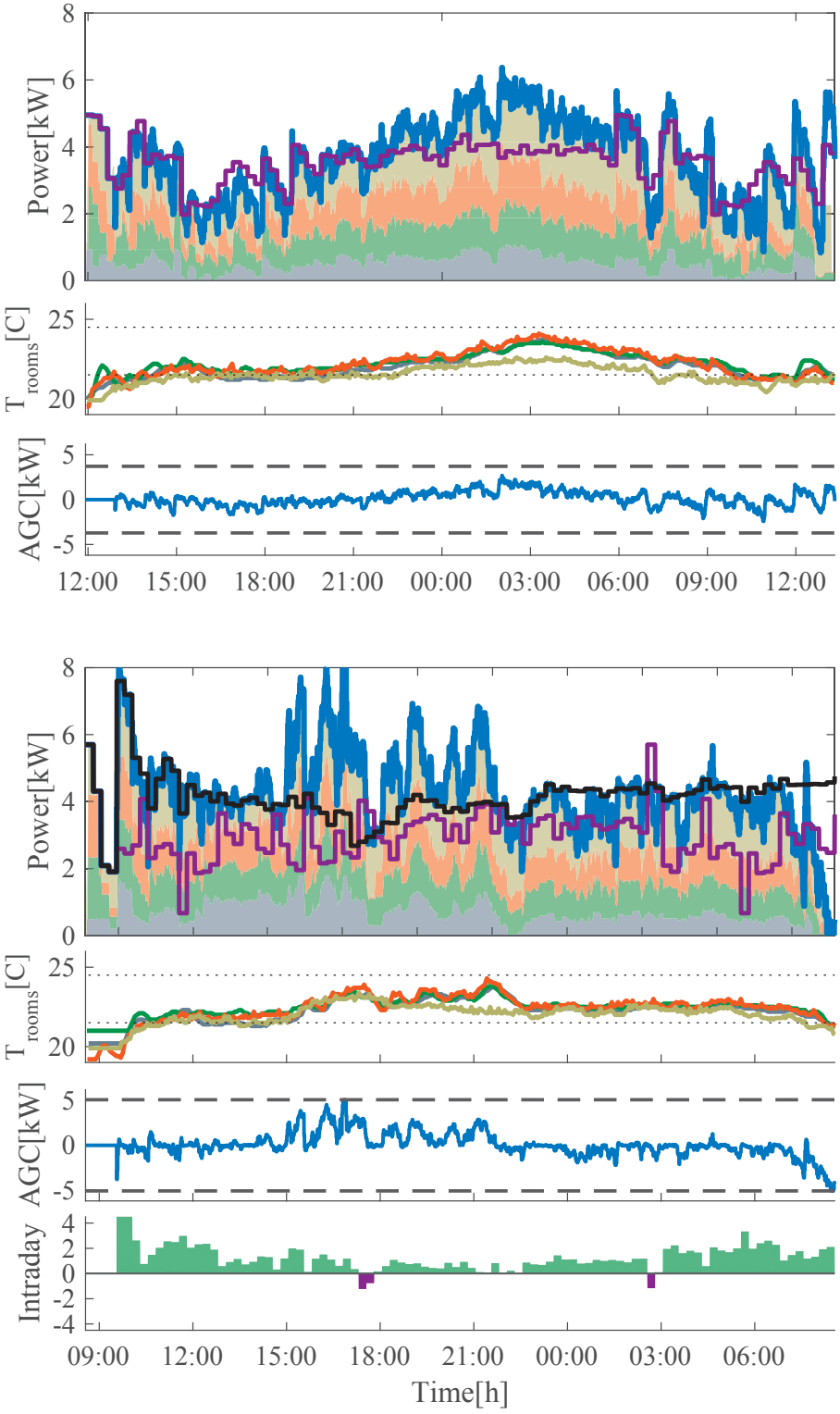

Figure E.3 – Experiments from 05/03/2016, no intraday (top) and 04/03/2016, intraday(bottom). $\beta = 1.5°C$. Capacities: ± 3.7 and ± 5.1kW

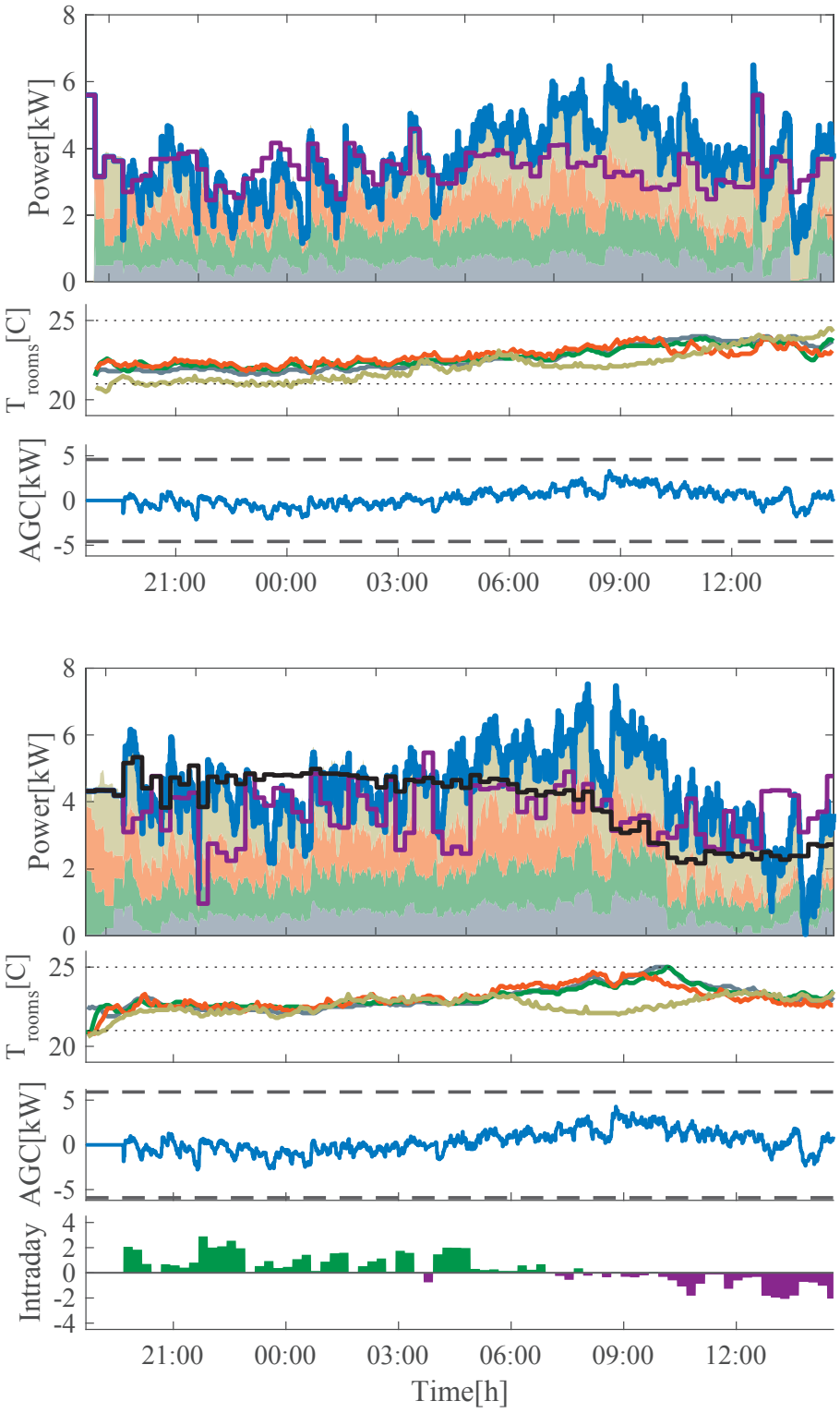

Figure E.4 – Experiments from 10/03/2016, no intraday (top) and 08/03/2016, intraday(bottom). $\beta = 2^{o}$C. Capacities: $\pm$4.6.9 and $\pm$5.9kW

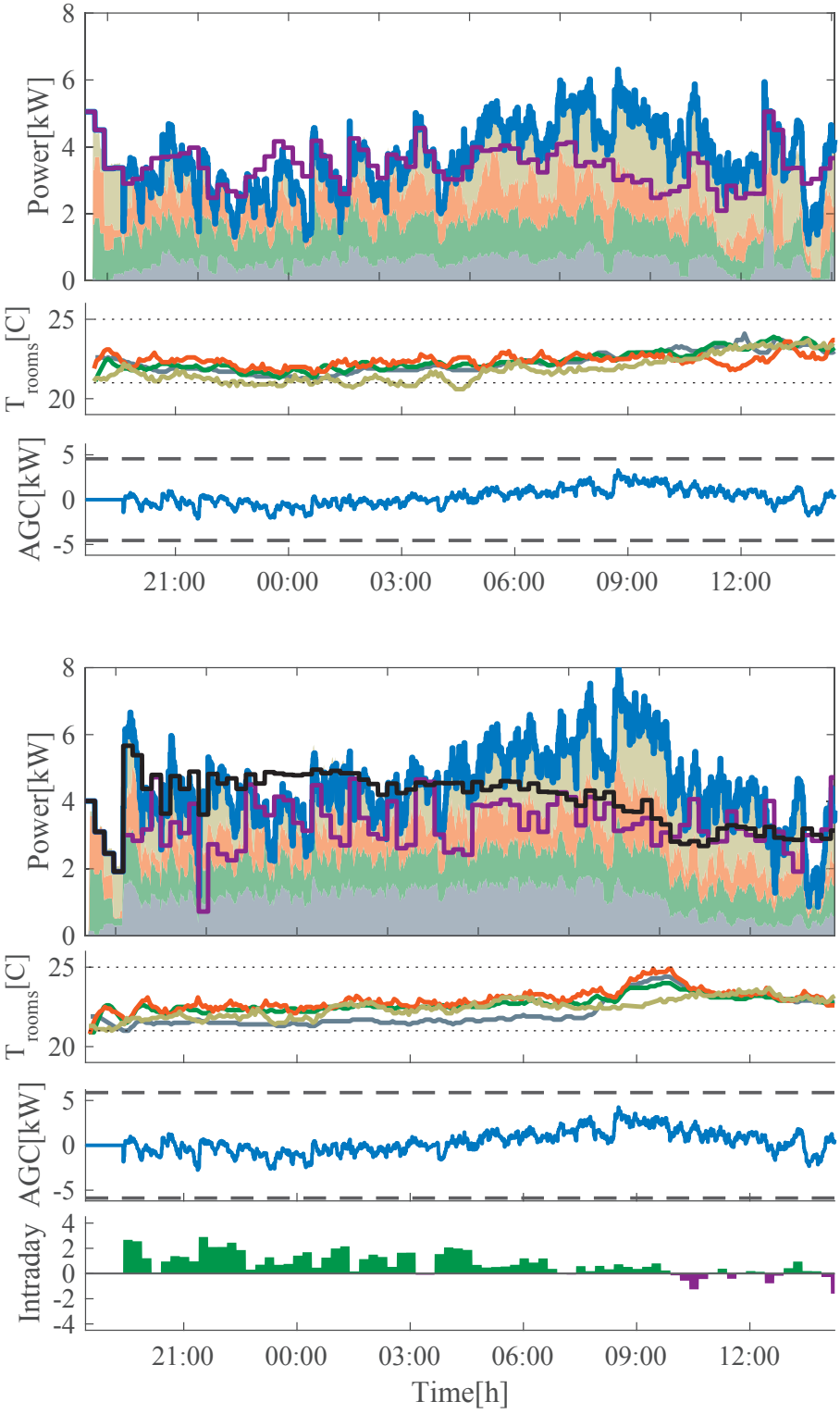

Figure E.5 – Experiments from 14/03/2016, no intraday (top) and 15/03/2016, intraday(bottom). $\beta = 2^o$C. Capacities: $\pm$4.6 and $\pm$5.9kW

the reference temperature, respectively. In the case of the intraday trades, by compensating the AGC in the intraday market, the temperature is maintained more consistently close to the reference.

Finally, in Figure E.5, we can also observe, how the transactions tend to be biased up on average to maintain the temperature closer to the reference temperature.

8 Conclusion

8.1 Summary

We have started by presenting the toolbox OpenBuild. This Matlab toolbox facilitates the design of predictive controllers for buildings by:

1. Extracting controller-ready models for the thermodynamics of buildings using standard building description data. These models feature a good prediction quality and help estimating the thermal power required in the building accurately. They also come with realistic input data modeling the effect of occupants, equipment and weather, that allow simulating building controllers in realistic conditions.

2. Providing a co-simulation interface with EnergyPlus that allows to test these models on a trusted simulation environment for validation.

Next, we have presented the robust tracking commitment problem. This problem formulation was directly motivated by our main question related to the provision of grid services with buildings and loads in general: How can we capture the flexibility of a load in its power consumption, both synthetically and as accurately as possible. To answer this question, the robust tracking commitment essentially formulates a multi-stage robust optimization problem for a system subject to uncertainties, but with the particularity that the set in which the uncertainty lies is part of the decision variables. This set can for example capture the set of all power consumption tracking requests a load can follow. In an effort to formalize the problem in a general setting, particular care was needed in order to make sure that the decisions are not taken considering information that is not supposed to be available at the time of the decision. This required the introduction of information structures and we showed how to modulate the uncertainty sets while taking this into account. Special cases of interest are listed where the robust tracking commitment problem can be formulated and solved tractably for large problem instances. An example of a building offering reserves to the grid illustrates the approach and the concept of 'virtual battery' is discussed in detail.

The last part of the thesis puts into practice the concepts developed in the second part. It reports the experiments conducted in the LADR experimental platform, a part of

our laboratory equipped with sensors and electric heaters for control experiments. It is demonstrated that we are able to satisfactorily evaluate the amount of secondary frequency control the system can provide, emulating the rules of the Swiss ancillary services market. We focused there on two aspects:

- The trade-off between comfort and flexibility, whereby the comfort constraint are set at different levels and we observe the resulting bids accordingly increase.
- The influence of the intraday market, which allows to readjust the power consumption baseline up to one hour before delivery. By explicitly modeling the recourse to the intraday market through the use of appropriate information structures, we see that the system can offer more flexibility at an increased level of comfort when using the intraday market.

8.2 Future directions

The topic of flexibility modeling is attracting a growing attention and numerous contributions suggest future directions in this domain. Starting from the elements presented in this thesis, four promising research venues are briefly presented here.

8.2.1 Data-driven modeling of buildings with OpenBuild

As we discussed in part I, the process of building model identification is heavy and requires large amount of experimental data. Even when precise description data is not available, OpenBuild can construct a structural model based on the geometry of the building. In this structural model, a handful of parameters could be identified to match the output of the EnergyPlus simulation (or field data) and the prediction of the model. This could be performed automatically using the already existing code structure of OpenBuild. Using this approach would allow to benefit from the processing power of OpenBuild, especially regarding the impact of the sun which is time varying during the day and therefore cannot be captured very well by a time-invariant linear model (as we have observed for room SW in the LADR experimental setup in section 7.3). Efforts in this direction have been initiated through master projects, but no conclusive result can be reported yet.

8.2.2 Computational aspects of large scale robust optimization

We have seen how to recast a problem with adjustable uncertainty set into a standard robust optimization problem. This allowed us to leverage known results from the literature to identify tractable instances of the problem in large dimensions, based on a dual reformulation of the problem. It is frequent to start from a very large dimensional problem due to the large system dimension and the very large horizon considered. The dual reformulation causes a massive increase of the number of variables to consider, sometimes rendering the problem too large. Moreover, this approach is only applicable under structural assumption on the problem. Considering these limitations, alternative methods have been proposed to solve

robust optimization problems. [98] propose a 'cutting-set' method where the problem is solved in an alternating fashion: the decision variable is computed with a finite subset of the constraint; based on that decision, a pessimizing realization of the uncertainty is computed by maximizing the constraint function on the uncertainty set. That pessimizer is then added to the surrogate uncertainty set and the procedure is repeated until convergence. It has been reported in [12] that despite no general conclusion can be derived concerning the computational advantage of the cutting set method compared to the dual reformulations, the cutting set method can outperform reformulations in some cases.

We have developed preliminary results exploring this type of methods, which are presented in the manuscript:

Tomasz T. Gorecki and Colin N. Jones. "Constrained bundle methods with inexact minimization applied to the energy regulation provision". In: *IFAC World Congress (accepted)*. Toulouse, France, July 2017

In this work, an alternative method is proposed to solve large scale robust optimization problems. It combines ideas from the cutting set method of [98] and of the bundle method of [127] for constrained nonsmooth optimization. Instead of assuming exact solutions to the minimization subproblems within the bundle method iterations, we propose to use an approximate solution to the minimization step and in particular to use the alternating direction method of multipliers (ADMM) [17] to perform this step efficiently. Beside taking advantage of the celebrated robustness properties of ADMM, we saw that obtaining low accuracy solutions to the minimization quickly allows to solve larger problems faster.

This method is demonstrated on 'flexibility commitment problems' arising in power systems applications. We show how the method proposed allows to tackle instances that could not be solved using convex reformulations. They also provide only slightly suboptimal solutions on smaller instance faster and thanks to the monotonic feasibility property of the bundle method used, usually provide feasible solutions.

This work is still under progress and can be extended to exploit more advanced bundle methods, explore other minimization methods than ADMM, and perform a more comprehensive comparison of the methods proposed.

8.2.3 Infinite horizon tracking

We have listed a number of ways to get infinite horizon guarantees for the robust tracking commitment problem. They rely on the knowledge of invariant sets of different kinds. As we have seen, there is no known method to compute robust controlled invariant sets for an adjustable uncertainty set. Some preliminary results have been developed that identify special cases where invariant sets for tracking can be computed while the uncertainty sets is optimized. Due to a very limited applicability, these results have been left out of the thesis but further work in this area may bring more satisfying infinite horizon guarantees. Finally, the infinite horizon tracking case with time-correlated uncertain sets, such as the virtual battery case, is probably the most interesting case of study, but remains relatively unexplored.

8.2.4 Distributed versions of the robust tracking commitment problem

We have been mostly concerned with characterizing the flexibility of one resource. It is expected that a large number of resources need to be aggregated in order to be offer significant flexibility to the grid. For example, secondary frequency control requires minimum bids of $\pm$ 5MW in Switzerland, which can rarely be met by a single building or resource. Therefore, aggregation schemes are required to pool resources together. It follows that an appropriate scheme needs to be devised to evaluate the flexibility of a pool of participants, and dispatch the tracking requirement in an appropriate way. In addition, issues regarding what data is shared arise in this situation due to privacy concerns.

A method to compute the flexibility of a collection of participants has already been proposed in [15]. It relies on the ADMM algorithm. Approximate methods relying on the robust tracking commitment can be imagined, which yield a minimum amount of communication. In its simplest form, each load could compute a set of possible references it can follow, for example solving a robust tracking commitment problem, using the full knowledge of its model and constraints. The reference set would be broadcasted to the aggregator which would choose one trajectory in the combination of all the reference sets of all participants. This requires only one round trip of communication between the aggregator and the providers in total for the period of time considered. Naturally, a closed loop version of the algorithm can be implemented, where the participants would update their reference sets over time, based on updated information and forecast. The effect of such a scheme on the closed behavior of the system, as well as its suboptimality is unclear and require a detailed investigation. Iterative schemes to improve on this simple version can also be imagined.

Bibliography

[1] Aleksandar S. Anđelković, Igor Mujan, and Stojanka Dakić. "Experimental validation of a EnergyPlus model: Application of a multi-storey naturally ventilated double skin façade". In: *Energy and Buildings* 118 (2016), pp. 27 –36. ISSN: 0378-7788. DOI: http://dx.doi.org/10.1016/j.enbuild.2016.02.045.

[2] ASHRAE. "Supervisory Control Strategies and Optimization". In: *2011 ASHRAE Handbook - HVAC Applications*. 2011.

[3] E. Atam and L. Helsen. "Control-Oriented Thermal Modeling of Multizone Buildings: Methods and Issues: Intelligent Control of a Building System". In: *IEEE Control Systems* 36.3 (2016), pp. 86–111. ISSN: 1066-033X. DOI: 10.1109/MCS.2016.2535913.

[4] Mesut Avci, Murat Erkoc, Amir Rahmani, and Shihab Asfour. "Model predictive HVAC load control in buildings using real-time electricity pricing". In: *Energy and Buildings* 60 (May 2013), pp. 199–209. ISSN: 0378-7788. DOI: 10.1016/j.enbuild.2013.01.008.

[5] M. Balandat, F. Oldewurtel, Mo Chen, and C. Tomlin. "Contract design for frequency regulation by aggregations of commercial buildings". In: *2014 52nd Annual Allerton Conference on Communication, Control, and Computing (Allerton)*. Sept. 2014, pp. 38–45. DOI: 10.1109/ALLERTON.2014.7028433.

[6] Miroslav Barić, Saša V. Raković, Thomas Besselmann, and Manfred Morari. "Max–Min Optimal Control of Constrained Discrete-time Systems". In: *IFAC Proceedings Volumes*. Vol. 41. 17th IFAC World Congress. 2008, pp. 8803–8808. DOI: 10.3182/20080706-5-KR-1001.01488.

[7] S. Barot and J. A. Taylor. "An outer approximation of the Minkowski sum of convex conic sets with application to demand response". In: *2016 IEEE 55th Conference on Decision and Control (CDC)*. Dec. 2016, pp. 4233–4238. DOI: 10.1109/CDC.2016.7798912.

[8] A. Ben-Tal, L. El Ghaoui, and A. Nemirovski. *Robust Optimization*. Princeton University Press, 2009.

[9] Aharon Ben-Tal, Dick den Hertog, and Jean-Philippe Vial. "Deriving robust counterparts of nonlinear uncertain inequalities". en. In: *Mathematical Programming* 149.1-2 (Feb. 2014), pp. 265–299. ISSN: 0025-5610, 1436-4646. DOI: 10.1007/s10107-014-0750-8.

[10] S. Bengea, V. Adetola, K. Kang, M. J. Liba, D. Vrabie, R. Bitmead, and S. Narayanan. "Parameter estimation of a building system model and impact of estimation error on closed-loop performance". In: *2011 50th IEEE Conference on Decision and Control and European Control Conference*. 2011, pp. 5137–5143. DOI: 10.1109/CDC.2011.6161302.

[11] Willy Bernal, Madhur Behl, Truong X Nghiem, and Rahul Mangharam. "MLE + : A Tool for Integrated Design and Deployment of Energy Efficient Building Controls". In: *Proceedings of the Fourth ACM Workshop on Embedded Sensing Systems for Energy-Efficiency in Buildings*. 2012, pp. 123–130.

[12] Dimitris Bertsimas, Iain Dunning, and Miles Lubin. "Reformulation versus cutting-planes for robust optimization". In: *Computational Management Science* 13.2 (July 2015), pp. 195–217. ISSN: 1619-697X, 1619-6988. DOI: 10.1007/s10287-015-0236-z.

[13] Dimitris Bertsimas and Angelos Georghiou. "Design of Near Optimal Decision Rules in Multistage Adaptive Mixed-Integer Optimization". In: *Operations Research* 63.3 (Apr. 2015), pp. 610–627. ISSN: 0030-364X. DOI: 10.1287/opre.2015.1365.

[14] Dimitris Bertsimas, Vishal Gupta, and Nathan Kallus. "Data-Driven Robust Optimization". In: *arXiv:1401.0212 [math]* (Dec. 2013). arXiv: 1401.0212.

[15] Altuğ Bitlislioğlu, Tomasz T. Gorecki, and Colin N. Jones. "Robust Tracking Commitment with Application to Demand Response". In: *IEEE Transactions on Automatic Control* (2016).

[16] Franco Blanchini and Stefano Miani. *Set-Theoretic Methods in Control*. 1st. Birkhäuser Basel, 2007. ISBN: 0-8176-3255-7 978-0-8176-3255-7.

[17] Stephen Boyd, Neal Parikh, Eric Chu, Borja Peleato, and Jonathan Eckstein. "Distributed Optimization and Statistical Learning via the Alternating Direction Method of Multipliers". In: *Found. Trends Mach. Learn.* 3.1 (Jan. 2011), pp. 1–122. ISSN: 1935-8237. DOI: 10.1561/2200000016.

[18] J. E. Braun. "Reducing energy costs and peak electrical demand through optimal control of building thermal storage". In: *ASHRAE transactions* 96.2 (1990), pp. 876–888.

[19] James E. Braun and Nitin Chaturvedi. "An Inverse Gray-Box Model for Transient Building Load Prediction". In: *HVAC&R Research* 8.1 (2002), pp. 73–99. DOI: 10.1080/10789669.2002.10391290.

[20] D.S. Callaway and I.A. Hiskens. "Achieving Controllability of Electric Loads". In: *Proceedings of the IEEE* 99.1 (Jan. 2011), pp. 184 –199. ISSN: 0018-9219. DOI: 10.1109/JPROC.2010.2081652.

[21] M. C. Campi and S. Garatti. "Wait-and-judge scenario optimization". en. In: *Mathematical Programming* (July 2016), pp. 1–35. ISSN: 0025-5610, 1436-4646. DOI: 10.1007/s10107-016-1056-9.

[22] Salvatore Carlucci. *Thermal comfort assessment of buildings*. Springer, 2013.

[23] W. J. Cole, E. T. Hale, and T. F. Edgar. "Building energy model reduction for model predictive control using OpenStudio". In: *2013 American Control Conference*. 2013, pp. 449–454. DOI: 10.1109/ACC.2013.6579878.

[24] Drury B. Crawley, Jon W. Hand, Michaël Kummert, and Brent T. Griffith. "Contrasting the capabilities of building energy performance simulation programs". In: *Building and Environment* 43.4 (2008), 661–673. ISSN: 03601323. DOI: 10.1016/j.buildenv.2006.10.027.

[25] Drury B. Crawley, Linda K. Lawrie, Frederick C. Winkelmann, W.F. Buhl, Y.Joe Huang, Curtis O. Pedersen, Richard K. Strand, Richard J. Liesen, Daniel E. Fisher, Michael J. Witte, and Jason Glazer. "EnergyPlus: creating a new-generation building energy simulation program". In: *Energy and Buildings* 33.4 (2001), pp. 319–331. ISSN: 03787788. DOI: 10.1016/S0378-7788(00)00114-6.

[26] S. Di Cairano and F. Borrelli. "Constrained tracking with guaranteed error bounds". In: *2013 IEEE 52nd Annual Conference on Decision and Control (CDC)*. Dec. 2013, pp. 3800–3805. DOI: 10.1109/CDC.2013.6760469.

[27] Justin R. Dobbs and Brandon M. Hencey. "Model Predictive HVAC Control with Online Occupancy Model". In: *arXiv:1403.4662 [cs]* (Mar. 2014).

[28] DOE. *Auxiliary EnergyPlus Programs*. Tech. rep. 2013.

[29] US DOE. *EnergyPlus Engineering Reference*. 2012.

[30] Erik Ela, Michael Milligan, and Brendan Kirby. *Operating reserves and variable generation*. Tech. rep. 2011, pp. 275–3000.

[31] Switzerland Bundesamt fur Energie. *La Stratégie énergétique 2050 après la votation finale au Parlement*. 2015.

[32] of the European Parliament. *Directive 2010/31/EU on Building Energy efficiency*. May 2010.

[33] Luca Fabietti, Tomasz T. Gorecki, Faran A. Qureshi, Altuğ Bitlislioğlu, Ioannis Lymperopoulos, and Colin N. Jones. "Experimental Implementation of Frequency Regulation Services Using Commercial Buildings". In: *IEEE Transactions on Smart Grid* PP.99 (2016), pp. 1–1. ISSN: 1949-3053. DOI: 10.1109/TSG.2016.2597002.

[34] P. Falugi and D.Q. Mayne. "Model predictive control for tracking random references". In: *Control Conference (ECC), 2013 European*. July 2013, pp. 518–523.

[35] Poul O. Fanger. "Thermal comfort. Analysis and applications in environmental engineering." In: *Thermal comfort. Analysis and applications in environmental engineering.* (1970).

[36] M. P. Fanti, A. M. Mangini, M. Roccotelli, F. Iannone, and A. Rinaldi. "A natural ventilation control in buildings based on co-simulation architecture and Particle Swarm Optimization". In: *2016 IEEE International Conference on Systems, Man, and Cybernetics (SMC)*. 2016, pp. 002621–002626. DOI: 10.1109/SMC.2016.7844634.

[37] B. Francis. "The Linear Multivariable Regulator Problem". In: *SIAM Journal on Control and Optimization* 15.3 (May 1977), pp. 486–505. ISSN: 0363-0129. DOI: 10.1137/0315033.

[38] R Freire, G Oliveira, and N Mendes. "Predictive controllers for thermal comfort optimization and energy savings". In: *Energy and Buildings* 40.7 (2008), pp. 1353–1365. ISSN: 03787788. DOI: 10.1016/j.enbuild.2007.12.007.

[39] Robert M. Freund. "Postoptimal analysis of a linear program under simultaneous changes in matrix coefficients". In: *Mathematical Programming Essays in Honor of George B. Dantzig Part I*. Springer, 1985, pp. 1–13.

[40] Matthias D. Galus, S. Koch, and G. Andersson. "Provision of Load Frequency Control by PHEVs, Controllable Loads, and a Cogeneration Unit". In: *IEEE Transactions on Industrial Electronics* 58.10 (2011), pp. 4568–4582. ISSN: 0278-0046. DOI: 10.1109/TIE.2011.2107715.

[41] Angelos Georghiou, Wolfram Wiesemann, and Daniel Kuhn. "Generalized decision rule approximations for stochastic programming via liftings". en. In: *Mathematical Programming* (May 2014), pp. 1–38. ISSN: 0025-5610, 1436-4646. DOI: 10.1007/s10107-014-0789-6.

[42] E.G. Gilbert and Kok Tin Tan. "Linear systems with state and control constraints: the theory and application of maximal output admissible sets". In: *IEEE Transactions on Automatic Control* 36.9 (Sept. 1991), pp. 1008–1020. ISSN: 0018-9286. DOI: 10.1109/9.83532.

[43] LUCA GIULIONI. *Stochastic Model Predictive Control with application to distributed control systems*. Politecnico di Milano, 2015.

[44] L. Gkatzikis, I. Koutsopoulos, and T. Salonidis. "The Role of Aggregators in Smart Grid Demand Response Markets". In: *IEEE Journal on Selected Areas in Communications* 31.7 (July 2013), pp. 1247–1257. ISSN: 0733-8716. DOI: 10.1109/JSAC.2013.130708.

[45] Ravi Gondhalekar, Frauke Oldewurtel, and Colin N. Jones. "Least-restrictive robust periodic model predictive control applied to room temperature regulation". In: *Automatica* 49.9 (Sept. 2013), pp. 2760–2766. ISSN: 0005-1098. DOI: 10.1016/j.automatica.2013.05.009.

[46] Tomasz T. Gorecki, Altuğ Bitlislioğlu, Giorgos Stathopoulos, and Colin N. Jones. "Guaranteeing input tracking for constrained systems: theory and application to demand response". In: *the 2015 American Control Conference (ACC)*. 2015.

[47] Tomasz T. Gorecki, Luca Fabietti, Faran A. Qureshi, and Colin N. Jones. "Experimental Demonstration of Buildings Providing Frequency Regulation Services in the Swiss Market". In: *Energy and Buildings(accepted)* (2017).

[48] Tomasz T. Gorecki and Colin N. Jones. "Constrained bundle methods with inexact minimization applied to the energy regulation provision". In: *IFAC World Congress (accepted)*. Toulouse, France, July 2017.

[49] Tomasz T. Gorecki and Faran A. Qureshi. *OpenBuild Manual*.

[50] Tomasz T. Gorecki, Faran A. Qureshi, and Colin N. Jones. "OpenBuild : An Integrated Simulation Environment for Building Control". In: *2015 IEEE Multi-Conference on Systems and Control (MSC)*. 2015.

[51] Bram L. Gorissen, İhsan Yanikoğlu, and Dick den Hertog. "A practical guide to robust optimization". In: *Omega* 53 (June 2015), pp. 124–137. ISSN: 0305-0483. DOI: 10.1016/j.omega.2014.12.006.

[52] Paul J. Goulart, Eric C. Kerrigan, and Jan M. Maciejowski. "Optimization over state feedback policies for robust control with constraints". In: *Automatica* 42.4 (Apr. 2006), pp. 523–533. ISSN: 0005-1098. DOI: 10.1016/j.automatica.2005.08.023.

[53] Rob Guglielmetti, Dan Macumber, and Nicholas Long. "OpenStudio: an open source integrated analysis platform". In: *Proceedings of the 12th Conference of International Building Performance Simulation Association*. 2011.

[54] R. Halvgaard, N.K. Poulsen, H. Madsen, and J.B. Jorgensen. "Economic Model Predictive Control for building climate control in a Smart Grid". In: *Innovative Smart Grid Technologies (ISGT), 2012 IEEE PES*. Jan. 2012, pp. 1 –6. DOI: 10.1109/ISGT.2012.6175631.

[55] H. Hao, Y. Lin, A. S. Kowli, P. Barooah, and S. Meyn. "Ancillary Service to the Grid Through Control of Fans in Commercial Building HVAC Systems". In: *IEEE Transactions on Smart Grid* 5.4 (July 2014), pp. 2066–2074. ISSN: 1949-3053. DOI: 10.1109/TSG.2014.2322604.

[56] H. Hao, B. M. Sanandaji, K. Poolla, and T. L. Vincent. "Aggregate Flexibility of Thermostatically Controlled Loads". In: *IEEE Transactions on Power Systems* 30.1 (Jan. 2015), pp. 189–198. ISSN: 0885-8950. DOI: 10.1109/TPWRS.2014.2328865.

[57] H. Hao, B.M. Sanandaji, K. Poolla, and T.L. Vincent. "Aggregate Flexibility of Thermostatically Controlled Loads". In: *IEEE Transactions on Power Systems* Early Access Online (2014). ISSN: 0885-8950. DOI: 10.1109/TPWRS.2014.2328865.

[58] Ion Hazyuk, Christian Ghiaus, and David Penhouet. "Optimal temperature control of intermittently heated buildings using Model Predictive Control: Part I – Building modeling". In: *Building and Environment* 51 (2012), pp. 379 –387. ISSN: 0360-1323. DOI: http://dx.doi.org/10.1016/j.buildenv.2011.11.009.

[59] Robert H Henninger, Michael J Witte, and Drury B Crawley. "Analytical and comparative testing of EnergyPlus using IEA HVAC BESTEST E100–E200 test suite". In: *Energy and Buildings* 36.8 (Aug. 2004), pp. 855–863. ISSN: 0378-7788. DOI: 10.1016/j.enbuild.2004.01.025.

[60] Gregor P. Henze, Anthony R. Florita, Michael J. Brandemuehl, Clemens Felsmann, and Hwakong Cheng. "Advances in Near-Optimal Control of Passive Building Thermal Storage". In: *Journal of Solar Energy Engineering* 132.2 (2010), p. 021009. ISSN: 01996231. DOI: 10.1115/1.4001466.

[61] Gregor P. Henze, Doreen E. Kalz, Simeng Liu, and Clemens Felsmann. "Experimental Analysis of Model-Based Predictive Optimal Control for Active and Passive Building Thermal Storage Inventory". In: *HVAC&R Research* 11.2 (2005), pp. 189–213. ISSN: 1078-9669. DOI: 10.1080/10789669.2005.10391134.

[62] Martin Herceg, Michal Kvasnica, Colin N. Jones, and Manfred Morari. "Multi-parametric toolbox 3.0". In: *Control Conference (ECC), 2013 European*. IEEE, 2013, pp. 502–510.

[63] M. Houwing, R.R. Negenborn, and B. De Schutter. "Demand Response With Micro-CHP Systems". In: *Proceedings of the IEEE* 99.1 (Jan. 2011), pp. 200 –213. ISSN: 0018-9219. DOI: 10.1109/JPROC.2010.2053831.

[64] Jianjun Hu and Panagiota Karava. "A state-space modeling approach and multi-level optimization algorithm for predictive control of multi-zone buildings with mixed-mode cooling". In: *Building and Environment* 80 (Oct. 2014), pp. 259–273. ISSN: 0360-1323. DOI: 10.1016/j.buildenv.2014.05.003.

[65] IRENA. *Battery storage for renewables: Market status and technology outlook*. Tech. rep. 2015.

[66] Colin Jones, Eric C. Kerrigan, and Jan Maciejowski. *Equality set projection: A new algorithm for the projection of polytopes in halfspace representation*. Tech. rep. Cambridge University Engineering Dept, 2004.

[67] K. J. Kircher and K. M. Zhang. "Testing building controls with the BLDG toolbox". In: *2016 American Control Conference (ACC)*. 2016, pp. 1472–1477. DOI: 10.1109/ACC.2016.7525124.

[68] NEIL E. KLEPEIS, WILLIAM C. NELSON, WAYNE R. OTT, JOHN P. ROBINSON, ANDY M. TSANG, PAUL SWITZER, JOSEPH V. BEHAR, STEPHEN C. HERN, and WILLIAM H. ENGELMANN. "The National Human Activity Pattern Survey (NHAPS): a resource for assessing exposure to environmental pollutants". en. In:

Journal of Exposure Science and Environmental Epidemiology 11.3 (July 2001), pp. 231–252. ISSN: 1053-4245. DOI: 10.1038/sj.jea.7500165.

[69] Darin Koblick. *Vectorized Solar Azimuth and Elevation Estimation*. 2013.

[70] Stephan Koch, Johanna L. Mathieu, and Duncan S. Callaway. "Modeling and control of aggregated heterogeneous thermostatically controlled loads for ancillary services". In: *Proc. PSCC*. 2011, pp. 1–7.

[71] D. Kolokotsa, A. Pouliezos, G. Stavrakakis, and C. Lazos. "Predictive control techniques for energy and indoor environmental quality management in buildings". In: *Building and Environment* 44.9 (Sept. 2009), pp. 1850–1863. ISSN: 0360-1323. DOI: 10.1016/j.buildenv.2008.12.007.

[72] T. Kostiainen, I. Welling, M. Lahtinen, K. Salmi, E. Kähkönen, and J. Lampinen. "Modeling of Subjective Responses to Indoor Air Quality and Thermal Conditions in Office Buildings". In: *HVAC&R Research* 14.6 (Nov. 2008), pp. 905–923. ISSN: 1078-9669. DOI: 10.1080/10789669.2008.10391046.

[73] Michael Kummert, Philippe Andre, and Jacques Nicolas. "Optimal heating control in a passive solar commercial building". In: *Solar Energy* 69 (2001), pp. 103–116.

[74] Xiwang Li and Jin Wen. "Review of building energy modeling for control and operation". In: *Renewable and Sustainable Energy Reviews* 37 (Sept. 2014), pp. 517–537. ISSN: 1364-0321. DOI: 10.1016/j.rser.2014.05.056.

[75] D. Limon, I. Alvarado, T. Alamo, and E. F. Camacho. "MPC for tracking piecewise constant references for constrained linear systems". In: *Automatica* 44.9 (Sept. 2008), pp. 2382–2387. ISSN: 0005-1098. DOI: 10.1016/j.automatica.2008.01.023.

[76] D. Limon, I. Alvarado, T. Alamo, and E. F. Camacho. "Robust tube-based MPC for tracking of constrained linear systems with additive disturbances". In: *Journal of Process Control* 20.3 (Mar. 2010), pp. 248–260. ISSN: 0959-1524. DOI: 10.1016/j.jprocont.2009.11.007.

[77] Y. Lin, P. Barooah, S. Meyn, and T. Middelkoop. "Demand side frequency regulation from commercial building HVAC systems: An experimental study". In: *American Control Conference (ACC), 2015*. July 2015, pp. 3019–3024. DOI: 10.1109/ACC.2015.7171796.

[78] Y. Lin, P. Barooah, S. Meyn, and T. Middelkoop. "Experimental Evaluation of Frequency Regulation From Commercial Building HVAC Systems". In: *IEEE Transactions on Smart Grid* 6.2 (Mar. 2015), pp. 776–783. ISSN: 1949-3053. DOI: 10.1109/TSG.2014.2381596.

[79] Yashen Lin, T. Middelkoop, and P. Barooah. "Issues in identification of control-oriented thermal models of zones in multi-zone buildings". In: *2012 IEEE 51st Annual Conference on Decision and Control (CDC)*. Dec. 2012, pp. 6932–6937. DOI: 10.1109/CDC.2012.6425958.

[80] A. Lorca and X.A. Sun. "Adaptive Robust Optimization With Dynamic Uncertainty Sets for Multi-Period Economic Dispatch Under Significant Wind". In: *IEEE Transactions on Power Systems* 30.4 (July 2015), pp. 1702–1713. ISSN: 0885-8950. DOI: 10.1109/TPWRS.2014.2357714.

[81] Ioannis Lymperopoulos, Faran A. Qureshi, Truong Nghiem, Ali Ahmadi Khatir, and Colin N. Jones. "Providing ancillary service with commercial buildings: the Swiss perspective". In: vol. 48. Vancouver, Canada, 2015, pp. 6–13.

[82] Ioannis Lymperopoulos, Faran A. Qureshi, Truong Nghiem, Ali Ahmadi Khatir, and Colin N. Jones. "Providing ancillary service with commercial buildings: the Swiss perspective". In: *IFAC-PapersOnLine* 48.8 (2015). 9th (IFAC) Symposium on Advanced Control of Chemical Processes (ADCHEM), June 2015, pp. 6 –13.

[83] Jingran Ma, Joe Qin, Timothy Salsbury, and Peng Xu. "Demand reduction in building energy systems based on economic model predictive control". In: *Chemical Engineering Science* 67.1 (Jan. 2012), pp. 92–100. ISSN: 0009-2509. DOI: 10.1016/j.ces.2011.07.052.

[84] Jingran Ma, S.J. Qin, Bo Li, and T. Salsbury. "Economic model predictive control for building energy systems". In: *Innovative Smart Grid Technologies (ISGT), 2011 IEEE PES*. Jan. 2011, pp. 1 –6. DOI: 10.1109/ISGT.2011.5759140.

[85] Y. Ma, A. Kelman, A. Daly, and F. Borrelli. "Predictive Control for Energy Efficient Buildings with Thermal Storage: Modeling, Stimulation, and Experiments". In: *IEEE Control Systems* 32.1 (Feb. 2012), pp. 44 –64. ISSN: 1066-033X. DOI: 10.1109/MCS.2011.2172532.

[86] Yudong Ma, Francesco Borrelli, Brandon Hencey, Brian Coffey, Sorin Bengea, and Philip Haves. "Model Predictive Control for the Operation of Building Cooling Systems". In: *IEEE Transactions on Control Systems Technology* 20.3 (May 2012), pp. 796–803. ISSN: 1063-6536. DOI: 10.1109/TCST.2011.2124461.

[87] M. Maasoumy, C. Rosenberg, A Sangiovanni-Vincentelli, and D.S. Callaway. "Model predictive control approach to online computation of demand-side flexibility of commercial buildings HVAC systems for Supply Following". In: *American Control Conference (ACC), 2014*. June 2014, pp. 1082–1089. DOI: 10.1109/ACC.2014.6858874.

[88] Mehdi Maasoumy and Alberto Sangiovanni-Vincentelli. "Smart Connected Buildings Design Automation: Foundations and Trends". In: *Foundations and Trends® in Electronic Design Automation* 10.1-2 (2016), pp. 1–143. ISSN: 1551-3939. DOI: 10.1561/1000000043.

[89] D. Madjidian, M. Roozbehani, and M. A. Dahleh. "Battery capacity of deferrable energy demand". In: *2016 IEEE 55th Conference on Decision and Control (CDC)*. Dec. 2016, pp. 4220–4225. DOI: 10.1109/CDC.2016.7798910.

[90] Urban Maeder, Francesco Borrelli, and Manfred Morari. "Linear offset-free Model Predictive Control". In: *Automatica* 45.10 (Oct. 2009), pp. 2214–2222. ISSN: 0005-1098. DOI: 10.1016/j.automatica.2009.06.005.

[91] Urban Maeder and Manfred Morari. "Offset-free reference tracking with model predictive control". In: *Automatica* 46.9 (Sept. 2010), pp. 1469–1476. ISSN: 0005-1098. DOI: 10.1016/j.automatica.2010.05.023.

[92] K. Margellos, P. Goulart, and J. Lygeros. "On the Road Between Robust Optimization and the Scenario Approach for Chance Constrained Optimization Problems". In: *IEEE Transactions on Automatic Control* 59.8 (Aug. 2014), pp. 2258–2263. ISSN: 0018-9286. DOI: 10.1109/TAC.2014.2303232.

[93] Nuno M. Mateus, Armando Pinto, and Guilherme Carrilho da Graça. "Validation of EnergyPlus thermal simulation of a double skin naturally and mechanically ventilated test cell". In: *Energy and Buildings* 75 (2014), pp. 511 –522. ISSN: 0378-7788. DOI: http://dx.doi.org/10.1016/j.enbuild.2014.02.043.

[94] Peter May-Ostendorp, Gregor P. Henze, Charles D. Corbin, Balaji Rajagopalan, and Clemens Felsmann. "Model-predictive control of mixed-mode buildings with rule extraction". In: *Building and Environment* 46.2 (Feb. 2011), pp. 428–437. ISSN: 03601323. DOI: 10.1016/j.buildenv.2010.08.004.

[95] D. Q. Mayne, J. B. Rawlings, C. V. Rao, and P. O. M. Scokaert. "Constrained model predictive control: Stability and optimality". In: *Automatica* 36.6 (June 2000), pp. 789–814. ISSN: 0005-1098. DOI: 10.1016/S0005-1098(99)00214-9.

[96] D.Q. Mayne, M.M. Seron, and S.V. Raković. "Robust model predictive control of constrained linear systems with bounded disturbances". In: *Automatica* 41.2 (Feb. 2005), pp. 219–224. ISSN: 0005-1098. DOI: 10.1016/j.automatica.2004.08.019.

[97] Giorgio Metta, Paul Fitzpatrick, and Lorenzo Natale. "Yarp: Yet another robot platform". In: *International Journal of Advanced Robotic Systems* 3.1 (2006), p. 8.

[98] Almir Mutapcic and Stephen Boyd. "Cutting-set methods for robust convex optimization with pessimizing oracles". In: *Optimization Methods and Software* 24.3 (June 2009), pp. 381–406. ISSN: 1055-6788. DOI: 10.1080/10556780802712889.

[99] D. Subbaram Naidu and Craig G. Rieger. "Advanced control strategies for heating, ventilation, air-conditioning, and refrigeration systems—An overview: Part I: Hard control". In: *HVAC&R Research* 17.1 (2011), pp. 2–21. ISSN: 1078-9669. DOI: 10.1080/10789669.2011.540942.

[100] A. Nayyar, M. Negrete-Pincetic, K. Poolla, and P. Varaiya. "Duration-differentiated energy services with a continuum of loads". In: *53rd IEEE Conference on Decision and Control*. Dec. 2014, pp. 1714–1719. DOI: 10.1109/CDC.2014.7039646.

[101] T.X. Nghiem and G.J. Pappas. "Receding-horizon supervisory control of green buildings". In: *American Control Conference (ACC), 2011*. July 2011, pp. 4416 –4421.

[102] Xuan Truong Nghiem, Altug Bitlislioğlu Altuğ, Tomasz T. Gorecki, Faran Ahmed Qureshi, and Colin Jones. "OpenBuildNet Framework for Distributed Co-Simulation of Smart Energy Systems". In: *Proceedings of the 14th International Conference on Control, Automation, Robotics and Vision*. 2016.

[103] J. F. Nicol and M. A. Humphreys. "Adaptive thermal comfort and sustainable thermal standards for buildings". In: *Energy and Buildings*. Special Issue on Thermal Comfort Standards 34.6 (July 2002), pp. 563–572. ISSN: 0378-7788. DOI: 10.1016/S0378-7788(02)00006-3.

[104] Office fédéral de l'énergie (OFEN). *Ex-Post-Analyse des schweizerischen Energieverbrauchs 2000 bis 2013*. Tech. rep. 2014.

[105] F. Oldewurtel, A. Ulbig, A. Parisio, G. Andersson, and M. Morari. "Reducing peak electricity demand in building climate control using real-time pricing and model predictive control". In: *2010 49th IEEE Conference on Decision and Control (CDC)*. Dec. 2010, pp. 1927 –1932. DOI: 10.1109/CDC.2010.5717458.

[106] Frauke Oldewurtel, Theodor Borsche, Matthias Bucher, Philipp Fortenbacher, Marina Gonzalez Vaya Tobias Haring, Johanna L. Mathieu, Olivier Megel, Evangelos Vrettos, and Goran Andersson. "A framework for and assessment of demand response and energy storage in power systems". In: *Bulk Power System Dynamics and Control - IX Optimization, Security and Control of the Emerging Power Grid (IREP), 2013 IREP Symposium*. 2013, pp. 1–24. DOI: 10.1109/IREP.2013.6629419.

[107] Frauke Oldewurtel, Alessandra Parisio, Colin N. Jones, Dimitrios Gyalistras, Markus Gwerder, Vanessa Stauch, Beat Lehmann, and Manfred Morari. "Use of model predictive control and weather forecasts for energy efficient building climate control". In: *Energy and Buildings* 45 (Feb. 2012), pp. 15–27. ISSN: 03787788. DOI: 10.1016/j.enbuild.2011.09.022.

[108] Frauke Oldewurtel, David Sturzenegger, and Manfred Morari. "Importance of occupancy information for building climate control". In: *Applied Energy* 101 (Jan. 2013), pp. 521–532. ISSN: 0306-2619. DOI: 10.1016/j.apenergy.2012.06.014.

[109] Luis Pérez-Lombard, José Ortiz, and Christine Pout. "A review on buildings energy consumption information". In: *Energy and Buildings* 40.3 (2008), pp. 394–398. ISSN: 0378-7788. DOI: 10.1016/j.enbuild.2007.03.007.

[110] S. Privara, Z. Vana, D. Gyalistras, J. Cigler, C. Sagerschnig, M. Morari, and L. Ferkl. "Modeling and identification of a large multi-zone office building". In: *2011 IEEE International Conference on Control Applications (CCA)*. Sept. 2011, pp. 55 –60. DOI: 10.1109/CCA.2011.6044402.

[111] S. Prívara, Z. Váňa, D. Gyalistras, J. Cigler, C. Sagerschnig, M. Morari, and L. Ferkl. "Modeling and identification of a large multi-zone office building". In: *2011 IEEE International Conference on Control Applications (CCA)*. 2011, pp. 55–60. DOI: 10.1109/CCA.2011.6044402.

[112] F. A. Qureshi, I. Lymperopoulos, A. Ahmadi Khatir, and C. N. Jones. "Economic Advantages of Office Buildings Providing Ancillary Services with Intraday Participation". In: *IEEE Transactions on Smart Grid* PP.99 (2016), pp. 1–1. ISSN: 1949-3053. DOI: 10.1109/TSG.2016.2632239.

[113] Faran A. Qureshi, Tomasz T. Gorecki, and Colin N. Jones. "Model Predictive Control for Market-Based Demand Response Participation". In: *Proceedings of the 19th IFAC World congress*. Cape Town, South Africa, 2014.

[114] Faran Ahmed Qureshi, Tomasz T. Gorecki, and Colin N. Jones. "Model Predictive Control for Market-Based Demand Response Participation". In: *19th World Congress of the International Federation of Automatic Control*. 2014.

[115] S. V. Rakovic, M. Baric, and M. Morari. "Max-min control problems for constrained discrete time systems". In: *2008 47th IEEE Conference on Decision and Control*. Dec. 2008, pp. 333–338. DOI: 10.1109/CDC.2008.4739218.

[116] S. V. Raković, E. C. Kerrigan, D. Q. Mayne, and K. I. Kouramas. "Optimized robust control invariance for linear discrete-time systems: Theoretical foundations". In: *Automatica* 43.5 (May 2007), pp. 831–841. ISSN: 0005-1098. DOI: 10.1016/j.automatica.2006.11.006.

[117] S. V. Raković, B. Kouvaritakis, R. Findeisen, and M. Cannon. "Homothetic tube model predictive control". In: *Automatica* 48.8 (Aug. 2012), pp. 1631–1638. ISSN: 0005-1098. DOI: 10.1016/j.automatica.2012.05.003.

[118] Sasa Raković. "Invention of Prediction Structures and Categorization of Robust MPC Syntheses". In: ed. by Mircea Lazar. Aug. 2012, pp. 245–273. DOI: 10.3182/20120823-5-NL-3013.00038.

[119] S.V. Raković, E.C. Kerrigan, D.Q. Mayne, and J. Lygeros. "Reachability analysis of discrete-time systems with disturbances". In: *IEEE Transactions on Automatic Control* 51.4 (Apr. 2006), pp. 546–561. ISSN: 0018-9286. DOI: 10.1109/TAC.2006.872835.

[120] S.V. Raković, B. Kouvaritakis, M. Cannon, C. Panos, and R. Findeisen. "Parameterized Tube Model Predictive Control". In: *IEEE Transactions on Automatic Control* 57.11 (Nov. 2012), pp. 2746–2761. ISSN: 0018-9286. DOI: 10.1109/TAC.2012.2191174.

[121] S.V. Raković and M. Barić. "Parameterized Robust Control Invariant Sets for Linear Systems: Theoretical Advances and Computational Remarks". In: *IEEE Transactions on Automatic Control* 55.7 (July 2010), pp. 1599–1614. ISSN: 0018-9286. DOI: 10.1109/TAC.2010.2042341.

[122] Y.G. Rebours, D.S. Kirschen, M. Trotignon, and S. Rossignol. "A Survey of Frequency and Voltage Control Ancillary Services mdash;Part I: Technical Features". In: *IEEE Transactions on Power Systems* 22.1 (Feb. 2007), pp. 350–357. ISSN: 0885-8950. DOI: 10.1109/TPWRS.2006.888963.

[123] Y.G. Rebours, D.S. Kirschen, M. Trotignon, and S. Rossignol. "A Survey of Frequency and Voltage Control Ancillary Services mdash;Part II: Economic Features". In: *IEEE Transactions on Power Systems* 22.1 (Feb. 2007), pp. 358–366. ISSN: 0885-8950. DOI: 10.1109/TPWRS.2006.888965.

[124] Ibrahim Reda and Afshin Andreas. "Solar position algorithm for solar radiation applications". In: *Solar Energy* 76.5 (2004), pp. 577–589. ISSN: 0038-092X. DOI: 10.1016/j.solener.2003.12.003.

[125] Sullivan Royer, Stéphane Thil, Thierry Talbert, and Monique Polit. "A procedure for modeling buildings and their thermal zones using co-simulation and system identification". In: *Energy and Buildings* 78 (2014), pp. 231 –237. ISSN: 0378-7788. DOI: http://dx.doi.org/10.1016/j.enbuild.2014.04.013.

[126] Swissgrid SA. *Basic principles of ancillary service products*. Tech. rep. 2015.

[127] Claudia Sagastizábal and Mikhail Solodov. "An infeasible bundle method for nonsmooth convex constrained optimization without a penalty function or a filter". In: *SIAM Journal on Optimization* 16.1 (2005), pp. 146–169.

[128] Malte Schönemann. "Multiscale Simulation Modeling Concept for Battery Production Systems". In: *Multiscale Simulation Approach for Battery Production Systems*. Cham: Springer International Publishing, 2017, pp. 59–129. ISBN: 978-3-319-49367-1. DOI: 10.1007/978-3-319-49367-1_4.

[129] Pervez Hameed Shaikh, Nursyarizal Bin Mohd Nor, Perumal Nallagownden, Irraivan Elamvazuthi, and Taib Ibrahim. "A review on optimized control systems for building energy and comfort management of smart sustainable buildings". In: *Renewable and Sustainable Energy Reviews* 34 (June 2014), pp. 409–429. ISSN: 1364-0321. DOI: 10.1016/j.rser.2014.03.027.

[130] A. Shapiro, D. Dentcheva, and A. P. Ruszczyński. *Lectures on Stochastic Programming: Modeling and Theory*. Society for Industrial and Applied Mathematics, Philadelphia, 2009.

[131] Siemens. *Energy efficiency in building automation and control*. Tech. rep. 2011.

[132] F. Sossan, E. Namor, R. Cherkaoui, and M. Paolone. "Achieving the Dispatchability of Distribution Feeders Through Prosumers Data Driven Forecasting and Model Predictive Control of Electrochemical Storage". In: *IEEE Transactions on Sustainable Energy* 7.4 (Oct. 2016), pp. 1762–1777. ISSN: 1949-3029. DOI: 10.1109/TSTE.2016.2600103.

[133] H Spindler and L Norford. "Naturally ventilated and mixed-mode buildings - Part II: Optimal control". In: *Building and Environment* 44.4 (Apr. 2009), pp. 750–761. ISSN: 03601323. DOI: 10.1016/j.buildenv.2008.05.018.

[134] Giorgos Stathopoulos, Harsh Shukla, Alexander Szucs, Ye Pu, and Colin N. Jones. "Operator Splitting Methods in Control". In: *Foundations and Trends® in Systems and Control* 3.3 (2016), pp. 249–362. ISSN: 2325-6818. DOI: 10.1561/2600000008.

[135] Oliver Stein. "How to solve a semi-infinite optimization problem". In: *European Journal of Operational Research* 223.2 (Dec. 2012), pp. 312–320. ISSN: 0377-2217. DOI: 10.1016/j.ejor.2012.06.009.

[136] D. Sturzenegger, D. Gyalistras, M. Morari, and R.S. Smith. "Model Predictive Climate Control of a Swiss Office Building: Implementation, Results, and Cost-Benefit Analysis". In: *IEEE Transactions on Control Systems Technology* PP.99 (2015), pp. 1–1. ISSN: 1063-6536. DOI: 10.1109/TCST.2015.2415411.

[137] D. Sturzenegger, Dominik Keusch, Leonardo Muffato, Dominique Kunz, and R. Smith. "Frequency-Domain Identification of a Ventilated Room for MPC". In: *IFAC World Congress on Automatic Control*. Cape Town, South Africa, Aug. 2014, pp. 593–598.

[138] David Sturzenegger, Dimitrios Gyalistras, Manfred Morari, and Roy S. Smith. "Semi-automated modular modeling of buildings for model predictive control". In: *Proceedings of the Fourth ACM Workshop on Embedded Sensing Systems for Energy-Efficiency in Buildings*. BuildSys '12. New York, NY, USA: ACM, 2012, pp. 99–106. ISBN: 978-1-4503-1170-0. DOI: 10.1145/2422531.2422550.

[139] David Sturzenegger, Dimitrios Gyalistras, Vito Semeraro, Manfred Morari, and Roy S Smith. "BRCM Matlab Toolbox: Model generation for model predictive building control". In: *American Control Conference (ACC), 2014*. IEEE. 2014, pp. 1063–1069.

[140] Leo Su and Leslie K. Norford. "Demonstration of HVAC chiller control for power grid frequency regulation—Part 1: Controller development and experimental results". In: *Science and Technology for the Built Environment* 21.8 (Nov. 2015), pp. 1134–1142. ISSN: 2374-4731. DOI: 10.1080/23744731.2015.1072449.

[141] Leo Su and Leslie K. Norford. "Demonstration of HVAC chiller control for power grid frequency regulation—Part 2: Discussion of results and considerations for broader deployment". In: *Science and Technology for the Built Environment* 21.8 (Nov. 2015), pp. 1143–1153. ISSN: 2374-4731. DOI: 10.1080/23744731.2015.1072455.

[142] Swissgrid. *Overview of ancillary service products*.

[143] Swissgrid. *Test for secondary control capability*. Tech. rep. 2012.

[144] Paulo Cesar Tabares-Velasco, Craig Christensen, and Marcus Bianchi. "Verification and validation of EnergyPlus phase change material model for opaque wall assemblies". In: *Building and Environment* 54 (2012), pp. 186 –196. ISSN: 0360-1323. DOI: http://dx.doi.org/10.1016/j.buildenv.2012.02.019.

[145] Jasna Tomić and Willett Kempton. "Using fleets of electric-drive vehicles for grid support". In: *Journal of Power Sources* 168.2 (June 2007), pp. 459–468. ISSN: 03787753. DOI: 10.1016/j.jpowsour.2007.03.010.

[146] US Department of Energy: Office of Energy Efficiency and Renewable Energy. *Commercial Reference Buildings*.

[147] Zdeněk Váňa, Jiří Cigler, Jan Široký, Eva Žáčeková, and Lukáš Ferkl. "Model-based energy efficient control applied to an office building". In: *Journal of Process Control* 24.6 (2014). Energy Efficient Buildings Special Issue, pp. 790 –797. ISSN: 0959-1524. DOI: http://dx.doi.org/10.1016/j.jprocont.2014.01.016.

[148] E. Vrettos, KuanLin Lai, F. Oldewurtel, and G. Andersson. "Predictive Control of buildings for Demand Response with dynamic day-ahead and real-time prices". In: *Control Conference (ECC), 2013 European*. July 2013, pp. 2527–2534.

[149] E. Vrettos, F. Oldewurtel, and G. Andersson. "Robust Energy-Constrained Frequency Reserves From Aggregations of Commercial Buildings". In: *IEEE Transactions on Power Systems* PP.99 (2016), pp. 1–14. ISSN: 0885-8950. DOI: 10.1109/TPWRS.2015.2511541.

[150] Evangelos Vrettos, Emre C. Kara, Jason MacDonald, Göran Andersson, and Duncan S. Callaway. "Experimental Demonstration of Frequency Regulation by Commercial Buildings - Part I: Modeling and Hierarchical Control Design". In: *arXiv:1605.05835 [math]* (May 2016). arXiv: 1605.05835.

[151] Evangelos Vrettos, Emre C. Kara, Jason MacDonald, Göran Andersson, and Duncan S. Callaway. "Experimental Demonstration of Frequency Regulation by Commercial Buildings - Part II: Results and Performance Evaluation". In: *arXiv:1605.05558 [math]* (May 2016). arXiv: 1605.05558.

[152] Evangelos Vrettos, Frauke Oldewurtel, Goran Andersson, and Fengthian Zhu. "Robust Provision of Frequency Reserves by Office Building Aggregations". In: *Proceedings of the 19th IFAC World Congress*. Cape Town, South Africa, 2014.

[153] J. Warrington, P. Goulart, S. Mariethoz, and M. Morari. "Policy-Based Reserves for Power Systems". In: *IEEE Transactions on Power Systems* 28.4 (Nov. 2013), pp. 4427–4437. ISSN: 0885-8950. DOI: 10.1109/TPWRS.2013.2269804.

[154] WBCSD. *Transforming the Market: Energy efficiency in buildings*. Tech. rep. 2009.

[155] Michael Wetter. "Co-Simulation of Building Energy and Control Systems with the Building Controls Virtual Test Bed". In: *Journal of Building Performance Simulation* August (2011).

[156] Michael Wetter and Philip Haves. "A MODULAR BUILDING CONTROLS VIRTUAL TEST BED FOR THE INTEGRATION OF HETEROGENEOUS SYSTEMS". In: *IBPSA-USA Journal* 3.1 (2008), pp. 69–76.

[157] Qingyuan Zhang, Joe Huang, and Siwei Lang. "Development of typical year weather data for Chinese locations/Discussion". In: *ASHRAE transactions* 108 (2002), p. 1063.

[158] X. Zhang, M. Kamgarpour, P. Goulart, and J. Lygeros. "Selling robustness margins: A framework for optimizing reserve capacities for linear systems". In: *2014 IEEE 53rd Annual Conference on Decision and Control (CDC)*. Dec. 2014, pp. 6419–6424. DOI: 10.1109/CDC.2014.7040396.

[159] Xiaojing Zhang, Maryam Kamgarpour, Angelos Georghiou, Paul Goulart, and John Lygeros. "Robust optimal control with adjustable uncertainty sets". In: *Automatica* 75 (Jan. 2017), pp. 249–259. ISSN: 0005-1098. DOI: 10.1016/j.automatica.2016.09.016.

[160] Xiaojing Zhang, G. Schildbach, D. Sturzenegger, and M. Morari. "Scenario-based MPC for energy-efficient building climate control under weather and occupancy uncertainty". In: *Control Conference (ECC), 2013 European*. July 2013, pp. 1029–1034.

[161] L. Zhao, H. Hao, and W. Zhang. "Extracting flexibility of heterogeneous deferrable loads via polytopic projection approximation". In: *2016 IEEE 55th Conference on Decision and Control (CDC)*. Dec. 2016, pp. 6651–6656. DOI: 10.1109/CDC.2016.7799293.

[162] L. Zhao and W. Zhang. "A geometric approach to virtual battery modeling of thermostatically controlled loads". In: *2016 American Control Conference (ACC)*. July 2016, pp. 1452–1457. DOI: 10.1109/ACC.2016.7525121.

[163] Peng Zhao, Gregor P. Henze, Sandro Plamp, and Vincent J. Cushing. "Evaluation of commercial building HVAC systems as frequency regulation providers". In: *Energy and Buildings* 67 (Dec. 2013), pp. 225–235. ISSN: 0378-7788. DOI: 10.1016/j.enbuild.2013.08.031.

[164] J. Zhen and D. den Hertog. "Computing the Maximum Volume Inscribed Ellipsoid of a Polytopic Projection". In: *CentER Discussion Paper Series* 2015-004 (Jan. 2015).

[165] Datong Zhou, Qie Hu, and Claire J. Tomlin. "Model Comparison of a Data-Driven and a Physical Model for Simulating HVAC Systems". In: *CoRR* abs/1603.05951 (2016).

[166] Günter M. Ziegler. *Lectures on polytopes*. Vol. 152. Springer Science & Business Media, 2012.

Tomasz Gorecki

24 chemin de la fourmi, 1010 LAUSANNE, Switzerland
+(41) 7 82 00 37 80
tomh.gorecki@orange.fr
Skype: tomek.gorecki269
French, born
26.09.1990

- PhD in Control Engineering
- Proficient in French, English and German
- Looking for international experience in the field of Energy or Autonomous systems

EDUCATION

Since 09.2012 — **PhD in Control Engineering,** **Swiss Institute of Technology at Lausanne (EPFL)**
Automatic control lab
Graduation expected in May 2017
Advisor: Prof. Colin Jones, colin.jones@epfl.ch

09.2009 – 06.2012 — **Mines ParisTech,** **Paris, France**
Master degree in Mechanical Engineering
Ranked in top 3 French Engineering schools
GPA: 3.6/4 (Average of students in year: 3.0/4)

09.2010 – 01.2011 — **California Institute of Technology,** **Pasadena, USA**
Department of Applied and Computational Mathematics
Exchange semester
Research project in Probability theory

WORK EXPERIENCE

Since 09.2012 — **Teaching Assistant**
- Graduate teaching assistant in five classes (BSc and MSc level)
- Coaching of a team of students in EPFL mobile robotics competition
- Supervision of 5 semester and 3 master projects

06.2011 – 09.2011 — **DAIMLER** **Stuttgart, Germany.**
Team for optical control at Mercedes-Benz Cars.
Identification and study of surface defects on complex manufactured pieces and evaluation of measurement systems as part of a project of automation of the quality control for automatic gearbox production lines.

PROJECTS

Since 09.2012 — **Ancillary services with buildings**
- Study of fast power consumption modulation with building heating systems for grid support services
- Design of novel optimization-based controllers for systems under uncertainty.
- Economic study of building participation in ancillary services market.

LADR experimental testbed
- Design of a controllable heating system for control experiments in a living laboratory.
- Software design for the control and data logging (MATLAB + Python/Django)
- Experiment design and implementation for system identification and real-time control of power consumption.

Openbuild toolbox

- Building thermodynamics modeling toolbox. Physical modelling of buildings to extract controller-ready mathematical models.
- Developed in MATLAB and available under GPL license. Interfaces with modeling software EnergyPlus for data extraction and co-simulation.
- *Openbuild* has been used in several teaching and research projects in and outside our laboratory.

01.2012 – 06.2012 **Master thesis** **The French Aerospace Lab (ONERA)**

Cooperative guidance methods for drone fleets

- Design of trajectory planning methods for the guidance of multi-agent systems. Use of optimization-based methods and implementation in MATLAB.

LANGUAGE

French	Mother tongue
English	C1, proficient
German	B2, good written and spoken

SKILLS

Mathematics	Optimization: convex and non-convex programming techniques, optimization under uncertainty (robust and stochastic programming) Control theory (in particular Predictive Control) System identification
Programming	Working knowledge: MATLAB Basic knowledge: Python, SQL, Java

VOLUNTEER ACTIVITY

Hand'escape	**Treasurer et co-founder, 2010-2012** We designed a technical kit for wheelchairs. A functional prototype has been constructed and tested. Finalists in two national innovation competitions
Handivalides Mines ParisTech	**Co-president, 2011** We organized with other universities a national event for promoting a better understanding of handicap-related issues.
Voyage Promo Mines ParisTech	**Secretary of the association, 2012** Organization of a trip for the students of the university (budget : 160 000€)

INTERESTS

Interests	Sports. Climbing. Piano. Photography.